AGARD-R-734

AGARD

ADVISORY GROUP FOR AEROSPACE RESEARCH & DEVELOPMENT

7 RUE ANCELLE 92200 NEUILLY SUR SEINE FRANCE

AGARD REPORT No.734

The Flight of Flexible Aircraft in Turbulence — State-of-the-Art in the Description and Modelling of Atmospheric Turbulence

NORTH ATLANTIC TREATY ORGANIZATION

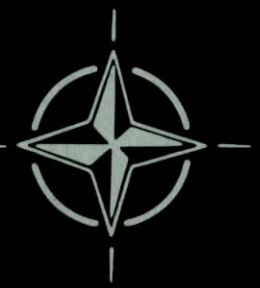

UNCLASSIFIED

AGARD-R-734

NORTH ATLANTIC TREATY ORGANIZATION

ADVISORY GROUP FOR AEROSPACE RESEARCH AND DEVELOPMENT

(ORGANISATION DU TRAITE DE L'ATLANTIQUE NORD)

AGARD Report No.734

THE FLIGHT OF FLEXIBLE AIRCRAFT IN TURBULENCE – STATE-OF-THE-ART IN THE DESCRIPTION AND MODELLING OF ATMOSPHERIC TURBULENCE

Papers presented at the 63rd Meeting of the Structures and Materials Panel of AGARD in Athens, Greece 28 September—3 October 1986.

THE MISSION OF AGARD

The mission of AGARD is to bring together the leading personalities of the NATO nations in the fields of science and technology relating to aerospace for the following purposes:

— Exchanging of scientific and technical information;

— Continuously stimulating advances in the aerospace sciences relevant to strengthening the common defence posture;

— Improving the co-operation among member nations in aerospace research and development;

— Providing scientific and technical advice and assistance to the Military Committee in the field of aerospace research and development (with particular regard to its military application);

— Rendering scientific and technical assistance, as requested, to other NATO bodies and to member nations in connection with research and development problems in the aerospace field;

— Providing assistance to member nations for the purpose of increasing their scientific and technical potential;

— Recommending effective ways for the member nations to use their research and development capabilities for the common benefit of the NATO community.

The highest authority within AGARD is the National Delegates Board consisting of officially appointed senior representatives from each member nation. The mission of AGARD is carried out through the Panels which are composed of experts appointed by the National Delegates, the Consultant and Exchange Programme and the Aerospace Applications Studies Programme. The results of AGARD work are reported to the member nations and the NATO Authorities through the AGARD series of publications of which this is one.

Participation in AGARD activities is by invitation only and is normally limited to citizens of the NATO nations.

Published December 1987

ISBN 92-835-0426-7

Printed by Specialised Printing Services Limited
40 Chigwell Lane, Loughton, Essex IG10 3TZ

FOREWORD

The papers collected together in this document were presented at a Workshop held by the Structures and Materials Panel on the Flight of Flexible Aircraft in Turbulence. Discussion centered on the collection and analysis of turbulence data obtained from commercial flights and also from specially equipped aeroplanes.

The reason for resuscitating a topic covered very fully by the Structures and Materials Panel some fifteen years ago is that the new technical capacity which has become available makes it possible to enlarge the existing data banks by a large factor and, furthermore, to improve the descriptions of atmosphere, (derived from all too few flight hours), which is still the foundation of the relevant airworthiness regulations.

Three of the presentations deal with the means for measuring actual time histories of turbulence, and the spectrum associated; most of the others took advantage of the Aircraft Integrated Data System (A.I.D.S.) to propose methods for collecting acceleration data and deriving gust statistics.

It is hoped that this comon effort will improve our knowledge of an environment which is of great importance for the new generation of aircraft being designed in the NATO community.

G.COUPRY
Chairman, Sub-Committee on
The Flight of Flexible Aircraft
in Turbulence

ABSTRACT

The Structures and Materials Panel of AGARD is studying the Flight of Flexible Aircraft in Turbulence. This, the first section of a two-part report, contains presentations given at the first of two Workshops on the State-of-the-Art in the Description and Modelling of Atmospheric Turbulence; topics covered here are (a) Measurements of Turbulence by Specially-equipped Aircraft and (b) Data Collection and Reduction of Incremental Accelerations observed in Commercial Flights.

***

Le Groupe de l'AGARD chargé de l'étude des Structures et des Matériaux étudie actuellement le vol des avions flexibles dans les turbulences. Ce document, qui est le premier chapitre d'un rapport comportant deux parties, contient les exposés qui ont été présentés lors du premier de deux ateliers sur l'état de l'art en ce qui concerne la définition et la modélisation de la turbulence atmosphérique; les thèmes abordés ici sont: (a) Mesures des turbulences par des avions spécialement équipés et (b) Procédures de recueil et d'exploitation des données concernant les incréments d'accélération observés sur les vols commerciaux.

CONTENTS

STATUS REVIEW OF ATMOSPHERE TURBULENCE AND AIRCRAFT RESPONSE

by

J.C.Houbolt
Chief Aeronautical Scientist
NASA Langley Research Center
M.S.243, Hampton, VA 23665
USA

ABSTRACT

A brief review is made of where we stand presently with respect to our understanding of aircraft encounter of atmospheric turbulence, both from the point of view of describing or modeling the turbulence and with respect to our ability to calculate resulting airplane loads.

Some of the more recent studies of gust measurements and of reducing airline gust response data are discussed. Special attention is given to gust analysis requirements as involved in airplane certification and whether there is a need for additional or different requirements. The paper concludes with the review of a recent study in which amazingly simple and universal gust response equations were discovered; the possible impact of these new findings on future work is indicated.

LIST OF SYMBOLS

Symbol:	Definition:
a	slope of the lift curve
A	response transfer coefficient as in $\sigma_{\Delta n} = A\sigma_w$
A_r	aspect ratio
c	wing chord
k	reduced frequency, $k = \frac{\omega c}{2V}$
k	reduced frequency for zero crossings, $k_o = \frac{\pi N_o c}{V}$
k_s	reduced short period frequency, $k_s = \frac{\omega_s c}{2V}$
L	integral scale
N_o	zero crossing per second, $N_o = \frac{V}{\pi c} k_o$
S	wing area
U_d, U_e, U_t	various gust intensity design values
V	airplane speed
W	airplane weight
α	angle of attack for airplane in level flight referred to the $C_L = 0$ crossing point
Δn	incremental load factor due to gusts
η	number of standard deviations
μ	mass parameter, $\mu = \frac{2W}{a\rho cgS}$
ρ	air density
σ_w	rms value for gust intensity
σ_1	combined severity and scale parameter, $\sigma_1 = \frac{\sigma_w}{\sqrt{\pi}\,(\frac{2L}{c})^{1/3}}$
ϕ_w	power spectrum for gusts
ω	angular frequency
Ω	a reduced frequency, $\Omega = \frac{\omega}{V}$

INTRODUCTION

This report gives a brief review of where we stand today with respect to measuring atmospheric turbulence, of modeling the turbulence in convenient analytical form for design use, and of our ability to design airplanes for turbulence encounter. It is perhaps worthwhile to mention that these considerations were covered in two review papers of some years ago.[1,2] Although the basic points and findings presented in these two papers still stand, there have been limited continuing efforts to obtain turbulence data, both in specialized and routine flights, and to reduce and interpret these data in a more consistent or universal manner. In turn the question arises of whether we need changes or improvements in our design approaches. It is fitting, therefore, that we get together to discuss some of our more recent findings and concerns about airplane turbulence encounter. The present report is not exhaustive in its coverage; the main attempt is to bring out some of the key concerns that are on the horizon so as to set the stage for discussion and interchange in this workshop.

MEASUREMENT AND ANALYSIS OF TURBULENCE

About a year ago, Murrow gave a paper before this group reviewing a number of turbulence study efforts that had been or were going on in the U.S.[3] He is giving an update to this paper today. In addition, 7 or 8 other papers are to be presented which review the work that has been going on in the U.S. and several countries in Europe on the measurement and analysis of atmospheric turbulence through the use of instrumented airplanes. I will, therefore, leave the review of the measurement and analysis of turbulence up to the authors that we will hear from subsequently in this workshop.

REDUCTION AND INTERPRETATION OF GUST ACCELERATION DATA

It has been a standard procedure to take measured airplane vertical acceleration data and to deduce the effective gust intensity that produced the acceleration by means of the equation

$$\Delta n = \frac{a \rho S V}{2W} K U_e \qquad (1)$$

where K is the K_g curve shown in figure 1[2]. The prime assumptions that led to this equation are that the airplane is a point mass with vertical degree of freedom only, and that the gust is a discrete gust that is uniform in the spanwise direction. When power spectral methods are considered, a similar equation results, except now it is found, as shown in the figure, that the alleviation factor K is not only a function of the mass parameter μ but also on the parameter $\frac{2L}{c}$, where L is the integral scale of turbulence. It is seen, then, that if measurement airplanes of different chords are used (and if L for a given altitude is chosen fixed) that the deduced value of U_e using the appropriate $\frac{2L}{c}$ curve will be quite different than the value found by using the K_g curve. Coupry has found that, through use of a family of $\frac{2L}{c}$ curves similar to that shown in figure 1, the deduced value of U_e tend to fall in a more consistent and narrower pattern (a less scattered curve formation) than obtained by use of the K_g curve.

There is, however, an important item still missing. Figure 1 results are for a single degree of freedom airplane. The results should be derived on the basis that the airplane has two degrees of freedom, namely vertical motion and pitch. Later in this paper results based on a two degree freedom system will be presented.

AIRCRAFT CERTIFICATION DUE TO GUST ENCOUNTER

In the U.S. there has been essentially no change for many years in the gust design requirements outlined in the FAR and in the Military Specifications, and no change seems to be forthcoming. Design is still largely based on the discrete gust formula (equation 1), and on the use of a power spectral approach. I would like to observe that the values of P and b, the proportion of time in turbulence and turbulence severity, as used in the PSD approach, have been for years regarded as "too severe," but they remain unchanged. As an attempt to improve this situation, updated P and severity values were derived and published in reference 4. I believe these updated values should be taken into account in any further deliberations we may have on changes or improvements in our design approaches.

IS THERE A NEED FOR A CHANGE IN GUST DESIGN PROCEDURES

Although the gust design procedures have essentially remained the same for years, at least here in the U.S., there is concern expressed from some quarters that perhaps some changes or additions to the design procedures are needed. Interest in changes has been especially focused because of a particular Statistical Discrete Gust analysis method that has been advocated by Jones of RAE Farnborough. In an attempt to bring out the concerns of various individuals more clearly, a gust specialist meeting was held in San Antonio, Texas, May 22, 1986.

The following is a listing in abbreviated form of some of the concerns or positions that various individuals expressed; this listing serves to indicate the tenor of the meeting.

1. There was concern that yet another method might be added to the six already required to obtain FAA/JAR certification (the six cited were: static elastic, PSD design envelope, PSD mission analysis, discrete tuned gust (CAA), round-the-clock and negative gusts (RLD).

2. Different methods give different loads:
   a. Static elastic gust loads gave original design
   b. U_σ = 85 gave lower loads
   c. 50 fps tuned gust and round-the-clock gusts gave greater weights
   d. Tuned discrete "too severe"

3. No difficulty in the PSD approach to handle balanced loads

4. PSD approach has practical problems

5. Time domain analysis should be used, particularly to handle non-linear systems

6. The Statistical Discrete Gust method should be developed further, especially as a tool for handling non-linearities

It is clear from this listing that the Structures and Materials people of AGARD must get together to form jointly a list of concerns that represent a consensus, and then to take steps to resolve these concerns. I offer a few comments about some of the items in the listing. Regardless of the design method, there is one item of commonality; that is, the gust severity must be stated in some way. The fact that different methods give different loads suggests that the severity values have not been chosen in a consistent way.

In a way the choice of gust severity values is sort of arbitrary, and is a way of covering up all our sins or ignorances in the simplifying assumptions we make in our analyses. Consider the incremental vertical acceleration that three different methods might indicate: the discrete gust approach may yield

$$\Delta n = .03\ U_d$$

while the power spectral approach may give

$$\Delta n = .0175\ U_\sigma$$

and the tuned gust method indicates

$$\Delta n = .0333\ U_t$$

We note that if we choose

$$U_d = 50 \text{ fps}$$

$$U_\sigma = 85.7$$

$$U_t = 45$$

then all three approaches lead to the same incremental load factor of 1.5. My feeling is that we have not done enough study of the type illustrated by these examples to establish the gust severity values in our various approaches, or to see if a consistent set of severity values can be established which, when applied to past aircraft, lead to consistent design loads.

With respect to the power spectral approach, I have found that it is quite versatile and can do just about anything that any other method can do. If individuals have found some difficulty in applying the approach, these difficulties should be brought out; I feel sure ways can be found to solve the apparent problem. Reference 1 and 5, for example, give ways for handling combined loads, in spite of the fact that some felt that this was not possible.

With respect to the Statistical Discrete Gust approach, I must admit that it appears complicated, that there seems to be a mystic or magic about it, and that the terminology used is confusing. I do not know that it has any real value or credibility. This situation suggests the following. Before the community at large can evaluate the SDG approach or understand its value the following should be done:

1. Outline the approach in a clear step by step manner, devoid of any needless jargon.

2. Show its application by way of a few examples, not connected with proprietary interests.

3. Show why it is considered to be necessary or what it can do that other approaches cannot.

4. Bring all interested parties together to make sure they all understand it clearly.

Through steps of the nature indicated gust specialists would then be better able to evaluate its usefulness, and in turn, judge whether it should be introduced as another analysis tool.

At the same time consideration should be given to another analysis approach, namely a time domain procedure. As an example of this approach, reference 6 presents a direct time history method for establishing gust loads for the often used case of an airplane with vertical motion freedom only. Gusts are synthesized in a Monte Carlo fashion to provide for a rather realistic nonstationary type of gust encounter. Figure 2, taken from reference 6 (figure 14 of this reference), illustrates the nature of the results obtained. The turbulence is seen to be quite nonstationary and very realistic in appearance; notice the isolated type gusts, and even the recurrences of large gusts in sequence. With the computer power we have available today there is no reason why the procedure given in this reference cannot be expanded to include two or more degrees of freedom. Direct time histories of loads would result, and no ambiguity in the interpretation of these loads should be present. Further development of this direct time history approach is highly recommended.

A word should be said about nonlinear systems. The argument is sometimes presented that newer design approaches, such as the SDG method, are needed to handle the response of nonlinear subsystems--such as gust load alleviation. I wish to caution that this argument is subject to question. When we analyze the response of an airplane to turbulence we make a number of simplifying assumptions--for many years, for example, we treated the airplane as a point mass with vertical motion only. The gusts felt by the airplane act in all directions, yet we treat the longitudinal and lateral response separately. We assume the gusts are uniform across the spans, but we know there is a spanwise variation just as there is a variation along the path of the airplane. The errors introduced by all these assumptions may easily equal or exceed any error that is introduced by treating a nonlinear subsystem in a linear way. Thus, there is little point in refining or introducing a new analysis so as to be able to take certain nonlinearities into account precisely, when all the rest of the assumptions are left to first order crudeness. The treatment, for example, of the airplane as a single degree of freedom or as a two degree of freedom system leads to vastly different response results, as a later figure will show.

SOME NEW REMARKABLY SIMPLE RESPONSE EQUATIONS

We hear rumblings that there are already too many gust analysis procedures. I must confess that I am going to compound the situation by showing the basis for still another approach. The results presented in this section are from some analyses I have made over the past several years. Just by rearranging the governing response equations in slightly different form, and by introducing a basic flight condition, I have found that the gust response results could be made to condense to an amazingly simple form. Only a summary of the results is given, without the supporting analysis. I urge gust specialists to study these results, and reexamine their analyses on the basis of the notions presented here; it is hoped that they will confirm these new findings and that they find their results also condense in similar fashion.

The analysis is a power spectrum approach and is based on an airplane with two degrees of freedom, vertical motion and pitch. Spanwise gust gradients are taken into account. The point spectrum chosen is the von Karman spectrum, but written in the following form:

$$\phi_w(k) = \sigma_1^2 \frac{\left(\frac{2L}{c}\right)^{5/3}\left[1 + \frac{8}{3}\left(1.339\,\frac{2L}{c}\,k\right)^2\right]}{\left[1 + \left(1.339\,\frac{2L}{c}\,k\right)^2\right]^{11/6}} \qquad (2)$$

where

$$\sigma_1^2 = \frac{\sigma_w^2}{\pi\left(\frac{2L}{c}\right)^{2/3}} \qquad (3)$$

This is an important step; it makes all the spectra pass through the same points at high frequencies, regardless of the scale of turbulence, see figure 3.

We should note that the inclusion of the pitch degree of freedom has a pronounced influence on the output response. To illustrate, figure 4, taken from reference 7, compares the distribution of response power for a single degree of freedom airplane with the two degree of freedom case. Even though equation 2 was used in both cases, we note that there is a lot of response at low frequencies for the single freedom case, and that the results depend on $\frac{2L}{c}$. By contrast, the response power at low frequencies is

virtually eliminated for the two degree of freedom airplanes, (because of airplane weathercocking), and instead the response power tends to concentrate around the short period frequency; we also find, because of the way we arranged equation 2, that the response is essentially independent of the value of $\frac{2L}{c}$.

The response equation for incremental vertical acceleration is found to be

$$\Delta n = \frac{a\rho SV}{2W} K(n\sigma_1) \tag{4}$$

$$= \frac{V}{cg\mu} K(n\sigma_1)$$

where $\mu = \frac{2W}{a\rho cgS}$, n refers to a chosen number of standard deviations, and where K is an alleviation factor given by

$$K = [\int f_0 f_1 f_2 f_3 \, dk]^{1/2} \tag{5}$$

In the equation for K, f_0 is the airplane transfer function, f_1 is the unsteady lift function for gust penetration effects, f_2 takes into account spanwise gust variation effects, and $f_3 = \frac{\Phi_w}{\sigma_1^2}$ reflects the input gust spectrum as given by equation 2. The specific equations used for the f_1 and f_2 are (unpublished work of the author)

$$f_1 = \frac{1}{1 + 2.32\nu k + \nu^2 k^2}$$

$$f_2 = \frac{1 + .55\, A_r k}{1 + .66\, A_r k + .34\, A_r^2 k^2}$$

where

$$\nu = \frac{1.5}{\beta} \frac{A_r}{3 + A_r\beta}$$

$$\beta = \sqrt{1 - M^2}$$

With the use of these f_1 and f_2 functions, there is no difficulty found in establishing realistic values of N_0, the zero crossing parameter.

The analysis was applied to a number of different airplanes. In a remarkable way, it was found that K could be given in very good approximation by

$$K = .95\sqrt{\mu} \tag{6}$$

for all the airplanes studied, and for practical purposes the results were found to be essentially independent of $\frac{2L}{c}$.

It is now useful to introduce the level flight conditions of the airplane, namely

$$W = \frac{a}{2} \rho V^2 S\alpha$$

where α is the angle of attack necessary to maintain level flight, relative to the $C_L = 0$ crossing point of the C_L versus α curve, see figure 5. This equation yields

$$V = \sqrt{\frac{\mu cg}{\alpha}} \tag{7}$$

If equation 3, 6, and 7 are inserted in equation 4, the value for Δn condenses to the following simple and universal result.

$$\Delta n = \frac{.07497}{c^{1/6}\sqrt{\alpha}} \frac{n\sigma_w}{L^{1/3}} \tag{8}$$

Note, apart from the gust parameter $\frac{\sigma_w}{L^{1/3}}$, the value of Δn is dependent esentially

only on α; the speed of the airplane, the weight, and the altitude are all automatically taken into account. The chord c enters in only a secondary way because of the sixth-root variation.

Now further, the value $\frac{\sigma_w}{L^{1/3}}$, is a combined parameter and it should be treated as such; there is no need to try to separate the severity σ_w and the scale L values. Consider turbulence data as obtained from an instrumented airplane. Generally, measured turbulence leads to well defined spectral values in the straight line portion of the spectrum (the $\Omega^{-5/3}$ fall-off portion), see figure 6. Equation 14 in reference 1 indicates that by taking any point along this straight line portion, the value of $\frac{\sigma_w}{L^{1/3}}$ is given by

$$\frac{\sigma_w}{L^{1/3}} = \left[1.919\ \Omega_1^{5/3}\ \phi_w(\Omega_1)\right]^{1/2} \tag{9}$$

Thus, $\frac{\sigma_w}{L^{1/3}}$ is a combined parameter that falls out naturally from measured spectral values; there is no need to establish separate values for σ_w and L.

Another point of interest can be made from equation 9. The equation indicates that $\frac{\sigma_w}{L^{1/3}}$ is a constant for a given set of spectral data; thus

$$\sigma_w \propto L^{1/3}$$

If we liken σ_w to gust severity U, and L to gust gradient distance H, then we have

$$U \propto H^{1/3}$$

a result which Jones has observed in his SDG approach. Thus his result obtained from examining sequential discrete type gust is not too surprising, since it apparently can be predicted by the power spectral approach.

The analysis also indicated the following general expression for all airplanes studied

$$N_o = \frac{V}{\pi c} k_o = \frac{1.084}{\sqrt{c\alpha}}$$

$$k_o = \frac{.496}{\mu^{.46}}$$

$$k_o = 1.29\ k_s^{.8}$$

A sumary of the results obtained when the Dryden type spectrum (Ω^{-2} fall-off) was used is as follows

$$\Delta n = \frac{.1547}{\sqrt{\alpha}} \frac{\eta\sigma_w}{\sqrt{L}}$$

$$N_o = \frac{V}{\pi c} k_o = \frac{.858}{\sqrt{c\alpha}} \tag{10}$$

$$k_o = \frac{.475}{\sqrt{\mu}}$$

$$k_o = 1.9\ k_s$$

$$\frac{\sigma_w^2}{L} = \frac{\pi}{3} \Omega_1^2\ \phi_w(\Omega_1)$$

The results for the load exceedance curves are also greatly simplified, but these results are not presented here.

Besides the simplified design equations, the results of this section provide a new way to deduce gust severity levels from measured acceleration data. Thus, if equations 3 and 6 are substituted into equation 4, the result is

$$\Delta n = .013211 \frac{V}{c^{2/3}\sqrt{\mu}} U_L \qquad (11)$$

where $U_L = \eta \frac{\sigma_w}{L^{1/3}}$; in this form V is in fps, and c is in feet. This equation is of universal form; the use in deriving characteristic atmospheric values of U_L from measured Δn's is recommended, just as U_e has been derived from an equation like equation 1 in the past. It is estimated that design values for U_L will be around 10.

We conclude this section by speculating what equations 8 and 10 might look like when presented in a design application form. Assume the equations have been applied to a number of existing aircraft in retrospect manner; essentially the intent would be to derive design choices for $\frac{\eta \sigma_w}{L^{1/3}}$ or $\frac{\eta \sigma_w}{\sqrt{L}}$. When examined in this way, results of the following very simple and generalized form may, for example, be found.

For a von Karman type spectral input,

$$\Delta n = \left(\frac{15}{c}\right)^{\frac{1}{6}} \frac{.50}{\sqrt{\alpha}}$$

or $$\Delta n = 1.5 \left(\frac{15}{c}\right)^{\frac{1}{6}} \sqrt{\frac{.11}{\alpha}}$$

or $$\Delta n = 1.5 \left(\frac{15}{c}\right)^{\frac{1}{6}} \sqrt{\frac{a}{5} \frac{.55}{C_L}}$$

and for the Dryden type spectral input,

$$\Delta n = \frac{.50}{\sqrt{\alpha}}$$

or $$\Delta n = 1.5 \sqrt{\frac{.11}{\alpha}}$$

or $$\Delta n = 1.5 \sqrt{\frac{a}{5} \frac{.55}{C_L}}$$

where c is in feet and α in radians represents the level flight angle of attack that is associated with some sort of average cruising condition for the airplane. The application of these amazingly simple equations gives directly the design incremental load factor for gust encounter. All conditions of flight speed, weight, and altitude are automatically taken into account. The consideration of these equations and the specific evaluation of the appropriate coefficients are recommended.

CONCLUDING REMARKS

The coverage in this paper indicates the following recommendations:

1. A unified and consistent way should be agreed upon for reducing gust acceleration data to gust severity values.
2. The P's and b's in the design regulations should be updated.
3. Gust severity levels in the various design approaches should be evaluated so as to give consistent design load values.

4. The SDG approach should be listed in a clear and simple step by step manner, and its advantages over other approaches, if any, should be brought out clearly by examples.

5. Consideration should be given to the development of a direct time history method for calculating gust loads, similar to the procedure used in reference 6.

6. Spectral data should be evaluated to yield the $\frac{\sigma_w}{L^{1/3}}$ parameter as given by equation 9.

7. The simplified gust design procedure presented herein should be examined for its universal applicability.

REFERENCES

1. Houbolt, J. C.; Steiner, R.; and Pratt, K. G.: Dynamic Response of Airplanes to Atmospheric Turbulence Including Flight Data on Input and Response. NASA TR R-199, June 1964.

2. Houbolt, J. C.: Atmospheric Turbulence. Reprint from AIAA Journal, Vol. 11, No. 4, April 1973, pp. 421-437.

3. Murrow, H. N.: A Perspective on the Status of Measurement of Atmospheric Turbulence in the U.S. NASA TM-87610, September 1985.

4. Houbolt, J. C.: Updated Gust Design Values for Use with AFFDL-70-106. Air Force Technical Report No. AFFDL-TR-73-148, November 1973.

5. Houbolt, J. C.: Exceedances of Structural Interaction Boundaries for Random Excitation. Reprint from AIAA Journal, Vol. 6, No. 11, November 1968, pp. 2175-2182.

6. Houbolt, J. C.; and Williamson, G. G.: A Direct Time History Study of the Response of an Airplane to Nonstationary Turbulence. Air Force Technical Report No. AFFDL-TR-74-148, January 1975.

7. Houbolt, J. C.; and Williamson, G. G.: Spectral Gust Response for an Airplane with Vertical Motion and Pitch. Air Force Technical Report No. AFFDL-TR-75-121, October 1975.

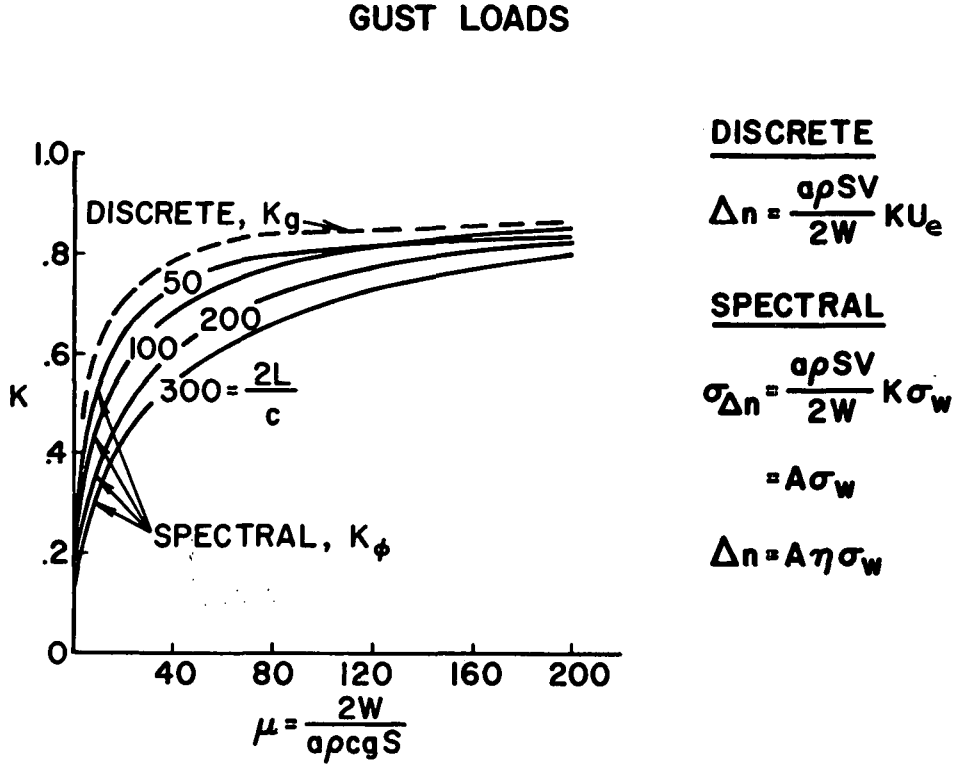

Figure 1.- Discrete and spectral equations for gust loads.

TIME HISTORY APPROACH

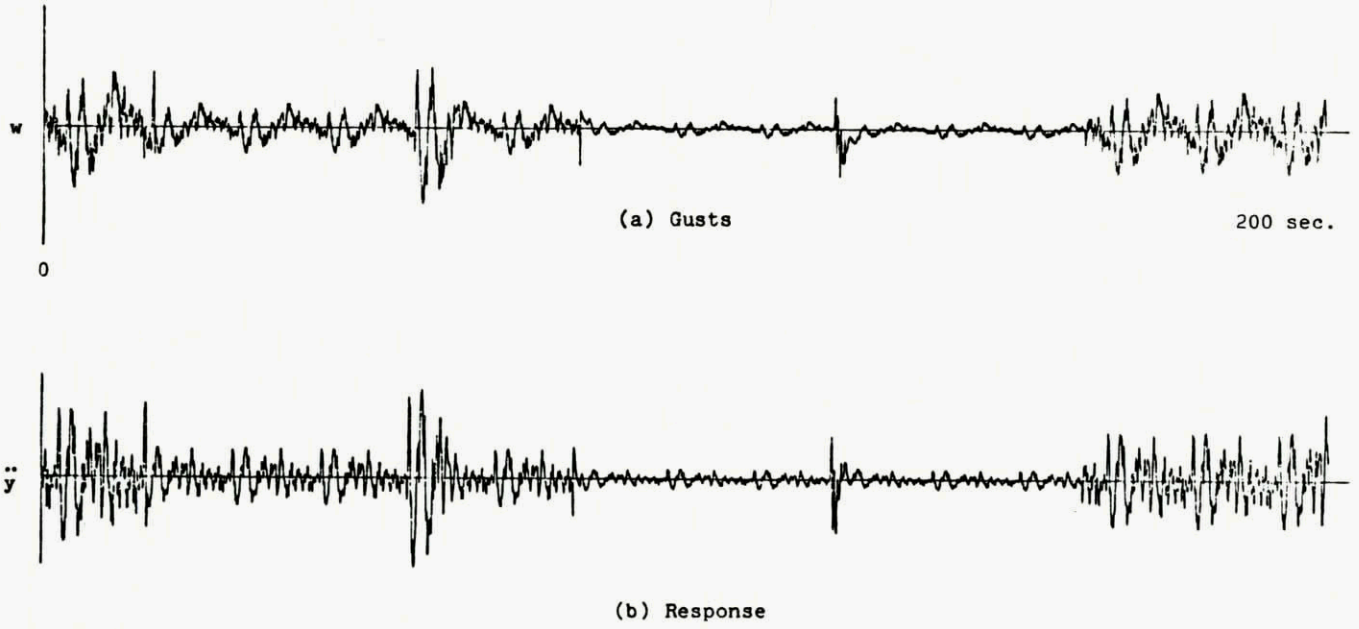

Figure 2.- Record portions illustrating the gusts and airplane response time histories.

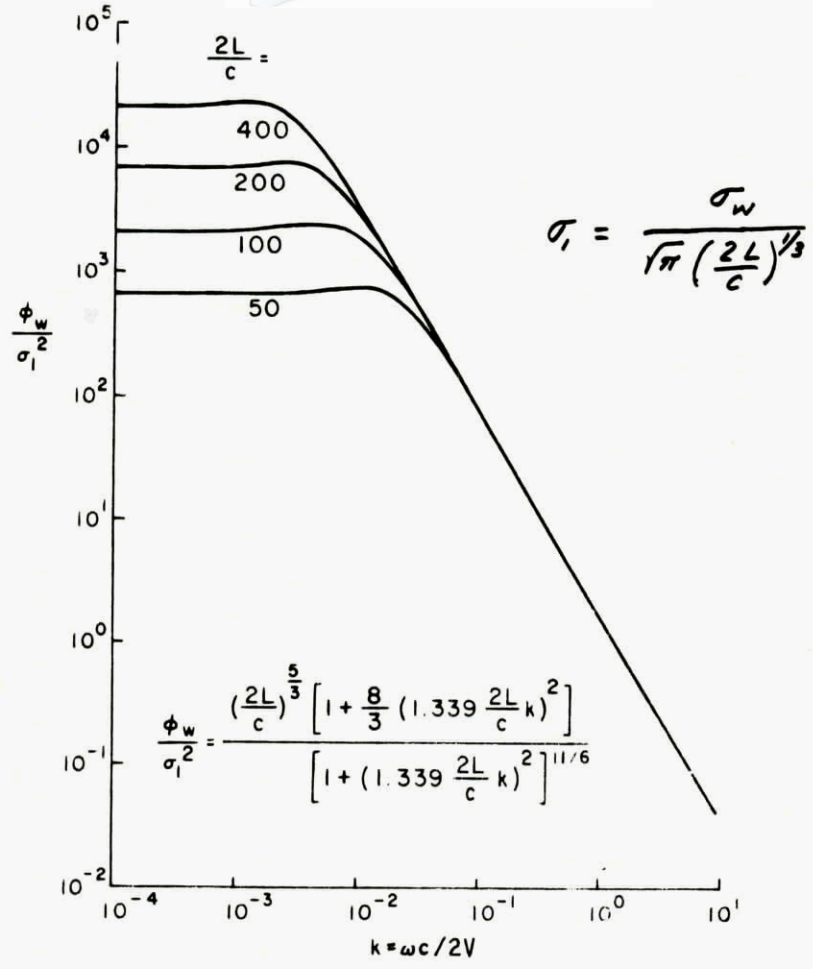

Figure 3.- Gust spectrum form used in analysis.

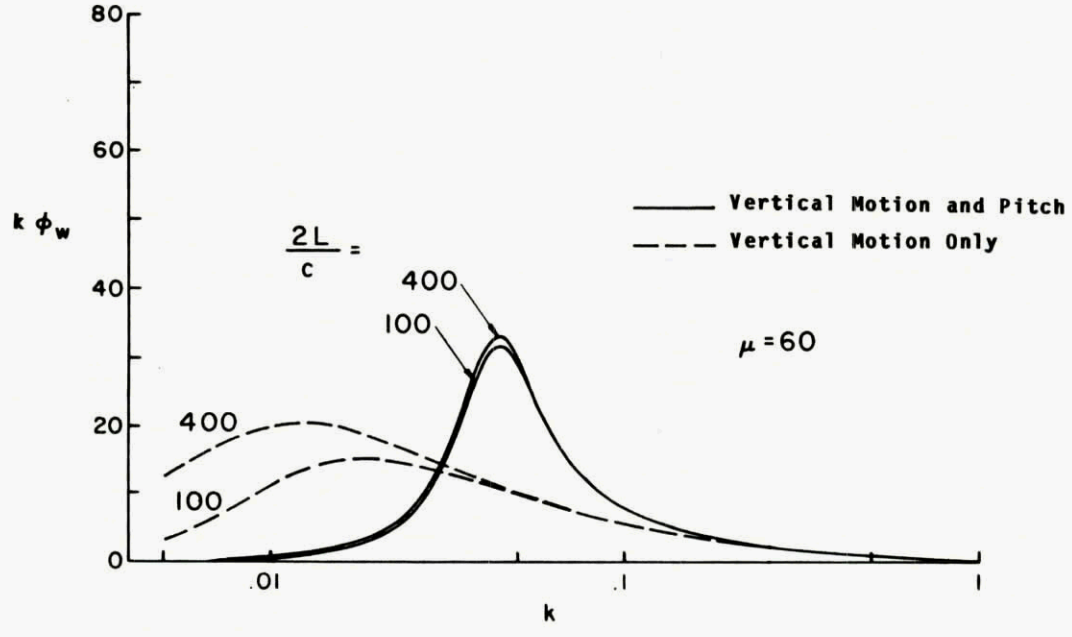

Figure 4.- Distribution of response power for one and two degrees of freedom.

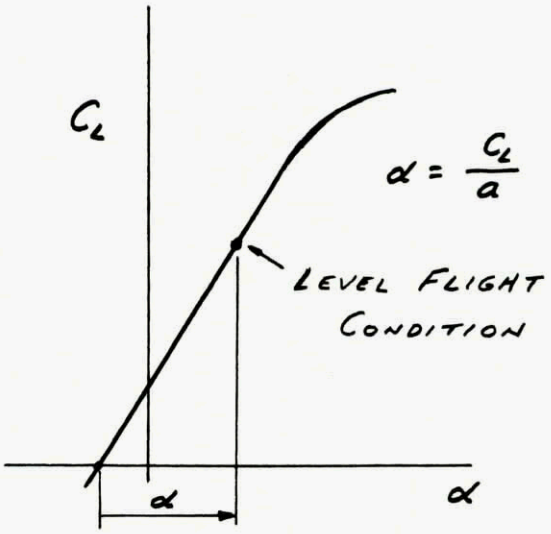

Figure 5.- Angle of attack used in gust loads equations.

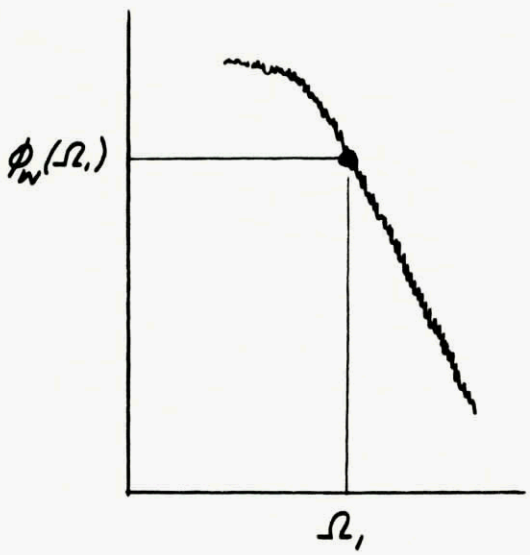

$$\frac{\sigma_w}{L^{1/3}} = \left[1.919\ \Omega_1^{5/3}\ \phi_w(\Omega_1)\right]^{1/2}$$

Figure 6.- The establishment of $\frac{\sigma_w}{L^{1/3}}$ from measured gust spectra.

A SUMMARY OF ATMOSPHERIC TURBULENCE MEASUREMENTS WITH SPECIALLY-EQUIPPED AIRCRAFT IN THE U.S.A.

By H. N. Murrow
NASA Langley Research Center
Hampton, Virginia 23665

ABSTRACT

This paper summarizes the technique of measurement of atmospheric turbulence in the form of true gust velocity. Specific aspects pointed out are related to NASA programs conducted over the last 15 years. Liberal use is made of references for details. Some recommendations resulting from a Spring 1986 workshop on atmospheric turbulence are also presented.

LIST OF SYMBOLS

ℓ	distance between inertial platform accelerometers and flow direction sensors
V_{ax}, V_{ay}, V_{az}	east-west, north-south, and vertical aircraft velocities
V	true airspeed
ΔV	airspeed increment from the mean value, referenced to beginning of data run
σ	rms value
Ψ	heading
α	angle-of-attack
β	angle-of-sideslip
θ	pitch attitude
ϕ	roll attitude
$\Delta\Psi$	heading increment from mean value for the run
$\overline{\quad}$	bar over a symbol indicates mean value for a data run
$\dot{}$	dot over a symbol indicates time derivative

INTRODUCTION

A number of flight investigations have been conducted to measure atmospheric turbulence. In many cases the aircraft itself is the sensor and values of "derived" gust velocity are provided using the relationship shown on the left hand portion of figure 1. Useful comparisons can be made of gust encounter statistics between different aircraft with a differentiating parameter that includes wing loading, lift-curve slope, and a gust alleviation factor. The actual air velocity fluctuations in the atmosphere, or true gust velocity, however, can be determined if a sensor with good frequency resonse characteristics, such as an angle-of-attack vane for the vertical gust velocity component, is mounted on a rigid boom a distance forward of the aircraft adequate to eliminate upwash effects, and if the aircraft motions can be accurately measured to provide corrections to the basic flow vane measurements. The equation on the right-hand side of figure 1 is an example, indicating that a time history of true gust velocity will result. The primary purpose of this paper is to describe various aspects of true gust velocity measurements made in recent years in the U.S. with emphasis on NASA programs. As an additional point of interest, some recommendations resulting from a workshop on atmospheric turbulence held at NASA-Langley in April 1986 are included.

AIRCRAFT AND PURPOSE OF MEASUREMENTS

The photograph in figure 2 is of an airplane (B-57B) that was specially instrumented by NASA to provide accurate true gust velocity measurements over a broad frequency range but with special emphasis on the low frequency or long wavelength region (refs. 1,2). Atmospheric turbulence power spectra are usually thought of as conforming to the von Karman expression where the intensity or standard deviation, σ, and an integral scale value, L, can be used to define a particular power spectrum. The L value locates the "knee" or break in the spectrum curve. Conventional aircraft principal responses to gusts occur at frequencies higher than the break, but for very large and

very fast flexible aircraft, significant responses would occur at very long wavelengths, or frequencies below the break (ref. 3). A major purpose of the program described in ref. 1 was to identify the spectral shape for atmospheric turbulence associated with various meteorological conditions and at altitudes between sea level and 50,000 ft. The same instrumentation system was also installed in the aircraft shown in the photograph of figure 3 to obtain data at altitudes up to 65,000 ft. Unfortunately, due to incompatibility of the nose boom arrangement with another experiment system with higher priority, only a small amount of data were obtained at the higher altitudes. Later, the airplane of fig. 2 was modified to include booms at the wing tips (shown in figure 4) to allow spanwise gradients of turbulence to be measured (wing span about 60 ft., ref. 4). Another NASA aircraft has been instrumented to measure atmospheric turbulence to support analysis of data from atmospheric constituent samplings. A photograph of the nose boom on this aircraft is given in figure 5.

Another highly instrumented NASA aircraft is shown in figure 6. The purpose of flights of this aircraft is to study hazards involved in flight operations in severe storms (ref. 5). The primary emphasis to to characterize lightning hazards. The instrumentation system provides atmospheric turbulence measurements (true gust velocity) and most flights have been made in a storm environment; however, up to this time the only turbulence data analysis performed has been for derived gust velocity values.

The National Center for Atmospheric Research (NCAR) has also instrumented several aircraft to acquire true gust velocity measurements (ref. 6); however, the flight samplings have been primarily in support of other atmospheric research experiments. Both fixed and free vanes have been utilized as the primary sensors. Some recent work at NCAR has centered on providing atmospheric turbulence measurements with a system of five pressure measurements on the surface of a special nose section on the aircraft (ref. 7). Efforts are underway at the present time to validate the system.

EQUATIONS, DATA, AND DATA PROCESSING

The equations utilized for determination of the three components of gust velocity are shown in figure 7. For the NASA aircraft, lightweight mass-balanced balsa vanes provide the primary measurement for the vertical and lateral components and a special sensitive pressure transducer yields the longitudinal component. As shown on the figure, the other terms provide corrections to the primary measurement for aircraft motion. Measurements for aircraft motion corrections come from rate gyros and an inertial platform. In general, values used are increments from the mean value for the run. Figures 8 and 9 list measurements (ref. 2) indicating ranges, allowable error (both amplitude and phase) for determination of gust velocity values within ± 1 fps for the ranges specified (nearly all flight measurements will be well within these ranges), and measured errors.

Flight data recording is as shown on figure 10. The principal measurements are provided as analog signals through onboard matched anti-aliasing filters. The low frequency signals from the inertial navigation system (INS) are digital signals and (for the spanwise gradient program) piezoelectric pressure transducers with digital signal outputs were utilized. All signals were played through a pulse code modulation conversion and recorded on a flight tape.

The post-flight data reduction shown on figure 11 involves first converting the flight tape to two tapes, one for the high frequency data channels at 200 samples per sec. and the other for the inertial navigation system data at 40 samples per sec. A wildpoint removal process and filtering of digital channels is performed and the resulting data are merged into an engineering units (EU) tape at 40 samples per sec. Gust velocity time histories are then derived according to the equations shown in figure 7 at 40 samples per sec. The resulting data tape (called SPANMAT for the case shown in the figure) can then be used for various statistical analyses. Power spectra can be provided to 20 Hz, however most data are not presented above 10 Hz.

Accuracy assessments are made according to the procedure given in ref. 8. Maneuvers are performed in smooth air, resulting in aircraft motions as large or larger than would be expected during data runs. Data are processed through the entire processing sequence with the final result being a time history of gust velocity which should be zero. The values obtained are an indication of adequacy of the correction procedure. Example cases are given in figures 12a-c. For the run in figure 12a the pilot performed large pitching maneuvers; the data of figure 12b are a result of large yawing motion and that of figure 12c for airspeed variations. The resulting gust velocities are satisfactory especially considering the magnitude of the aircraft motions.

As stated previously, the principal goal of the earlier sampling program with the B-57B was to provide estimates of the integral scale value, L, in the von Karman model. For this objective, the region of intrest in the power spectra was at the low values of frequency or inverse wavelength. For spanwise gradient studies, however, the values at the large inverse wavelengths (near the Nyquist frequency) are important (ref. 9). For the long wavelength emphasis, power estimates are desired at small frequency increments (Δf) in order to obtain estimates at very long wavelengths, however, to minimize scatter between individual power estimates, the statistical degrees of freedom (a linear

function of both f and record length) should be as large as possible, thus the two requirements are in conflict. Long records are always desired, however.

It is important to point out that due to a tuned frequency of the platform in inertial navigation systems, aircraft velocity measurements will oscillate at the so-called "Schuler" frequency (ref. 10) i.e. 84-minute period. This is relatively unimportant for turbulence measurements where measurements are deviations from the mean and runs are of 10 minutes or less, however, for wind or wind shear measurements where the total velocity measurements are used, the amplitude of the Schuler oscillation can lead to erroneous results. Figure 14 (from ref. 10) shows variations in peak velocity error measured after flights of from 1 - 6 hours duration. The amplitude of the oscillation is variable, but erroneous velocity indications of 3 meters/sec are common.

The sampling program with the B-57B aircraft has been terminated. Tapes containing three components of gust velocity associated with various meteorological phenomena are on file and are summarized in figure 15. Statistical degrees of freedom greater than 20 are desired. It should be pointed out that significantly larger values are obtained for horizontal gust velocity components. This is believed to be due to the fact that at the long wavelengths measured in this program, general wind patterns are detected, and, as seen in the power spectra presented in ref. 11, the power at long wavelengths does not conform to the von Karman model. These data are available for various statistical analyses. To date, some tapes have been provided in cooperation with the RAE (U.K.) and NLR (Netherlands).

RESULTS FROM ATMOSPHERIC TURBULENCE WORKSHOP

A workshop focused on various aspects of atmospheric turbulence related to aviation, rocket and space programs was held at the NASA Langley Research Center in April 1986. The proceedings are available (ref. 12). Attendees represented government, industry, and universities, and were expert in areas of measuring, modeling, predicting, and understanding processes of atmospheric turbulence. From the measurement standpoint, the following recommendations were made:

1. A repository should be established for all atmospheric turbulence data.

2. The existing data base should be updated, expanded and evaluated.

3. Measurements should be obtained in the 60-100K ft. altitude region.

Additional recommendations considered pertinent here include:

1. A standard, simple, quantitative, automated turbulence encounter reporting procedure should be established world-wide.

2. A systematic information/education program should be developed utilizing circulars and manuals.

3. Design procedures/criteria should be critically reviewed in regard to available data, analysis capabilities, design trends, and for vehicles such as helicopters.

4. A summary document should be established describing the various existing and proposed turbulence models and their applications.

CONCLUDING REMARKS

Flights of aircraft instrumented to measure true gust velocity time histories, and focused on atmospheric turbulence research, are essentially non-existent in the U.S. at the present time. The B-57B aircraft has been deactivated. Other aircraft with this capability are utilized primarily to support other programs. Requirements and procedures for acquiring detailed measurements were described. Existing data are on file and available for special analyses, however. Results of a workshop held in 1986 provided recommendations for future efforts.

REFERENCES

1. Murrow, Harold N.; and Rhyne, Richard H.: The MAT Project - Atmospheric Turbulence Measurements With Emphasis on Long Wavelengths. Proceedings of the Sixth Conference on Aerospace and Aeronautical Meteorology of the American Meteorological Society, Nov. 1974, pp. 313-316.

2. Meissner, Charles W., Jr.: A Flight Instrumentation System for Atmospheric Turbulence Data. NASA TN D-8314, 1976.

3. Rhyne, Richard H.; Murrow, Harold N.; and Sidwell, Kenneth: Atmospheric Turbulence Power Spectral Measurements to Long Wavelengths for Several Meteorological Conditions. Aircraft Safety and Operating Problems, NASA SP-416, 1976, pp. 271-286.

4. Camp, D.; Campbell, W.; Frost, W.; Murrow, H.; and Painter, W.: NASA's B-57B Gust Gradient Program. AIAA Journal of Aircraft, Vol. 21, No. 3, March 1984, pp. 175-182.

5. Deal, Perry L.; Keyser, Gerald L.; Fisher, Bruce D.; and Crabill, Norman L.: Thunderstorm Hazards Flight Research - Program Overview. AIAA-81-2412, Nov. 1981.

6. Lenschow, D. H.; Cullian, C. A.; Friesen, R. B.; and Brown, E. N.: The Status of Air Motion Measurements on NCAR aircraft. Preprints Fourth Symposium on Meteorological Observations and Instrumentation. American Meteorological Society, Denver, CO, pp. 433-438, 1978.

7. Brown, E. N.; Friehe, C. A.; and Lenschow, D. H.: The Use of Pressure Fluctuations on the Nose of an Aircraft for Measuring Air Motion. AMS Journal of Climate and Applied Meteorology, Vol. 22, No. 1, Jan. 1983, pp. 171-180.

8. Rhyne, Richard H.: Flight Assessment of an Atmospheric Turbulence Measurement System With Emphasis on Long Wavelengths. NASA TN D-8315, 1976.

9. Houbolt, John C.; and Sen, Asim: Cross-Spectral Functions Based on von Karman's Spectral Equation. NASA CR-2011, 1972.

10. Rhyne, Richard H.: Accuracy of Aircraft Velocities Obtained from Inertial Navigation Systems for Application to Airborne Wind Measurements. NASA TM 81826, 1980.

11. Murrow, Harold N.; McCain, William E.; and Rhyne, Richard H.: Power Spectral Measurements of Clear-Air Turbulence to Long Wavelengths for Altitudes Up to 14000 Meters. NASA TP-1979, 1982.

12. Anon (Edited by D. W. Camp and W. Frost): Proceedings of the Workshop on Atmospheric Turbulence Relative to Aviation, Missile, and Space Programs. NASA CP 2468, 1987.

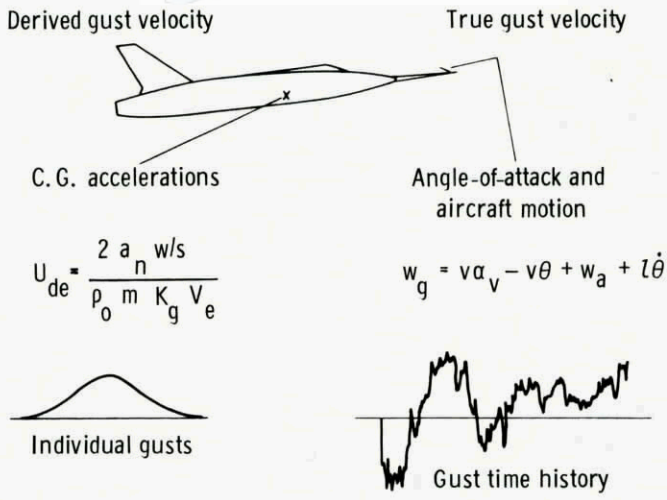

Figure 1 - Comparison of Derived and True Gust Velocity

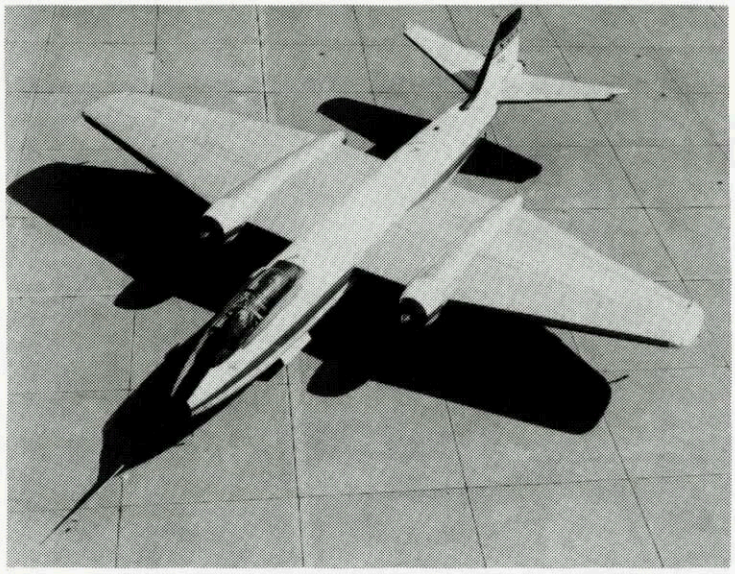

Figure 2 - B-57B Atmospheric Turbulence Sampling Airplane

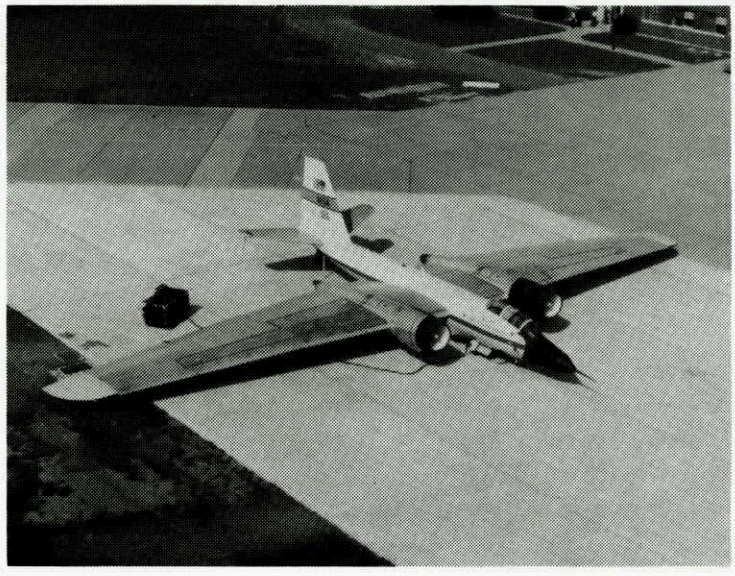

Figure 3 - System Installation on NASA B-57F Aircraft

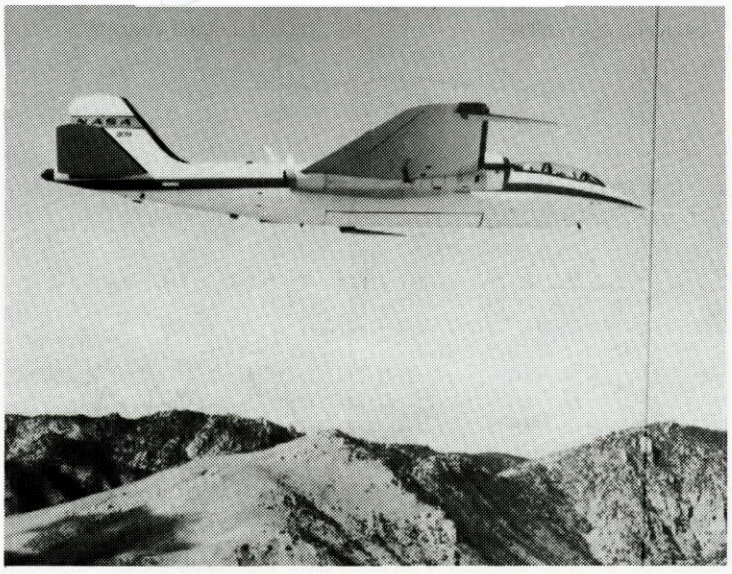

Figure 4 - B-57B Equipped to acquire Spanwise Gradient Data

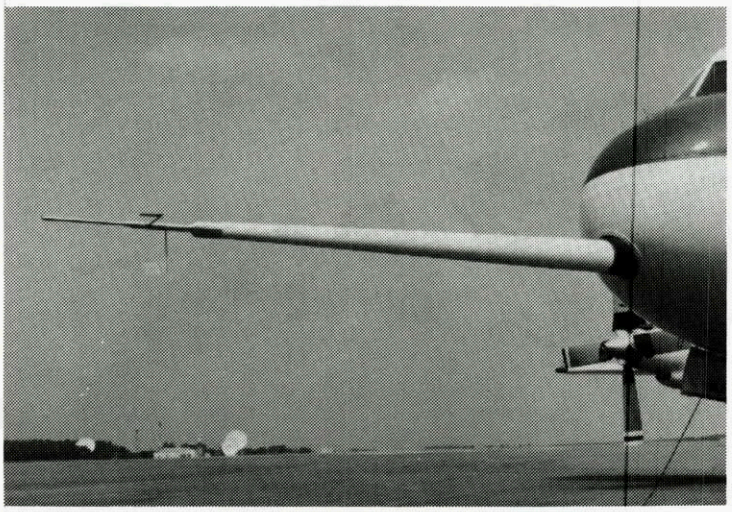

Figure 5 - Nose boom on NASA Electra Aircraft

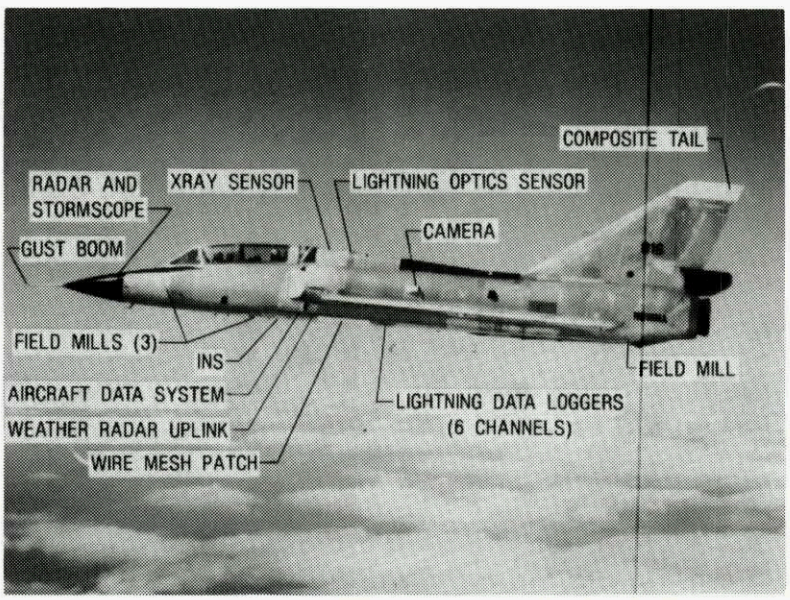

Figure 6 - Location of research sensors and equipment on the NASA F-106B aircraft

$$\text{Gust velocity component} = \left[\text{Primary measurement}\right] + \left[\text{Aircraft motion corrections}\right]$$

Longitudinal

$$u_g = [\Delta V] + \left[v_{ax} \sin \bar{\psi} + v_{ay} \cos \bar{\psi}\right]$$

Lateral

$$v_g = [V\beta] + \left[-V\Delta\psi + v_{ax} \cos \bar{\psi} - v_{ay} \sin \bar{\psi} + l\dot{\psi} + V\alpha\phi\right]$$

Vertical

$$w_g = [V\alpha] + \left[-V\theta + v_{az} + l\dot{\theta} - V\beta\phi\right]$$

Figure 7 - Equations for the determination of gust velocity component time histories

Measurement	Range	Overall system allowable error (1σ)	Measured system error @ 25°C
α, Balsa angle-of-attack flow vane	± 7.5°	.09° relative	.03 (.1)
β, Balsa angle-of-sideslip flow vane	± 7.5°	.09° relative	.03 (.1)
$\dot{\theta}$, pitch rate	± 1 R/sec	.012 R/sec	.01
$\dot{\psi}$, yaw rate	± 1/2 R/sec	.006 R/sec	.005
$\dot{\phi}$, roll rate	± 1 R/sec	.012 R/sec	.008
τ, free air temp (Total temp)	± 50°C	.555°C	.3°C
q_c, impact pressure	0-5 PSID	.03 PSI	.013
P_s, static pressure	0-15 PSIA	.1 PSI	.04
ΔP_s, incremental static pressure	± .25 PSID ± .1 PSID	.003 PSI	.0007 .0003
ΔP_T, incremental total pressure	± .25 PSID ± .1 PSID	.003 PSI	.0007 .0003
A_N, acceleration	± 1 G	.02 G	.008
time	0-365 days	.001 sec	

Figure 8 - Measurements list for MAT aircraft (B-57B)

Airborne inertial data system (AIDS)

Measurement	Range	Overall system allowable error (1σ)	Measured system error @ 25°C
A_X	1 G to -1 G	.006 G	.005
A_Y	1 G to -1 G	.006 G	.005
A_Z	3 G to -3 G	.018 G	.013
V_{AX}	± 100 FPS	.6 FPS	.4
V_{AY}	± 100 FPS	.6 FPS	.4
V_{AZ}	± 100 FPS	.6 FPS	.4
Φ	20 to 5°	.16°	.08
	5 to -5°	.12°	.04
	-5 to -20°	.16°	.08
θ	7.5 to 4°	.1°	.03
	4 to -4°	.08°	.03
	-4 to -7.5°	.1°	.03

Figure 8b - Measurements list continued (airborne inertial data system)

Measurement	Range	Overall system allowable error (1σ)	Measured system error @ 25°C
$\Delta\psi$	7.5	.08°	.09°
V_X	2000 FPS	15 FPS	6 FPS
V_Y	2000 FPS	15 FPS	6 FPS
ψ	0-360°	.5°	.7°

Figure 8c - Measurements list continued (airborne inertial data system)

Measurement	Full-scale range	Allowable phase error, degrees	Measured relative phase @ 1 Hz, degrees
θ	± 7.5°	± 1.5	-.75
$\Delta\psi$	± 7.5°	± 1.5	-.75
α and β	± 7.5°	± 1.7	.25
Φ	± 20°	± .92	-.75
$\dot{\theta}, \dot{\Phi}$	± 1 rad/sec	± 1.4	-1.5
$\dot{\psi}$	± .5 rad/sec	± 1.4	-1.5
A_X, A_Y	± 1 G	± .7	-1.25
A_Z	± 3 G	± .7	-1.25
V_{AX}, V_{AY}, V_{AZ}	± 100 FPS	± 1.4	-1.25
A_N	± 1 G	± 1.7	+1.1
ψ	- 0-360°	± 1.5	-.75
ΔP_{Total} Hi	± .25	± 1.7	
Lo	± .1	± 1.7	

Figure 9 - Measurements list concluded (phase matching)

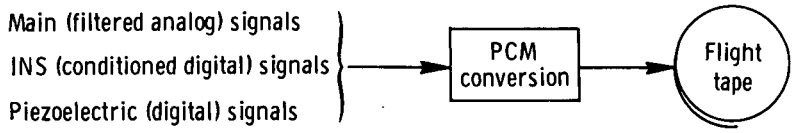

Figure 10 - Flight data recording

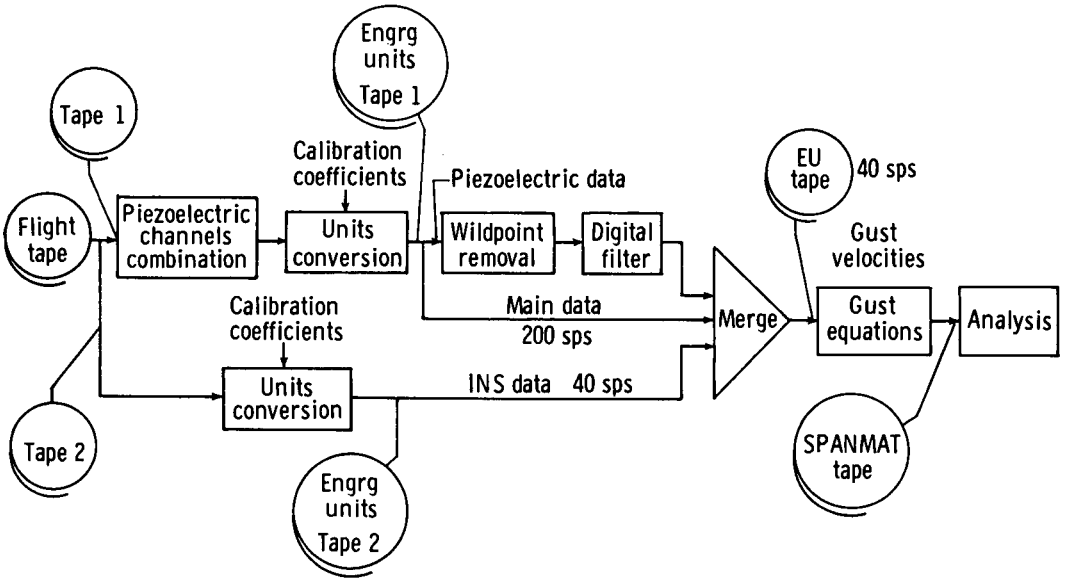

Figure 11 - Post-flight data reduction schematic

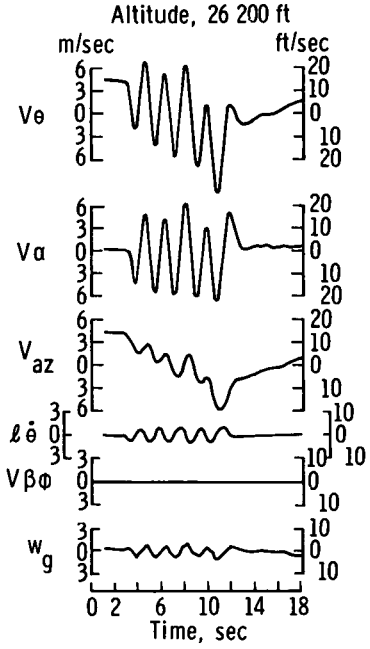

Figure 12 - Accuracy assessment with flight data

(a) vertical component

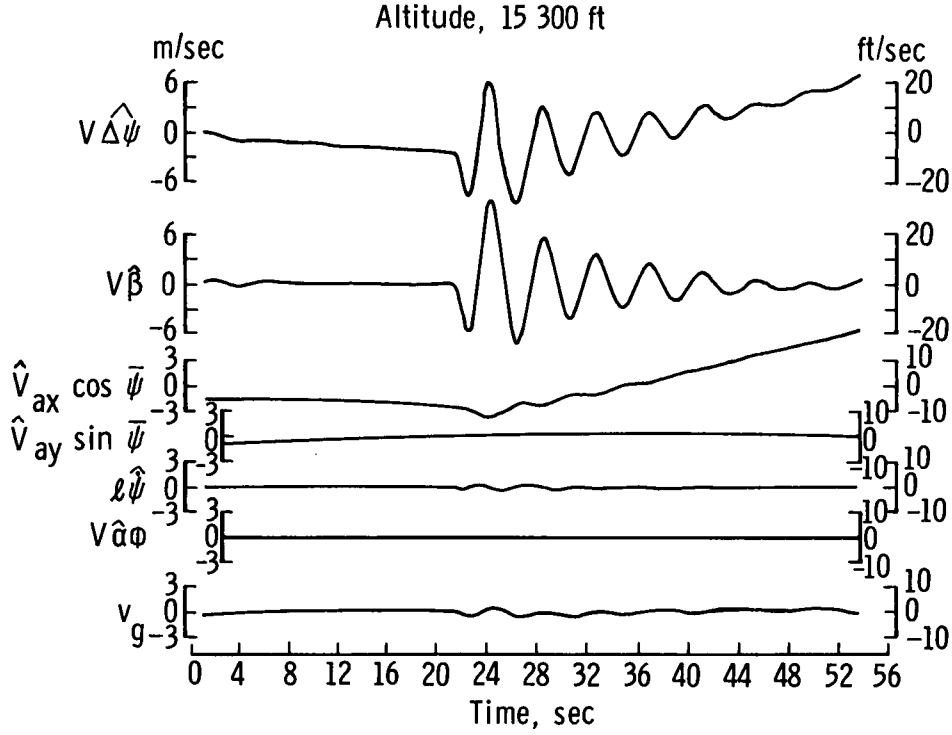

Figure 12 - Accuracy assessment continued

(b) lateral component

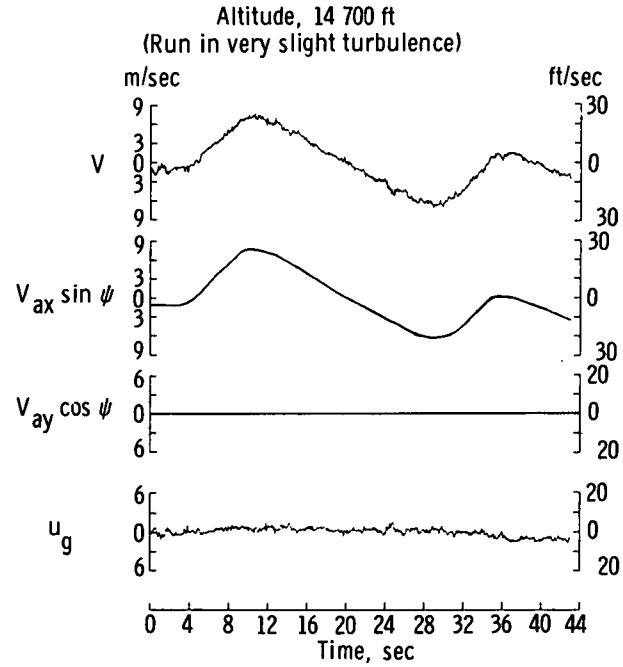

Figure 12 - Accuracy assessment concluded

(c) longitudinal component (run made in slight turbulence)

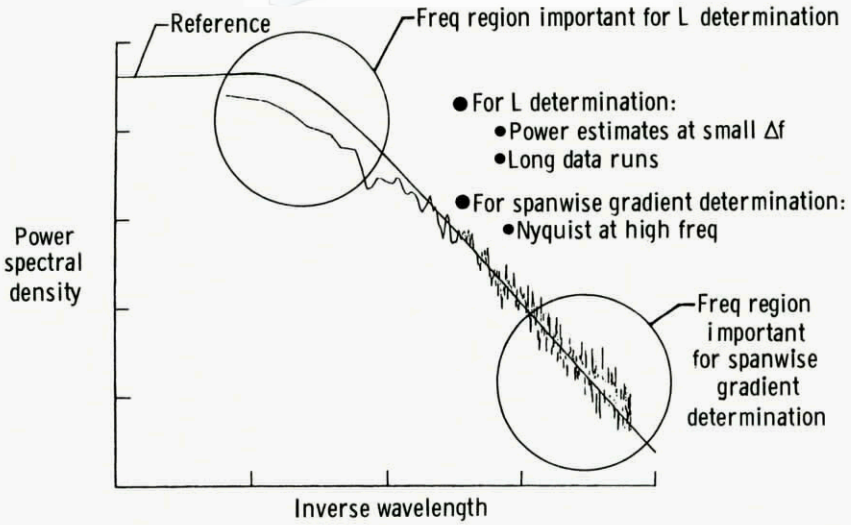

Figure 13 - Regions of Emphasis in Power Spectra

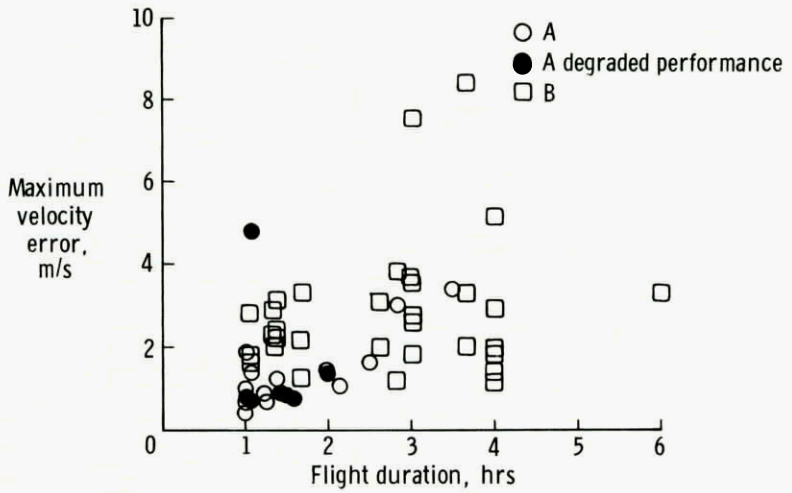

Figure 14 - Measured Schuler oscillation data on ramp after flight

Altitude (ft)	No. runs	Statistical D. O. F.	σ_w (ft/sec)	σ_v (ft/sec)
		Mountain wave/orographic (3 flts)		
~4-6K	9	13 - 40	4.6 - 7.3	4.7 - 21
9-15K	9	10 - 23	3.2 - 12.5	7.8 - 23
23-46K	3	21 - 40	3.5 - 4.4	6.3 - 17.7
		Wind-shear/jet stream (4 flts)		
19 - 35K	8	10 - 31	1.5 - 2.9	3.3 - 17
		(1 flt) Low-altitude convection (1 flt)		
1.5K	1	45	3.8	3.9
		Convection, sea-breeze convergence (flt)		
5.5 - 14.5K	6	11 - 21	4.6 - 7.8	7.2 - 10.3
		Complex effects (1 flt)		
42K	4	14 - 28	5 - 8	15.5 - 28.7

Figure 15 - Measured gust velocity time histories available

MEASUREMENT AND ANALYSIS OF LOW ALTITUDE ATMOSPHERIC TURBULENCE OBTAINED USING A SPECIALLY INSTRUMENTED GNAT AIRCRAFT

by

Dr G.W. Foster and J.G. Jones
Procurement Executive, Ministry of Defence
FS(B)1 Division, Royal Aircraft Establishment
Bedford MK41 6AE, England

AGARD SMP Workshop, Athens, September 1986

SUMMARY

Detailed measurements of atmospheric turbulence made by a specially instrumented Gnat aircraft at altitudes below one thousand feet over a variety of terrains are described. A programme of flying yielded about 400 runs for which time histories of the three components of turbulence are available. These runs are analysed to give parameters which summarise the statistical characteristics of the turbulence encountered. A very strong relationship between two parameters from the Statistical Discrete Gust analysis technique and one from the Power Spectral Density technique is identified.

LIST OF SYMBOLS

a	parameter defining overall rate of occurrence of ramps (or more accurately smooth increments), see Eq.(A-1)
A	intercept of straight line in PSD graph with 1 cycle per metre axis, see Eq.(2)
b	intensity parameter defining amplitude distribution of ramps (smooth increments), see Eq.(A-1)
F	gain of filter is 1/F, see Eq.(A-2)
H	length of ramp (smooth increments), see Fig 25
h	height
k	scaling parameter defining relative intensity of ramps (smooth increments) of differing lengths, see Eq.(A-1)
L	scale length of turbulence
L_{std}	standard scale length (2500 ft, 762 m) used in calculation of $\bar{\sigma}$, see Eqs.(7) and (9)
$n(S, x)$	density (when differencing over distance S) of rate of occurrence of peaks and troughs with size greater than x
$N'(H, w)$	density (at ramp length H) of rate of occurrence of ramps with amplitude greater than w
s	local slope of PSD curve (see Appendix)
S	differencing distance
t	time
u, u_g	component of velocity along aircraft body fixed x axis, component of turbulence velocity in that direction; positive forward
V_T	true airspeed
v, v_g	component of velocity along aircraft body fixed y axis, component of turbulence velocity in that direction; positive to starboard
w	amplitude of ramp (smooth increment), see Fig 25
w, w_g	component of velocity along aircraft body fixed z axis, component of turbulence velocity in that direction; positive downwards
x	size of peak or trough
x	aircraft body fixed axis, positive forward
y	aircraft body fixed axis, positive to starboard
z	aircraft body fixed axis, positive downwards
α	angle of attack
α	parameter defining overall rate of occurrence of peaks and troughs, see Eq.(A-2)
β	angle of sideslip or more accurately, as the tangent definitions of incidence angles are being used, flank angle attack, Ref 23
β	intensity parameter defining amplitude distribution of peaks and troughs, see Eq.(A-2)
Δt	sampling interval
κ	wave number that is cycles per unit distance
λ	width of filter is S/λ, see Eq.(A-2)
σ	standard deviation particularly of turbulence speed
$\bar{\sigma}$	estimate of turbulence intensity, see Eqs.(6) and (8)

σ_{diff} one standard deviation of the smoothed differenced signal sity, see Eqs.(6) and (8)

Φ power spectral density

1 INTRODUCTION

Between July 1981 and April 1983 Gnat XP 505* (Fig 1) undertook a flying programme to collect samples of measurements of atmospheric turbulence particularly at low altitude using special instrumentation installed for the task, Ref 1. Being a highly manoeuvrable fast jet, the Gnat was able to undertake flight profiles closely akin to operational strike aircraft over all types of terrain. The aim of the programme was to sample the turbulence encountered in a range of atmospheric conditions over various types of terrain and at a number of heights. It was not intended to gather statistics for the turbulence encountered during all flying of the Gnat. The resulting samples were analysed using both spectral and statistical discrete gust techniques with the intention of improving the turbulence models that are used in areas such as control system design and generation of synthetic turbulence. A subject of particular concern was the accurate modelling of the rates of occurrence and form of extreme gusts.

An RAE Report (Ref 2) has been published which presents a few examples of the turbulence measurements made by Gnat XP 505 and introduces the data reduction methods, including the types of statistical analysis, being applied to the flight recordings. A further Report (Ref 3) will soon be available giving details of the analysis of a large number of samples of the turbulence data. The present paper summarises some of the results.

2 FLIGHT PROGRAMME

A total of 389 turbulence sampling runs have been completely analysed. Fig 2 shows the approximate geographic locations within Britain of these runs together with an indication of the severity of turbulence $\overline{\sigma_v}$ (see below) encountered during each run. Note that the points in Fig 2 have been shifted slightly when necessary to avoid points overlaying one another.

Most of the sorties took place from RAE Bedford Airfield and there were a large number of flights in the Bedford local area. Flights over the Cotswolds, Severn/Wye valley area, and the mountains of South and Mid Wales gave a selection of terrains of increasing roughness. Two periods of flying from Kinloss in Scotland gave some runs over very rugged terrain and two such runs have been described in detail in Ref 2. Flights over the East Anglian Fens and the Suffolk coast gave examples of turbulence over smoother terrain, and to complete the picture there were some flights over the sea, mostly the North Sea off East Anglia. Each of the runs analysed was allotted a 'Terrain Roughness Rating' in the range 0 to 8, see Table 1.

In most cases the pilot made at least three runs along a particular straight track at radio altimeter heights of 250, 500 and 1000 ft (75, 150 and 300 m). Clearly, maintaining constant radio height over rough terrain was impossible and in these conditions these nominal heights tended to become minimum heights. The restriction to straight runs conflicted to some extent with the aim of sampling turbulence along realistic flight profiles for low level attack aircraft and so some runs were made with the aircraft manoeuvring to follow valleys and so forth. Unfortunately removing the effects of aircraft motion from the resulting flight data to give turbulence time histories without spurious gusts, a difficult task even for the wings-level runs (see below), proved unreliable for this type of flying and so it was not employed very much.

When possible runs at 100 ft radio height were made. However, the locations in which flying this low was permitted were very limited: the extreme North of Scotland, during the approach to RAE Bedford Airfield and over the sea. The pilots were understandably reluctant to operate this low over the sea due to the lack of visual height cues. Some runs at higher altitudes than 1000 ft were made, but finding turbulence here was more difficult.

As the total recording time was limited to 18 minutes the recorders were only switched on during runs. The pilot kept notes on the location and conditions of the various runs.

Because of the problems caused by getting water into the Conrad Yawmeter and miniature pitot pneumatic pipes which form part of the turbulence sensing system (see below), flying in rain was avoided. Water in these pipes would effect their dynamic response and could freeze so disabling the system completely. Data from flights where the pilot reported that rain had been penetrated was always reviewed carefully. Avoiding rain will of course have biased the meteorological conditions under which the data was gathered.

The data gathered during one particular flight, flight number 716, will be used as a representative example here. The pilot originally intended to perform runs in the

---

* Now on display in the Science Museum, London.

Brecon Beacons area of South Wales. However, as he saw there was rain over these mountains, he instead found a clear patch West of Birmingham and did four runs on a line running South from Bridgnorth, Fig 3. This flight path was across wind. Two of the runs recorded were heading North along sections of the ground track shown in Fig 3 and the other two heading South.

3 DATA CAPTURE AND HANDLING

3.1 Instrumentation

The instrumentation carried by Gnat XP 505 (Fig 4) is described in detail in Ref 1. The main air data sensors were pairs of Conrad Yawmeters and miniature pitot tubes on the extended nose probe of the aircraft, Fig 5. A Conrad Yawmeter consisted of two hypodermic steel tubes with angled ends, Fig 6. The pressure difference across each double tube was sensed and recorded. In addition to the Conrad Yawmeters on the nose probe, incidence and sideslip were also measured by wind vanes carried on the wing tip probes and the nose probe. Vanes with balsa wood blades were used as these give better frequency response than metal or carbon fibre vanes due to their low inertia, at the expense of being less robust.

An instrumentation pack occupied the rear cockpit and contained the MODAS digital tape recorder (Ref 4) used for data capture. This gave a 12 bit resolution, and the majority of instruments were recorded at 256 samples per second.

3.2 Data handling

Fig 7 summarises the flow of data during the post-flight analysis of an airborne recording. The first stage was to produce a computer compatible tape (known as REDUC tape) and 'quick look' pen plots of some of the instruments. Based on these plots and the pilot's reports, runs to be analysed were chosen. In general for the turbulence sampling programme these were picked to be representative sections between 60 and 90 sec long of the runs recorded by the pilot.

Program I11C, which is described in detail in Ref 1, was used to extract the chosen analysis runs from the REDUC tape and apply calibrations to yield time histories in engineering units for each instrument and derived quantity. These were stored on a Gnat data magnetic tape. Run names were assigned at this stage. In general the names used take the form Gnat 'Three digit flight number' 'two digit run number'.

The calibrations performed by program I11C included applying the results obtained from wind tunnel tests Ref 5 to get air flow directions and speed at the nose probe based on data from the Conrad Yawmeters and miniature pitot. I11C also de-skewed the sequential samples by using linear interpolation to synchronize the apparent sampling instant of the various instruments.

For flight 716 four analysis runs each of 90 sec duration were extracted from the flight recordings. These runs are named Gnat 71601,2,3 and 4. They are composed of the middle sections of each of the four runs recorded by the pilot. Fig 8 gives time history plots from some of the instruments for the first of these four runs. Note, in particular, the traces of barometric height and ground height (the latter is obtained by subtracting the radio altimeter reading from the former) which give an impression of the terrain crossed and the flight path taken over it. Time histories are also given in Fig 8 for the flow angles at the nose probe as measured both by the Conrad Yawmeters, labelled ALPHA(CY) and BETA(CY), and by the balsa vanes which are labelled ALPHA(NP) and BETA(NP). I11C does not correct for instrument dynamic characteristics and so pressure lags in pneumatic instruments have not been rectified at this stage.

3.3 Calculation of turbulence time histories

The next stage in the processing was to derive time histories of the atmospheric turbulence encountered during the analysis runs. This involved correcting for instrument dynamic behaviour and removing the effects of aircraft or, more accurately, sensor motion from the measurements of airflow speed and direction. We will here concentrate on the derivation of the three components of turbulence (u_g, v_g and w_g) using the airflow information from the pneumatic instruments at the nose probe (Conrad Yawmeters and miniature pitot). The use of data from the balsa wood wind vanes on the wing tip probes and on the nose probe, which give information about the spanwise variation of the turbulence, is discussed in Ref 6 and Ref 7.

3.3.1 Corrections for pneumatic pipe dynamics

The pressure transducers used by the Conrad Yawmeters and miniature pitot were situated in the nose bay of the aircraft and so there were pipe runs of 1.65 m between the pressure sensing orifices on the nose probe and these transducers. Between the inboard end of these pipes and the pressure transducers enclosed volumes (7.91 cc) were fitted to reduce the amount of 'organ-pipe' resonance; however, there was still a resonant peak between 16 and 18 Hz. Fig 9 shows the results of ground tests Ref 1 to investigate the frequency response of the pipes as installed in the airframe using oscillating pressure generators, and compares the measurements with predictions made using the theoretical method of Bergh and Tijdeman Ref 8. The agreement is excellent and so the theoretical method has been used to predict the behaviour in flight as shown in the figure.

Program TURB (see Fig 7) incorporates digital filters which attempt to correct the incidence and sideslip signals from the Conrad Yawmeters and the airspeed from the miniature pitot so as to remove the effects of this resonance. Fig 10 is an example of the frequency response of the Finite Impulse Response (FIR) digital filters used. This filter attenuates the signal around 17 Hz as required but introduces some amplification between 20 Hz and 55 Hz. Just beyond 20 Hz this is not unreasonable as the filter is correcting for the attenuation caused by the pipes in this region. In general though, introducing amplification at high frequencies is undesirable due to the effects it has on noise in the signal. Fortunately the combined effects of the pipes pneumatic attenuation beyond 20 Hz and the 25 Hz fourth order Butterworth analogue (electrical) antialiasing filters, which are applied to the signal before sampling in the aircraft's recording system, are together sufficient to remove completely any undesirable consequences from the amplification caused by these digital filters.

Based on the above mentioned theoretical method the dynamic behaviour of the pneumatic pipes was calculated for a range of pressures and temperatures covering the conditions which could be encountered in the pipes in flight. The characteristics of the digital filters used in program TURB were scheduled with the pressures and temperature at each instant in flight to match the expected behaviour of the pipes at the flight conditions.

3.3.2 Removal of sensor motion

To remove the component in the recorded airflow velocity which arises from the movement of the sensors in sympathy with the airframe so leaving just the motion of the air (the turbulence), the velocity of the airflow sensors at each instant in time during a run has to be obtained. This was achieved by integrating the recordings from inertial sensors, ie linear accelerometers and angular rate gyros. Such instruments were not mounted near the airflow sensors on the nose probe of the Gnat (though they were present at the ends of the wing tip probes) and so it was necessary to use the instruments mounted in the rear cockpit and assume the airframe and nose probe formed a rigid body between the instrumentation pack and the airflow sensors. If this assumption is not valid one would expect particular problems at frequencies corresponding to the natural modes of the airframe and nose probe. Ground resonance testing of an early version of the Gnat Ref 9 gave (with full underwing fuel tanks) a first wing symmetric bending mode at 9.1 Hz, asymmetric wing bending at 15.9 Hz and fuselage bending at 29.0 Hz. The nose probe fitted to Gnat XP 505 has a natural frequency of 31.4 Hz both laterally and normally. Only the first two of these are within the frequency range observable by the Conrad Yawmeters Fig 9 and no contamination at these frequencies has been seen in the turbulence power spectral densities produced (see below for some examples). Of course quasi-static distortion at lower frequencies may occur but the success achieved in removing contamination at the dutch roll and short period frequencies tends to indicate that this was not a problem.

The integration of kinematic equations which is part of the process of removing sensor motion tends to be very sensitive to zero offsets in the instruments; for example a zero offset in a lateral accelerometer will, when integrated, produce an increasing side velocity which, if uncorrected, would contaminate the estimated side gusts. Therefore, prior to using program TURB, an Instrument Compatibility Check (ICC) program developed at the RAE by Reid Ref 10 was applied to the available instrument time histories so as to estimate these zero offsets for each run. This ICC program also proved useful in analysing a series of manoeuvres in calm air to identify position error corrections for the instrumentation system, particularly upwash and sidewash correction factors.

Since the ICC program produces time histories for α, β and V_t based on the inertial instruments the difference between these and the observations will be the turbulence. However, it was found preferable to recompute the turbulence in the separate program, TURB, for several reasons. A major one was to allow the ICC program to work with only a very much thinned (but adequate) version of the time histories (usually eight samples per sec), so reducing the amount of storage and computation it required, while TURB could handle the data at the full sampling rate of the airflow sensors and so produce time histories of the three components of turbulence at 256 samples per sec. The ICC program passes values for initial conditions and zero offsets to TURB as shown in Fig 7.

It should be noted that the three components of turbulence produced by TURB are still with respect to an aircraft body axis system (head, side and normal). They are not components in earth axes (North, East and vertical), nor are they along-heading, across-heading and vertical which is an example of another possible set. It would be possible to resolve into either of the latter two systems using the pitch attitude and bank angle recordings and (for earth axes) the heading recording. However, the aim of the turbulence investigation programme was to gather data on the turbulence and gusts which are encountered, and have an influence upon, aircraft flying at low altitude. It thus seems preferable to produce turbulence records which allow such information to be extracted directly. Transforming into either of the other axes systems mentioned above might be extremely useful when, for example, carrying out comparisons with ground features but would not yield information which was directly useful in aircraft, as opposed to meteorological, studies. In practice the restriction to straight runs mentioned earlier, the fairly small pitch attitudes reached in the turbulence measuring runs and the pilot's efforts to keep the wings level mean that the normal component is very nearly the same as vertical component. The convention that in aircraft body axes z is downwards means that positive values of w_g correspond to DOWN gusts.

For dissemination to other users and long term storage, the time histories of the three components of turbulence produced by TURB were transferred to Gnat TURB magnetic tapes (Fig 7).

3.3.3 Assessment of extracted turbulence

Fig 11 shows the turbulence time histories for the first run in flight 716. The three components are labelled:

NP MP UG for Nose Probe, Miniature Pitot, based U component of Gust,

NP CY VG for Nose Probe, Conrad Yawmeter, based V component of Gust, and

NP CY WG for Nose Probe, Conrad Yawmeter, based W component of Gust.

To bring out the detail available more clearly Fig 12 shows the first second of the three components of Gnat 71601 with each individual sample plotted. The smoothing caused by the antialiasing filters and the pipes is apparent.

Fig 13 presents the power spectral densities of the turbulence components for the first two runs from flight 716 and compares them with the power spectra of the fine airspeed, β and α. The angles from the Conrad Yawmeters for β and α have been multiplied by the mean speed of the aircraft during a run so as to convert them to the same units, metres per sec, as the turbulence components v_g and w_g from program TURB with which they are being compared. The power spectra are plotted on log-log axes; the horizontal axes have the units Hertz (ie cycles per sec) and the vertical axes (m $s^{-1})2/Hz$. For turbulence which matches the von Karman model the power spectra should be flat at low frequencies, changing to a slope of -5/3 at higher frequencies. A straight line with slope -5/3 has thus been fitted to the turbulence spectra between 1 Hz and 10 Hz in each plot. In all cases the turbulence spectra follow this line upto almost 25 Hz at which point the antialiasing and pneumatic filters cause a sudden rapid attenuation of the signals, an effect already remarked upon in the time histories above. The removal of aircraft motion is apparent by comparing the v_g and w_g spectra at frequencies below 2 Hz with the corresponding untreated instrument spectra. Of particular note is the peak in β at the dutch roll frequency of the aircraft, 0.6 Hz, which has been completely removed from v_g.

The success achieved in correcting for the amplification caused by the pipe resonances between 10 Hz and 20 Hz can also be judged from the plots in Fig 13. For the u_g and v_g components this has, in all cases, been most satisfactorily done. However, in run Gnat 71602 the w_g component of turbulence still shows a slight 'hump' above the -5/3 straight line. It would appear that the size of the resonance in the α Conrad Yawmeter pipes in these two runs was greater than that predicted by the theoretical method. It will later become apparent that this affected many, though not all, of the w_g records to some extent. No explanation for this anomaly has been found.

In the v_g and w_g plots the introduction within TURB of the upwash correction factors means the turbulence power spectra fall somewhat below those derived directly from β and α even in those parts of the frequency range where neither sensor motion nor pipe dynamics contaminates the raw flow angles. It should be noted that the sidewash and correction factors have been assumed to be independent of frequency and the values identified at low frequency (around the aircraft's rigid body modes) have been taken as constants.

To allow a high resolution pressure transducer to be used on the miniature pitot pipe, a transducer with a limited range compares the miniature pitot pressure against the pressure in an enclosed volume. If the transducer approaches it limits, for example due to a large change in aircraft speed or height, then a valve between the miniature pitot pipe and the enclosed volume opens to equalise the pressure on either side of the transducer. For more details of this device see Ref 1. During the 5 to 6 second periods when this valve is open it has been necessary to make use of the coarse airspeed derived from the aircraft pitot system rather than the higher resolution and higher bandwidth signal from the miniature pitot system. Program I11C therefore inserts the coarse airspeed into the fine airspeed time history during periods when the valve is open.

In some records problems were encountered in ensuring the continuity of the resulting fine airspeed time history at the points where the valve opened or closed. Several improvements were made to the algorithm used by I11C to carry out this insertion so as to avoid the resulting spurious steps in fine airspeed, but the problem was most persistent and still afflicts some of the u_g traces.

3.4 Statistical analysis of turbulence time histories

3.4.1 Introduction to techniques

Two types of time series analysis have been applied to the time histories of turbulence produced by the Gnat.

The more familiar of these, Power Spectral Density (PSD) analysis, has already been used above. In essence, it involves considering the power in a signal in a series of (usually quite narrow) frequency bands; thus, conceptually one is investigating how the signal is composed of sinusoidal waves. The variation of the power spectral density Φ

with frequency or wave number κ (the inverse of wave length)* may be compared with theoretically derived spectra such as those proposed by von Karman (Ref 11) or Dryden (Ref 12). Parameters which characterise a sample of turbulence in these models may be identified. Fig 14 illustrates the spectral densities given by these two models for the across path components of turbulence (v_g and w_g) for two values of L, the scale length, which is a parameter that appears in both models.

PSD analysis is a well established tool for analysing atmospheric turbulence, and techniques for using the resulting information, for example in the aircraft design process, are widely employed. Its limitations are, however, often not appreciated and two of these deserve comment. First, the power spectra gives no information on the probability distribution of the signal or changes in the signal. Often, in applications where probability distributions are needed, the simple (but questionable) assumption is made that they are Gaussian (Normal) in form. Second, PSD analysis gives no information about the rate of occurrence or shape of discrete events in a signal whereas the occurrence of large discrete events is often critical in aircraft or control system design.

To complement the PSD technique, Jones (Ref 13, Ref 14 and Ref 15) has advocated a Statistical Discrete Gust (SDG) method which does give information about the statistical properties of changes and rates of change of signals. It is probably worth noting here that it is the distribution of changes in turbulence velocities rather than of absolute velocities which are of most importance to an aircraft. A brief introduction to SDG techniques is given in the Appendix.

3.4.2 Implementation of techniques

Program I11W (Ref 16) was the main tool used to carry out these types of analysis, Fig 7. A standard way of processing turbulence runs was chosen and implemented by two I11W USE-files (Ref 16). The first of these, I11WTURB (see Table 2a) configures I11W to read the files of observation data produced by program TURB and sets various items that are not to be left at their default values. In particular it should be noted that, for the calculation of the power spectral density by means of a Fast Fourier Transform technique, the data was split into blocks 4 sec long. Each block overlaps its neighbours by 50% and the linear trend was removed from each block (by subtracting the best least squares fit straight line from each block), but no window, such as Hanning (Ref 17), was used. The second USE-file, I11WRUN (see Table 2b), carried out the analysis of the three components of a turbulence run. Comments in these tables explain much of the details of the analyses being performed.

The output from I11W consists of three streams:

1 A line-printer type of listing (the 'main output file') giving a detailed account of the data read, analyses performed and results produced. Any errors which occurred are also noted here.

2 Graphs produced within I11WRUN by the PLOT THREE instruction of I11W. These summary plots contain information pertinent to both SDG and PSD analyses.

3 Parameters identified by fitting statistical models which are appended to three files: FITTABLES(/UG), FITTABLES(/VG) and FITTABLES(/WG). These files eventually contain the parameters for all 389 runs analysed.

Fig 15 presents the plot produced for one component of the first run from flight 716. The plot is composed of three graphs which illustrate different aspects of the analysis performed.

In the lower right corner is a power spectral density graph. The horizontal axis is wave number which has units cycles per metre while the vertical axis (which is labelled simply POWER), is power spectral density with units $(\text{metres/sec})^2$ per (cycle per metre). Log-log axes are again employed. The definition of power spectral density adopted in this paper is such that

$$\sigma^2 = \int_0^\infty \Phi(\kappa)\, d\kappa \qquad (1)$$

where σ is the standard deviation of the signal. The limits of integration, zero to plus infinity, not minus infinity to plus infinity, should be noted. The power spectral density estimates from the FFT algorithm are shown connected by a solid line while the broad band spectral estimates which arise as a by-product of the SDG analysis (Ref 16) are shown as individual points, square symbols. A straight line with fixed slope of -5/3 has been fitted to the four broad band points which have the highest wave numbers (the rightmost four); it will be noted that the von Karman model approaches a slope of -5/3

---

* Herein 'frequency' is used for quantities having the dimensions 'cycles per unit time', while 'wave number' is used those for having units 'cycles per unit distance'. As the earlier section was concerned with instrument characteristics it was convenient there to work with frequencies. For investigating turbulence it is better to employ wave number so that the results are not dependent on the speed of the sampling aircraft.

asymptotically for high wave numbers (see Fig 14). The range of these points is shown along the bottom of the graph. The exact wave number range will depend on the flight speed during each individual run but was approximately 0.01 cycles/m to 0.1 cycles/m (that is wave lengths between 100 m and 10 m); in terms of frequency the range is in fact always 2 Hz to 16 Hz. In many cases one could probably have included the next one or two broad band points with lower wave numbers in the fitting process as they too often fall on the -5/3 part of the spectrum but this would have meant applying an algorithm to find the straight part of the spectrum. Limiting the range to the four points was simpler. Going to higher wave numbers, the next broad band point would fall at a frequency of 32 Hz which is beyond where the anti-aliasing filters have started to attenuated the signal.

This fitted line has an equation of the form

$$\phi(\kappa) = A\kappa^{-5/3} \tag{2}$$

The value of A (which is the intercept of the fitted line at a wavenumber of 1 cycle per metre) is based only on the intensity of the high frequency content. A quantity known as $\bar{\sigma}$ is derived from A as follows. Starting from the von Karman expressions for the power spectral density (Ref 18), which are for the along path u_g component

$$\phi(\kappa) = 4\sigma^2 L \frac{1}{[1+(1.339L\ 2\pi\ \kappa)^2]^{5/6}} \tag{3}$$

where (Ref 18 Eq.9.38)

$$1.339 = \Gamma(\tfrac{1}{3})/[\sqrt{\pi}\ \Gamma(5/6)] \tag{4}$$

and for the across path components v_g and w_g

$$\phi(\kappa) = 2\sigma^2 L \frac{[1 + \frac{8}{3}(1.339L\ 2\pi\ \kappa)^2]}{[1 + (1.339L\ 2\pi\ \kappa)^2]^{11/6}} \tag{5}$$

a standard scale length, Lstd , of 2500 ft (762 m) is employed and $\bar{\sigma}$ is then the value which needs to be used for σ in the relevant Eq.(3) or Eq.(5) so as to match the fitted straight line at high wave numbers. The resulting equations for $\bar{\sigma}$ are for u_g

$$\bar{\sigma}_u = 26.94\sqrt{A_u} \tag{6}$$

where

$$26.94 = \tfrac{1}{2}\ (1.339 \times 2\pi)^{5/6}\ L_{std}{}^{1/3} \tag{7}$$

and for v_g and w_g

$$\bar{\sigma}_{v,w} = 23.35\sqrt{A_{v,w}} \tag{8}$$

where

$$23.33 = \sqrt{\tfrac{3}{4}}\ (1.339 \times 2\pi)^{5/6}\ L_{std}{}^{1/3} \tag{9}$$

The factors which appear above are employed in I11WRUN, see Table 2b.

Values of $\bar{\sigma}$ give estimates of the turbulence intensity which, unlike the values for the standard deviation of the original signal σ_{obs} , are not inflated by large low frequency components in the signal. Values of $\bar{\sigma}_v$ have been used as a guide to the turbulence intensity of each run. The values for the 389 runs analysed range from 0.3 m/s to 6.9 m/s. The symbols in Fig 2 are also based on $\bar{\sigma}_v$. Values for both $\bar{\sigma}$ and σ_{obs} for all three components of the runs from flight 716 are given in Table 3.

I11WRUN goes on to fit another straight line to the same four broad band spectral estimate points but without constraining the gradient. This fitted line is not plotted

but the gradient so identified is output to the FITTABLES and will later give a means of checking the validity of the proposition that the slope of the power spectral density is -5/3 in this wave number range. The gradients for the runs from flight 716 appear in Table 3.

The large graph on the left of the plot is the cumulative distribution produced by the SDG analysis. In this plot a value of 1/3 has been used for the scaling parameter k, which determines the relationship between the rates of occurrences of ramps of different lengths. This value of k is only appropriate for ramp lenghts (the patterns here being simple ramps) for which the local slope of the power spectral density graph for corresponding wave lengths is -5/3 (see Ref 2 and Ref 19); the corresponding wave lengths are twice the ramp lengths and wave number is the inverse of wave length. The four shortest ramp lengths thus usually collapse quite well using this value of k. The exact lengths of these ramps depends on the airspeed for each run but usually covers the range 5 m to 50 m, in many cases the next one or two ramp lengths also collapse into the same family, which extends the range upto 100 or 200 m.

The curve onto which the individual distributions collapse usually bends at the smallest values of x (x being the size of the peak or trough in the smoothed, differenced signal caused by the occurrence of a ramp in the original signal). Departure from a straight line for small x is not unexpected; see the discussion following Eq.(A-2). An interesting point is that almost every individual distribution intersects the $x = 0$ axis extremely close to $\lambda S\ n(S,x) = 0.2$. This indicates that with the particular thinning (that is decimation) applied to get each successive ramp length, and with the differencing and smoothing applied before spotting peaks and troughs, the resulting thinned, smoothed, differenced signal is so band limited that every fifth point is a peak or trough.

A straight line is fitted to the points of the cumulative distributions between one and four standard deviations of the smoothed, differenced signal for the four shortest ramp lengths. The range of $x/(FS^k)$ thus fitted for each pattern length is shown in the key in the top right hand corner of the cumulative distribution graph. This fitted line is shown on each cumulative distribution graph along with the α and β which can be derived from the intercept and slope of the line. These two parameters characterise the overall rate of occurrence of ramps in the signal and the amplitude distribution of the ramps. The α and β estimates, together with values for the standard deviations (ie 68.2% confidence intervals) on the estimates, are also appended to the FITTABLES so that the distributions and correlations of α and β for all the runs can be investigated. The estimates for the runs in flight 716 are given in Table 3.

The graph in the top right hand corner of Fig 15 shows the single most intense increment, that is the largest ramp, observed in the record for each ramp length. These are the end points of each distribution in the cumulative distribution graph presented in a different way. The line shown is based on the α and β derived from fitting the cumulative distribution points; using these values in Eq.(A-2) with $n(S,x) = 1/(\text{record length})$, that is a rate of occurrence of once in the distance covered by the run, the expected size of x that should occur once in the run can be derived for each of the range of pattern lengths. The deviation of the observed single most intense increment points from the line thus shows how well the model derived from fitting between one and four standard deviations predicts the tails of the distributions.

A further straight line is fitted to the cumulative distribution points between four and eight standard deviations of the smoothed, differenced signal for the same four ramp lengths. This line is not plotted but the α and β estimates are appended to the FITTABLES. This will allow the distributions of the intense increments (large ramps) to be investigated.

Table 3 gathers together the items identified from the four runs in flight 716. This Table also includes estimates of the scale length L which has been derived from the following formula

$$L = L_{std}\left(\frac{\sigma_{obs}}{\bar{\sigma}}\right)^3 \qquad (10)$$

There are several techniques for estimating the scale length of turbulence samples. Frost and Lin (Ref 20 Chapter V) discuss such techniques and the method adopted here is similar to their method No 3. The scale length is an important parameter in spectral descriptions of turbulence. Fig 14 gives an example of its influence on the shape of the power spectral density.

4 ASSEMBLED RESULTS

The preceding section has described how individual turbulence sampling runs were analysed. One of the main results of this analysis was estimates for a set of parameters which describe and summarise various statistical properties of the turbulence encountered. In this section we will be concerned with looking at the properties and distribution of each of the parameters across 389 runs which have been analysed in detail.

4.1 Power spectral density parameters

Fig 16 gives histograms for the slope of the line fitted to the power spectral density. The von Karman (Ref 11) model predicts a value of -5/3 (-1.667) for this slope and it will be seen that the mean values for the head gust u_g and side gusts v_g of -1.685 and -1.665 are quite remarkably close to this. For the normal gusts w_g, however, the mean value is -1.503. Two factors can be advanced as contributing to this anomaly. The first is an instrumentation problem which was introduced above when discussing the w_g power spectral density for run Gnat 71602. It there became apparent that the 'organ-pipe' resonance in the nose probe α Conrad Yawmeter pipes was not always being entirely removed by the corrective algorithm in program TURB. The increased power in the right hand part of the spectrum arising from this will tend to decrease (absolutely) the slope of the fitted line.

The second factor arises, however, from a real a property of the turbulence. Fig 17 shows scatter plots for the power spectral density slope for each run against the average radio heights.* Fig 17a is for runs over smoother terrains while Fig 17b is for the rougher terrains. It is noticeable that for the w_g component over all types of terrains (and in fact for the v_g component over smooth terrain) the power spectral density slope decreases for low altitudes. If the scale length is decreasing at these low altitudes it is possible that the left hand part of the spectrum being fitted no longer belongs to the -5/3 region but falls below this line, and so ought not to have been included in the fitting. Its inclusion will tend to reduce the slope of the fitted line.

To investigate more directly the wave length at which the power spectral density deviates from a -5/3 slope Fig 18 gives scatter plots for scale length, estimated using Eq.(10), against average radio height, again separated into smoother and rougher terrains. Once again the vertical axis is limited to 400 m and here the horizontal, scale length, axis, has been limited to 1500 m. Points giving values of L greater than 1500 m are all plotted just off the axis scale. Using Eq.(10) to estimate scale length means that a von Karman model (ie Eq.(3) for the u_g component or Eq.(5) for the v_g and w_g components) has been fitted to the observed spectra by taking σ equal to the standard deviation of the observations and choosing L so that the high wave number (high frequency) asymptote of Eq.(3) or Eq.(5), (whichever is required) matches as closely as possible the part of the observed spectrum between about 0.01 cycle/m and 0.1 cycle/m (see earlier discussion concerning exact range used) where a -5/3 slope is assumed to be appropriate. This technique produces three separate estimates for the scale length of the turbulence encountered during each run, one for each component. It is clear from the appearance of the scatter plots in Fig 18 that the estimates of scale length based on the u_g component tend to be longest (with many being very long over rough terrain) and those from the w_g component shortest. Although the scatter in these graphs (particularly over the rougher terrains) is enormous, there is some evidence of scale length increasing with altitude. Due to the scatter, trying to quantify the relationship is open to question, but taking scale length equal to altitude, as shown by the line on each graph, upto a height of 400 m (the limit of the information available here) would not be inconsistent with the data for the smoother terrains. Somewhat longer scale lengths are indicated for the rougher terrains, particularly for the horizontal components.

4.2 Statistical discrete gust parameters

The parameters available for each component of each run which characterise the turbulence in SDG terms are the values of α and β. We have available two pairs of α, β values for each run component; the first got from fitting the distribution of moderate to high intensity ramps (one to four standard deviations) in a time history, and the second from fitting the extreme ramps (four standard deviations onward).

For samples of turbulence which can be derived from one another by

(i) scaling the amplitude of the signal, and/or

(ii) stretching (or compressing) the duration of the signal, and/or

(iii) adding (or deleting) patches of quiescence in the signal,

a simple relationship holds between α, β and A (where A appears in Eq.(2) and is a measure of the intensity of the turbulence in the wave length region where k = 1/3 is appropriate). This relationship is:

$$\frac{\alpha\beta^2}{A} = \text{constant}$$

$$\therefore \alpha = \text{constant} \times \left(\frac{\beta}{\sqrt{A}}\right)^{-2} \qquad (11)$$

* The sensitivity setting used for the radio altimeter limited its range to just over 400 m and so the points shown above the 400 m line could be at any altitude greater than 400 m.

See Ref 21 for the derivation of Eq.(11). Scaling the amplitude of the signal changes β and $\sqrt{A}$ by the scaling factor, so their ratio is unchanged, while α, which measures the rate of occurrence of increments in the signal per ramp length, is also unchanged. Stretching the signal has the similar effects in that β and $\sqrt{A}$ change by the same factor (which is now a function of the amount of stretching and of k), while α is still unchanged. Adding patches of quiescence decreases α, the same total number of increments being diluted over a larger number of ramp lengths.

Scatter plots of α against $\beta/\sqrt{A}$ on log-log axes for each component of all the runs, using the first α, β pair (that is 1-4 standard deviation fitting) are shown in Fig 19.

There are good collapses to straight lines, particularly for the v_g and w_g components, but the straight line is somewhat steeper than the -2 given by Eq.(11). These collapses are all the more remarkable when it is realised that many of the points are derived from runs for which the value of k used (1/3) is not the most appropriate. In Fig 20 only those components where the slope of the power spectral density is between -1.600 and -1.733 have been accepted. Fitting straight lines to these points and taking average values over the three components gives

$$\alpha = 2.57 \left(\frac{\beta}{\sqrt{A}}\right)^{-2.53} \tag{12}$$

This line is shown in Fig 19.

A close examination of the left hand end of the three components in Fig 20 reveals that for these high values of α the points tend to lie above the fitted lines and a steeper slope than -2.53 might be appropriate for the high alpha region.

Eq.(12) is in terms of α, β and A. These parameters are products of the present analysis techniques. It is useful to recast this equation in terms of parameters which more directly characterise the turbulence such as:

(i) a and b, which appear in the SDG model of turbulence (see Appendix) and are related in a simple way to α and β, Eq.(A-3), and

(ii) σ and L, which appear in the von Karman model, Eq.(3) and Eq.(5).

Then

$$a = 3.85 \left(\frac{b}{\sqrt{A}}\right)^{-2.53} \tag{13}$$

where, for the u_g, head gust component

$$A = 0.115\ \sigma^2\ L^{-2/3} \tag{14}$$

and for the v_g and w_g, side and normal gust components

$$A = 0.153\ \sigma^2\ L^{-2/3}\ . \tag{15}$$

Fig 21 uses the second α, β pair, got from fitting the intense ramps in the records. As each point plotted here is based on far fewer occurrences than in the preceding figures, one would expect the uncertainty in each point to be greater and thus the much greater scatter in the points plotted. The line defined by Eq.(12) is shown on these graphs. This line is not a particularly good model for these sets of data, but it should be noted that it performs best (that is it intersects the scatter of points though its slope is too shallow) in the α range 0.1 to 1.0 (ie log10 (α) between -1 and 0). This is very nearly the range of α of the points in Fig 20, and it was these on which Eq.(12) was based. Even so, the marked differences between Fig 19 and Fig 21 tends to indicate that the parameters which characterise the rates of occurrence of the intense ramps in a patch of turbulence form a different family to those characterising even the moderate to large ramps.

Returning to the data shown in Fig 19, having established this strong connection between α, β and A one would clearly like to discover what determines where a particular patch of turbulence falls on the line defined by Eq.(12). To this end the time histories of the three v_g components with lowest α values are shown in Fig 22, while the three with highest α appear in Fig 23 (similar plots could have been presented for the u_g and w_g components).

It is immediately apparent that the low α runs, Fig 22, contain bursts of higher turbulence activity interspersed with periods of much lower activity. In the case of the v_g components of runs Gnat 72305 and Gnat 68901 there are periods of almost calm air between the turbulence encounters. The latter run is the outlying point at the low α

end of the v_g (centre) graph in Fig 19. It was gathered flying Easterly about 11 km south of Cairngorm in Scotland at a radio height of 360 m (barometric height 974 m) in cloudy weather. It is interesting to note that the α and $\beta/\sqrt{A}$ of this outlying point agree extremely closely with those found in Ref 22 for run 70-2 gathered by the Canadian National Aeronautics Establishment T33 aircraft flying into and through a thundercloud on 11 July 1977.

The high α runs, Fig 23 on the other hand, show an extremely continuous, highly packed character. It is worth emphasizing, particularly with regard to the production of synthetic turbulence for flight simulators, that turbulence which is this continuous is exceptional; runs Gnat 69806 and Gnat 69902 are the two outlying points at the high α end of Fig 19 v_g component. Most atmospheric turbulence has a character resembling the records from flight 716 (see Fig 11 for an example) the α values of which fall in the range 0.288 to 0.496.

The above observations based on a comparison of Fig 22 and Fig 23 do, therefore, confirm the model postulated at the start of this section. Records with low α values, and correspondingly high values of $\beta/\sqrt{A}$, do indeed have patches of quiescence, while high α records lack such patches completely and are highly packed in character.

The three low α runs in Fig 22 were in fact all at higher altitude (radio heights 239 m, over 400 m and 363 m) while the three high α runs were at extremely low altitudes (41 m, 27 m and 32 m). To see whether this is a general trend Fig 24 shows scatter plots of α against mean radio height for the points used in Fig 20 (that is with power spectral density slope between -1.600 and -1.733), separated into smoother Fig 24a and rougher Fig 24b terrains. There is no clear correlation of α with height, nor with terrain roughness. Plots for α against surface wind speed also showed no correlation.

5 CONCLUSIONS

The measurements of atmospheric turbulence made by Gnat XP 505 of RAE Bedford have been described. These were mainly at altitudes below 1000 ft over a variety of terrains within Britain. Processing of the data which was gathered yielded about 400 runs for which the time histories of the three components of turbulence, uncontaminated by aircraft motion and instrument characteristics, are available. Any deficiencies in these records have been noted.

These 400 runs have been analysed using both power spectral density and statistical discrete gust techniques to give a set of parameters which summarises the statistical characteristics of the turbulence encountered during each run. Assembling the results from all the runs confirmed the prediction of the von Karman model that the power spectral density decays at a rate of -5/3 and, furthermore, allowed a very strong relationship between two parameters from the statistical discrete gust technique and one from the power spectral density technique to be identified (Eq.(12) and Fig 19).

APPENDIX

AN INTRODUCTION TO STATISTICAL DISCRETE GUST TECHNIQUES

The purpose of SDG analysis is to investigate the rate at which ramp shaped gusts occur in flight through a turbulent atmosphere. The aim is to quantify the rate of occurrence of ramps which are bigger than a specified size and have length in a specified range, Fig 25. Such rates of occurrence can be used in theoretical studies of aircraft response to turbulence; it is particularly important to be able to quantify the rate of occurrence of big ramps with a length which, in some way, 'tunes' with the aircraft dynamics, so producing a violent response which leads to crew discomfort or even structural damage.

We define $N'(H,w)dH$ to be the number of ramps (or more accurately 'smooth increments') encountered per unit distance with length in the range H to $H + dH$ and size greater than w, Fig 26. An example of an analytic form for N' which has been found applicable to many atmospheric turbulence measurements is

$$N'(H,w) = \frac{a}{H^2} \exp\left(-\frac{w}{bH^k}\right) , \qquad (A-1)$$

where

a is a dimensionless parameter defining the overall rate of occurrence of smooth increments,

b is an intensity parameter defining the amplitude distribution of smooth increments (b has the dimensions velocity/length^k), and

k is a dimensionless scaling parameter which defines the relative intensity of smooth increments of differing lengths.

Fig 27 gives an impression of the surface defined by Eq.(A-1) and its interpretation.

To investigate the form of N' which describes a given time history requires a technique for quantifying the number and size of ramps in the record, followed by a means of fitting postulated analytic models to the observed distribution and identifying parameters in the models (such as a, b and k in Eq.(A-1)). One approach would be to attempt to detect and count the occurrence and size of smooth increments present in a time history for a specified set of length ranges. However, a more convenient and quicker method has been described in Ref 15. In this method, digital smoothing filters are applied to the sampled record to remove increments which are only maintained for an interval much shorter than a specified interval S (ie a low pass filter in the frequency domain), and the filtered record is differenced over a length S (ie the sample value at a distance S behind is subtracted from each sample; a high pass filter in the frequency domain). After this smoothing and differencing the occurrence and size of peaks* (or troughs) in the signal is counted. The result, for a particular choice of S, is an observed cumulative distribution $n(S,\times)$ of the number of peaks or troughs per unit distance of size greater than $\times$, for a series of levels of $\times$. The analysis is usually carried out for a number of different values of S.

Using this method means that the relationship between the distribution $n(S,\times)$ of peaks and troughs in the smoothed differenced signal has to be related to $N'(H,w)$ which is the distribution of smooth increments in the original record. The extrema in the smoothed, differenced signal will in fact arise from ramps with lengths H in a band surround S. The width of this band, δS will depend on the filters used.

As an example of the relationship between $n(S,\times)$ and $N'(H,w)$, if the latter has the exponential form of Eq.(A-1), then for large $\times$

$$n(S,\times) \simeq \frac{\alpha}{\lambda S} \exp\left(-\frac{\times}{\beta F S^k}\right) , \qquad (A-2)$$

where $\alpha = 0.89a$ $\beta = b/1.12$ } these corrections are to allow for the exact distribution of $n(S,\times)$ being approximated by an exponential form, (A-3)

λ depends on the range of ramp lengths let through by the filtering, the range effectively has a width $\delta S = S/\lambda$,

and F depends on the attenuation caused by the filtering, so $w = \times/F$.

---

* Hence the name "Peakspotter', although this is only a part of the computations carried out.

The derivation of Eq.(A-2) from Eq.(A-1) relies on $\times$ being 'large', and so might not be valid for low intensity ramps, see Appendix C of Ref 15.

Rearranging and taking logarithms, Eq.(A-2) gives

$$\log \lambda Sn(S,\times) = \log \alpha - \frac{1}{\beta} \frac{\times}{FS^k} . \qquad (A-4)$$

Analysis of a given record for a set of values of S and a series of values of $\times$ (at each S) yields pairs $(\times, n(S,\times))$. Plotting $\times/FS^k$ against $\log \lambda Sn(S,\times)$ should for each S produce points on a straight line and, furthermore, with the correct choice of k the points will collapse on a single straight line for all values of S. The single straight line has a slope $-1/\beta$ and intercept $\log \alpha$, from which a and b may be derived using Eq.(A-3).

In the above discussion it has been assumed that a, b and k in Eq.(A-1) are independent of H. In practice it may be necessary to use several values of k corresponding to different ranges of values of H.

It can be shown[19] that if $s(\kappa)$ is the local slope of the power spectral density curve (plotted on log-log axes) at the wave number corresponding to a particular value of H (ie at a wave number κ of $1/2H$), then the value of k to use at that H is

$$k(H) = \frac{-s(\kappa) - 1}{2} \qquad (A-5)$$

PSD plots thus give a good guide[13] to the ranges of H in which k is constant and the value of k to use in each range.

REFERENCES

1 G.W. Foster, R.L. Poulter. Gnat XP 505 atmospheric research aircraft - instrumetation and data processing.
RAE Technical Memorandum FS(B) 480 (1982).

2 G.W. Foster. Examples of low altitude atmospheric turbulence measurements by Gnat XP 505.
RAE Technical Report 83026 (1983).

3 G.W. Foster. Results of low altitude atmospheric turbulence measurements by Gnat XP 505.
RAE Technical Report to be published.

4 Technical information brochure for Modular Data Acquisition System (MODAS).
Plessey Avionics and Communications, April 1979.

5 G.W. Foster. Wind tunnel calibration of an aircraft pitot - static and flow direction measuring nose probe.
RAE Technical Report 80077 (1980).

6 W. Love. Analysis of Gnat data tapes.
Report for contract A81A/1996 Aeronautical Instrumentation Laboratories, Cranfield Institude of Technology (1985).

7 G.W. Foster. Measurements of the spanwise variation of atmospheric turbulence by Gnat XP 505.
RAE Technical Memorandum to be published.

8 H. Bergh, H. Tijdeman. Theoretical and experimental results for the dynamic response of pressure measuring system.
NLR Technical Report F238 (1965)

9 R.T.F. Vanstone. The ground resonance testing of the Gnat T Mk I.
Aerodynamics Department Report F/GT/7 Folland Aircraft Ltd (1962).

10 G.E.A. Reid. Validation of kinematic compatibility of flight data using parameter estimation methodology.
RAE Technical Report 81020 (1981).

11 T. von Karman. Progress in the statistical theory of turbulence.
Journal of Marine Research, Vol, 7, pp 252-264 (1948).

12 H.L. Dryden. A review of the statistical theory of turbulence.
Interscience Publishers, New York (1961).

13 J.G. Jones. Summary notes on the statistical discrete gust method.
RAE Technical Memorandum FS 323 (1980).

14 J.G. Jones. Response of linear and nonlinear systems to an atmospheric turbulence model involving the representation of fluctuations as discrete gust patterns.
RAE Technical Memorandum FS 429 (1981).

15 J.G. Jones, Ann Haynes. A peakspotter program applied to the analysis of increments in turbulence velocity.
RAE Technical Report 84071 (1984)

16 G.W. Foster, S.L. Gale. A computer program for random series analysis including the statistical discrete gust technique.
RAE Technical Memorandum FS(B) 565 (1984).

17 G.M. Jenkins, D.G. Watts. Spectral analysis and its applications.
Holden-Day (1969).

18 J. Taylor (editor). Manual on aircraft loads.
AGARDograph 83 (1965)

19 J.G. Jones. A theory for extreme gust loads on aircraft based on the representation of the atmosphere as a self-similar intermittent random process.
RAE Technical Report 68030 (1968).

20 W. Frost, Ming-Chan Ling. Statistical analysis of turbulence data from the NASA Marchal Space Flight Centre atmospheric boundary layer tower facility.
NASA CR 37373 (1983).

21 J.G. Jones, G.W. Foster, Ann Haynes. A relationship between the parameters describing atmospheric turbulence.
RAE Technical Memorandum to be published.

22 Ann Haynes. Analysis of atmospheric turbulence measurements recorded by a Canadian T33 aircraft.
RAE Technical Memorandum to be published.

23 Direction and incidence angles.
Engineering sciences data, aeronautical series, dynamic sub-series, item 67037.
Royal Aeronautical Society (1967).

Table 1

Terrain Roughness Ratings

Symbol	Rating	Description	Examples
Δ	0	Sea well away from land	
∇	1	Sea just offshore	
+	2	Flat land	East Anglian Fens
×	3	Not hilly	Bedfordshire
□	4	Rolling hills	Cotswolds, Severn valley
◊	5	Hills with peaks up to 2500'	Mid Wales, N.Scotland
○	6	Hills with peaks up to 3000'	South Wales, Brecon Beacons
✳	7,8	Mountains with peaks over 3000'	W.Coast Scotland

Symbols are used in figures 17, 18 and 24. Ratings up to 3.5 are considered to be 'smoother' terrains and over 3.5 are 'rougher'.

TABLE 2a
I11W Use-file I11WTURB

```
C I11WTURB  Configures I11W to read data from GNAT TURB files.
C
C No input parameters are required, and no parameters are changed by this
C  USE-file.
C
C Dr G.W.Foster  FS(B)1 R.A.E.

 ADDRESS  GENERAL AERO SECTION,FS(B)1,RAE BEDFORD

C Observation files start with 6 header records. Print 1,2,4,5 & 6 and also
C  try to interpret record 4 as an I11W instruction (in fact this record
C  carries the speed, radio and baro heights)...
  HEADER=6  REC1 1 8Ø  REC2 1 52  REC3 Ø Ø  REC4* 1 52  REC5 1 12Ø  REC6 1 12Ø
C Each data record carries a time and four samples (of each component)...
 LAYOUT TIME,SAMPLES 4
C As the original sampling was at an excessive rate ( 256 samples/sec after
C  passing through 25 Hz antialiasing filters ), smooth and thin to half this
C  rate as data is read...
 OBS  INERT  RATE=256
 ALTER 2 3 Ø.25 Ø.5 Ø.25
C Reset ( if possible & necessary ) number of points which can be acquired..
 SIZE MAX=12ØØØ

C Use a block size of 512 when carrying out Fast Fourier Fourier transform
C  ( with sampling rate reduced to 128 by ALTER this gives 4 second blocks and
C  a frequency resolution of Ø.25 Hz). Also overlap blocks by 5Ø% and remove
C  linear trend from each block ...
 FFT  BLOCK 512  OVERLAP Ø.5  DETREND  INERT

C When fitting Broad Band PSD estimates and Cumulative Distributions only
C  use the first 4 patterns.  Don't fit PSD's beyond 2Ø Hz and restrict range
C  of FFT PSD estimates used in fitting to that covered by Broad Band points
C  that are being fitted...
 RANGES PATTERNS 1 4  FREQ 1.ØE-1Ø 2Ø.Ø  TIED
C When fitting PSDs ignore FFT estimates and only fit Broad Band estimates that
C  arise from PDA (Pattern Detector Algorithm) ...
 WEIGHTS FFT Ø.Ø PDA 1.Ø

P
P Setup by I11WTURB completed.
P
 EXIT
```

Table 2b
I11W Use-file I11WRUN

```
C I11WRUN  To carry out a standardised analysis on the three components
C  of a Gnat turbulence sampling run. Plotting is produced and results are
C  appended to FITTABLES for each component.
C
C Parameter usage ( * mandatory, others optional i.e. may be null ) :-
C * F=Run name (eg GNAT 535Ø1). File name is got by concatenating (/TURB) .
C   E=Extra clauses to go in OBS instruction (eg UPTO 9Ø.Ø).
C   P=Mininimum number of peaks or troughs on which a point in the U component
C      Cumulative Distribution must be based for point to be taken into account
C      during FIT CD. Default is 5 if P is null.
C
C N.B. I11WTURB should have been used for setup before using I11WRUN
C
C Dr G.W.Foster FS(B)1 R.A.E.

T %F  HEAD GUST , Ug
C FORTRAN format required to pick out Ug from data records and pass a TYPE of
C  Nose Probe Miniature Pitot Ug to any tables produced ...
 FORMAT(F8.3,4(F6.2,12X))      TYPE=NP MP UG
C Read Ug observations ...
 OBS  %E  FILE %F
C Carry out Fast Fourier Transform and Pattern Detector Algorithm for Power
C  Spectral Density and Statistical Discrete Gust type of analysis respectively..
 FFT
 PDA
C When fitting CD only fit points from 1 to 4 sigma ( std devns ) and for
C  Ug minimise the effects of spurious steps caused by operation of
C  pneumatic equalisation valve ( see P= above ) ...
 RANGE  LEVELS 11 4Ø  PEAKS %P 5
C Now fit a straight line of fixed slope -5/3 to the PSD estimates that are
C  within ranges (using relevant factor to estimate sigma_bar for a standard
C  scale length of 25ØØ'=762m) ; also fit CD to estimate alpha and beta ...
 FIT  PSD SLOPE=-1.667 FACTOR=26.95  &  CD
C Plot FFT and Broad Band PSDs (with fitted line), CD (also with its fitted
C  line), and Single Most Intense Increment (with projection of fitted CD
C  line,) then append characteristics of fitted lines to Ug FITTABLES...
 PLOT  THREE
 TAB  FITS  FILE FITTABLES(/UG)
C Now fit CD points from 4 to 8 sigma and the PSD with a line of any slope
C  and add results to FITTABLE(/UG)...
 RANGES  LEVELS 41 81
 FIT  PSD FREE  &  CD
 TAB  FITS
```

Table 2b (concluded)

```
T %F  SIDE GUST , Vg
C Reread observation file with new FORMAT to access Nose Probe Conrad
C  Yawmeter based Vg...
 FORMAT(F8.3,4(6X,F6.2,6X))     TYPE=NP CY VG
 OBS
 FFT
 PDA
C Do not restrict number of peaks & troughs required for a point to be fitted
C  as miniature pitot valve operations do not effect Vg ...
 RANGE  LEVELS 11 40  PEAKS 1
 FIT  PSD SLOPE=-1.667  FACTOR=23.35 & CD  ! FACTOR is different for along path
                                           !  spectrum Ug to that for across path
                                           !  spectra Vg and Wg )
 PLOT  THREE
 TAB  FITS  FILE FITTABLES(/VG)
 RANGE  LEVELS 41 81
 FIT  PSD FREE  &  CD
 TAB  FITS


T %F  NORMAL GUST , Wg
 FORMAT(F8.3,4(12X,F6.2))       TYPE=NP CY WG
 OBS
 FFT
 PDA
 RANGE  LEVELS 11 40
 FIT  PSD SLOPE=-1.667  FACTOR=23.35 & CD
 PLOT  THREE
 TAB  FITS  FILE FITTABLES(/WG)
 RANGE  LEVELS 41 81
 FIT  PSD FREE  &  CD
 TAB  FITS


C Tidy up where appropriate ...
 RANGE  LEVELS 1 81
 TAB  RESET

P
P Completed I11WRUN standard analysis of %F
 EXIT
```

Table 3

Results from GNAT flight 716

Run	Radio ht. m		Sigma obs m/s	Sigma bar m/s	L m	PSD slope	Fitting 1 to 4 std devns alpha	Fitting 1 to 4 std devns beta m/s / m^1/3	Fitting 4 to 8 std devns alpha	Fitting 4 to 8 std devns beta m/s / m^1/3
GNAT 716Ø1	172	Ug	1.27	1.54	425	-1.688 (Ø.Ø33)	Ø.338 (Ø.Ø12)	Ø.128 (Ø.ØØ1)	Ø.Ø55 (Ø.Ø25)	Ø.186 (Ø.Ø2Ø)
		Vg	1.74	2.59	231	-1.668 (Ø.ØØ7)	Ø.369 (Ø.Ø23)	Ø.238 (Ø.ØØ4)	Ø.Ø17 (Ø.ØØ4)	Ø.487 (Ø.Ø25)
		Wg	1.89	2.22	473	-1.564 (Ø.Ø1Ø)	Ø.3Ø9 (Ø.Ø12)	Ø.225 (Ø.ØØ3)	Ø.Ø4Ø (Ø.ØØ8)	Ø.348 (Ø.Ø15)
GNAT 716Ø2	1Ø9	Ug	1.35	1.97	247	-1.668 (Ø.ØØ3)	Ø.331 (Ø.Ø12)	Ø.164 (Ø.ØØ2)	Ø.747 (Ø.341)	Ø.15Ø (Ø.Ø1Ø)
		Vg	2.ØØ	3.Ø2	223	-1.828 (Ø.ØØ7)	Ø.366 (Ø.Ø2Ø)	Ø.275 (Ø.ØØ4)	Ø.173 (Ø.Ø73)	Ø.298 (Ø.Ø2Ø)
		Wg	1.28	2.51	1Ø1	-1.522 (Ø.Ø32)	Ø.3Ø8 (Ø.Ø25)	Ø.251 (Ø.ØØ6)	Ø.Ø18 (Ø.ØØ4)	Ø.5ØØ (Ø.Ø31)
GNAT 716Ø3	349	Ug	1.Ø8	1.36	376	-1.657 (Ø.Ø35)	Ø.431 (Ø.Ø19)	Ø.1Ø3 (Ø.ØØ1)	1.515 (2.178)	Ø.ØØ7 (Ø.Ø14)
		Vg	1.71	2.11	4Ø4	-1.665 (Ø.ØØ2)	Ø.496 (Ø.Ø43)	Ø.175 (Ø.ØØ4)	Ø.996 (1.171)	Ø.164 (Ø.Ø22)
		Wg	1.17	1.94	167	-1.647 (Ø.Ø22)	Ø.288 (Ø.ØØ9)	Ø.197 (Ø.ØØ2)	Ø.Ø43 (Ø.ØØ7)	Ø.3Ø1 (Ø.Ø1Ø)
GNAT 716Ø4	11Ø	Ug	1.38	2.15	2Ø2	-1.726 (Ø.Ø16)	Ø.342 (Ø.Ø14)	Ø.176 (Ø.ØØ2)	Ø.115 (Ø.Ø9Ø)	Ø.2Ø8 (Ø.Ø3Ø)
		Vg	1.94	2.82	248	-1.67Ø (Ø.Ø15)	Ø.425 (Ø.Ø27)	Ø.25Ø (Ø.ØØ4)	Ø.235 (Ø.Ø88)	Ø.279 (Ø.Ø16)
		Wg	1.84	2.44	328	-1.475 (Ø.Ø2Ø)	Ø.292 (Ø.Ø24)	Ø.247 (Ø.ØØ6)	Ø.Ø19 (Ø.ØØ5)	Ø.477 (Ø.Ø34)

NOTE Values shown in parentheses are standard deviations on preceeding estimates

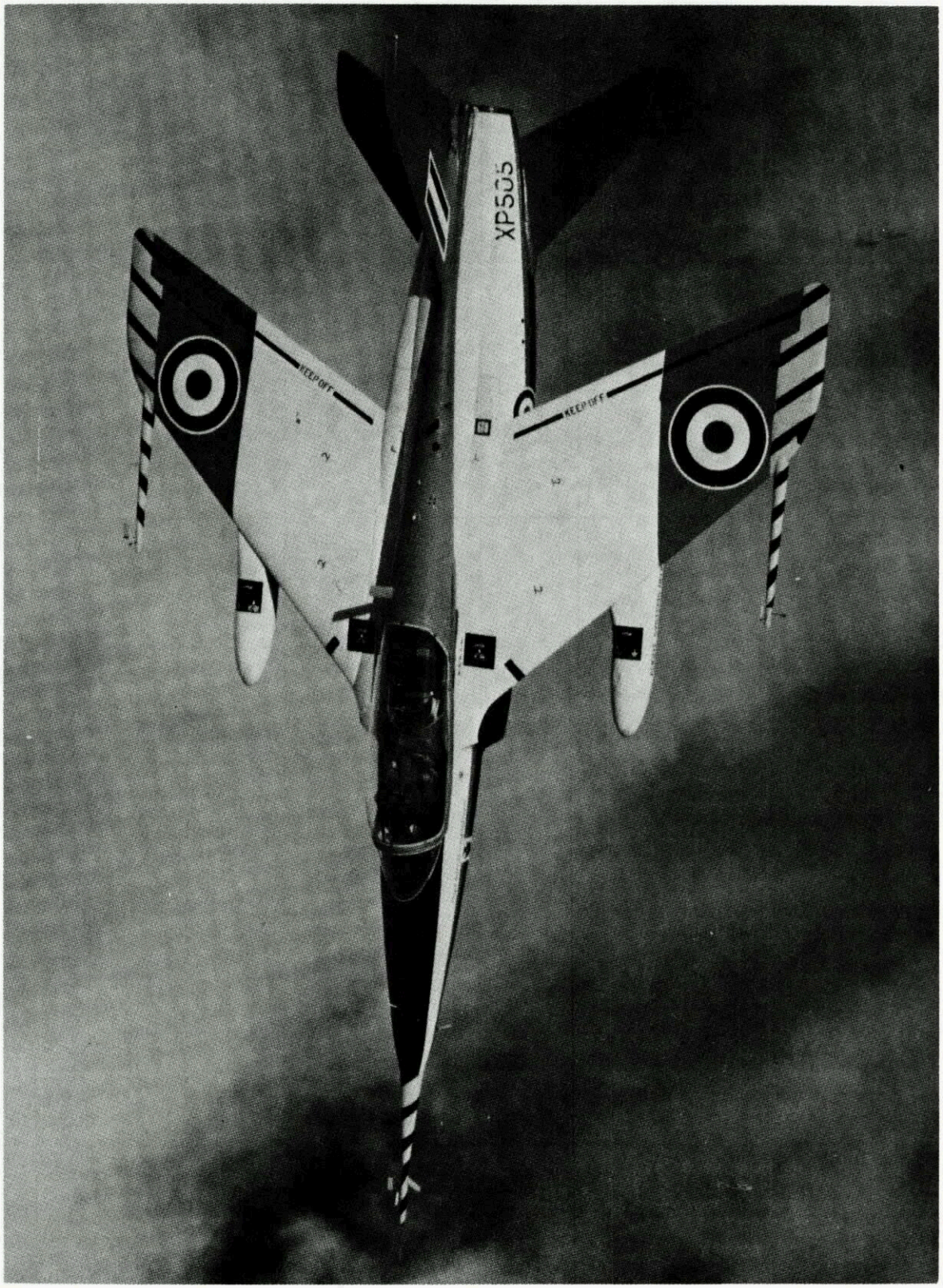

Fig 1 Gnat XP505

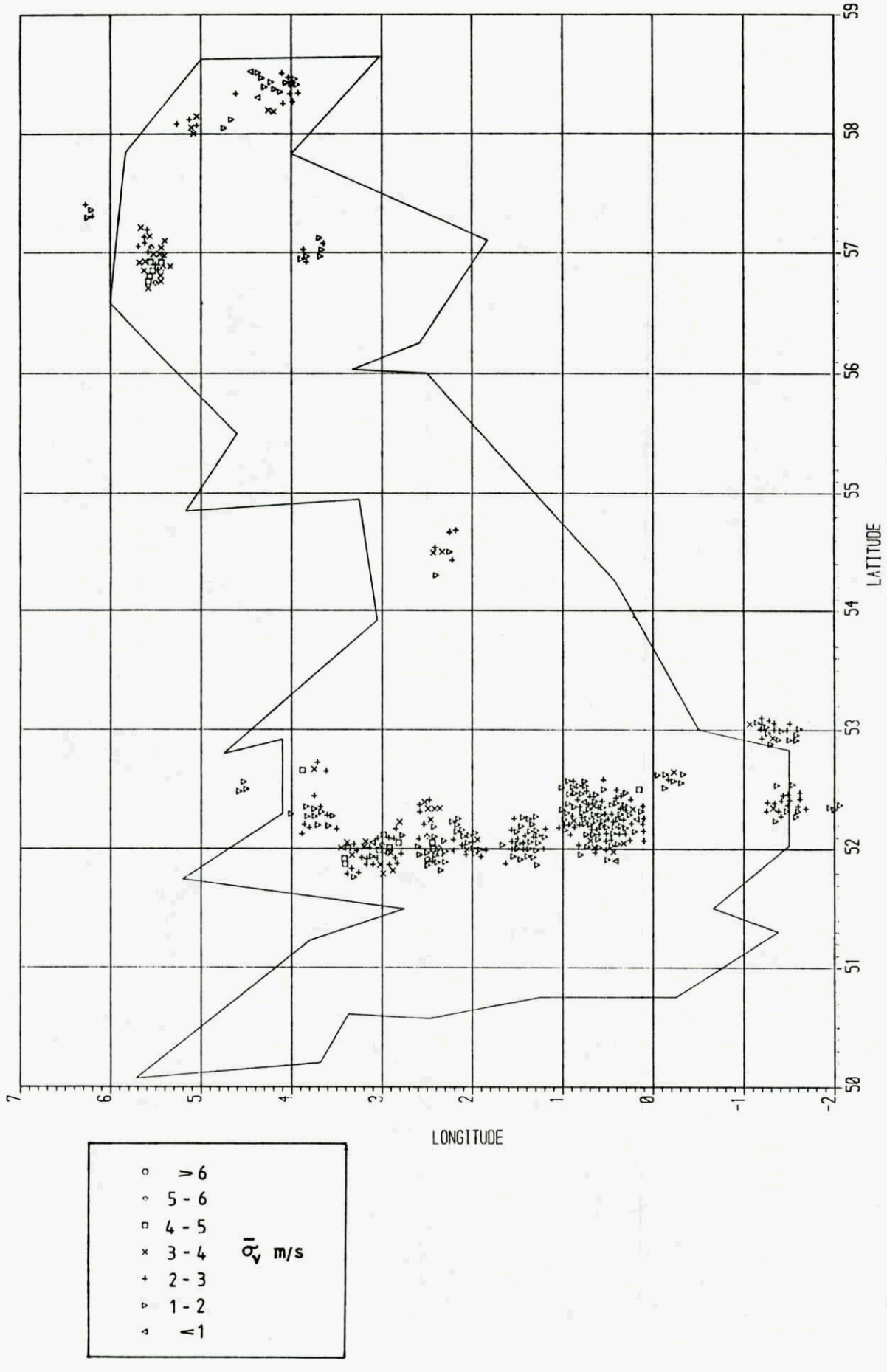

Fig 2 Locations of turbulence sampling runs

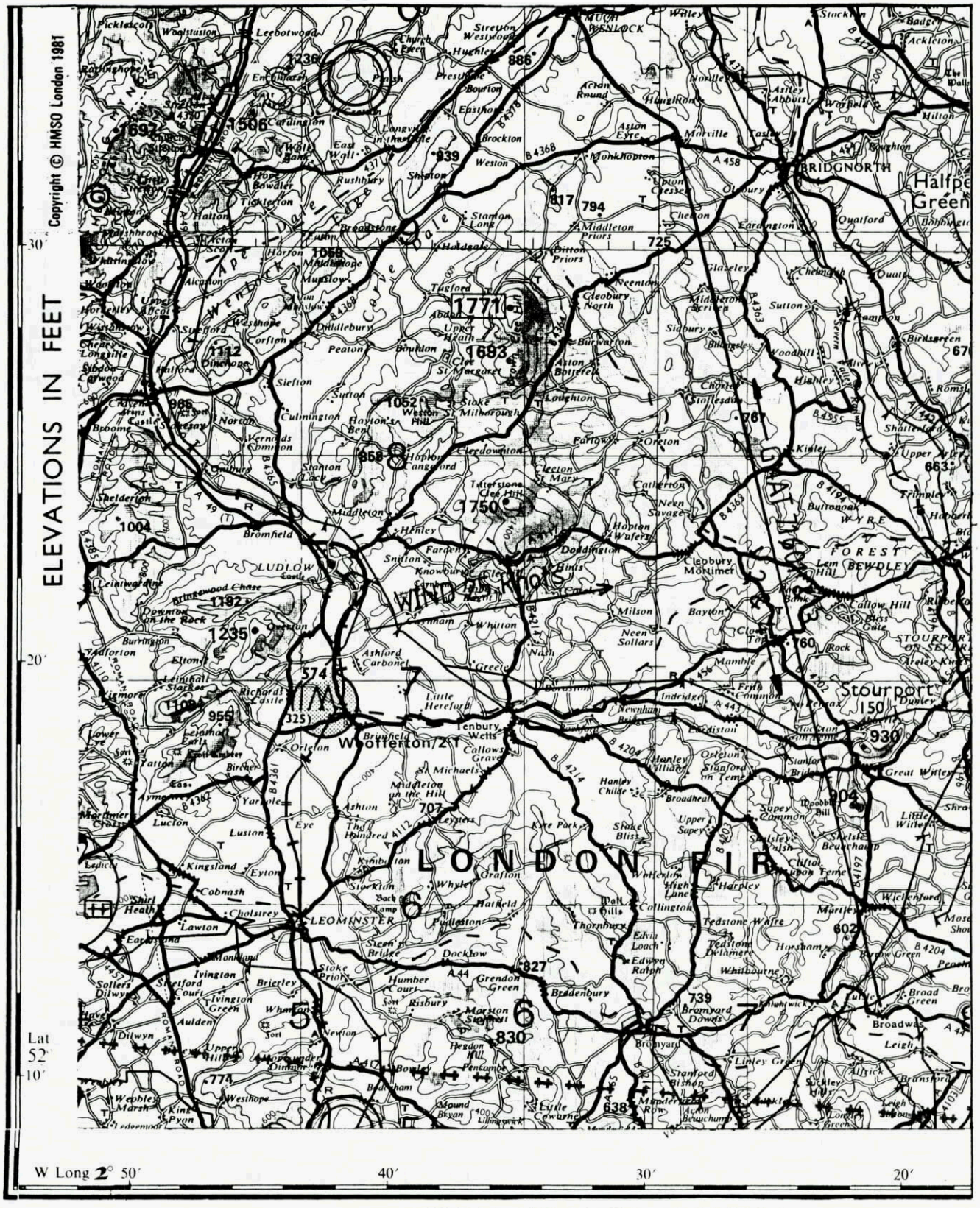

SCALE 1:250 000 TRANSVERSE MERCATOR PROJECTION

KILOMETRES 10 5 0 10 20

Fig 3 Ground tracks of runs from flight 716

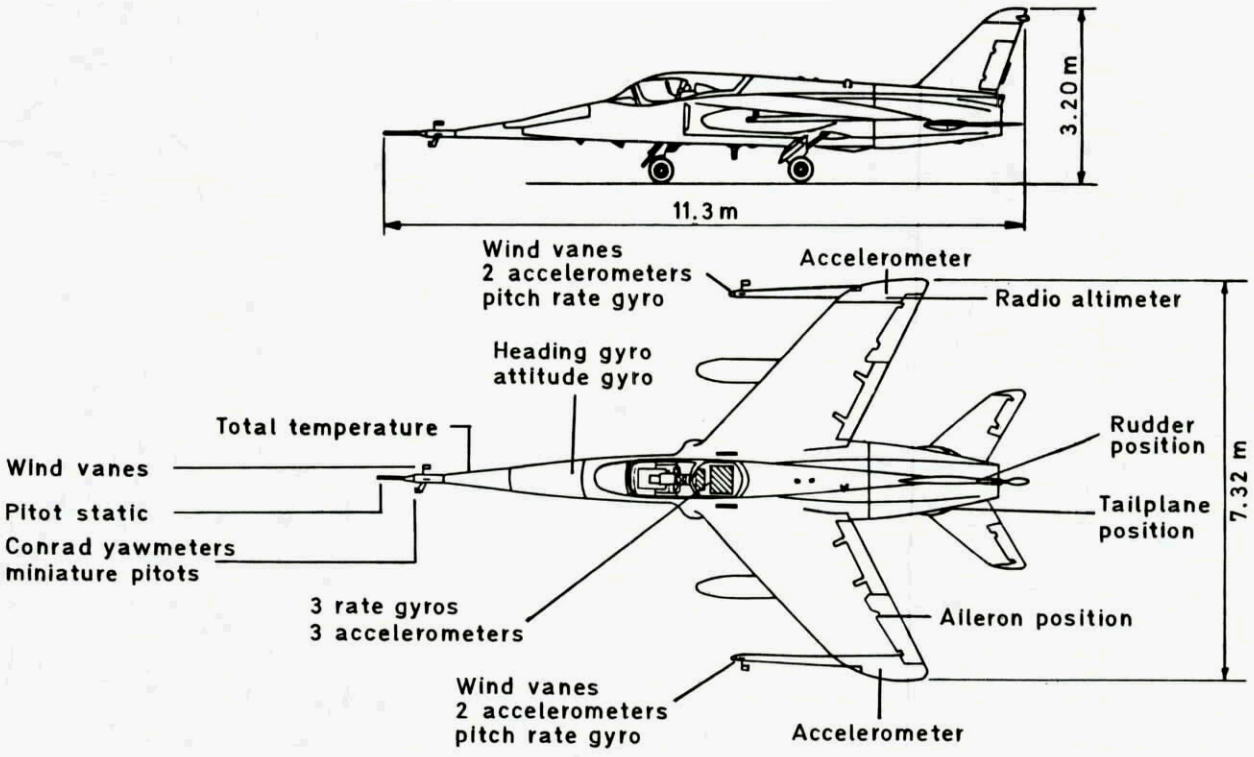

Fig 4 Gnat XP505 instrumentation

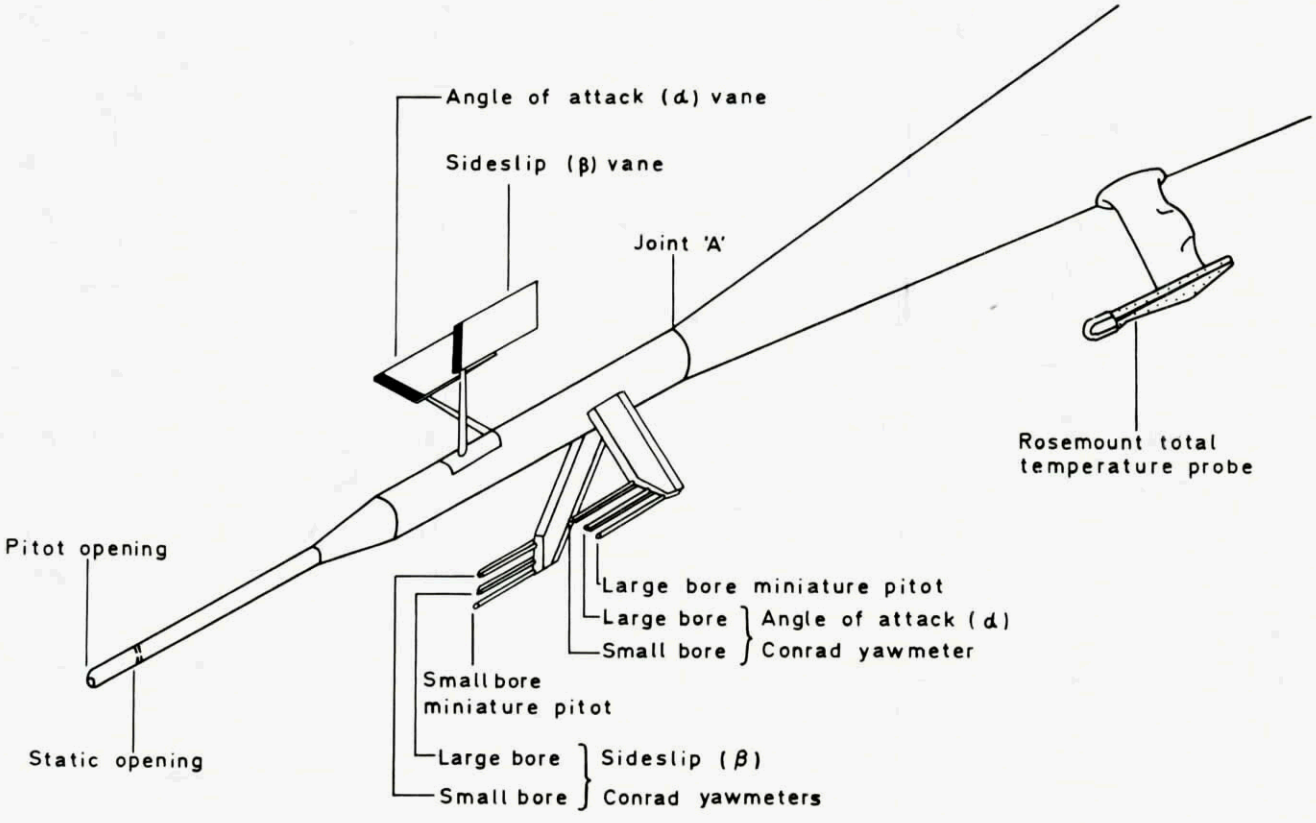

Fig 5 The nose probe assembly

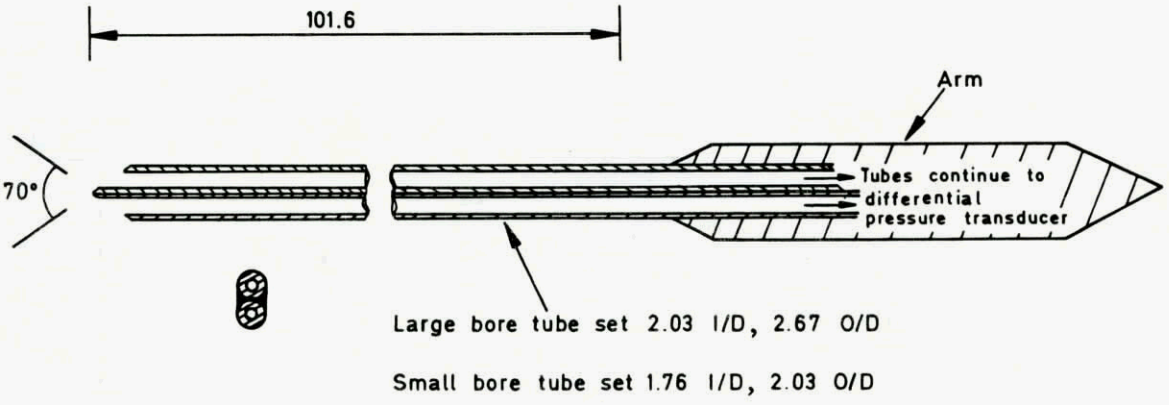

Scale twice full size
All dimensions in millimetres

Fig 6 Cross section of Conrad Yawmeter

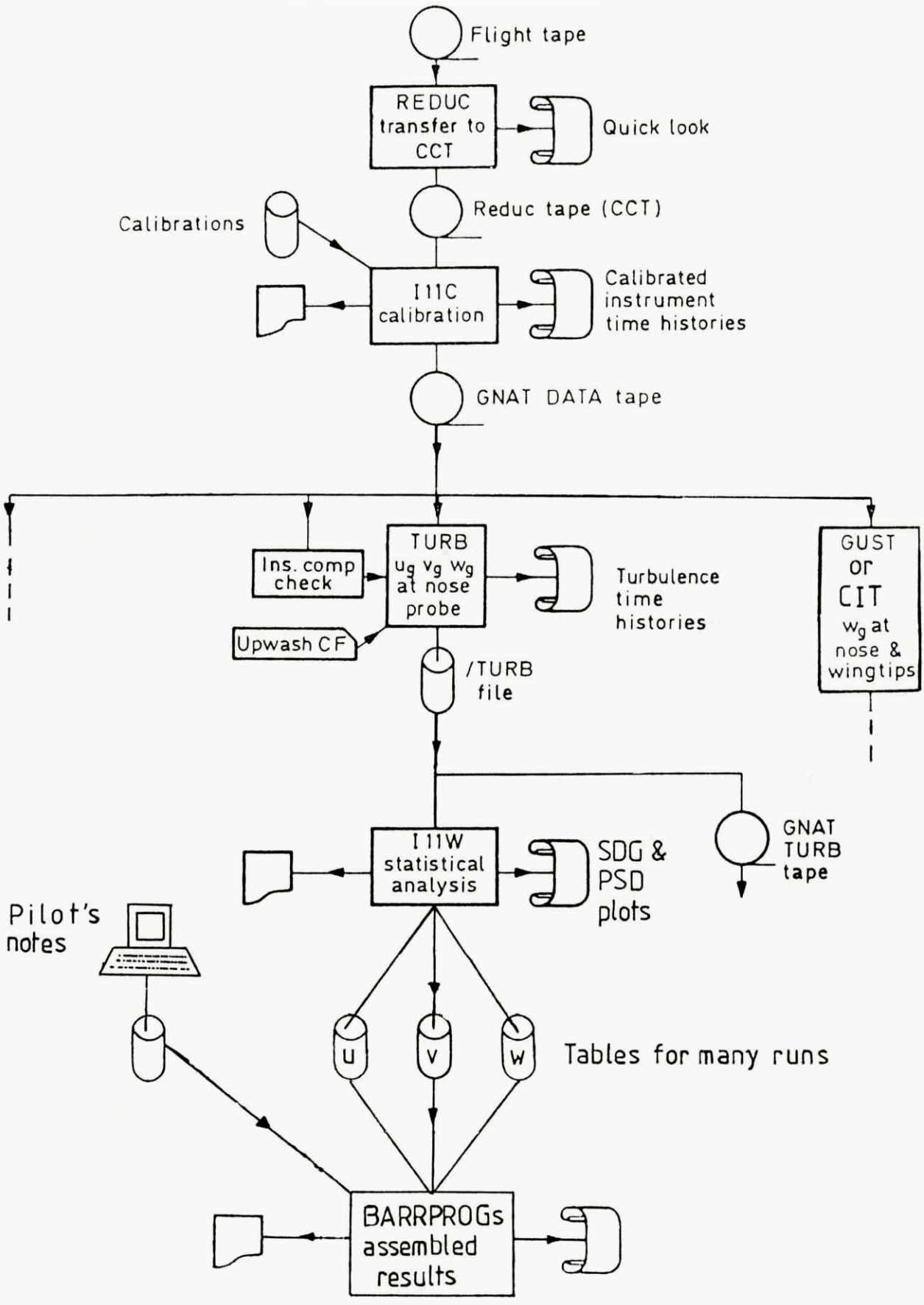

Fig 7 Processing of turbulence measurements

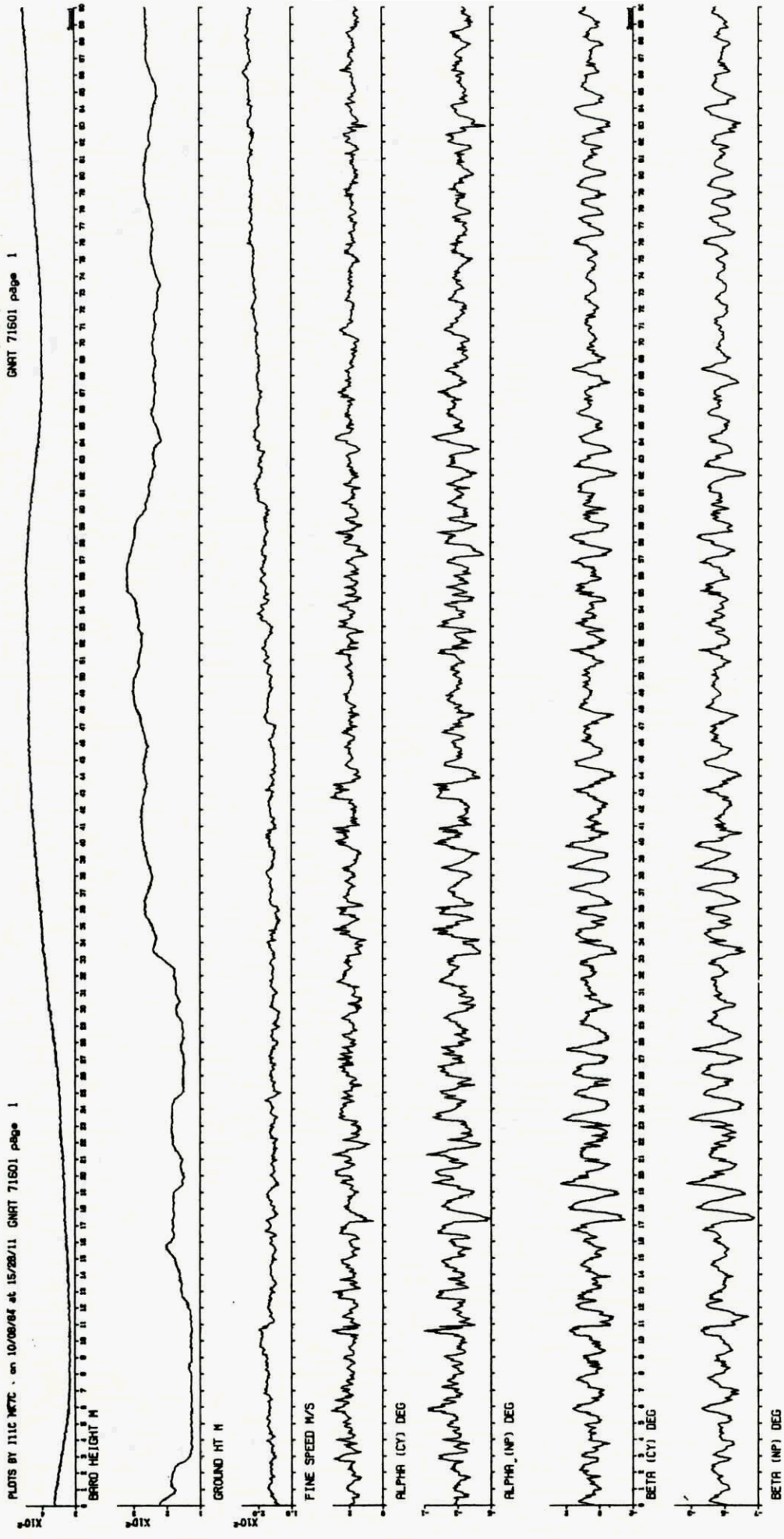

Fig 8 GNAT 71601 Instrument time histories

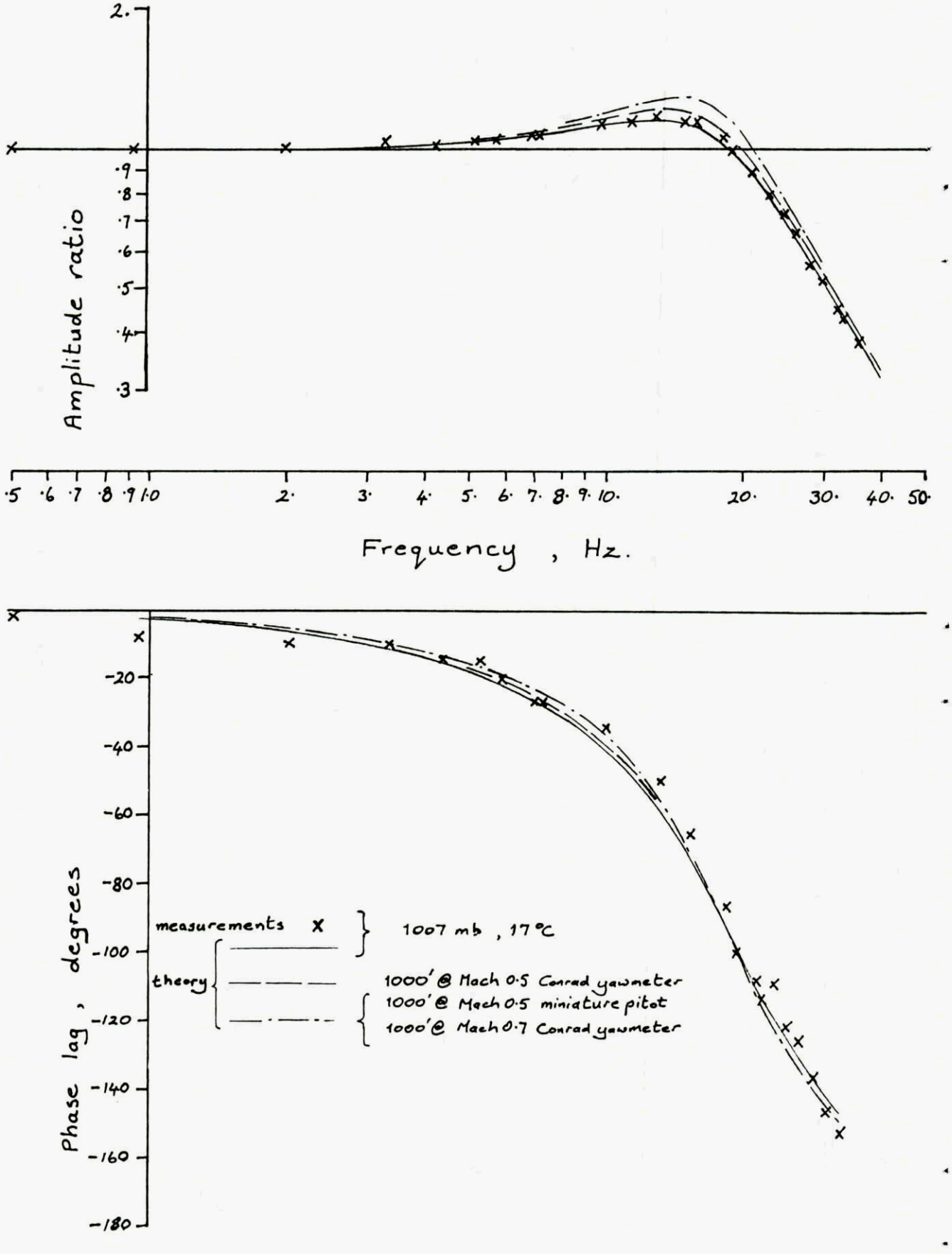

Fig 9 Frequency response of pneumatic piping

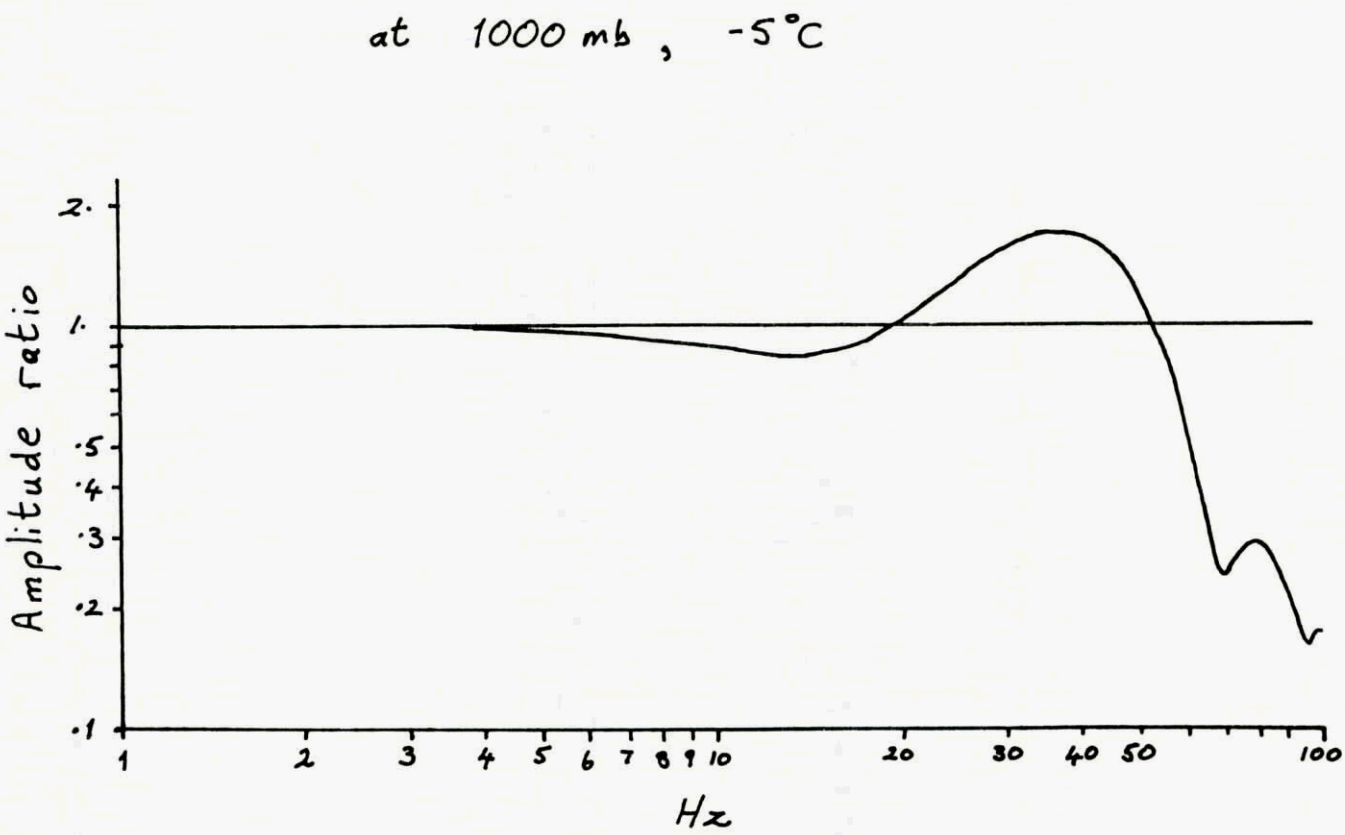

Fig 10 Typical frequency response of digital filter

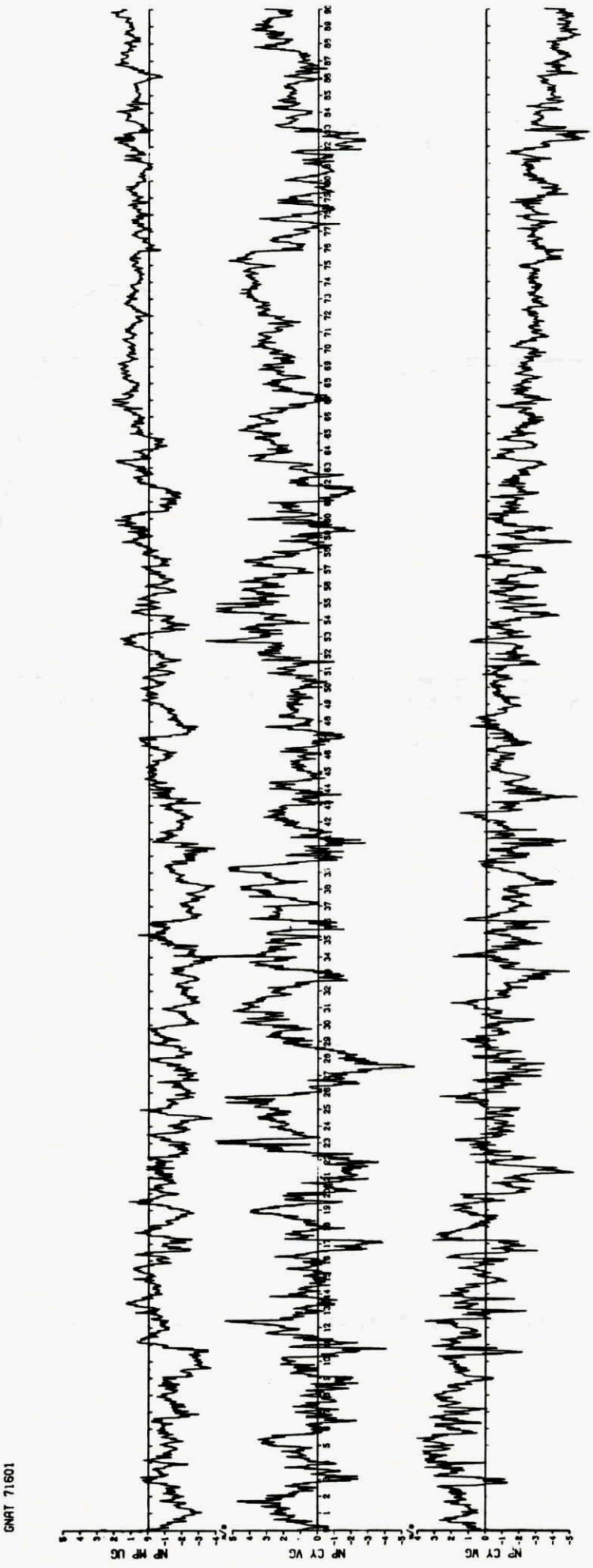

Fig 11 GNAT 71601 Three components of turbulence at nose probe - time histories

GNAT 71601 Ug component of turbulence. First second of run

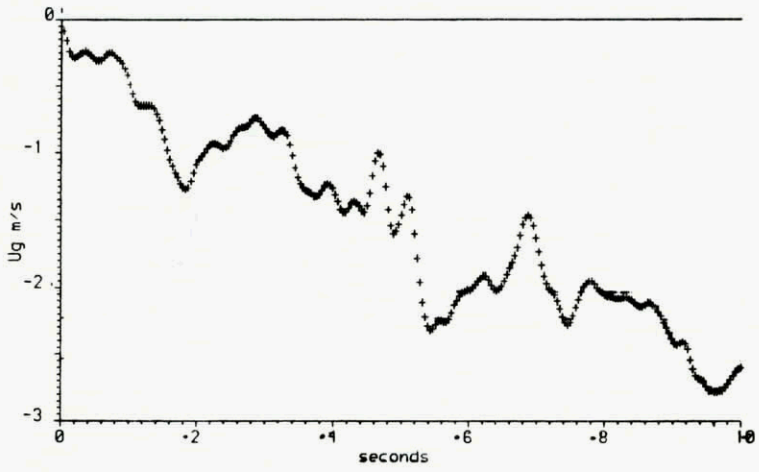

GNAT 71601 Vg component of turbulence. First second of run

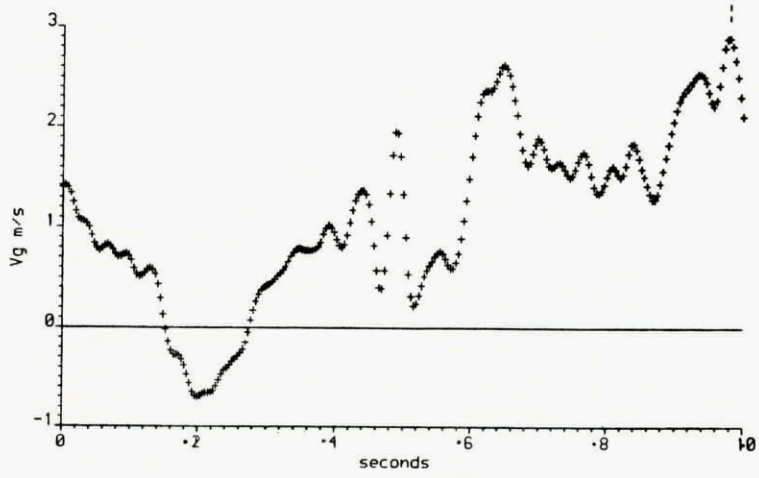

GNAT 71601 Wg component of turbulence. First second of run

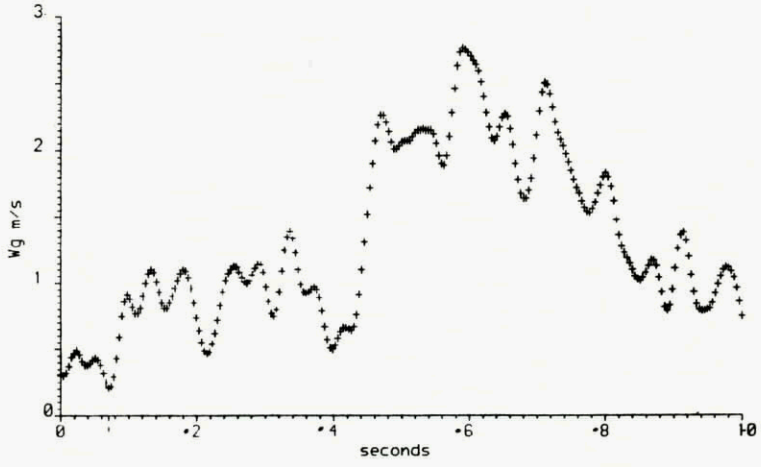

Fig 12 First second of GNAT 71601. Three components of turbulence - time histories

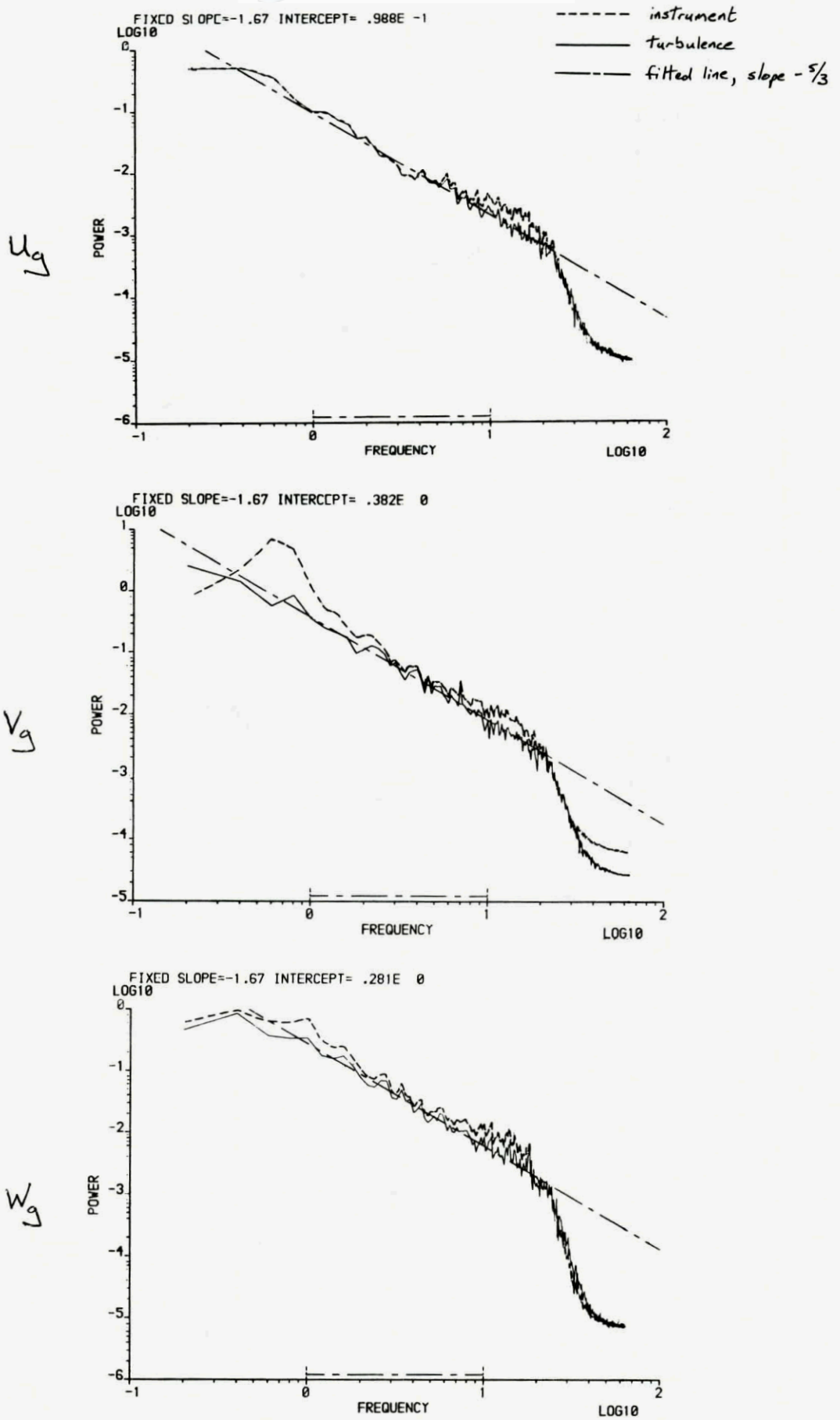

Fig 13a GNAT 71601 Comparison of instrument and turbulence power spectral densities

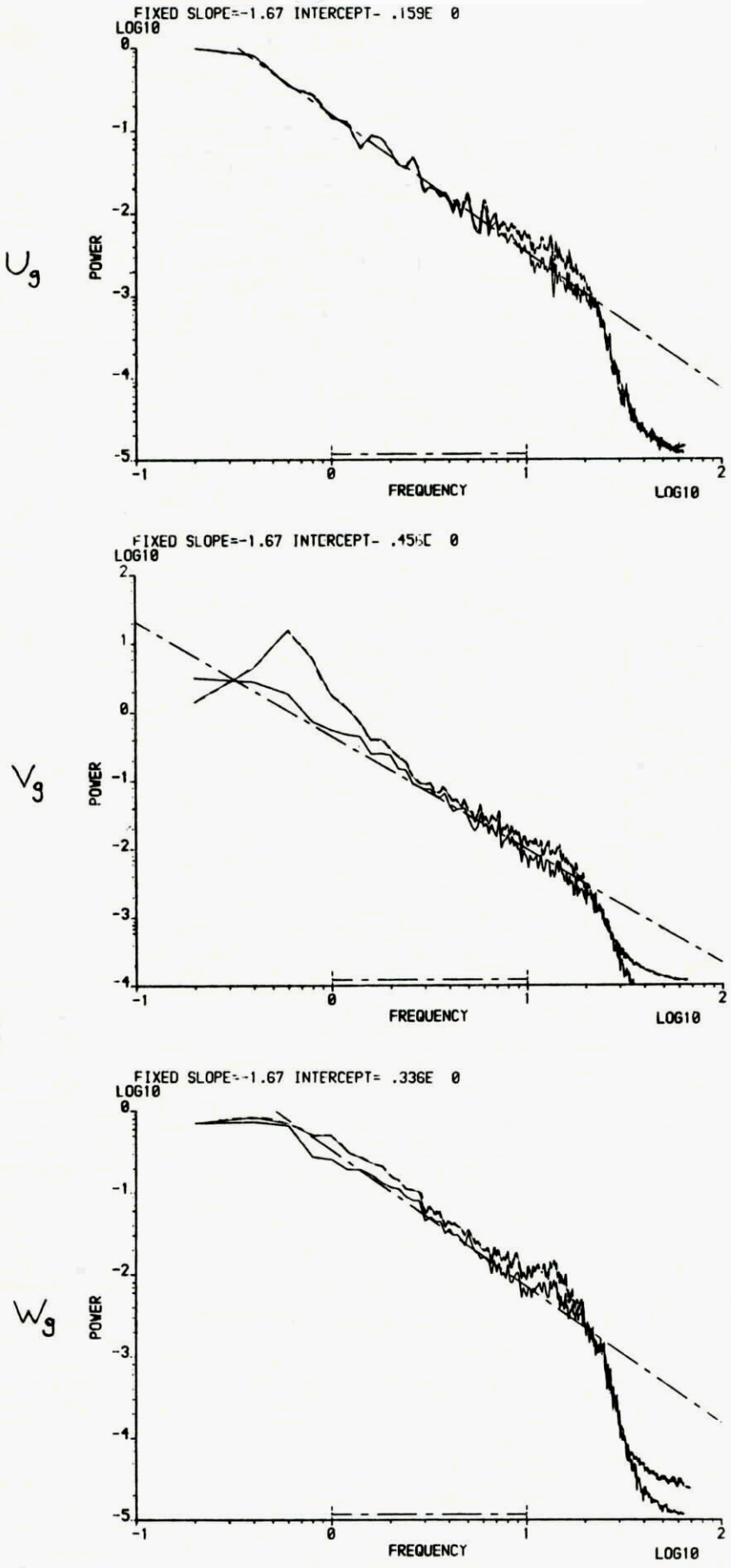

Fig 13b GNAT 71602 Comparison of instrument and turbulence power spectral densities

Across path components v_g and w_g

——— von Kármán $2\sigma^2 L \dfrac{1+{}^{8}/_{3}(1.339L\,2\pi K)^2}{\left[1+(1.339\,L\,2\pi K)^2\right]^{11/6}}$

..... Dryden $2\sigma^2 L \dfrac{1+3(L2\pi K)^2}{\left[1+(L2\pi K)^2\right]^2}$

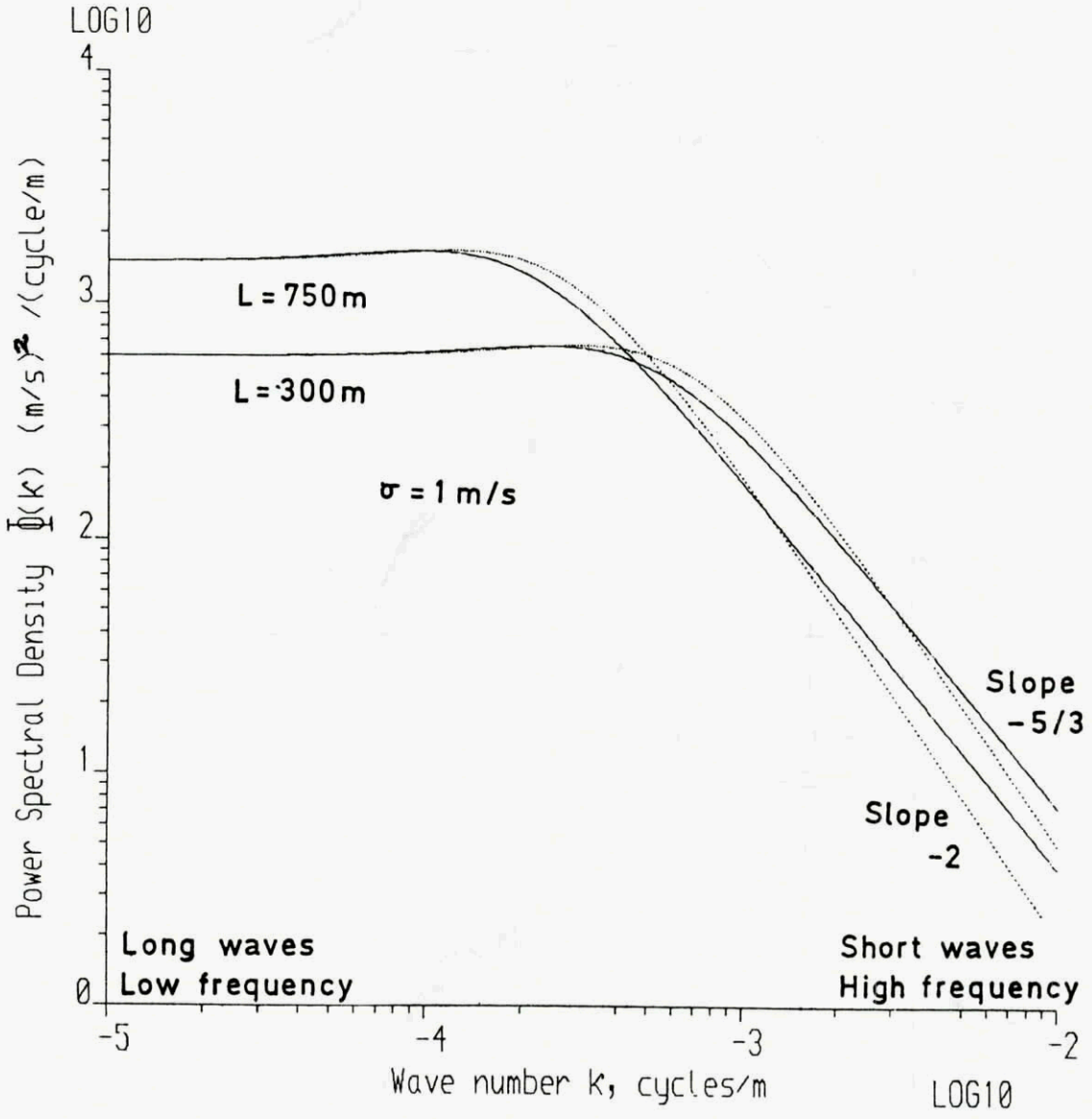

Fig 14 Theoretical forms for turbulence power spectral density

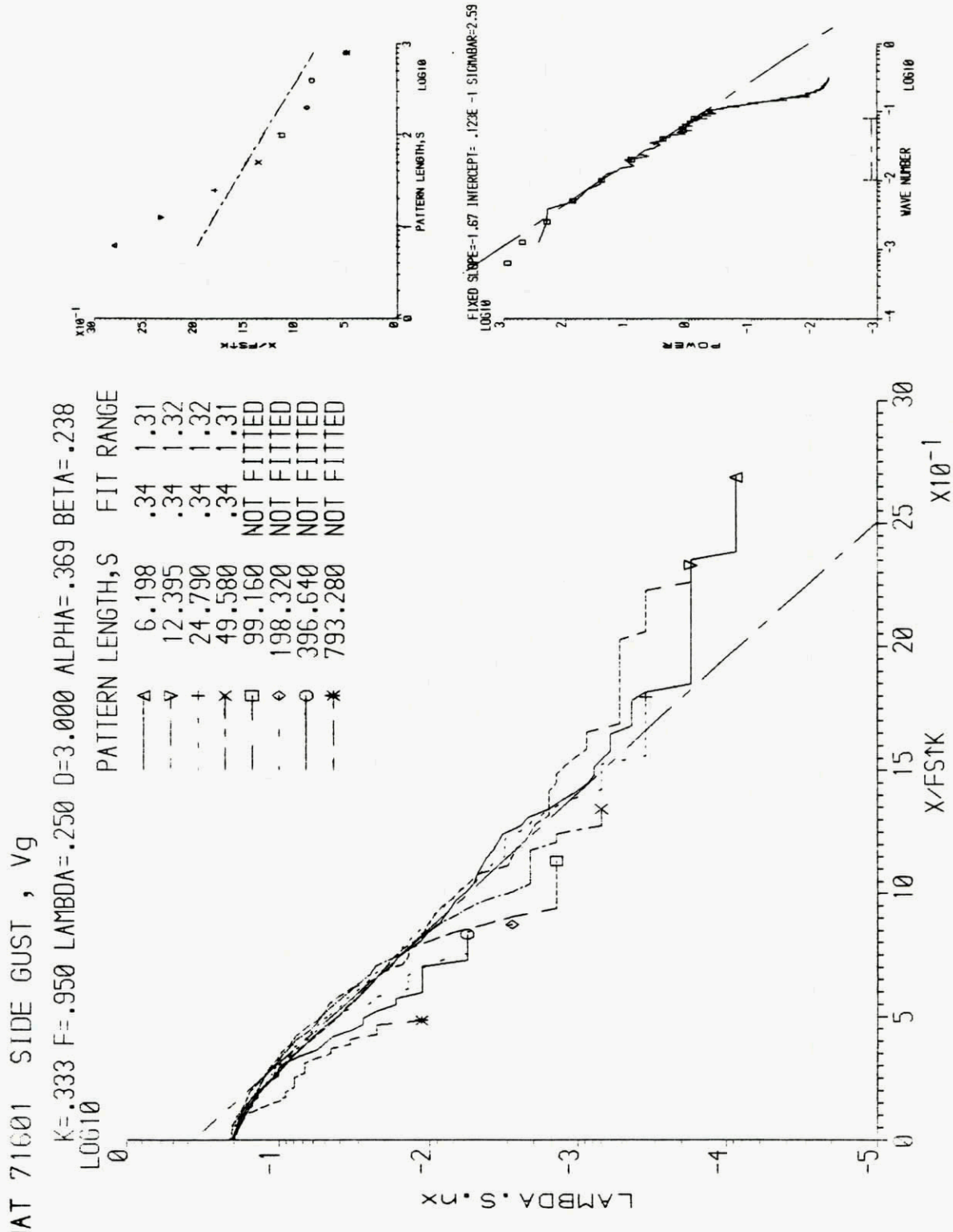

Fig 15 GNAT 71601 Summary plot of statistical analyses for vg turbulence component

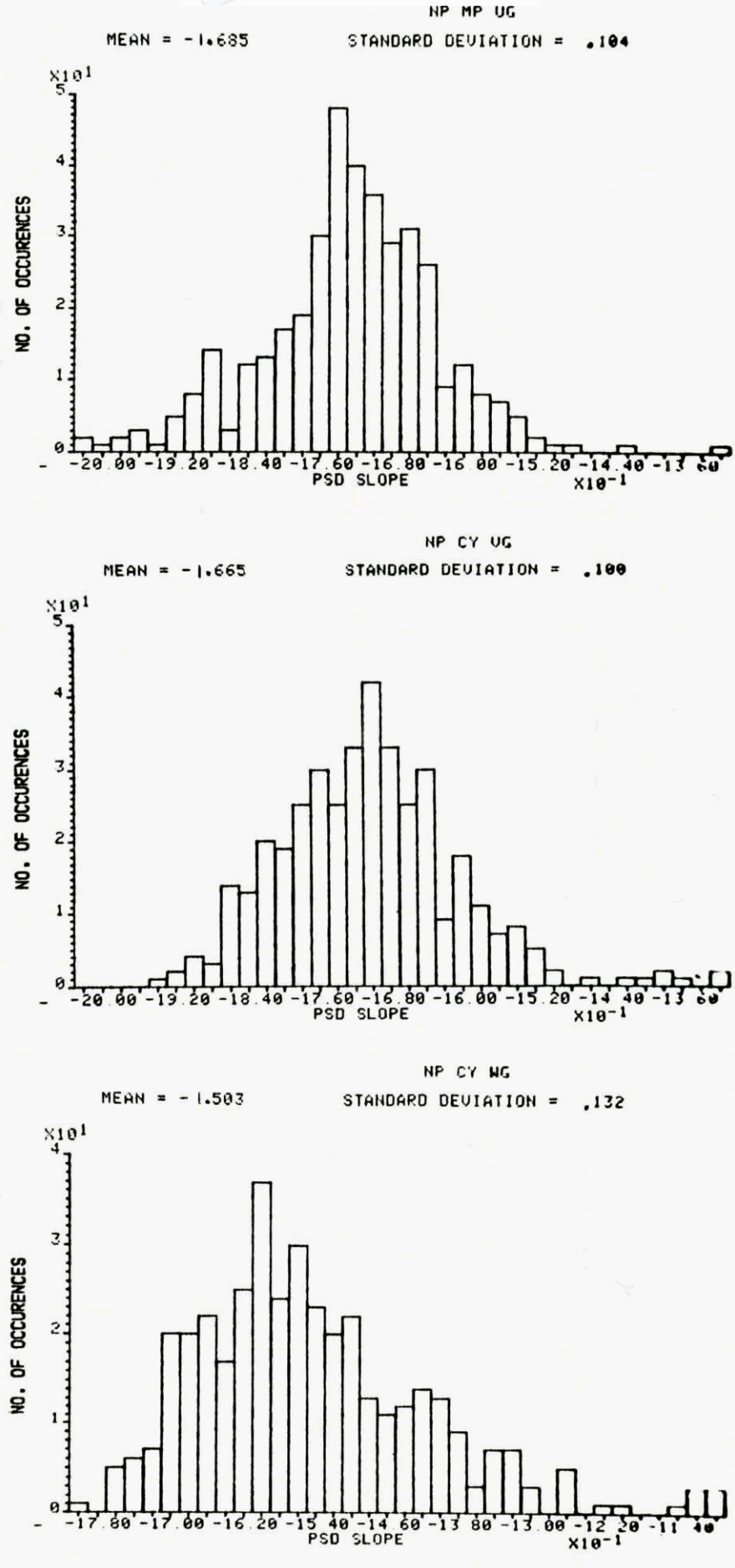

Fig 16 Distributions of fitted power spectral density slopes

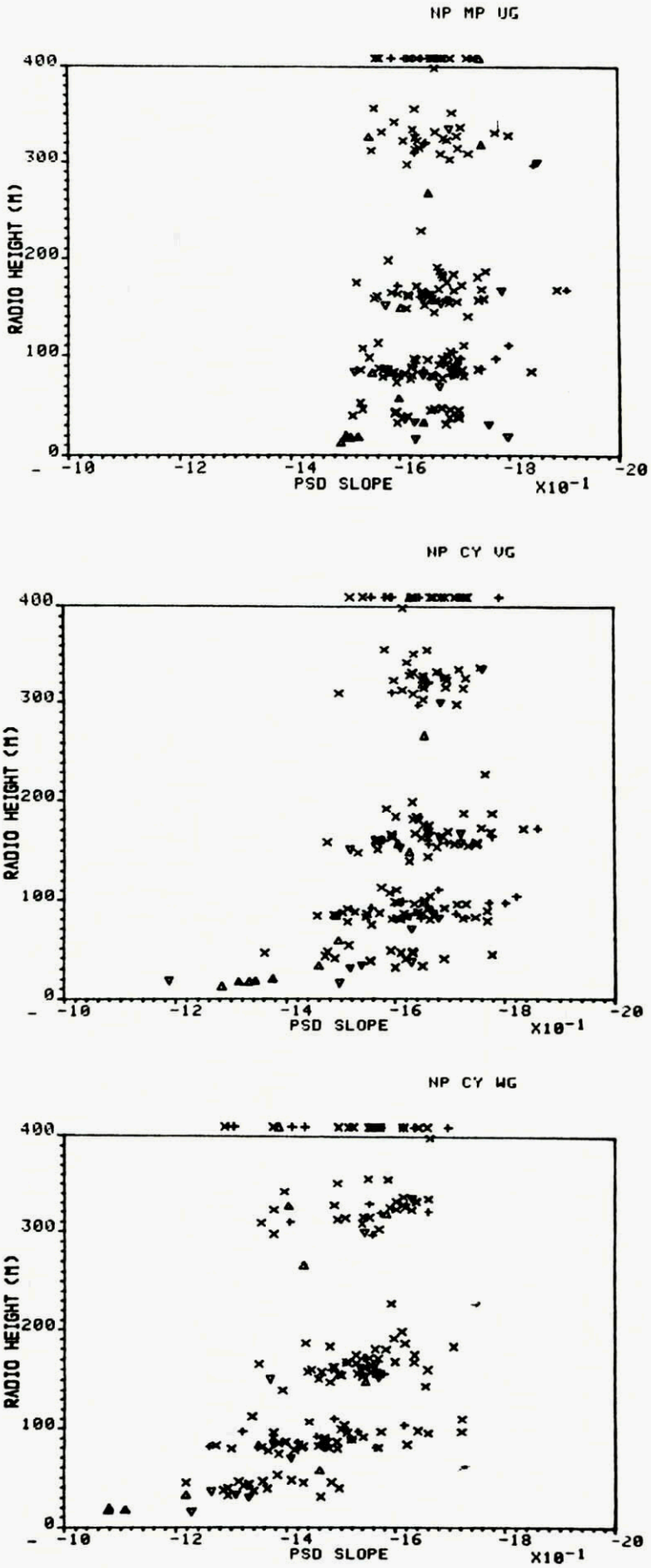

Fig 17a Variation of fitted power spectral density slopes with height; smoother terrains

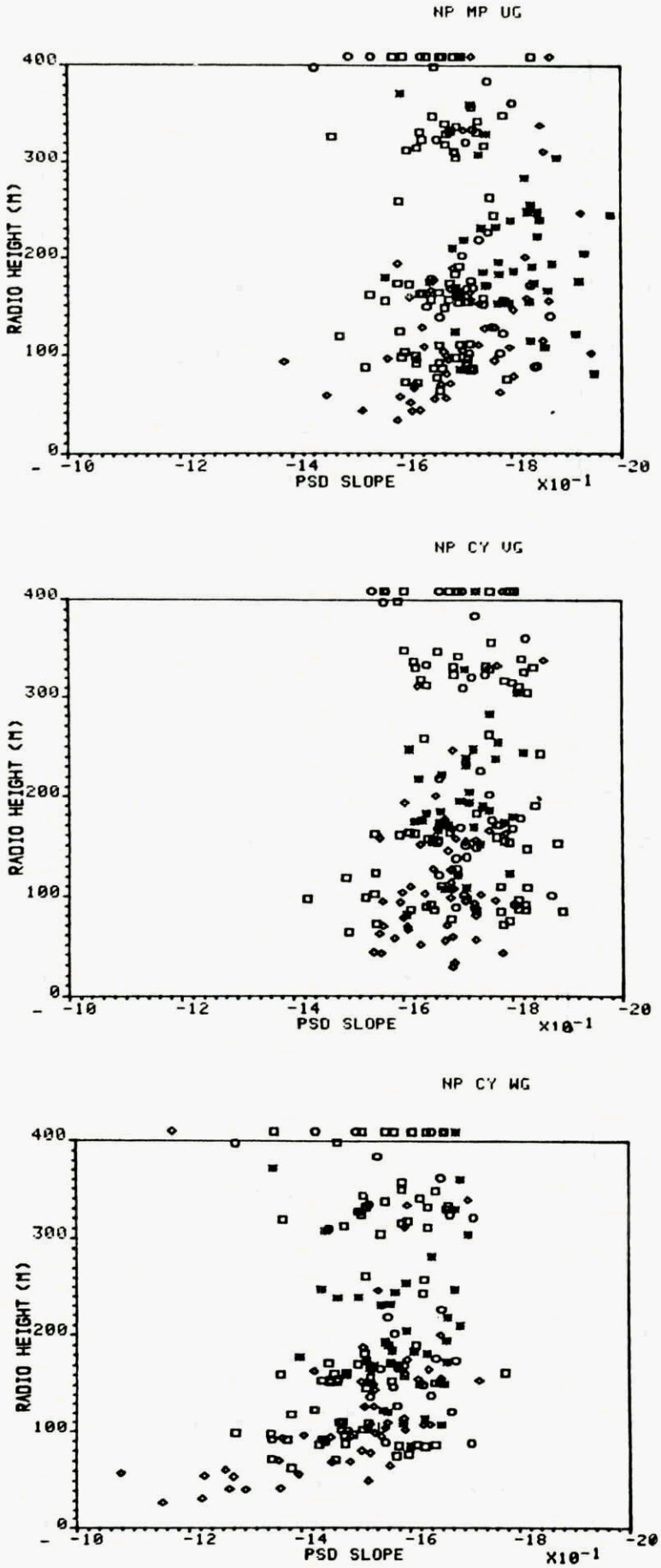

Fig 17b Variation of fitted power spectral density slopes with height; rougher terrains

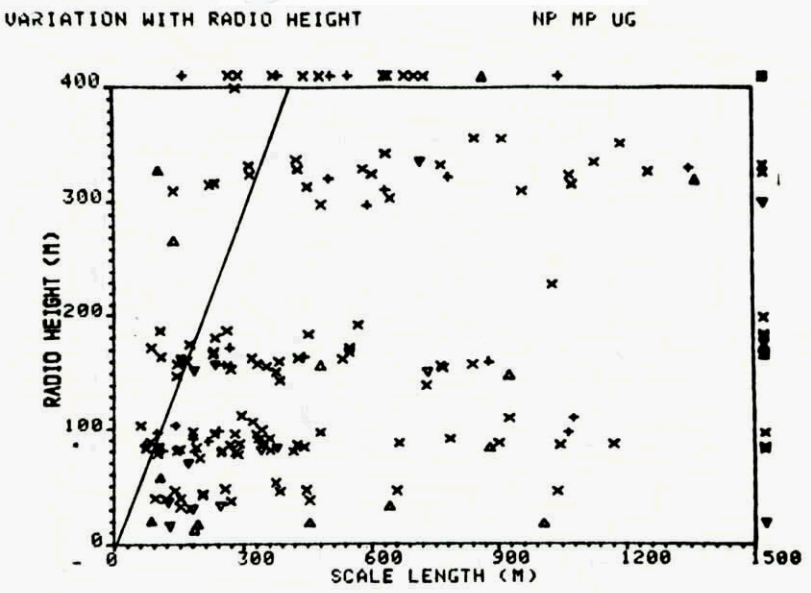

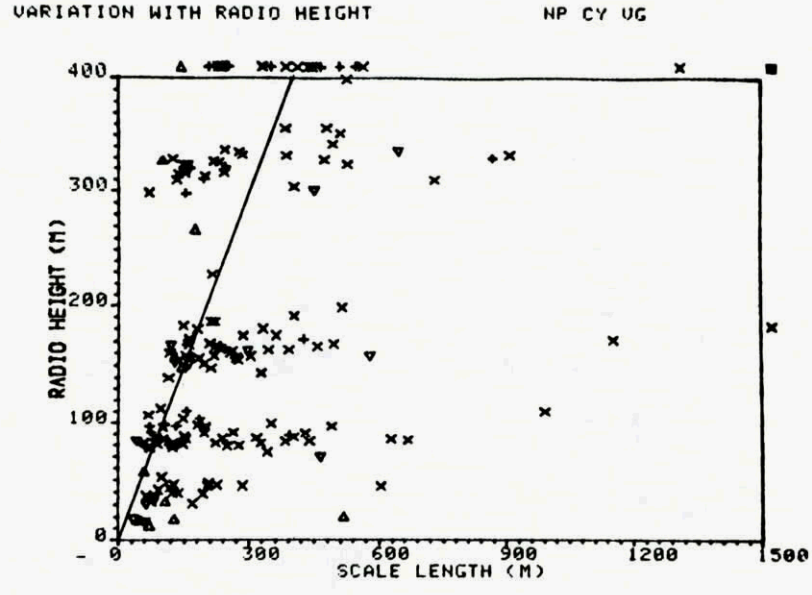

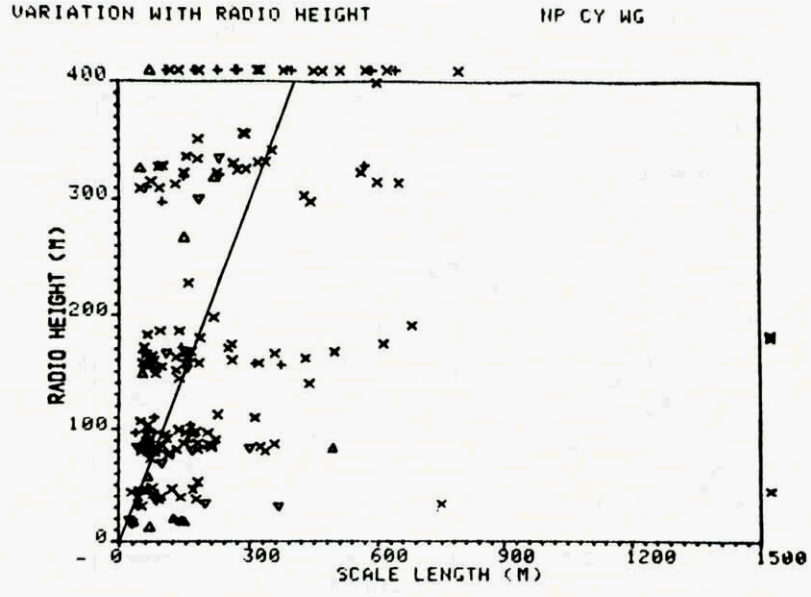

Fig 18a Variation of scale length with height; smoother terrains

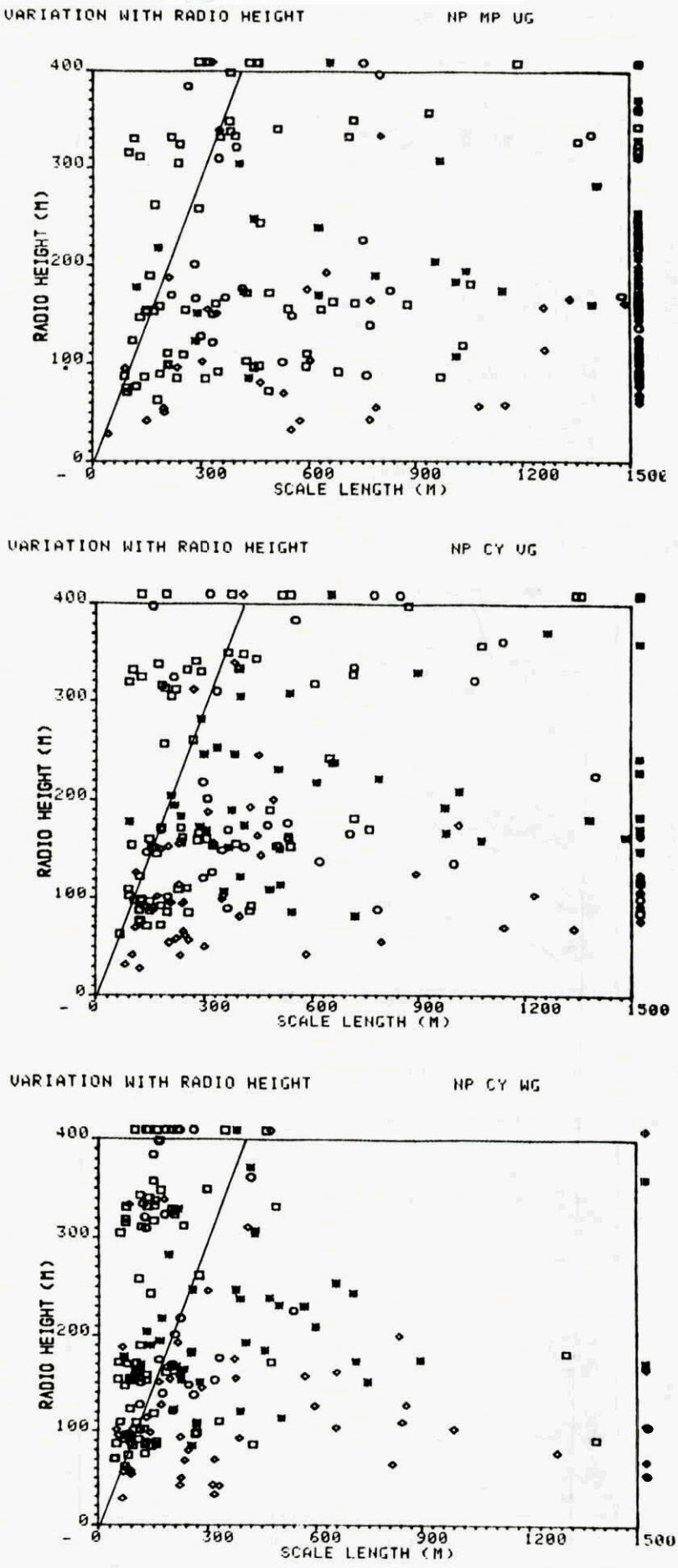

Fig 18b Variation of scale length with height; rougher terrains

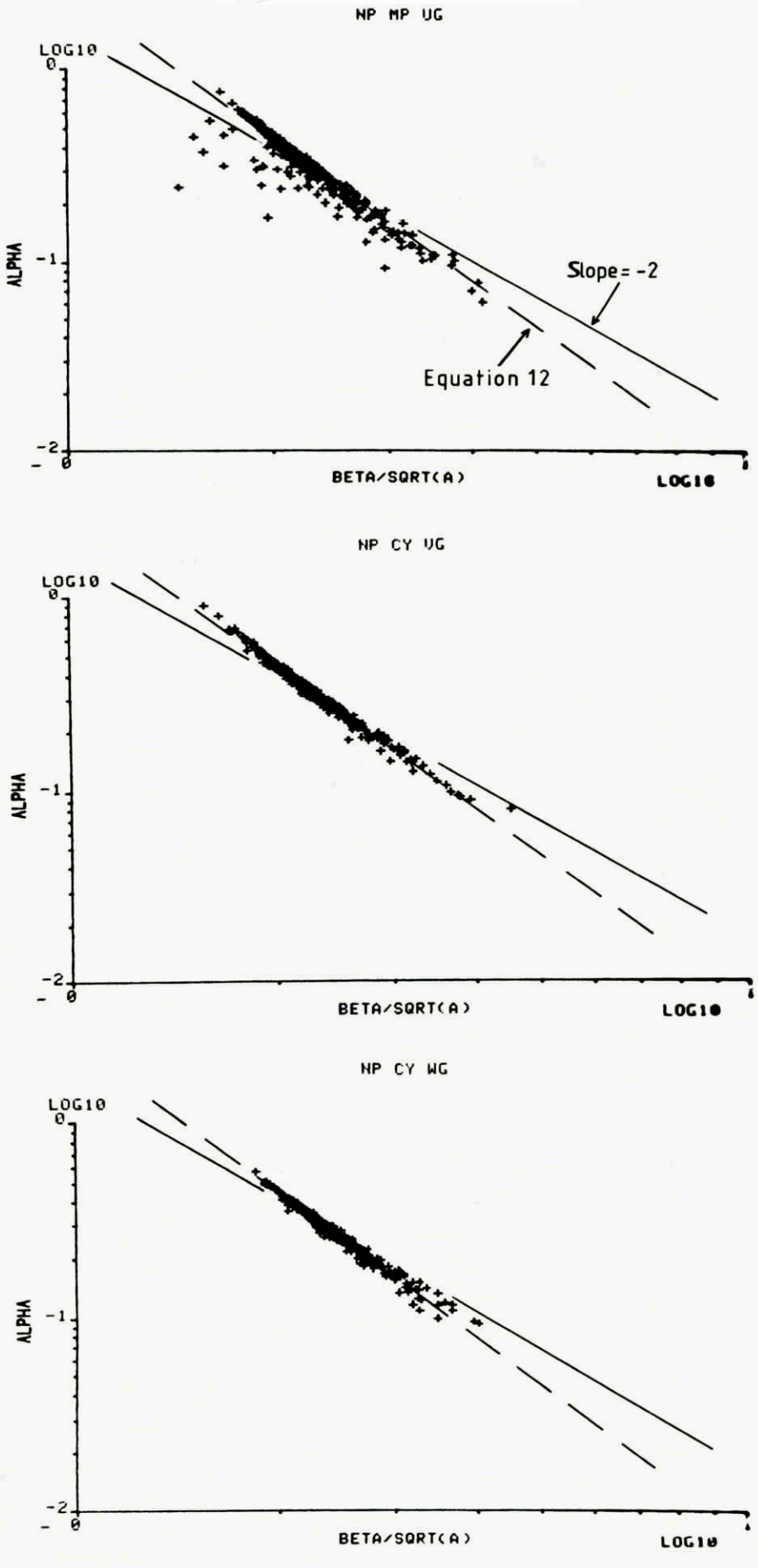

Fig 19 α versus $\beta/\sqrt{A}$, all runs, α & β from 1-4σ fitting ; 3 components

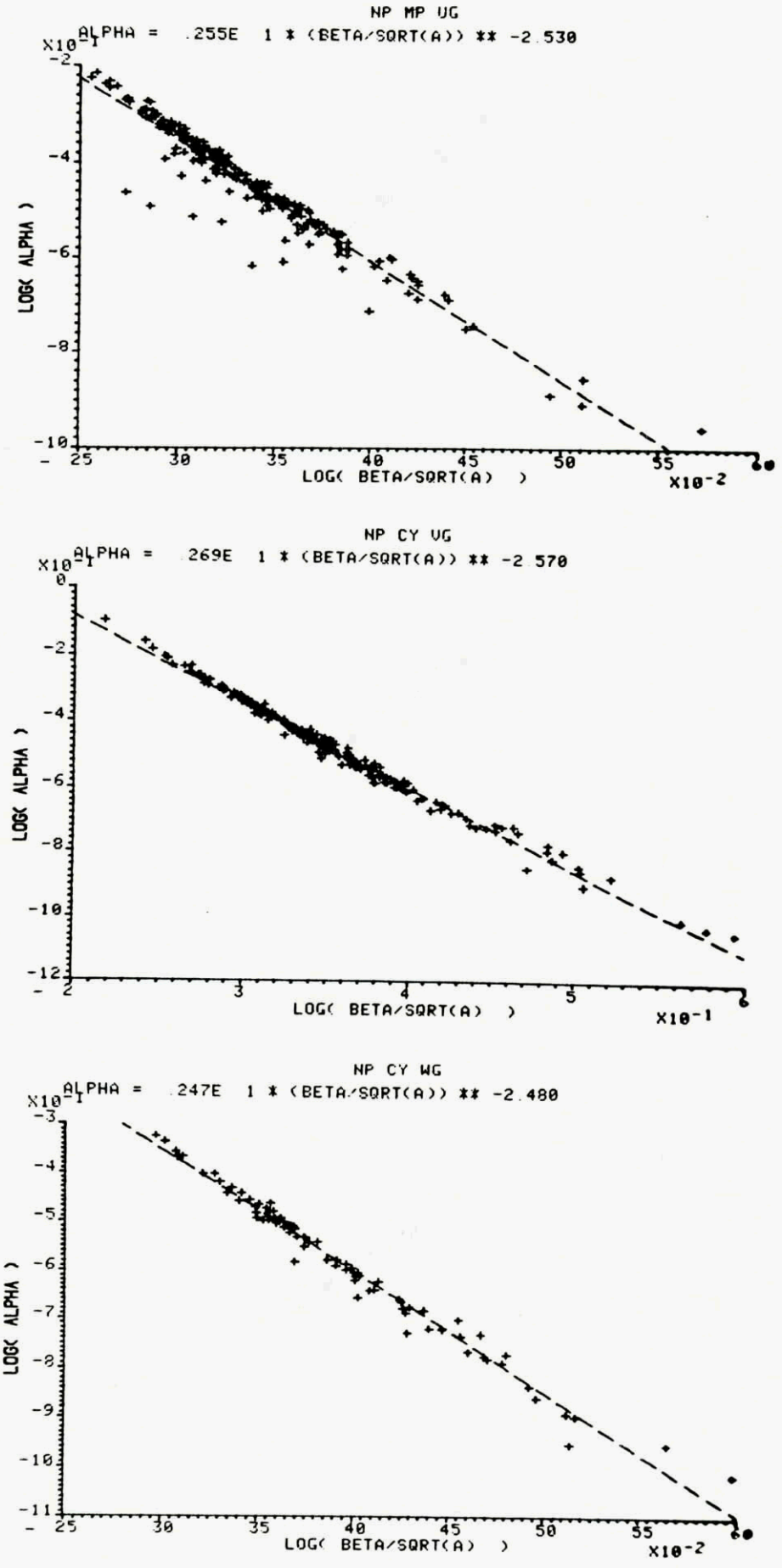

Fig 20 α versus $\beta/\sqrt{A}$, runs with PSD slope near -5/3, 3 components

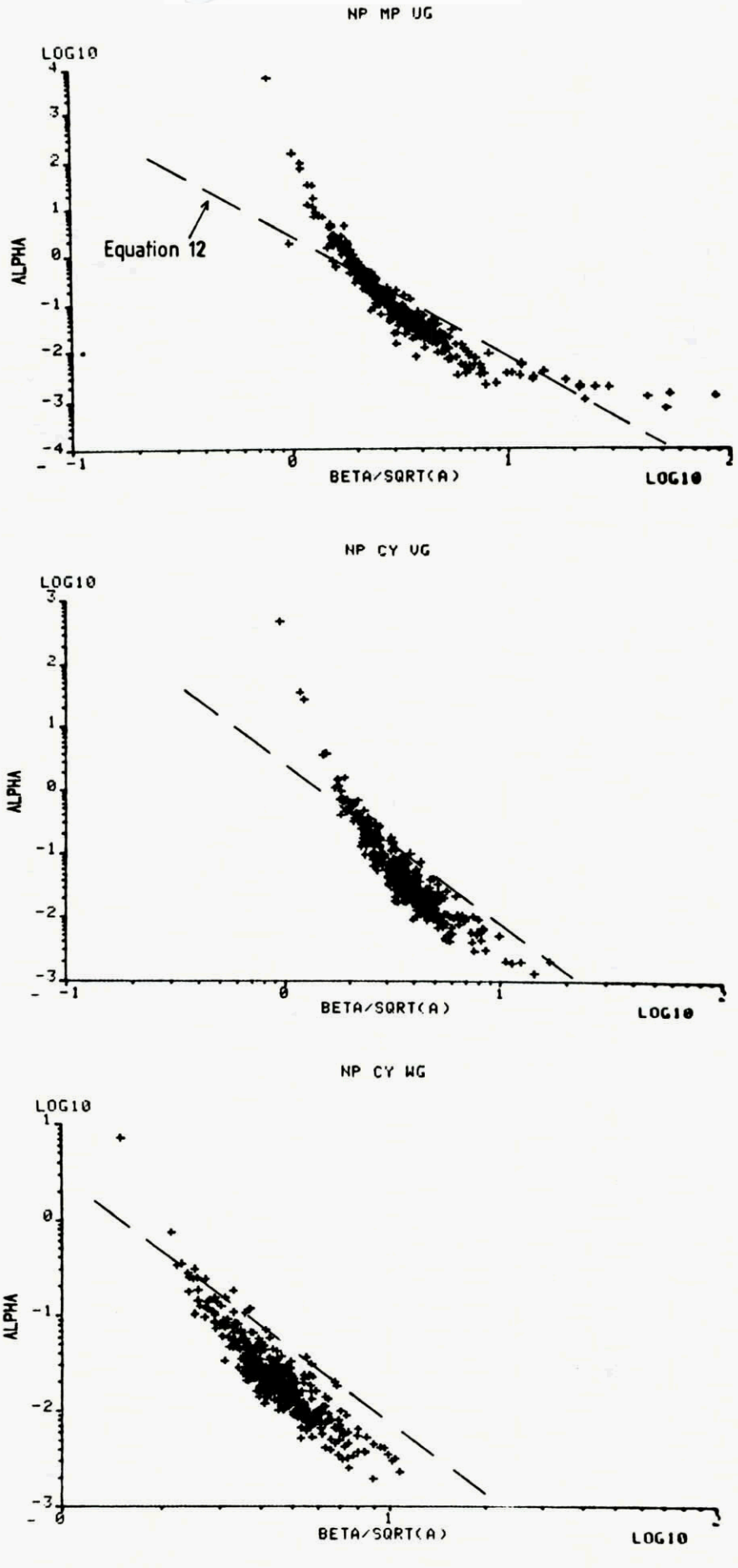

Fig 21 α versus $\beta/\sqrt{A}$, all runs, α & β from $>4\sigma$ fitting; 3 components

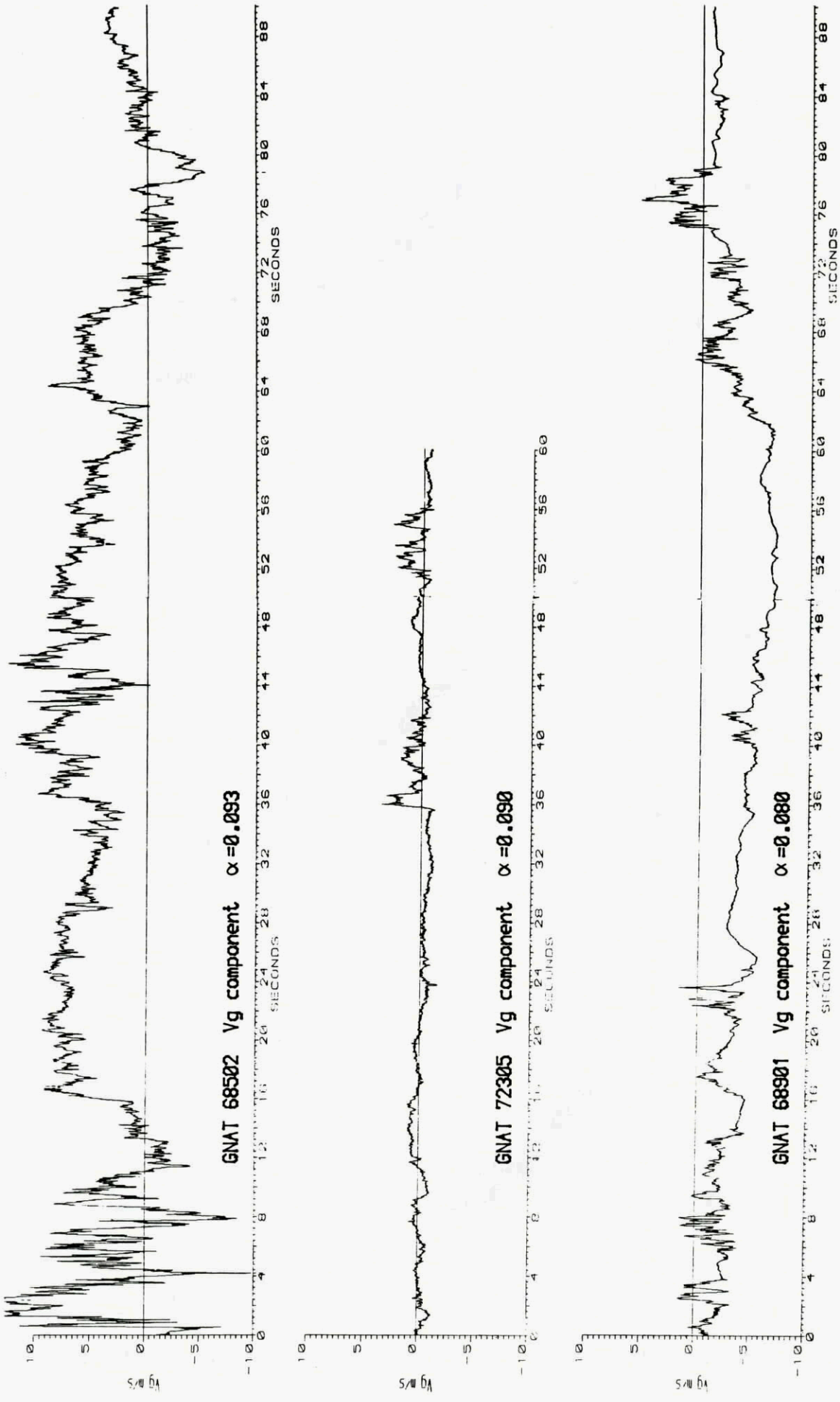

Fig 22 Three vg time histories which give lowest α values

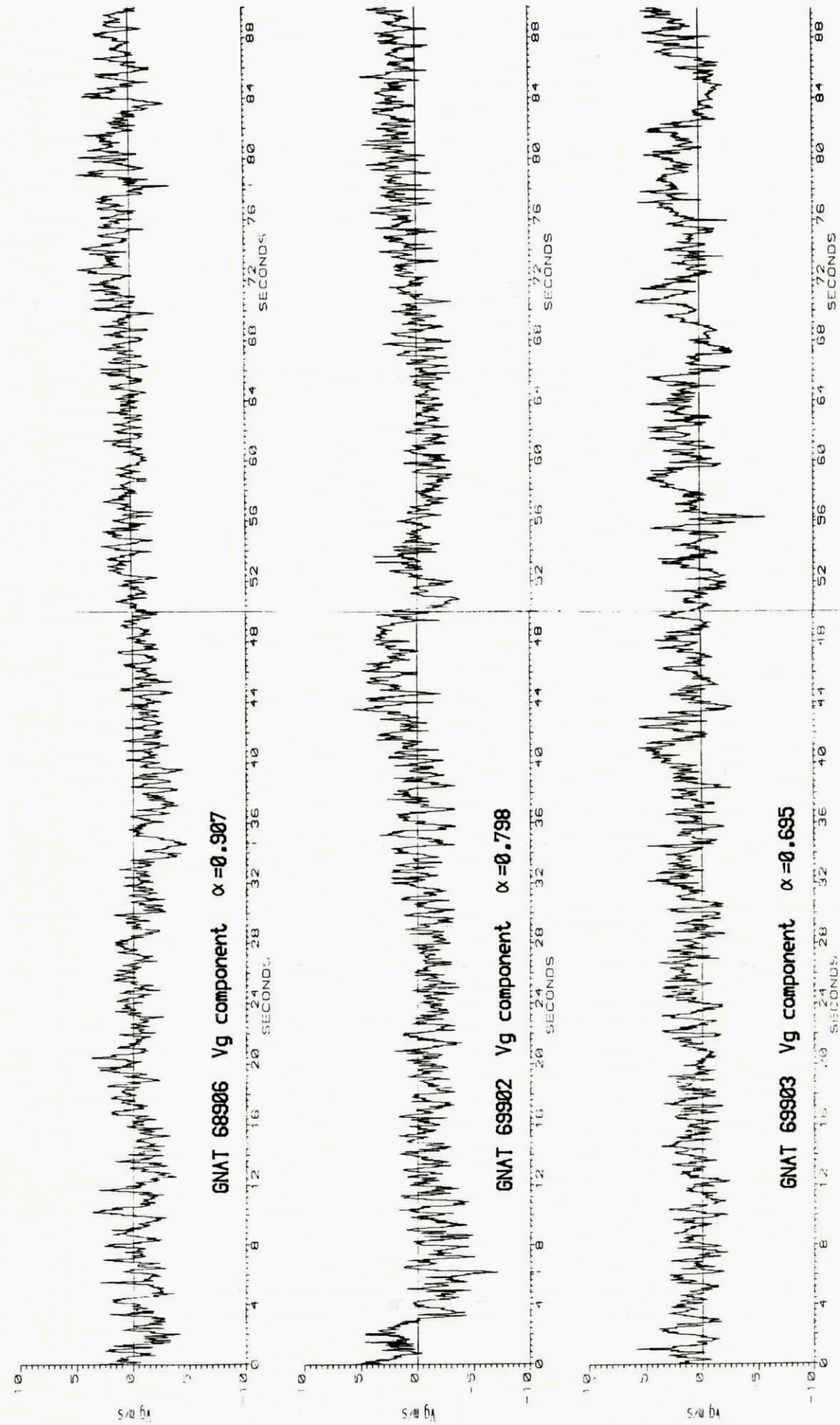

Fig 23 Three vg time histories which give highest α values

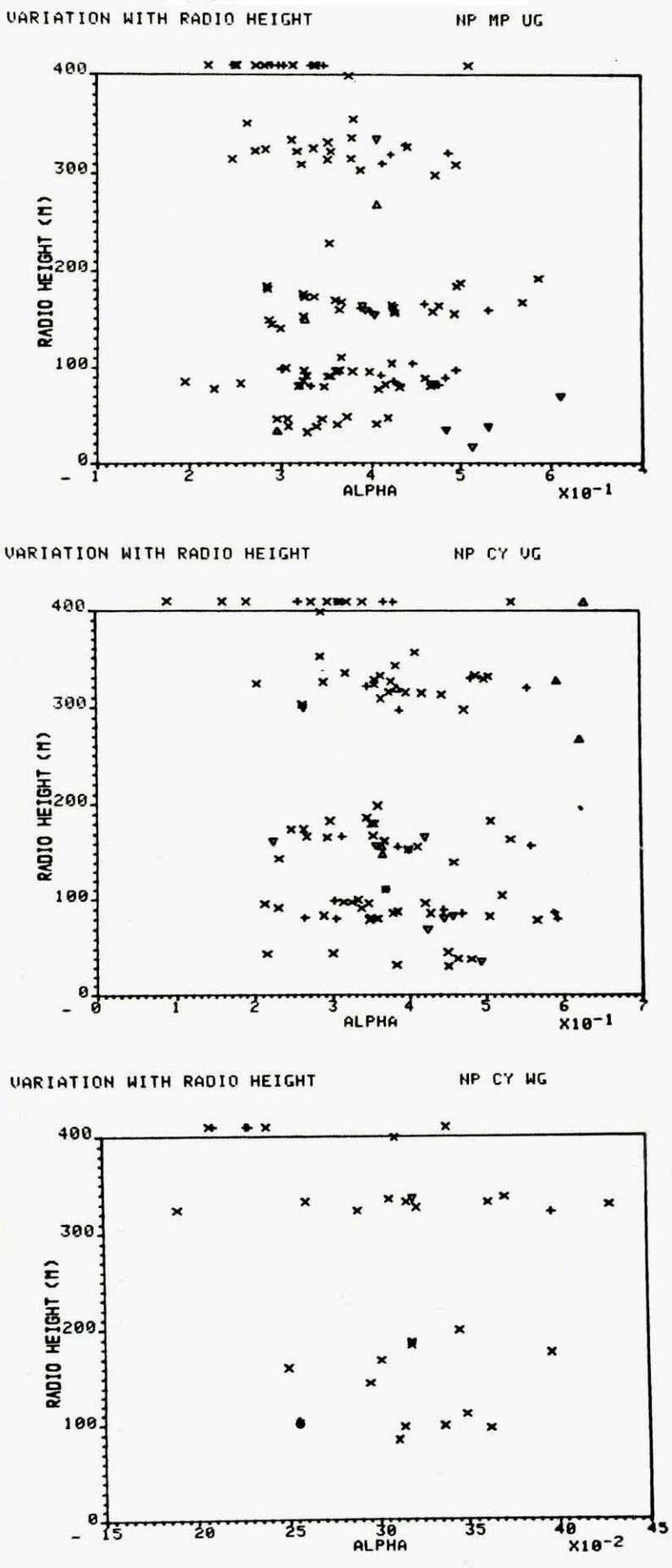

Fig 24a Variation of α with height; smoother terrains

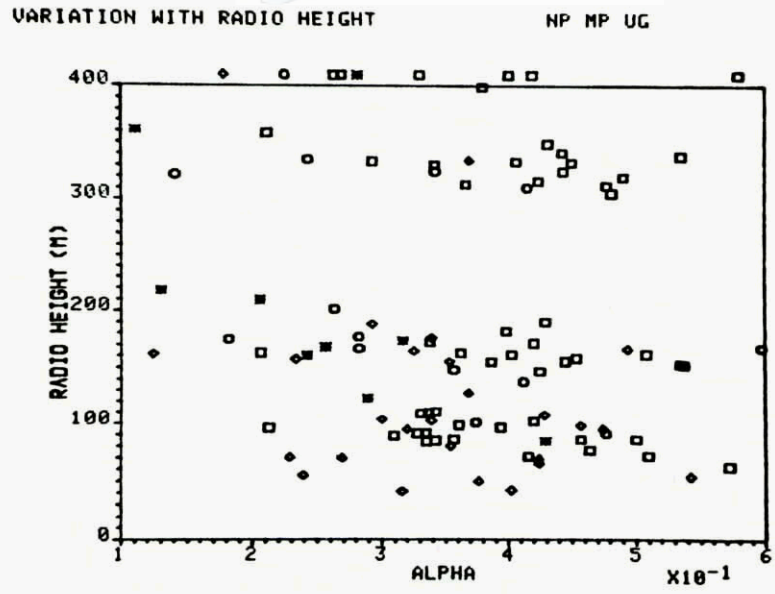

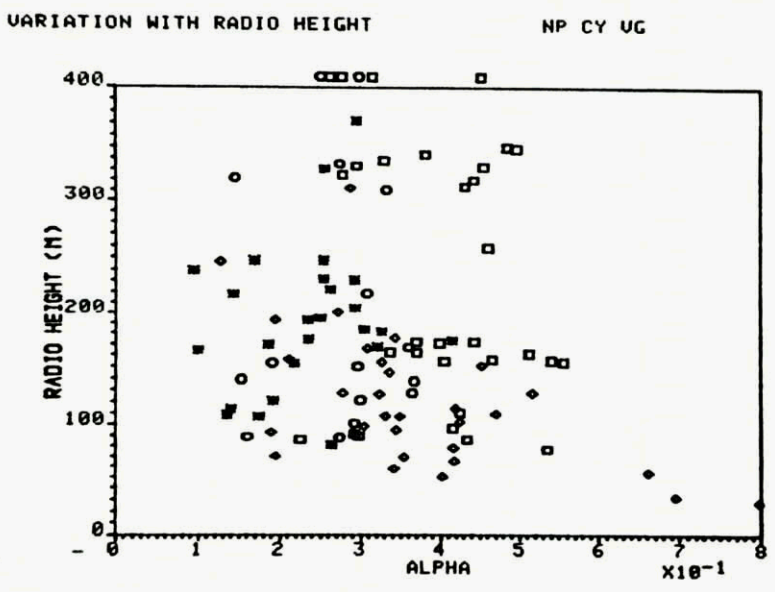

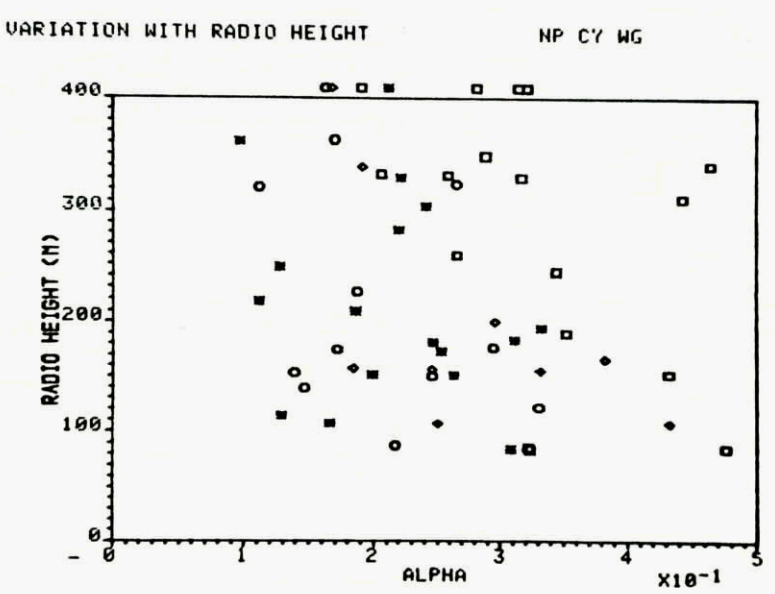

Fig 24b Variation of α with height; rougher terrains

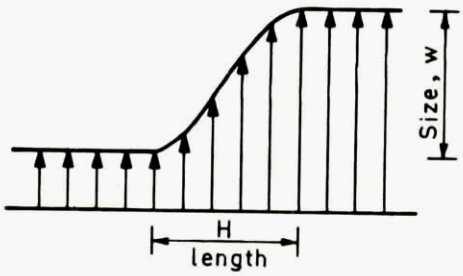

Fig 25 A ramp shaped gust

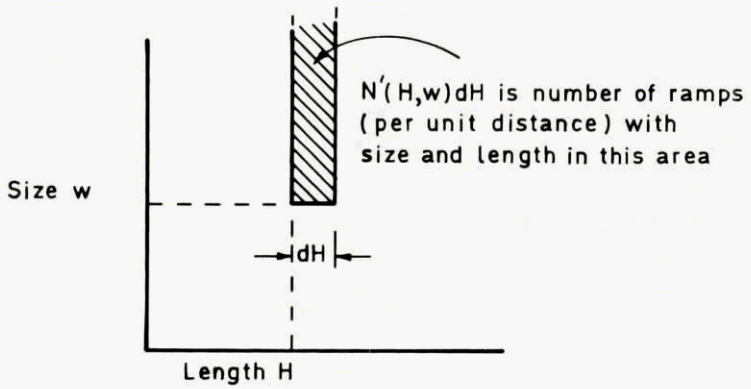

Fig 26 Definition of N'(H,w)

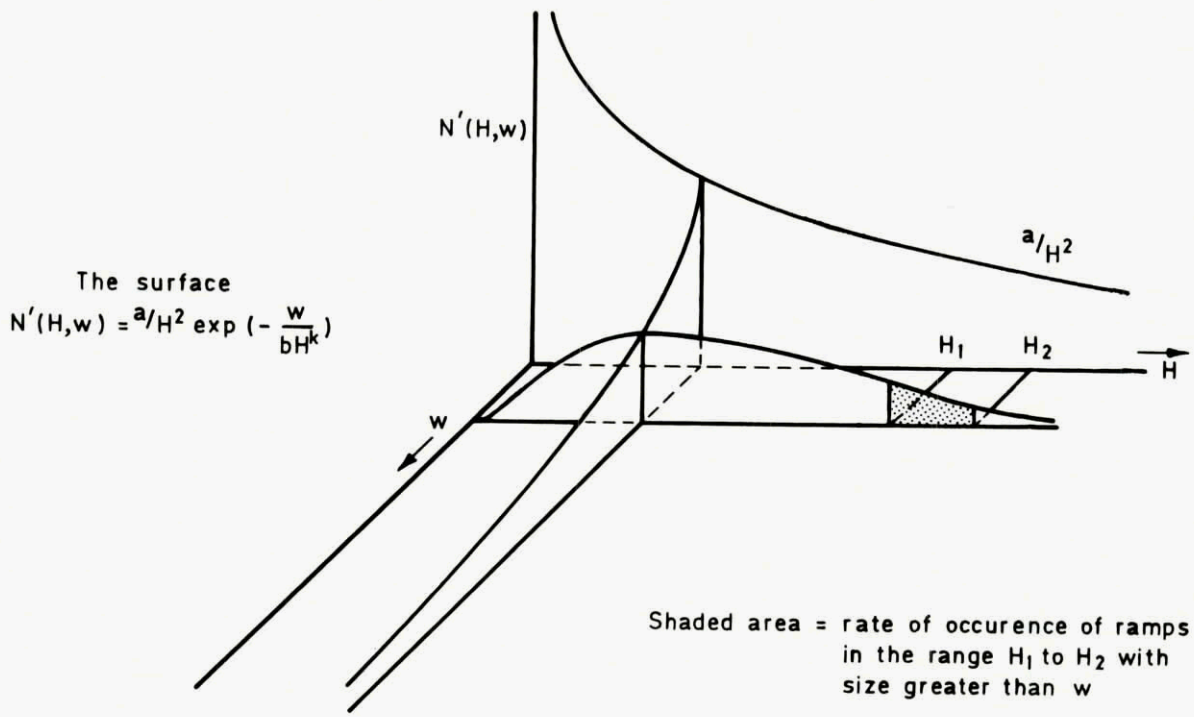

Fig 27 The surface N'(H,w)

AN INTERIM COMPARISON OF OPERATIONAL CG RECORDS IN TURBULENCE ON SMALL AND LARGE CIVIL AIRCRAFT

by

J.Taylor
Consultant
32 Limes Avenue
Camberley, Surrey
UK

Summary

Operational records have been made on British Airways aircraft for the period May 1980 to April 1985 and analysed for about 650,000 flying hours on a number of different aircraft. Records have been obtained for about 2 to 5 minutes of Normal Acceleration, Pitch Angle, Roll Angle, Height and Speed for nearly all those events which had an increment of 1g or more i.e. 29 events; similar records have also been obtained for nearly all those events with an increment of 0.5g or more with flaps down for the period May 1983 to April 1985 i.e. 33 events.

An interim examination of the 29 events with 1 excess g or more, with special emphasis on 15 of them (3 BAC 1-11, 2 737's, 3 Tristar and 7 747's), is made and includes an estimate of the interaction of manoeuvres and turbulence, an estimate of the frequency of occurrence of high level intensity gusts and of the equiprobability relationships of gust levels and gust gradients. It is found that gusts that are important for a particular response are strongly dependent on the rate per 5 Km at which zero crossings occur in that response. Using the Kaynes[5] formulae for gust intensity and zero crossings it is found that the equiprobability relationships of gust levels and gust gradients can be represented on a single diagram for all sizes of aircraft at all heights.

This work was done as a Contract with British Aerospace under the excellent supervision of Mr H Hitch.

1. Introduction.

As a result of the arrangements made on 3 Oct 1983 for British Airways to supply British Aerospace with SESMA Events 23B "High Normal Acceleration Flight" and further arrangements with CAA on 25 Aug 1986 a total of 62 events have been made available for the present investigation. The total of 62 listings is made up of 29 with an increment of 1g or more (2 Trident, 5 BAC 1-11, 3 B737, 2 B757, 5 Tristar and 12 B747) for the 5 year period May 1980 to April 1985 and 33 with an increment of 0.5g or more with flaps out (2 B757 and 31 B747) for the two year period May 1983 to April 1985. All the data from these listings of height, speed, pitch angle, roll angle and normal acceleration at the CG has been copied on to floppy discs to be used in the complete investigation.

This paper is an interim report and is based entirely on the data from the 29 events with an increment of 1g or more, and especially on 15 of them; it is complementary to the paper[1] by G.Coupry, which is based on all the peaks with an increment of 0.5g or more for the same 5 years. In order to facilitate this presentation, it, for the most part, omits the data from the Trident and B757 to conform with Coupry's main comparison of B747, Tristar, BAC 111 and B737. Table 1 is an extract from reference 1 and shows the total hours analyzed on these 4 aircraft.

An essential requirement for the description of turbulence for modern aircraft, especially those that are relying on active controls for gust load alleviation (GLA), is that the gust patterns shall be identified in addition to retaining an adequate description of the intermittently continuous nature of the turbulence. Neither discrete gust types nor spectral types of current requirements give an adequate description of the turbulence. Whilst spectral procedures are of a form that is suitable for calculating standard deviations of responses from standard deviations of continuous turbulence no information is normally available of the nature of the individual gusts. In this respect they are deficient for GLA aircraft and requirements, additional to those covered by the spectral requirements, are needed. Whilst discrete gust requirements use gust shapes in their basic procedures, the development of them to cover continuous turbulence has not resulted in a sufficiently precise description of relationships between peaks and gradient distances for GLA aircraft.

Early in the development of discrete gust requirements it was appreciated that the aircraft properties were important in defining the gust shape that produced the gust loads and the gust gradient was defined in terms of chord lengths. More recent[2] work indicates that an important characteristic is the rate at which zero crossings occur, which means that a reliable method of determining the number of zero crossings is required. This recent work uses a spectral method of describing continuous turbulence that is of a form suitable for making a study of the the nature of the individual gusts. The distributions of gust velocities and a number of aircraft responses were examined together with the distributions of their derivatives. All were found to have the following probability density.

$$U(x_1) = (1/\sigma^2\pi)^{1/2} \int_0^1 \exp(-x_1^2/4\sigma^2 x^2)\,dx \qquad \text{----------(1)}$$

where $U(x_1)$ = the probability density of x_1

σ^2 = the variance of x_1

(equation 11 of Reference 2)

It was found that the distribution of the levels crossed for the variates were appropriate to that, that would occur when the variate and its derivative were independent. In order to give more confidence in calculated values of zero crossings, the measured data from a T33 and from a Canberra that were used in reference 2 was subjected to a stricter test for independence in reference 3. It was found for both aircraft that for vertical gust velocity and for normal acceleration at a point near the CG of the aircraft the correlation coefficient between each parameter and its derivative was very small; procedures for obtaining relationships between peaks and gust gradient distances were developed from the T33 and Canberra data and will be used on the British Airways data for the 5 year period.

2. Time-Histories.

Whenever there is known to be an error in the original recordings the line where it occurs is identified by inserting a minus sign before the frame number and as the errors may not be in the data that is being used it was decided to plot the records to check for drop-outs before rejecting data. This method was used[2] successfully on the CAADRP special events of British Airways, where the number of drop-outs was large.

Preliminary plots were made near those frames that were known to have errors. These errors were negligible in Events 2122, 7406, 4215, 3273, 0849, 3007, 3840, 1195 and 4178. They were serious in 3427 and 1692. For

those in which the errors were serious all the frames identified as having errors are omitted in the plots of pitch angle, roll angle and normal acceleration at the centre of gravity of the aircraft in Figure 1A-G for the whole record of each of the SESMA Events with an acceleration increment of 1g or more. The errors in Event 1692 occur such a long time before the start of the turbulence that simple interpolation of the records to replace the errors would have a negligible effect on any results obtained.

A visual examination of Figures 1A-G suggests that in addition to the frames that were identified as possibly containing errors there were 2 other events that appeared to have drop-outs. These are in the g record of the Tristar in Event 2854 and in the pitch record of the Tristar in Event 3427. The drop-out in 2854 is a single reading and is replaced by a simple interpolation. There are so many frames identified as containing errors in Event 3427 that the whole record must be regarded with suspicion and is therefore not used in this paper. For this interim report a further 13 of the remaining 28 events are omitted as follows:

2 Tridents and 2 B757's (Events 4882, 3420, 2514 and 4100) so that the comparison will be on BAC 111, B737, B747 and Tristar as in Ref. 1.
4 Events for which the weight of the aircraft is not known (Events 3938, 3273, 1521 and 2122) to avoid an error due to the possibility of a bad estimate of the weight.
2 Events that are of much longer duration than the others (Events 1195 and 4178): examination of the records of Event 4178 shows that the maximum g increment is slightly less than 1g i.e. 0.96g. However both Events should be of considerable value for the full Report.
3 Events that are of short duration (Events 7099, 4887 and 3120) in which the total number of gusts involved would not appreciably affect any results obtained without them.

3. Procedure for determining gust peaks and their gradient distances.

The gradient distance is estimated from a knowledge of the derivative. The procedure for calculating the derivative at a point is the same as the one used in Reference 1; the cubic through the two points each side of the point under consideration is calculated and the tangent at the point is taken to be the gradient at that point.

The peaks are identified as the highest magnitudes between successive zero crossings thus requiring the nomenclature of +ve peaks and -ve peaks. An empirical procedure is used to calculate the gradients of these individual gusts. For the purpose of Design Requirements it is convenient to assume a gust shape of (1 - cos) so it was decided that the gradients should be chosen so that any coefficients that were used in conjunction with the peak magnitude and the maximum derivative would be identical to those for a (1 - cos) shape. Thus for normal acceleration

$$H = (\pi/2)(G_{max}/\dot{G}_{max}) \quad \text{----------(2)}$$

where
H = the gradient distance.
G = the range of normal acceleration from the appropriate trough.
$\dot{G}$ = the rate of change of normal acceleration with respect to distance.

For a gust sequence made up entirely of gusts of (1-cos) shape, each starting at the 1 G datum, with no gaps between gusts and alternately +ve and -ve peaks the average gradient distance H would be 1/4 of the

average distance between zero crossings in one direction i.e. 4HN(0) = 1. For the condition in which each trough has the opposite sign to its associated peak, the average would be 4HN(0) = 2. It seems appropriate therefore to present the data in the non-dimensional unit 4HN(0); it is convenient to regard 4HN(0) = 1 as standard, as the H would correspond more directly with that used in current Design Requirements. For convenience in grouping data at different heights, H is given in metres X (square root rel. air density).

Having identified the peaks a decision has to be taken on which maximum derivatives should be associated with the entry to, and exit from the gust and also the value of the appropriate troughs. To facilitate making this decision, 4 seconds of the more intense turbulence in each of the T33 and Canberra time-histories of gust velocity and CG normal acceleration were selected[4] for special examination. A number of procedures were tried and the following is the one that appeared to be the most consistent and the most likely to give similar values for the gradient distances of the vertical gust velocity and for normal acceleration at a point near the CG of the aircraft.

A. Choose the largest magnitude of the derivative that occurs at the the peak or between it and the time that the derivative passes through zero.
B. Choose the largest range from peak to trough with the same restrictions.

4. Relationship of peaks and ranges and gradient distance.

The response of normal acceleration near the centre of gravity of the aircraft is such that when the oscillations due to structural vibrations are removed the cumulative distribution of peaks does not differ much from that for the level crossings. This is achieved in the plots of peaks and gradient distances by replacing all troughs with the same sign as their associated peaks by the datum value whilst retaining the same gradient. The distribution of level crossings is given by

$$N(x_1) = 4/3(1/2\pi)(\sigma_D/\sigma)\int_0^1 \exp(-x_1^2/4\sigma_x^2)dx \quad \text{----------(4)}$$

(equation 14 of Reference 2)

Different aircraft have different zreo crossings N(0). It seems however from the considerations presented in paragraph 3 that the non-dimensional parameter of 4HN(0) should give an opportunity of comparing different aircraft. The variation in zero crossings will also depend on the presence of long wavelengths, particularly for the low levels of turbulence. The long wavelengths will have less effect on the higher levels of peaks and also there will be a greater overshoot of the troughs and less variation in distance between zero crossings. Thus for the reasons given in paragraph 1 above, it will be more likely for the average of 4HN(0) to be nearer 2 than 1. It should be noticed that the values of the zero crossings of x_1 are given by putting $x_1 = 0$ in equation (4), which reduces to

$$N(0) = 4/3(1/2\pi)(\sigma_D/\sigma) \quad \text{----------(5)}$$

This equation (5) will be used to calculate the zero crossings N(0)for the recorded time-histories. It is identical to that normally given in terms of the spectral density.

5. SESMA Records.

5.1 Kaynes Response Factors

The records that have been taken from the listings of SESMA Events include the weight of the Aircraft at the time that the maximum increment of g occurs. The records are tabulated in successive frames, each for one second; each frame has normal acceleration at 8 readings per second, pitch angle and roll angle at 2 or 4 per second, depending on the aircraft, and speed and height at 1 per second and also there is a frame number, which gives the time in seconds to an arbitrary scale. By identifying the frame in which the maximum increment of g occurs the associated speed and height can be identified. These have been found for each of the Events and are presented in Table 2. In addition to this basic data, the Lift Coefficient, the Maximum Gust Velocity, the Gust Response Factor and the Zero Crossings are also given. The Lift Coefficient was provided by CAA for a number of the Events, the remainder being allocated the arbitrary value 5 for this paper. The Gust Response Factors and the Zero Crossings are calculated by the Kaynes procedure[5] for Two-dimensional Spectra of Turbulence using a scale of turbulence of 1000 ft divided by the relative air density (σ), which is the scale used[6] in 1965 with the Hall Response Factor. Coupry[1] also uses Hall but with a scale of 440 m divided by $(\sigma)^{1/2}$. Thus, Coupry has similar scales of turbulence to the ones used in this paper except that they would tend to be higher at low altitude and lower at high altitude.

It is considered that as the data being examined is for 650,000 flying hours over a period of 5 yeàrs it should give an opportunity to compare the results for different aircraft and check to what extent the description of the gusts becomes independent of the aircraft that is used for the measurements. It is considered that the data should be sufficient to make a comparison between measured and calculated values of zero crossings.

5.2 Separation of Turbulence and Manoeuvres

As mentioned in paragraph 2 fifteen SESMA Events have been selected for the study of the g response of small and large aircraft in severe Atmospheric Turbulence. All the records contain severe turbulence and the first step in the analysis is to determine the durations for which the analysis should be made. Analytical methods were used in the earlier work[2&4] to do this but it can be seen from the records of Figure 1 that it is rare for a particular traverse of severe turbulence to have an intensity that varies appreciably and a visual inspection is probably the best that can be done to identify the time boundaries to the nearest second. Having selected the durations of the severe portions of the traverses, the characteristics of the turbulence will first be examined by reducing the response into components of turbulence and of manoeuvres, whether or not the manoeuvre was produced by the turbulence. It has been shown[7] for a range of aircraft that it was possible to select a frequency below which the amount of turbulence was small. It corresponds to a wavelength of about 2000 metres for all the aircraft examined in this present paper. Thus for this study of turbulence it is adequate to select a single filtering frequency of 0.12 HZ for all the traverses. It would be necessary to make a more refined selection for detailed studies of the manoeuvres themselves for in such a case it would be preferable to select a higher frequency to include more of the manoeuvre contribution even at the expense of having a little more turbulence.

The upper frequency for which g records and direct measurements of turbulence gave similar records was also discussed in the earlier work[4] on the present subject. This of course had had to be done on research flights

but it was considered that an upper limit of 2 HZ would be a good choice for BAC 1-11 and Trident. This limit does not change rapidly with size of aircraft and it is thought that it would be suitable also for the larger aircraft. Fortunately all the SESMA records are at 8 g readings per second which is associated with a filter at 2 HZ. All the events have been filtered at 0.12 HZ to give the components above and below 0.12 HZ. The intensities of the g, pitch angle and roll angle have been calculated for the duration of each severe traverse of turbulence and are given in Table 3. The correlation factors of the three parameters in pairs have been calculated for a range of delay times. The maximum correlation factors and their appropriate delay times in 1/8 second units are also given in the Table. A preliminary examination of the relationship between the manoeuvres and the turbulence suggests that the variation in intensity of the manoeuvre component does not seem to depend on either the aircraft or the intensity of the turbulence for the recorded traverses, all of which had an increment of $1g_4$ or more. It has an RMS value of about 0.1g in all cases; the earlier work[4] on BAC 1-11 and Trident for a lower limit of 0.6g for the g increment also showed a manoeuvre contribution of 0.1g RMS value.

5.3 Turbulence components

The complete records of the severe portions of the traverses are taken as a means of estimating the characteristics of the turbulence data obtained from the SESMA records. Whilst there are very few troughs that have the same sign as the peaks it was considered that no Design Requirement was needed to incur such a condition. It was decided therefore that it would be preferable to replace any trough with the same sign as the peak by a trough at 1g, but retaining the same maximum gradient; this has the effect of increasing the gradient distance in proportion to the increase in range from peak to trough. When the long wavelengths are removed from the records to produce the turbulence components between 0.12 HZ and 2 HZ, the total number of peaks is increased and some of these, usually small ones, have troughs of the same sign as their associated peaks and should be modified by the method just described. Firstly, the frequency range 0.12 to 2 HZ, corresponding to the turbulence component, will be examined. The peaks and ranges have been plotted against gradient distances for each traverse in non-dimensional form using the method that was developed in the earlier work[4]. The Zero Crossings are calculated from equation (5), using the measured values for the standard deviations of the g and of its derivative. For comparison between different traverses, including the ones that had been taken on CAADRP Events with g increments of 0.6g and above, equiprobability curves have been included that were deduced from the 487 up peaks of the CAADRP records as follows: the locus of points, in which there are 5 gusts of higher magnitude and of lower gradient distance, was determined, which is 1 % of the total. Similarly a locus for 24 gusts, which is about 5 % of the total was also determined. In order to obtain an equiprobability line for the ranges, those ranges associated with peaks greater than the 5 % equiprobability line were used. The appropriate 1 % equiprobability line for ranges is also plotted in the figures. All of the traverses have records that are consistent with these equiprobability lines. Figure 2 shows a comparison of large and small aircraft. The upper diagrams are for peak up gusts, each showing the gradients on exit and entry to the peak and the ranges associated with those peaks above the 5% equiprobability line. The lower 2 diagrams are for the peak down gusts. In each figure the two left hand diagrams are for a small aircraft and the right hand ones for a large one. As these figures are plotted on non-dimensional scales of S.D. of gust intensity and of 4HN(0), the scales in m/sec CAS and m.(square root of relative air density) are different for

each diagram. Fig 2A is for a BAC 1-11 and a Tristar each at 13700 ft and Fig 2B is for a B737 and a B747 at 23000 ft. In all cases the records fit equally well on the non-dimensional basis. To illustrate the effect of size, scales have been included of gust gradient distance in mX(square root of the relative air density); this particular unit of gradient distance is chosen because the calculated value of N(0)/(square root of the relative air density) is less dependent on height than N(0); see Table 2. It will be seen that the two small aircraft have much the same gradient distances on these scales at the different heights as have the large aircraft but there is a ratio of about 5 to 7 between the small and large aircraft at both heights.

All the records for all the heights have been combined in Figure 3. In this case they have been grouped on the non-dimensional basis. The value of turbulence intensity chosen was a standard deviation of 5 m/second CAS calculated with the Kaynes Response Factor. As it had been noticed in the examination of the individual records that the measured N(0)'s did not differ much from the Kaynes calculated value it was decided to use the calculated values in each case. This has the advantage that the comparison of different traverses and of different aircraft are all made for Kaynes Response Factors and Zero Crossings.

The value of 5 m/sec CAS for standard deviation of turbulence intensity that was chosen for Fig 3 was deliberately selected to be a little on the high side of the actual average for the records taken and in consequence the number of gusts outside the 1 % equiprobability line is about 2 or 3 at any point; the total number of up gusts is 622 so that there would have been an expected number of about 6 had the average intensity been taken. The associated range of 1% equiprobability is about 1.6 times the peaks as had occurred with the CAADRP records.

5.4 Turbulence and manoeuvres combined

It was stated in paragraph 5.2 that there is no marked relationship between the manoeuvre g and the turbulence g at different heights or overall g intensity (for traverses with a g increment of 1g or more) or between aircraft. The standard deviation of the manoeuvre of all the severe portions of the traverses was about 0.1 g, which is about 1.6 m/sec CAS, so the probable manoeuvre (i.e. the magnitude that is as likely to be above or below the actual one at a specified time) is about 1 m/sec CAS. It seems that an overall addition of 1 m/sec CAS to give an indication of the manoeuvre contribution for each traverses would be a reasonable one to use. Likewise some value has to be used for the intensity of the turbulence as a basis for comparison and it seems reasonable to use 5 m/sec CAS as was used in paragraph 5.3 for the turbulence components. Figure 4 gives a plot of all the records of the basic g data of the severe turbulence combined. They are compared with equiprobability lines for an RMS value of 5 m/sec CAS plus a constant value 1 m/sec CAS to account for the manoeuvre contribution in the 1 % line. This would represent the expected limit for a traverse with a standard deviation of 5 m/sec CAS and containing 100 up gust peaks. Such a traverse would be of the order of 30 km, which is about 3 times the average length of the 15 SESMA traverses that have been examined. An examination of Fig 4 shows that the number of gusts more severe than this at any point is about 2 or 3 so that on the assumption that the 15 traverses examined accounted for half the total in the 29 traverses recorded, the limit load would have occurred about 5 times during the 650,000 flying hours.

The total records of Fig 4 are separated into several height bands in Fig 5; Fig 5A shows the records below 15000 ft and presents the small and large aircraft separately. The agreement between the small and large

aircraft is good and represents about the same number of flying hours. The limit load line represents about the limit of each set of records. Fig 5B shows similar records for 15000 to 25000 ft. The agreement between small and large aircraft is good but the gusts for each are rather below the limit line. This is accounted for to some extent by the flying hours for each set being a little under half those below 15000 ft. Fig 5C shows the records for flying above 25000 ft. In this case the large aircraft had about 7 times as many flying hours as the small ones and in consequence there were no traverses by the BAC 1-11 and the B737. However there was one traverse made by the Trident so this has been compared with the large aircraft. The Trident results are rather few but do not seem to be incompatible with those on the large aircraft, which are a good sample and agree well with the proposed limit load. There are about 1 or 2 gusts above the limit at each point.

It may be concluded that the 1 % equiprobability lines of peaks and ranges for different gradient distances on Fig 4 are the same for all aircraft and for all heights when the normal acceleration at the CG is converted to gusts by using a scale of turbulence of 1000 ft/(air density) and Kaynes values for Gust Response Factors and Zero Crossings; the gust gradient distance that is shown is for an N(0) of 0.007/m X (sq rt of relative air density) and would need amending for any other value.

5.5 Frequency of peak gusts at different heights

In the present analysis each peak that is recorded, is the maximum value between zero crossings and their distribution should be the same as the number of level crossings. The total number that were recorded for all aircraft are given in Table 4. In the same Table are given the corresponding numbers for the turbulence components only. As would be expected the turbulence has rather more small peaks but fewer large ones. The number that occur at 11 m/sec in the basic data are about the same as the number at 10 m/sec in the turbulence component only; this is the amount that is assumed for the 1% equiprobability line in Figure 5.

Coupry[1] has made a study of all the peaks above 0.5 g that occurred on the BAC 1-11, B737, Tristar and B747 during the same 5 year period. At each height band Coupry found that, by using the Hall Response Factor, there was agreement between the different aircraft. A similar result would have been achieved with the Kaynes Response Factors although the actual values would have been slightly different. He found that there was a factor of about 10 between the number of gusts at 7 m/sec and the number at 11 m/sec. All Coupry's gusts were, of course, for the basic data. This paper is concerned only with the severe traverses that included an and are presented in Table 5 for different height bands and for small and large aircraft. As would be expected the total number of gusts at about 11 m/sec is far fewer than Coupry found from a study of all the traverses that included an increment of 0.5g or more. However Table 5 shows the factor between 7 m/sec and 11 m/sec to be about 3 rather than 10. Also the factor is about the same for the different heights and for small and large aircraft.

6. Conclusions.

Data has been collected from 650,000 flying hours on BAC 1-11, B737, Tristar and B747 of speed, height, normal acceleration at the CG, pitch angle and roll angle for those occasions when an increment of 1 g or more occurred. After filtering at 0.12 HZ to separate predominantly manoeuvres

from turbulence, an examination of the records, where the g fluctuations were severe, showed that the gradient distances of the gusts were strongly dependent on the zero crossings. It was found that the relationship between peaks and gradient distances was statistically the same for all aircraft and at all heights, as one preselected from an earlier study using non-dimensional scales of gust velocity in terms of standard deviations and gust gradient distance in terms of 4HN(0). There is a probability of about 0.01 that there are no peaks with a gradient distance less than 0.8 times 4HN(0), the gust velocity then increases steadily with gradient distance to an asymptotic value of about 3.7 standard deviations. The manoeuvres were on average the equivalent of about 1 m/sec CAS and no dependence was found on the severity of the turbulence, for the records examined which all had an increment of 1g or more, or on the height or on the type of aircraft.

7. Proposal.

A model of turbulence is proposed in a form that is identical for all heights as follows:

A. A traverse of 30 Km.
B. Continuous Turbulence with an RMS value of 5 m/sec CAS and a scale of turbulence of 1000 ft/(air density), normal accelerations at the CG and non-dimensional gust gradient distances being calculated using Kaynes Response Factors and Zero Crossings for Two-dimensional Spectra of Turbulence.
C. An additional manoeuvre component that is the equivalent of 1 m/sec CAS gust.

The resultant equiprobability line that is produced for gust velocities and gradient distances is such that it is considered that for any point on it there would have been about 5 occurences that were more severe in the 650,000 flying hours recorded.

8. Future Developments.

For the most part only 15 traverses have been used in the present paper. It is expected that this study will be continued to take account of the other 13 with increments of 1g or more and the one with 10 minute duration and an increment of 0.96g. To this end further information is required on aircraft weights (presumably from British Airways), Lift Coefficients (possibly indirectly from the firms through Mr Coupry) and Flight Profiles for the B757 and Trident (from CAA or Mr Coupry). It is hoped also to examine the 32 events with an increment of 0.5g or more with flaps down and to include in this investigation a more refined study of the interaction of gusts and manoeuvres: in this study the two events (1195 and 4178) of 10 minute duration should be of considerable value, especially for taking account of pitch and roll angles.

References

1.	G. COUPRY	Analyse statistique de la turbulence atmospherique.	R.T.4/3567 050 R Fev 1986
2.	J. TAYLOR	Atmospheric Turbulence Loads of Aircraft.	Jour.R.Ae.S. Dec 1977
3.	J. TAYLOR	Gust description for active control technology. Report on responses to turbulence of a T33 and a Canberra and a calculated response of a BAC 1-11: application to selected CAADRP special events.	Report No WBR/JT/4. 19 Dec 1979
4.	J. TAYLOR	Gust description for active control technology.	WBR/JT/6 25 Nov 1981
5.	I.W. KAYNES	Aircraft Centre of Gravity Response to Two-Dimensional Spectra of Turbulence	R & M 3665 June 1970
6.	J. TAYLOR	Manual on Aircraft Loads.	AGARDograph No 83 (1965) Pergamon
7.	J. TAYLOR	Mathematical Model for the Separation of Gust and Manoeuvre Loads of Civil Aircraft.	LBF Rep. No FB-141(1979)

Table 1: Flight profiles of B-747, BAC 1-11, B-737, Tristar during recording period May 1980 to April 1985.
(Extract from ONERA Report No RT 4/3567 RY 050 R)

PROFIL DE VOL COHERENTS ET CORRECTIONS DE CALCUL DE W

NIVEAUX	B_747	% PROFIL	BAC_111	% PROFIL	V %	B_737	% PROFIL	V %	TRISTAR	% PROFIL	V %	ECH.
0_100	6 200 000	3.1	11 000 000	46.6	10.0	2 200 000	6.2	20.0	2 200 000	5.9	2.0	474
100_200	6 800 000	3.5	3 500 000	14.8	13.0	2 400 000	6.8	7.0	1 800 000	4.9	0.0	555
200_300	25 800 000	13.0	6 100 000	25.8	1.0	12 000 000	33.8	12.0	7 600 000	20.5	8.0	657
300_400	159 000 000	80.4	3 000 000	12.8	10.0	18 900 000	53.2	20.0	25 400 000	68.7	12.0	798
TOTAL NM	197 800 000		23 600 000			35 500 000			37 000 000			
HEURES ANALYSEES	410 200		64 280			96 700			87 000			
NM / HEURE	496		363			368			425			

Tableau: VII

Table 2: Peak G Increments and Gust Velocities for Kaynes Response Factors

Units: Height ft, CAS Knots, Weight Kg, UK m/sec CAS

Date	Event	Aircraft	Height	CAS	Weight	G	CLA	UK	K	NO/m.SQRσ
Jan 82	4882	TRIDENT 3	7105	356	54130	2.36	5	16.86	.6044	.00657
Sep 83	3420	TRIDENT 3	29600	309	57510	-.38	4.957	-19.78	.6453	.00699
Oct 81	3938	BAC 1-11	5100	280	0	2.16	5	0	0	0
Jul 82	7099	BAC 1-11	18795	250	32650	2.16	5.217	16.35	.5763	.00789
Jun 83	2312	BAC 1-11	13745	264	36880	-.26	5.262	-18.37	.5908	.00752
Jun 84	2291	BAC 1-11	7560	261	32570	0	5.05	-14.18	.5655	.00761
Oct 84	3396	BAC 1-11	22835	321	33390	2.18	6.141	11.61	.5587	.00828
Jul 80	2124	TRISTAR 5	29170	298	136200	-.06	6.106	-13.1	.5724	.0057
Aug 82	7406	TRISTAR 2	15750	339	162200	-.03	5.445	-14.43	.6073	.00505
Aug 83	3427	TRISTAR 1	32100	282	168900	2.05	6.089	16.13	.6199	.00545
Aug 84	2854	TRISTAR 2	13780	279	136300	-.07	5.286	-16.54	.5788	.00528
Sep 84	3120	TRISTAR 2	7030	274	156300	-.04	5.236	-18.56	.5909	.00501
May 80	1692	B747-136	10231	338	303000	2.3	5	22.38	.6336	.00393
Aug 81	3273	B747-136	11077	225	0	-.27	5	0	0	0
May 82	6556	B747-136	35336	278	248500	-.05	5.182	-17.49	.63	.00469
Mar 83	0849	B747-136	31122	312	288100	2.14	5	19.39	.6605	.00436
May 83	1521	B747-136	21979	311	0	-.03	5	0	0	0
Jun 83	2108	B747-136	35062	293	255300	2.11	5.63	16.86	.6197	.00476
May 84	2122	B747-136	16127	308	0	-.15	5	0	0	0
Aug 84	3007	B747-136	11919	321	214600	2.04	4.949	14.99	.57	.00462
Mar 81	1195	B747-236	10917	307	239600	-.18	5	-19.13	.5857	.00442
Aug 80	2766	B747-236	28301	316	330000	2.18	5	21.77	.6885	.00411
Dec 83	4887	B747-236	7441	305	218100	2.03	4.832	16.31	.5684	.00451
Nov 84	3840	B747-236	22992	308	217000	-.08	5	-15.62	.5926	.00461
Oct 81	4178	B737-236	10317	263	45990	.04	5.943	-15.78	.6112	.00724
Oct 84	3841	B737-236	23251	282	44700	-.2	6.36	-16.59	.6154	.00759
Dec 84	4215	B737-236	4282	283	52300	-.18	5	-22.51	.6615	.00653
Jul 84	2514	B757-236	10610	222	71000	-.1	5	-20.65	.5843	.00608
Dec 84	4100	B757-236	17540	288	78800	-.06	5	-16.28	.6109	.00608

Table 3. Maximum Correlation factors for high and low frequency ranges.

FX= Normal acceleration: FY= Pitch angle: FZ= Roll angle: Delay in 1/8 s

S3420H Event 3420:TRIDENT 3 ABOVE 0.12 HZ
MEANS : -6.7162800E-04 G .00218542 DEG -.0356498 DEG
STANDARD DEVIATIONS : .284913 G .649459 DEG 1.21575 DEG

DELAYS			DATA RANGE		CORRELATION FACTORS		
X	Y	Z	1st	Last	YZ	ZX	XY
0	1	2	633	776	-.327343	-.0873074	.53518

S3420L Event 3420:TRIDENT 3 BELOW 0.12 HZ
MEANS : .829027 G -2.70081 DEG -5.11438 DEG
STANDARD DEVIATIONS : .0927831 G .761625 DEG 1.55925 DEG

DELAYS			DATA RANGE		CORRELATION FACTORS		
X	Y	Z	1st	Last	YZ	ZX	XY
16	0	32	633	776	-.823342	-.718706	.830008

S2312H Event 2312: BAC 1-11 ABOVE 0.12 HZ
MEANS : .00108365 G -.00766522 DEG .00205662 DEG
STANDARD DEVIATIONS : .215441 G .616854 DEG 2.10113 DEG

DELAYS			DATA RANGE		CORRELATION FACTORS		
X	Y	Z	1st	Last	YZ	ZX	XY
0	1	2	769	1280	.010763	-.00934637	.561159

S2312L Event 2312: BAC 1-11 BELOW 0.12 HZ
MEANS : 1.08141 G -1.84996 DEG -2.68636 DEG
STANDARD DEVIATIONS : .0846458 G .885138 DEG 3.47466 DEG

DELAYS			DATA RANGE		CORRELATION FACTORS		
X	Y	Z	1st	Last	YZ	ZX	XY
0	16	0	769	1280	.255019	.163109	-.622876

S2291H Event 2291: BAC 1-11 ABOVE 0.12 HZ
MEANS : .00198248 G -.0255688 DEG -.0760713 DEG
STANDARD DEVIATIONS : .252256 G .703512 DEG 1.66429 DEG

DELAYS			DATA RANGE		CORRELATION FACTORS		
X	Y	Z	1st	Last	YZ	ZX	XY
0	1	1	609	848	-.394586	-.312375	.741735

S2291L Event 2291: BAC 1-11 BELOW 0.12 HZ
MEANS : .999764 G 6.6158 DEG 8.14909 DEG
STANDARD DEVIATIONS : .0595804 G 2.53522 DEG 14.3512 DEG

DELAYS			DATA RANGE		CORRELATION FACTORS		
X	Y	Z	1st	Last	YZ	ZX	XY
0	0	0	609	848	.897294	.0969994	.154865

S3396H Event 3396: BAC 1-11 ABOVE 0.12 HZ
MEANS : -.00129893 G -.0040137 DEG -.108592 DEG
STANDARD DEVIATIONS : .355479 G .725579 DEG 2.03519 DEG

DELAYS			DATA RANGE		CORRELATION FACTORS		
X	Y	Z	1st	Last	YZ	ZX	XY
0	1	5	305	448	.761282	.406605	.721726

S3396L Event 3396: BAC 1-11 BELOW 0.12 HZ
MEANS : .938866 G .612266 DEG 5.07595 DEG
STANDARD DEVIATIONS : .163479 G .518717 DEG 4.06298 DEG

DELAYS			DATA RANGE		CORRELATION FACTORS		
X	Y	Z	1st	Last	YZ	ZX	XY
0	0	12	305	448	.47421	.595132	.196102

S7406H Event 7406:TRISTAR 2 ABOVE 0.12 HZ
MEANS : -.00228538 G -.0042986 DEG .0502858 DEG
STANDARD DEVIATIONS : .272732 G .576228 DEG .738288 DEG

DELAYS			DATA RANGE		CORRELATION FACTORS		
X	Y	Z	1st	Last	YZ	ZX	XY
0	0	0	673	832	.0920076	.31177	.709478

S7406L Event 7406:TRISTAR 2 BELOW 0.12 HZ
MEANS : 1.06296 G .171798 DEG -1.25653 DEG
STANDARD DEVIATIONS : .0331955 G 1.07648 DEG .471031 DEG

DELAYS			DATA RANGE		CORRELATION FACTORS		
X	Y	Z	1st	Last	YZ	ZX	XY
0	0	0	673	832	-.608684	.352461	-.518874

A2854H Event 2854:TRISTAR 2 ABOVE 0.12 HZ
MEANS : 1.1376100E-04 G .00287301 DEG -.0131956 DEG
STANDARD DEVIATIONS : .236582 G .334967 DEG .940596 DEG

DELAYS			DATA RANGE		CORRELATION FACTORS		
X	Y	Z	1st	Last	YZ	ZX	XY
0	0	0	1009	1456	.0983201	.054446	.520848

A2854L Event 2854:TRISTAR 2 BELOW 0.12 HZ
MEANS : 1.00997 G 1.32335 DEG .502977 DEG
STANDARD DEVIATIONS : .139908 G .910943 DEG 2.81771 DEG

DELAYS			DATA RANGE		CORRELATION FACTORS		
X	Y	Z	1st	Last	YZ	ZX	XY
0	0	16	1009	1456	-.181802	.516627	.222447

S2108H Event 2108: B747-136 ABOVE 0.12 HZ
MEANS : .00036737 G 8.9320900E-04 DEG .0073864 DEG
STANDARD DEVIATIONS : .164694 G .27144 DEG 1.32923 DEG

DELAYS			DATA RANGE		CORRELATION FACTORS		
X	Y	Z	1st	Last	YZ	ZX	XY
0	3	8	705	1264	-.281496	-.00270872	.336328

S2108L Event 2108: B747-136 BELOW 0.12 HZ
MEANS : 1.00712 G .964744 DEG -.901056 DEG
STANDARD DEVIATIONS : .17723 G .676524 DEG 2.04932 DEG

DELAYS			DATA RANGE		CORRELATION FACTORS		
X	Y	Z	1st	Last	YZ	ZX	XY
24	0	24	705	1264	.402269	.300759	.340173

S3007H Event 3007: B747-136 ABOVE 0.12 HZ
MEANS : -1.1822200E-04 G -4.3621800E-04 DEG .0191628 DEG
STANDARD DEVIATIONS : .215137 G .462984 DEG 2.87718 DEG

DELAYS			DATA RANGE		CORRELATION FACTORS		
X	Y	Z	1st	Last	YZ	ZX	XY
0	1	0	273	1200	-.0235883	.0442625	.68096

S3007L Event 3007: B747-136 BELOW 0.12 HZ
MEANS : 1.01793 G 5.72281 DEG -4.28014 DEG
STANDARD DEVIATIONS : .101932 G 2.04877 DEG 5.45108 DEG

DELAYS			DATA RANGE		CORRELATION FACTORS		
X	Y	Z	1st	Last	YZ	ZX	XY
0	0	0	273	1200	-.151025	-.0489775	.124286

S2766H Event 2766: B747-236 ABOVE 0.12 HZ
MEANS : -.0055872 G .00232767 DEG .0018346 DEG
STANDARD DEVIATIONS : .159254 G .388459 DEG 1.37193 DEG

DELAYS			DATA RANGE		CORRELATION FACTORS		
X	Y	Z	1st	Last	YZ	ZX	XY
0	1	0	785	1856	-.0385997	-.0589124	.405825

S2766L Event 2766: B747-236 BELOW 0.12 HZ
MEANS : 1.00426 G 2.19105 DEG .818921 DEG
STANDARD DEVIATIONS : .0800375 G .957353 DEG 4.77989 DEG

DELAYS			DATA RANGE		CORRELATION FACTORS		
X	Y	Z	1st	Last	YZ	ZX	XY
0	0	0	785	1856	.0813661	-.298544	-.0667383

S3840H Event 3840: B747-236 ABOVE 0.12 HZ
MEANS : 2.0538900E-04 G 7.9736400E-04 DEG .0103565 DEG
STANDARD DEVIATIONS : .132994 G .189266 DEG .979984 DEG

DELAYS			DATA RANGE		CORRELATION FACTORS		
X	Y	Z	1st	Last	YZ	ZX	XY
0	3	3	337	1280	.0491688	.18225	.3842

S3840L Event 3840: B747-236 BELOW 0.12 HZ
MEANS : 1.0043 G -.818812 DEG -.486473 DEG
STANDARD DEVIATIONS : .0457844 G .249209 DEG 1.1314 DEG

DELAYS			DATA RANGE		CORRELATION FACTORS		
X	Y	Z	1st	Last	YZ	ZX	XY
16	0	0	337	1280	7.0743300E-05	-.263743	-.276775

S3841H Event 3841: B737-236 ABOVE 0.12 HZ
MEANS : 1.4194900E-04 G .0031141 DEG .0358954 DEG
STANDARD DEVIATIONS : .175802 G .343547 DEG 1.99628 DEG

DELAYS			DATA RANGE		CORRELATION FACTORS		
X	Y	Z	1st	Last	YZ	ZX	XY
0	1	0	193	800	.138002	.131795	.622381

S3841L Event 3841: B737-236 BELOW 0.12 HZ
MEANS : .983355 G 6.06562 DEG -1.24518 DEG
STANDARD DEVIATIONS : .0458048 G .851696 DEG 5.11181 DEG

DELAYS			DATA RANGE		CORRELATION FACTORS		
X	Y	Z	1st	Last	YZ	ZX	XY
24	0	0	193	800	-.81175	-.177463	.428057

S4215H Event 4215: B737-236 ABOVE 0.12 HZ
MEANS : 7.0700400E-05 G .0121224 DEG -.0301281 DEG
STANDARD DEVIATIONS : .189235 G .430809 DEG 1.68623 DEG

DELAYS			DATA RANGE		CORRELATION FACTORS		
X	Y	Z	1st	Last	YZ	ZX	XY
0	1	0	513	880	-.0333623	.124009	.544358

S4215L Event 4215: B737-236 BELOW 0.12 HZ
MEANS : 1.1006 G 11.5379 DEG -14.5876 DEG
STANDARD DEVIATIONS : .0634441 G 1.57981 DEG 2.38636 DEG

DELAYS			DATA RANGE		CORRELATION FACTORS		
X	Y	Z	1st	Last	YZ	ZX	XY
24	0	0	513	880	-.732248	.299184	-.333289

S2514H Event 2514: B757-236 ABOVE 0.12 HZ
MEANS : -8.9614800E-04 G -.00271682 DEG 4.0438100E-04 DEG
STANDARD DEVIATIONS : .136574 G .283509 DEG .864455 DEG

DELAYS			DATA RANGE		CORRELATION FACTORS		
X	Y	Z	1st	Last	YZ	ZX	XY
1	0	0	433	1280	-.0969021	-.116327	.653894

S2514L Event 2514: B757-236 BELOW 0.12 HZ
MEANS : .991171 G 3.85949 DEG -.560308 DEG
STANDARD DEVIATIONS : .0694474 G 1.4774 DEG 1.72334 DEG

DELAYS			DATA RANGE		CORRELATION FACTORS		
X	Y	Z	1st	Last	YZ	ZX	XY
0	0	0	433	1280	-.108312	-.200144	.301106

S4100H Event 4100: B757-236 ABOVE 0.12 HZ
MEANS : -4.5974200E-04 G -.00933281 DEG -.00595636 DEG
STANDARD DEVIATIONS : .237438 G .524469 DEG 1.35167 DEG

DELAYS			DATA RANGE		CORRELATION FACTORS		
X	Y	Z	1st	Last	YZ	ZX	XY
1	0	3	673	1056	.10054	-.0542255	.435143

S4100L Event 4100: B757-236 BELOW 0.12 HZ
MEANS : .992236 G 4.41809 DEG -7.54922 DEG
STANDARD DEVIATIONS : .058153 G .836178 DEG 4.27861 DEG

DELAYS			DATA RANGE		CORRELATION FACTORS		
X	Y	Z	1st	Last	YZ	ZX	XY
0	24	0	673	1056	.669673	-.606129	-.525818

S1692H Event 1692: B747-136 ABOVE 0.12 HZ
MEANS : -.00213454 G -.00125734 DEG .0323204 DEG
STANDARD DEVIATIONS : .222053 G .229502 DEG .742128 DEG

DELAYS			DATA RANGE		CORRELATION FACTORS		
X	Y	Z	1st	Last	YZ	ZX	XY
0	0	0	993	1280	-.0408431	-.14641	.531771

S1692L Event 1692: B747-136 BELOW 0.12 HZ
MEANS : 1.01492 G -1.03469 DEG 1.85864 DEG
STANDARD DEVIATIONS : .110003 G .769284 DEG 5.99823 DEG

DELAYS			DATA RANGE		CORRELATION FACTORS		
X	Y	Z	1st	Last	YZ	ZX	XY
8	8	0	993	1280	.809759	.645595	.488497

S6556H Event 6556: B747-136 ABOVE 0.12 HZ
MEANS : .00160106 G -.00282157 DEG -.00322656 DEG
STANDARD DEVIATIONS : .156647 G .314962 DEG .716239 DEG

DELAYS			DATA RANGE		CORRELATION FACTORS		
X	Y	Z	1st	Last	YZ	ZX	XY
0	1	4	793	1080	.426071	.0876508	.343273

S6556L Event 6556: B747-136 BELOW 0.12 HZ
MEANS : .998976 G 1.19723 DEG 1.39607 DEG
STANDARD DEVIATIONS : .1237 G .678963 DEG 1.20206 DEG

DELAYS			DATA RANGE		CORRELATION FACTORS		
X	Y	Z	1st	Last	YZ	ZX	XY
16	0	0	793	1080	.39115	-.120793	.470509

S0849H Event 0849: B747-136 ABOVE 0.12 HZ
MEANS : 5.0745100E-04 G .0244487 DEG .0781514 DEG
STANDARD DEVIATIONS : .223391 G .474397 DEG 1.0074 DEG

DELAYS			DATA RANGE		CORRELATION FACTORS		
X	Y	Z	1st	Last	YZ	ZX	XY
2	7	0	369	496	.443893	-.29513	.432568

S0849L Event 0849: B747-136 BELOW 0.12 HZ
MEANS : 1.03461 G 1.66111 DEG -.431447 DEG
STANDARD DEVIATIONS : .0961925 G .49709 DEG .753322 DEG

DELAYS			DATA RANGE		CORRELATION FACTORS		
X	Y	Z	1st	Last	YZ	ZX	XY
0	16	16	369	496	.900847	.755186	.940895

S2124H Event 2124:TRISTAR 5 BELOW 0.12 HZ
MEANS : -.00308003 G -.014584 DEG .0160968 DEG
STANDARD DEVIATIONS : .24004 G .644584 DEG 1.36544 DEG

DELAYS			DATA RANGE		CORRELATION FACTORS		
X	Y	Z	1st	Last	YZ	ZX	XY
10	8	0	101	244	-.59295	-.276175	.550899

S2124L Event 2124:TRISTAR 5 BELOW 0.12 HZ
MEANS : .886899 G 1.73001 DEG 7.60991 DEG
STANDARD DEVIATIONS : .154663 G 1.54673 DEG 7.48874 DEG

DELAYS			DATA RANGE		CORRELATION FACTORS		
X	Y	Z	1st	Last	YZ	ZX	XY
24	0	0	101	244	-.631406	.783082	-.841888

Table 4. Comparison of numbers of gusts from the basic data on all aircraft at all heights and from the data above 0.12 Hz.

Gusts	Number of gusts larger than stated value					
	Basic Data			Data above 0.12 HZ		
m/sec	-ve	+ve	Total	-ve	+ve	Total
0	503	507	1010	627	622	1249
1	336	361	697	409	431	840
2	252	267	519	296	306	602
3	175	204	379	197	204	401
4	122	153	275	126	146	272
5	86	99	185	88	83	171
6	56	75	131	61	55	116
7	37	57	94	43	43	86
8	27	35	62	28	31	59
9	21	24	45	23	19	42
10	18	19	37	16	15	31
11	16	14	30	12	7	19
12	13	10	23	11	5	16
13	12	9	21	9	4	13
14	11	6	17	7	4	11
15	9	5	14	6	3	9
16	8	5	13	4	3	7
17	4	3	7	3	3	6
18	3	3	6	2	2	4
19	2	3	5	2	1	3
20	2	2	4	1	1	2

Table 5. Comparison of numbers of gusts from the basic data on Small and Large Aircraft at different heights.

BELOW 15000 FT. BASIC DATA.

Gusts	Number of gusts larger than stated value					
	BAC 1-11 & B737			TRISTAR & B747		
m/sec	-ve	+ve	Total	-ve	+ve	Total
0	73	74	147	104	104	208
1	47	61	108	71	72	143
2	38	52	90	56	59	115
3	28	48	76	44	45	89
4	20	42	62	32	37	69
5	17	33	50	23	25	48
6	11	23	34	18	20	38
7	8	14	22	11	16	27
8	7	10	17	8	11	19
9	4	5	9	6	9	15
10	4	5	9	5	7	12
11	4	3	7	4	5	9
12	4	2	6	2	4	6
13	3	1	4	2	4	6
14	3	0	3	2	3	5
15	2	0	2	2	2	4
16	2	0	2	2	2	4
17	2	0	2	1	1	2
18	2	0	2	1	1	2
19	1	0	1	1	1	2
20	1	0	1	1	1	2

15000-25000 FT. BASIC DATA.

Gusts	Number of gusts larger than stated value					
	BAC 1-11 & B737			TRISTAR & B747		
m/sec	-ve	+ve	Total	-ve	+ve	Total
0	76	77	153	97	98	195
1	57	58	115	52	55	107
2	44	41	85	26	31	57
3	27	26	53	20	23	43
4	14	17	31	14	13	27
5	9	5	14	9	7	16
6	4	4	8	4	4	8
7	4	4	8	2	3	5
8	2	2	4	2	1	3
9	2	2	4	2	0	2
10	2	1	3	2	0	2
11	2	1	3	2	0	2
12	2	0	2	2	0	2
13	2	0	2	2	0	2
14	2	0	2	2	0	2
15	2	0	2	1	0	1
16	2	0	2	0	0	0
17	0	0	0	0	0	0
18	0	0	0	0	0	0
19	0	0	0	0	0	0
20	0	0	0	0	0	0

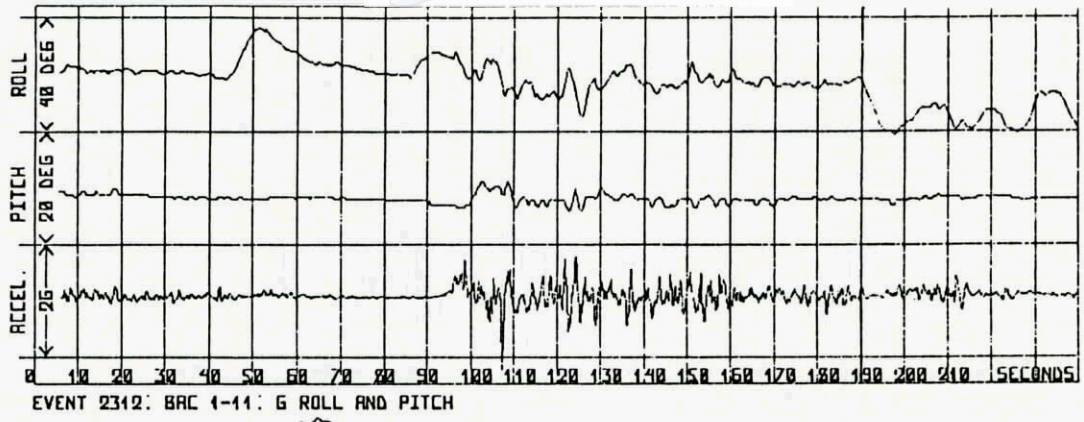

EVENT 2312: BAC 1-11: G ROLL AND PITCH

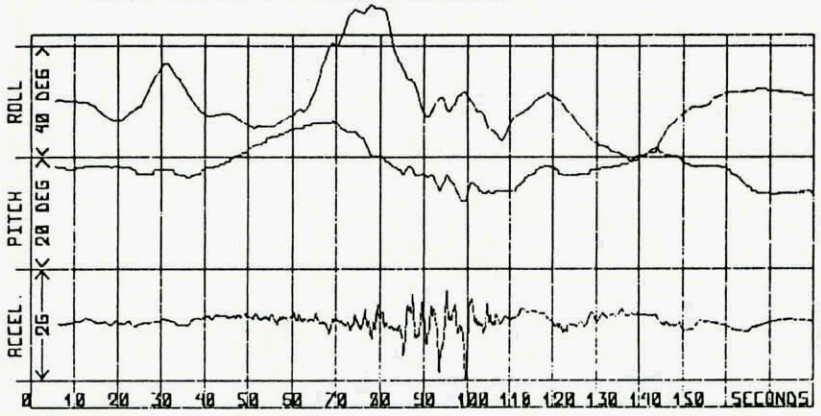

EVENT 2291: BAC 1-11: G ROLL AND PITCH

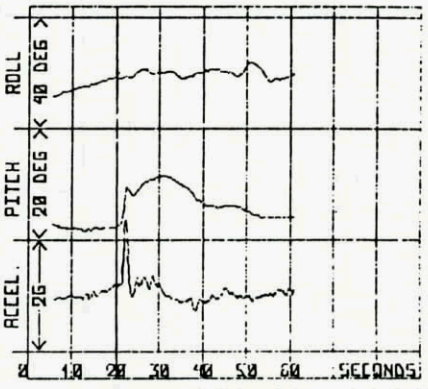

EVENT 4982: TRIDENT 3: G ROLL AND PITCH

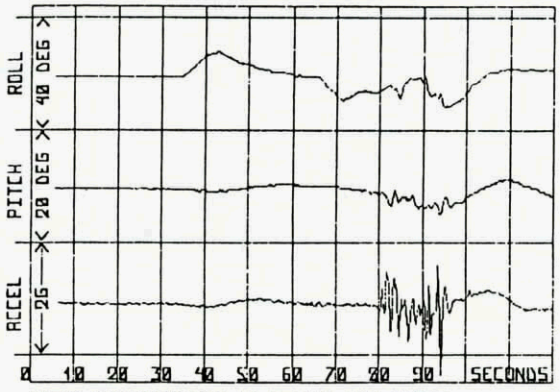

EVENT 3420: TRIDENT 3: G ROLL AND PITCH

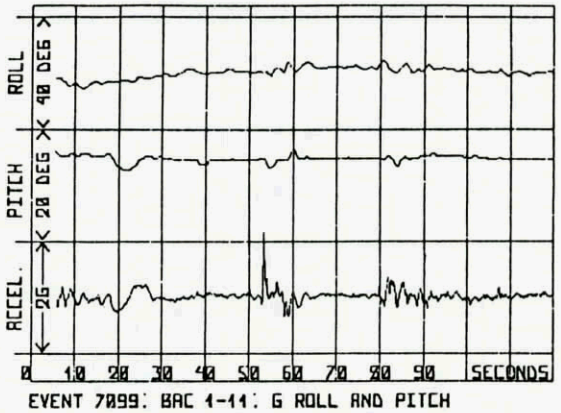

EVENT 7099: BAC 1-11: G ROLL AND PITCH

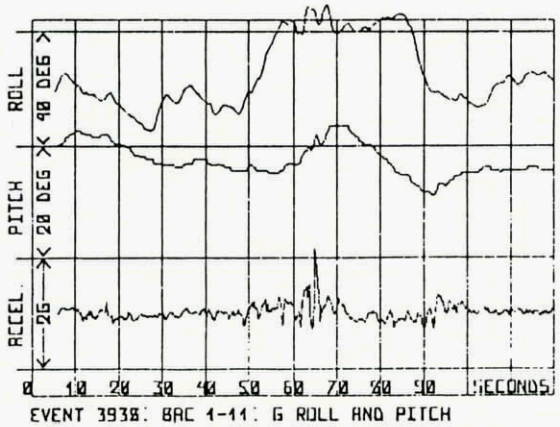

EVENT 3938: BAC 1-11: G ROLL AND PITCH

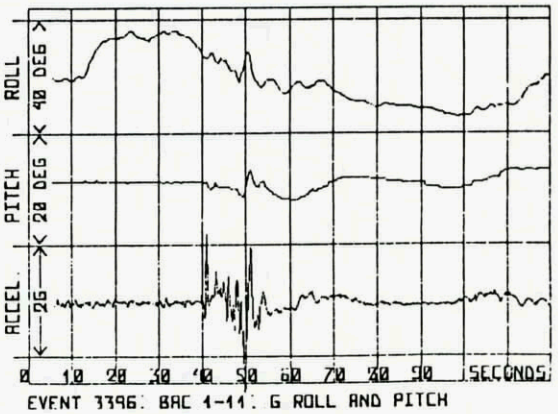

EVENT 3396: BAC 1-11: G ROLL AND PITCH

Fig.1A SESMA Events with Increment Greater than 1G

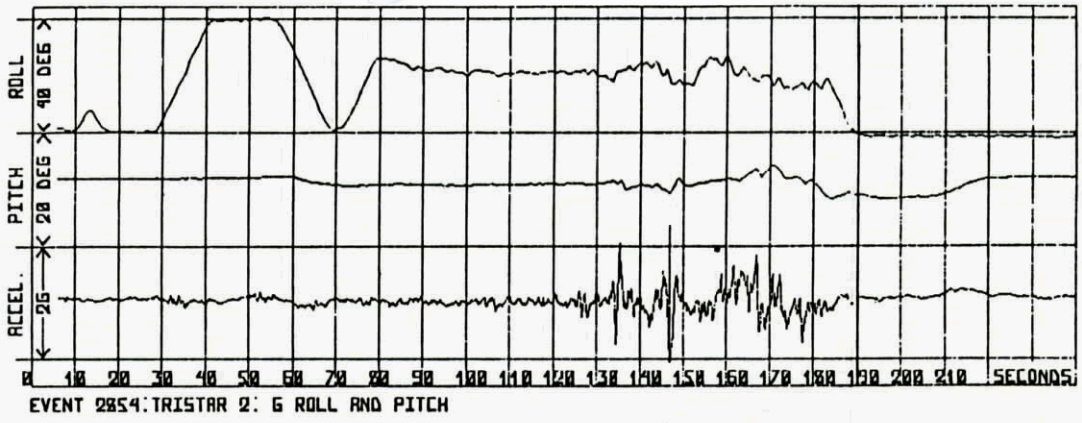

EVENT 2854:TRISTAR 2: G ROLL AND PITCH

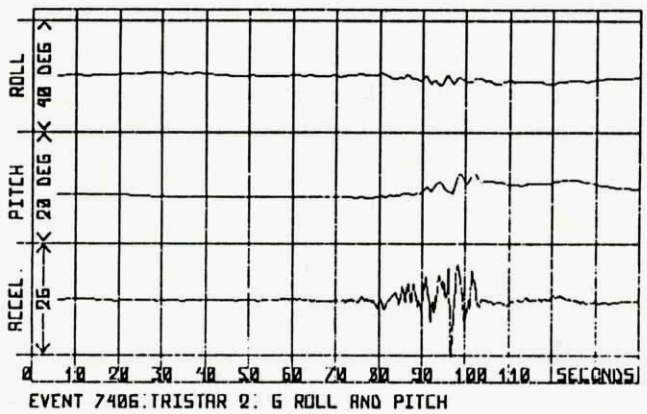

EVENT 7406:TRISTAR 2: G ROLL AND PITCH

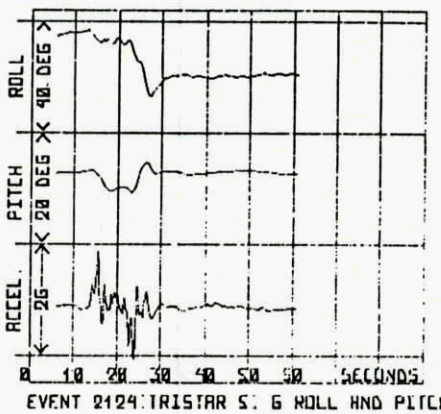

EVENT 2124:TRISTAR 5: G ROLL AND PITCH

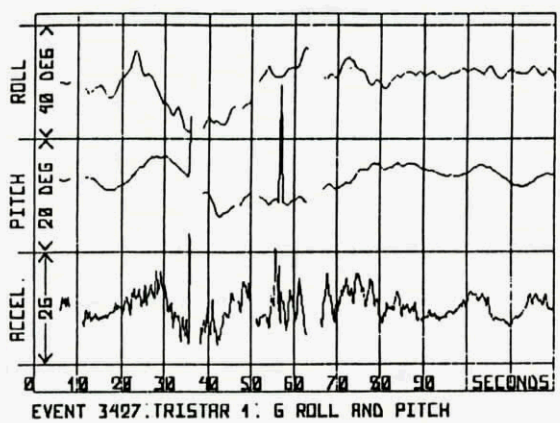

EVENT 3427:TRISTAR 1: G ROLL AND PITCH

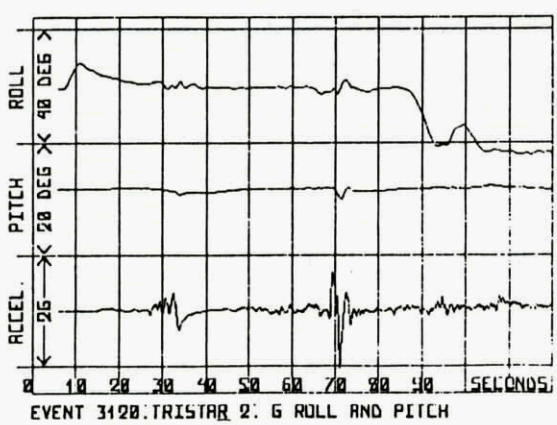

EVENT 3120:TRISTAR 2: G ROLL AND PITCH

Fig.1B SESMA Events with Increment Greater than 1G

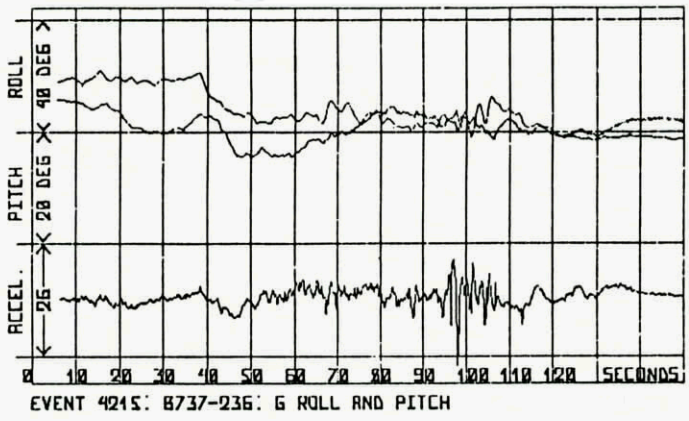

EVENT 4215: B737-236: G ROLL AND PITCH

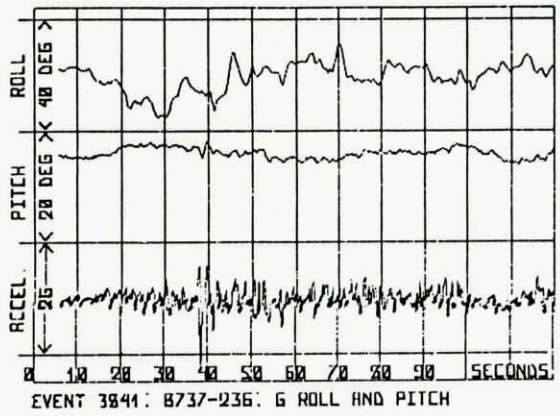

EVENT 3841: B737-236: G ROLL AND PITCH

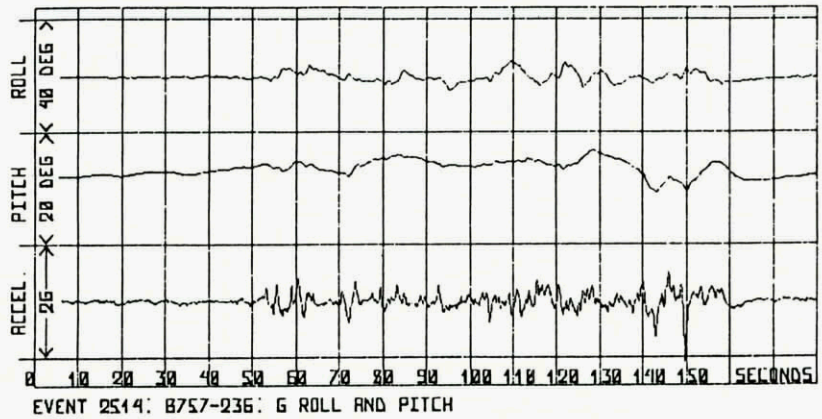

EVENT 2514: B757-236: G ROLL AND PITCH

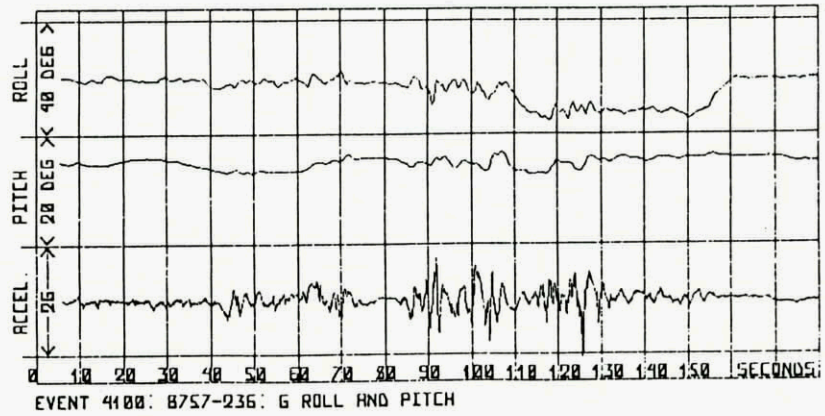

EVENT 4100: B757-236: G ROLL AND PITCH

Fig.1C SESMA Events with Increment Greater than 1G

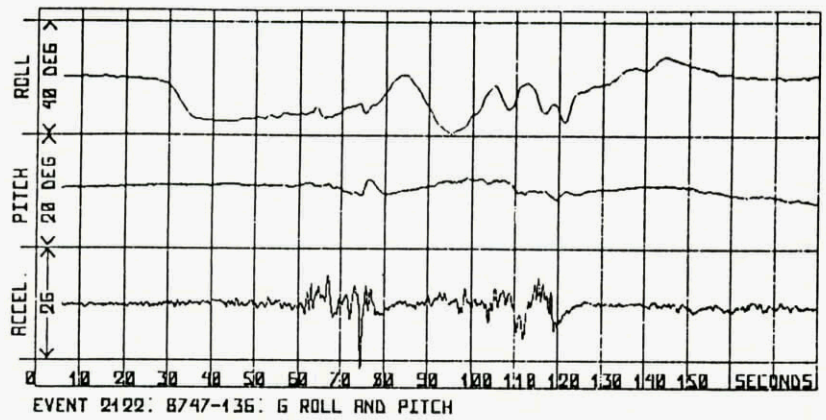

EVENT 2122: B747-136: G ROLL AND PITCH

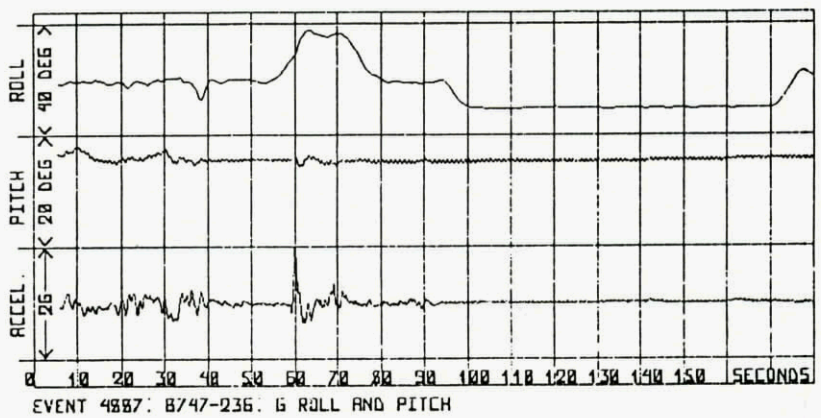

EVENT 4887: B747-236: G ROLL AND PITCH

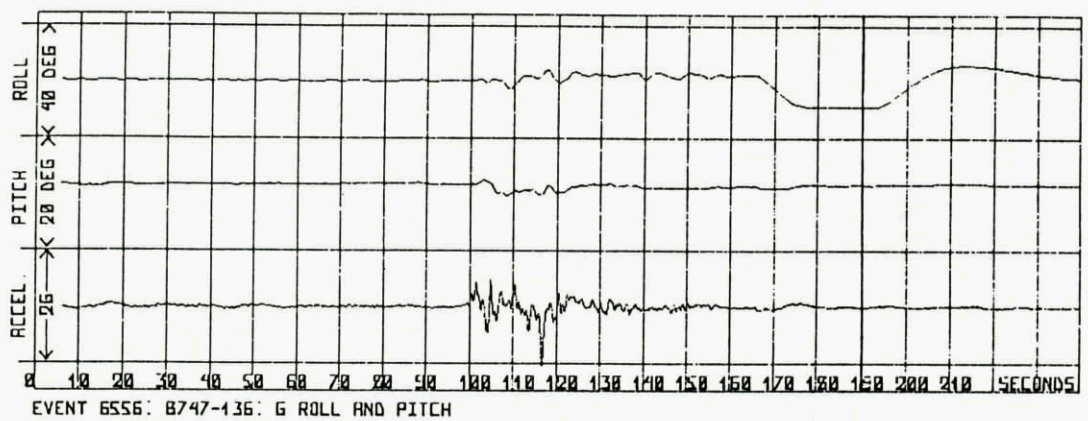

EVENT 6556: B747-136: G ROLL AND PITCH

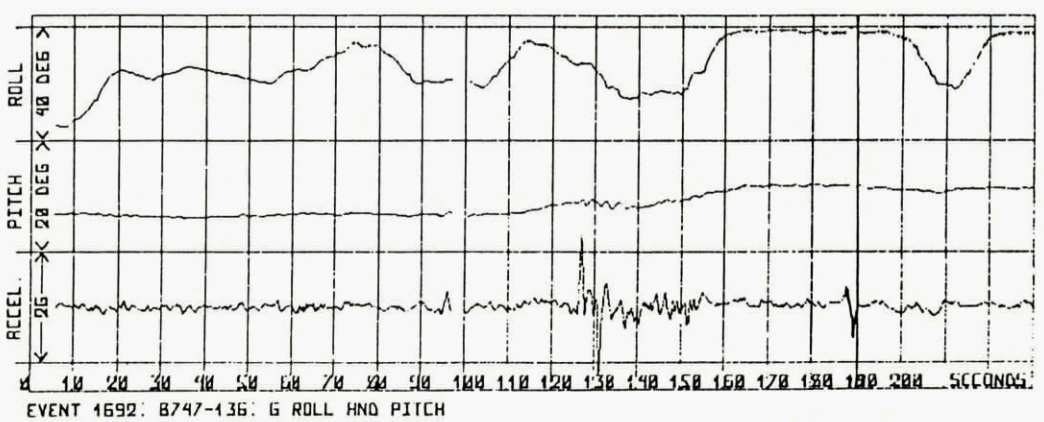

EVENT 1692: B747-136: G ROLL AND PITCH

Fig.1D SESMA Events with Increment Greater than 1G

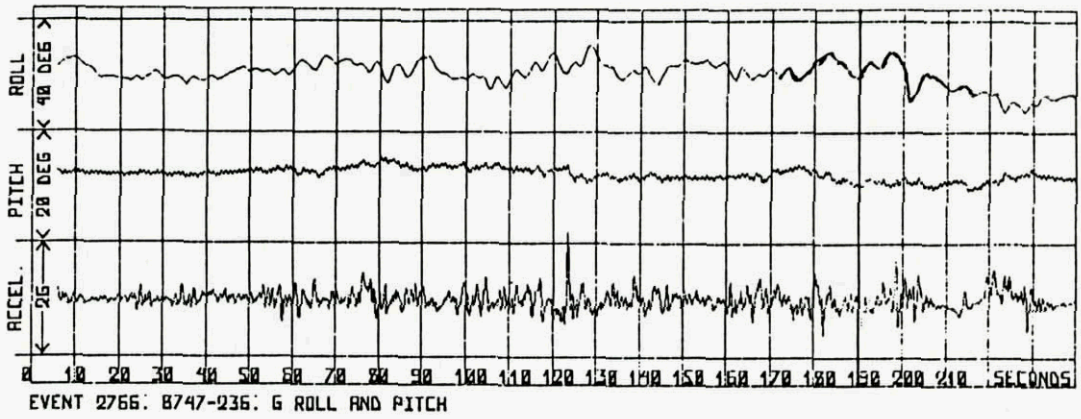

EVENT 2766: B747-236: G ROLL AND PITCH

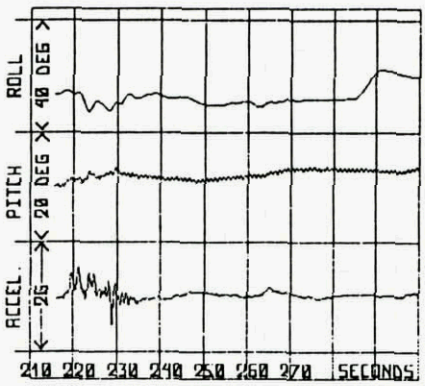

EVENT 2766: B747-236: G ROLL AND PITCH

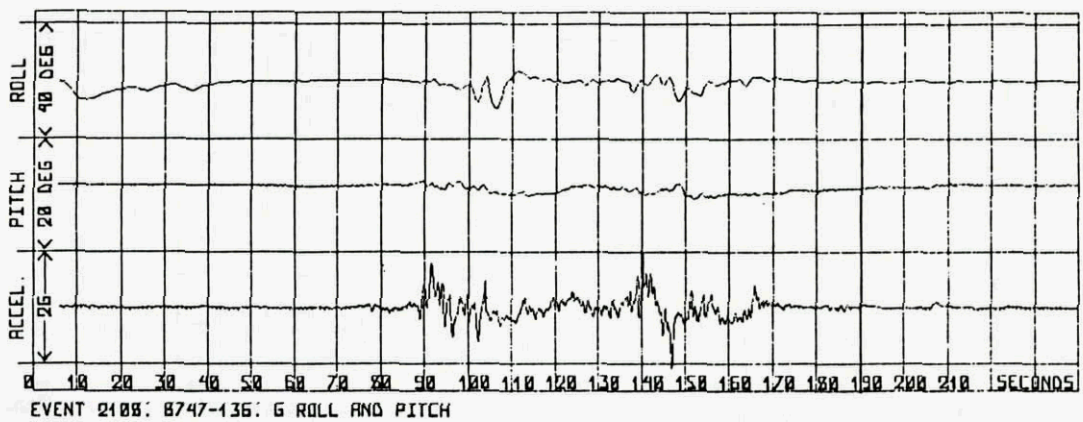

EVENT 2100: B747-136: G ROLL AND PITCH

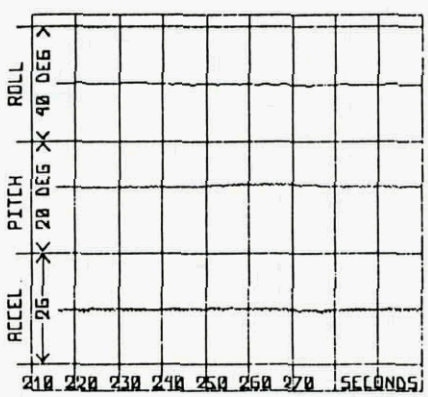

EVENT 2100: B747-136: G ROLL AND PITCH

Fig.1E SESMA Events with Increment Greater than 1G

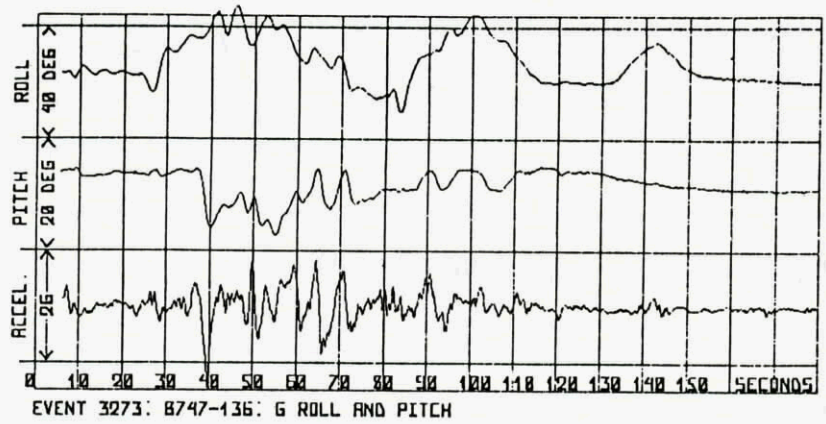

EVENT 3273: B747-136: G ROLL AND PITCH

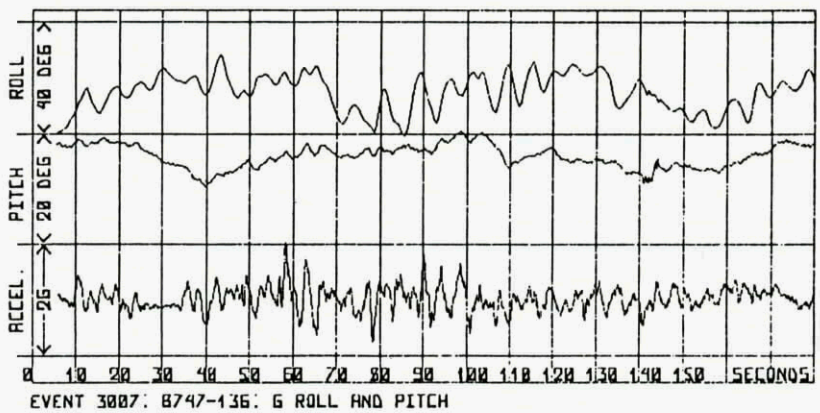

EVENT 3007: B747-136: G ROLL AND PITCH

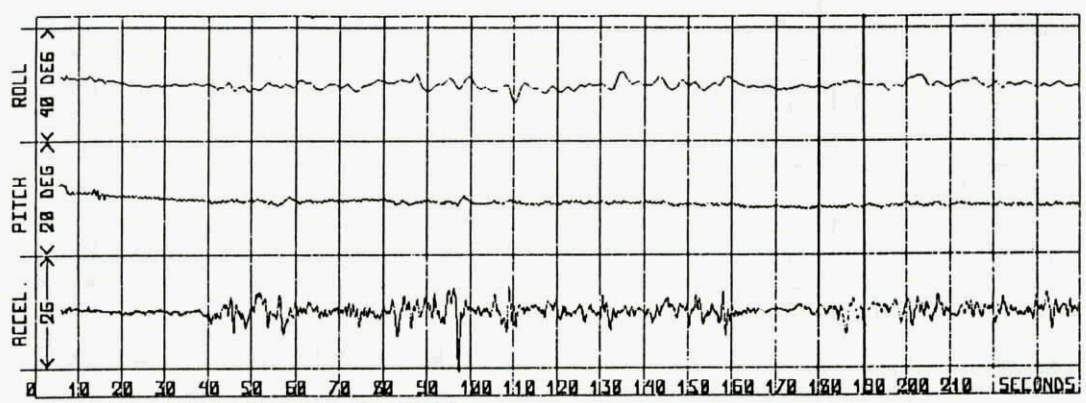

EVENT 3840: B747-236: G ROLL AND PITCH

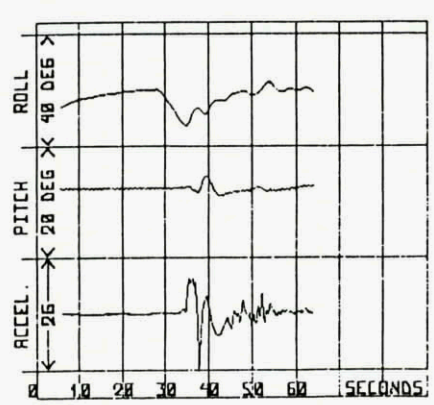

EVENT 1521: B747-136: G ROLL AND PITCH

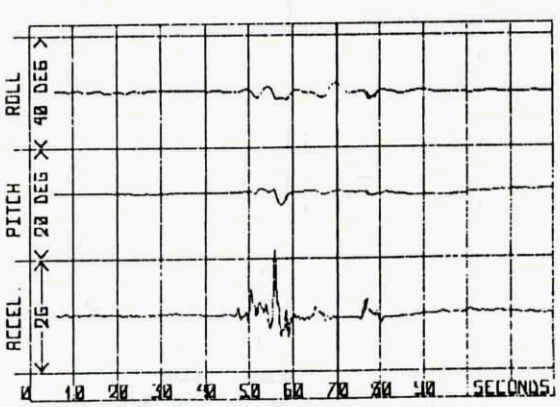

EVENT 0849: B747-136: G ROLL AND PITCH

Fig.1F SESMA Events with Increment Greater than 1G

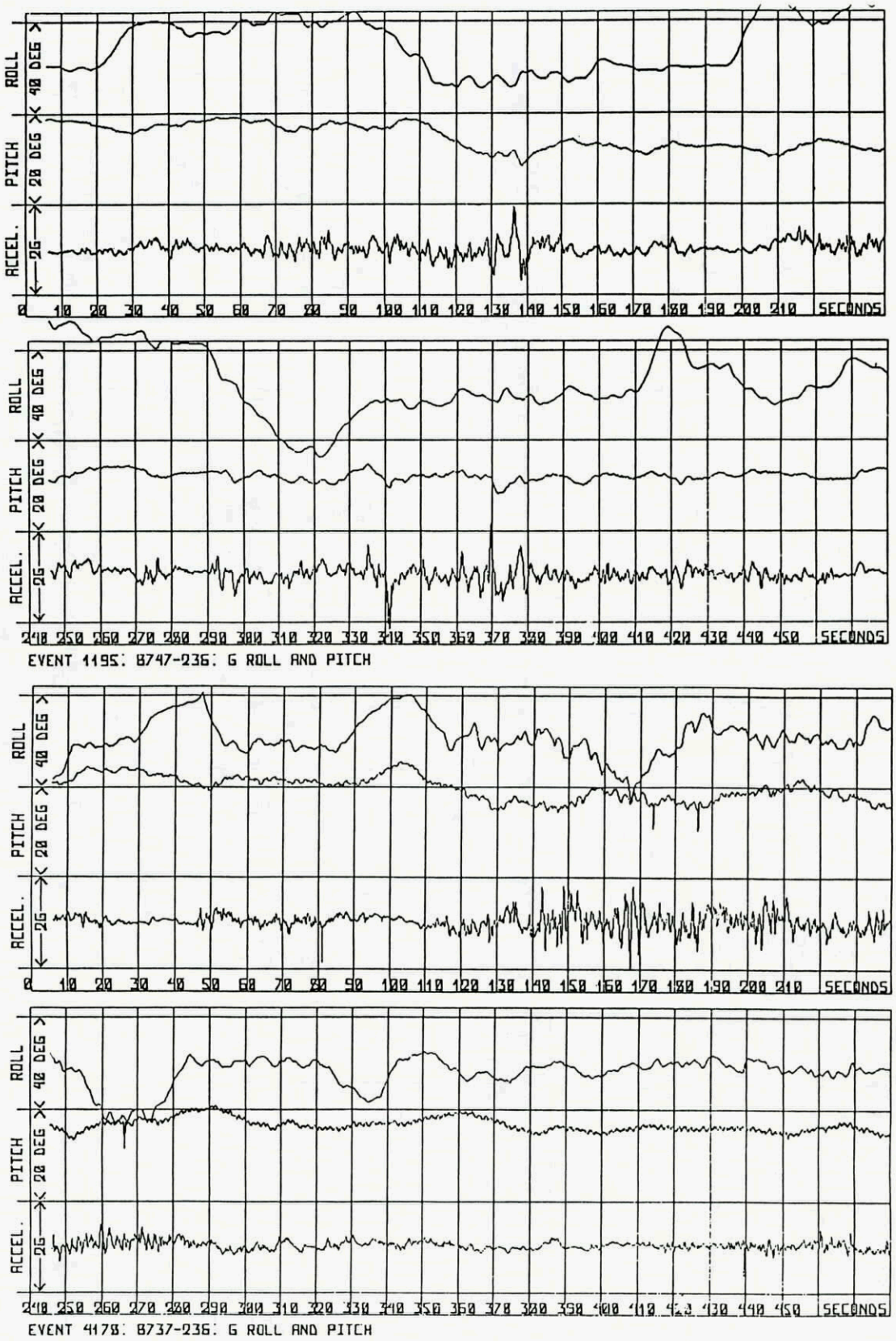

Fig.1G SESMA Events with Increment Greater than 1G

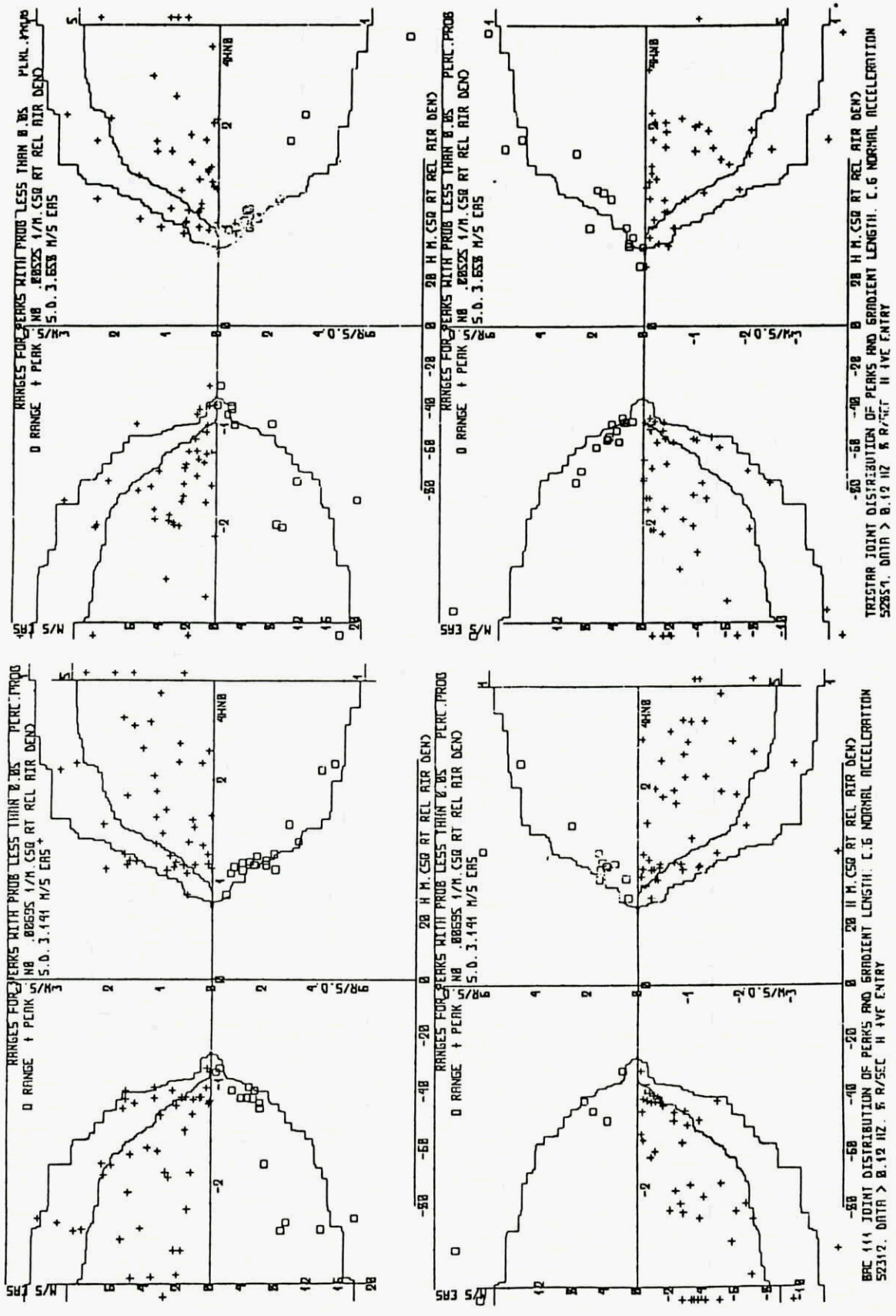

Fig.2A Comparison of BAC 1-11 and TRISTAR in Severe Turbulence
13700 ft. Turbulence Component 0.12 to 2 HZ

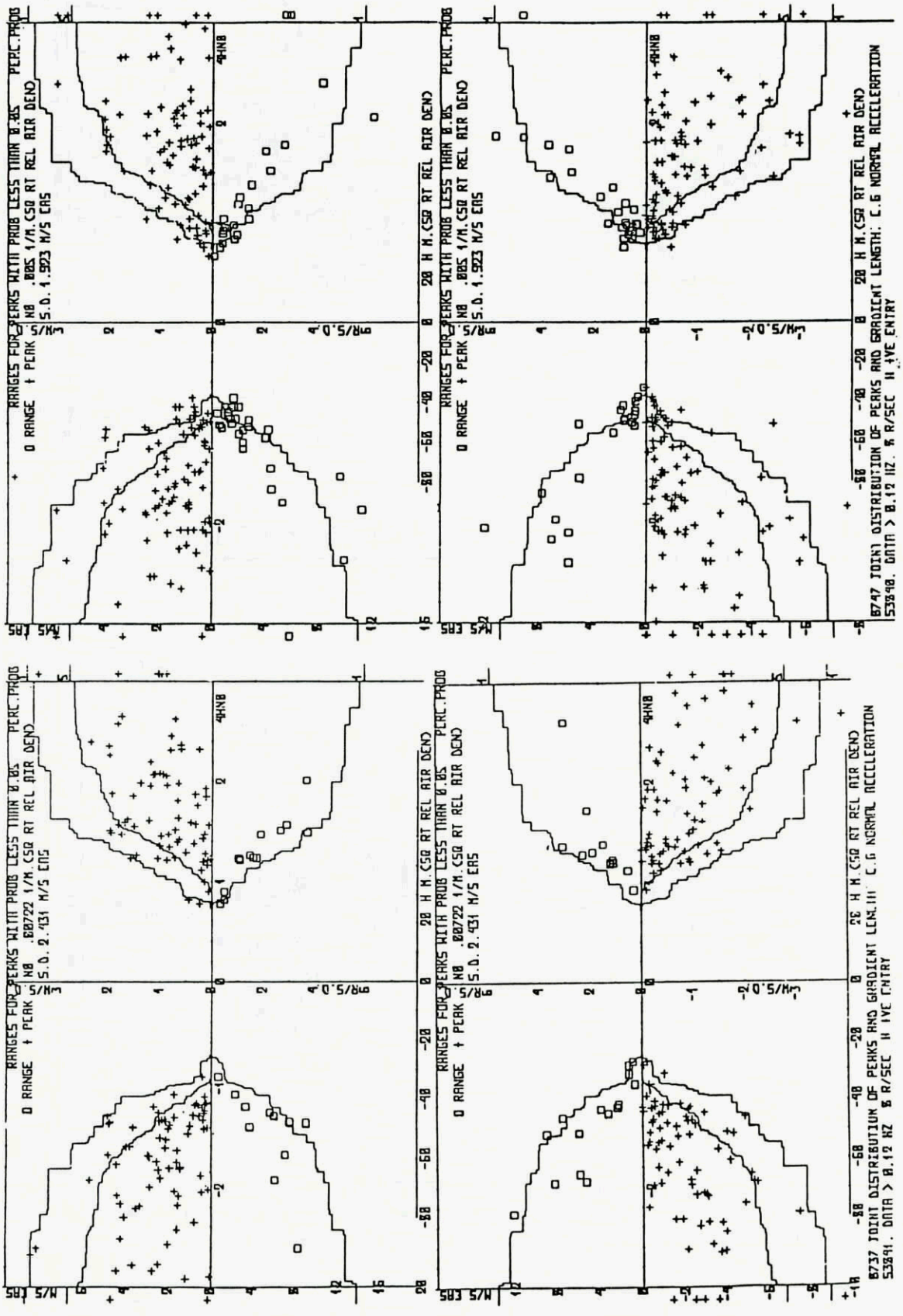

Fig.2B Comparison of B737 and B747 in Severe Turbulence
23000 ft. Turbulence Component 0.12 to 2 HZ

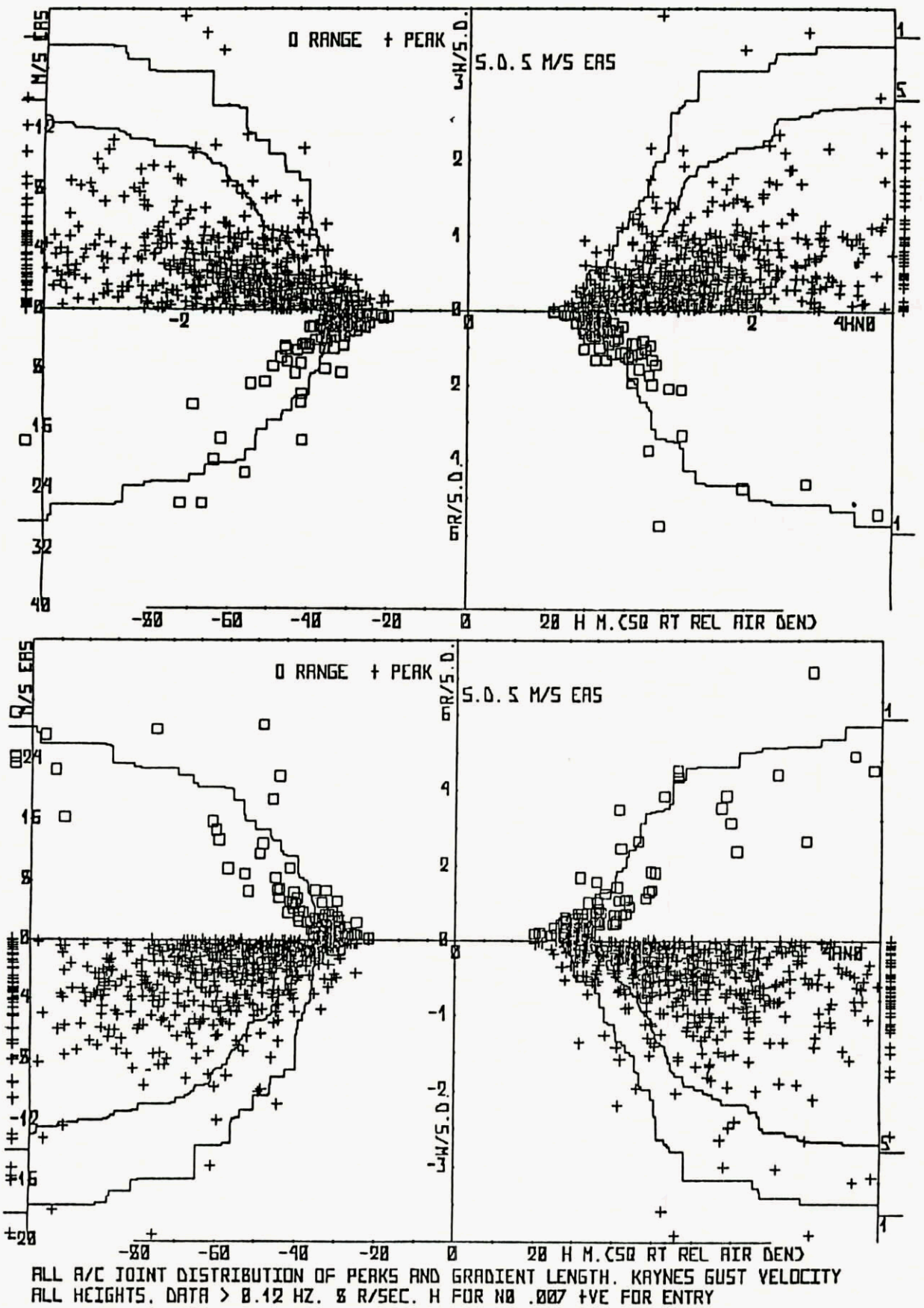

Fig.3 Gust Peaks and Gradient Distances for Severe Turbulence for all Aircraft at all Heights. Turbulence Component 0-12 to 2 HZ

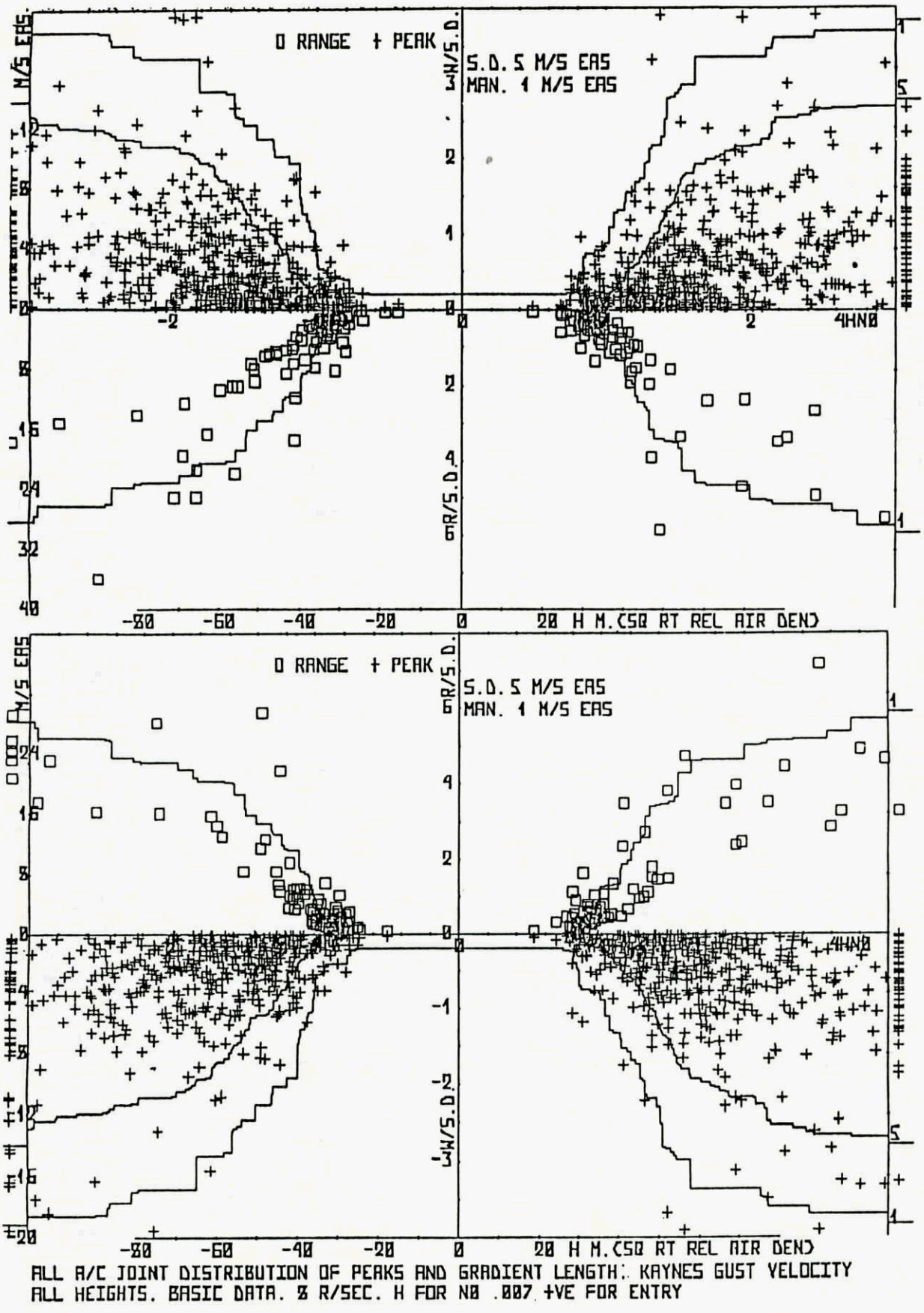

Fig.4 Gust Peaks and Gradient Distances for Severe Turbulence for all Aircraft at all Heights. Basic Data 0 to 2 HZ

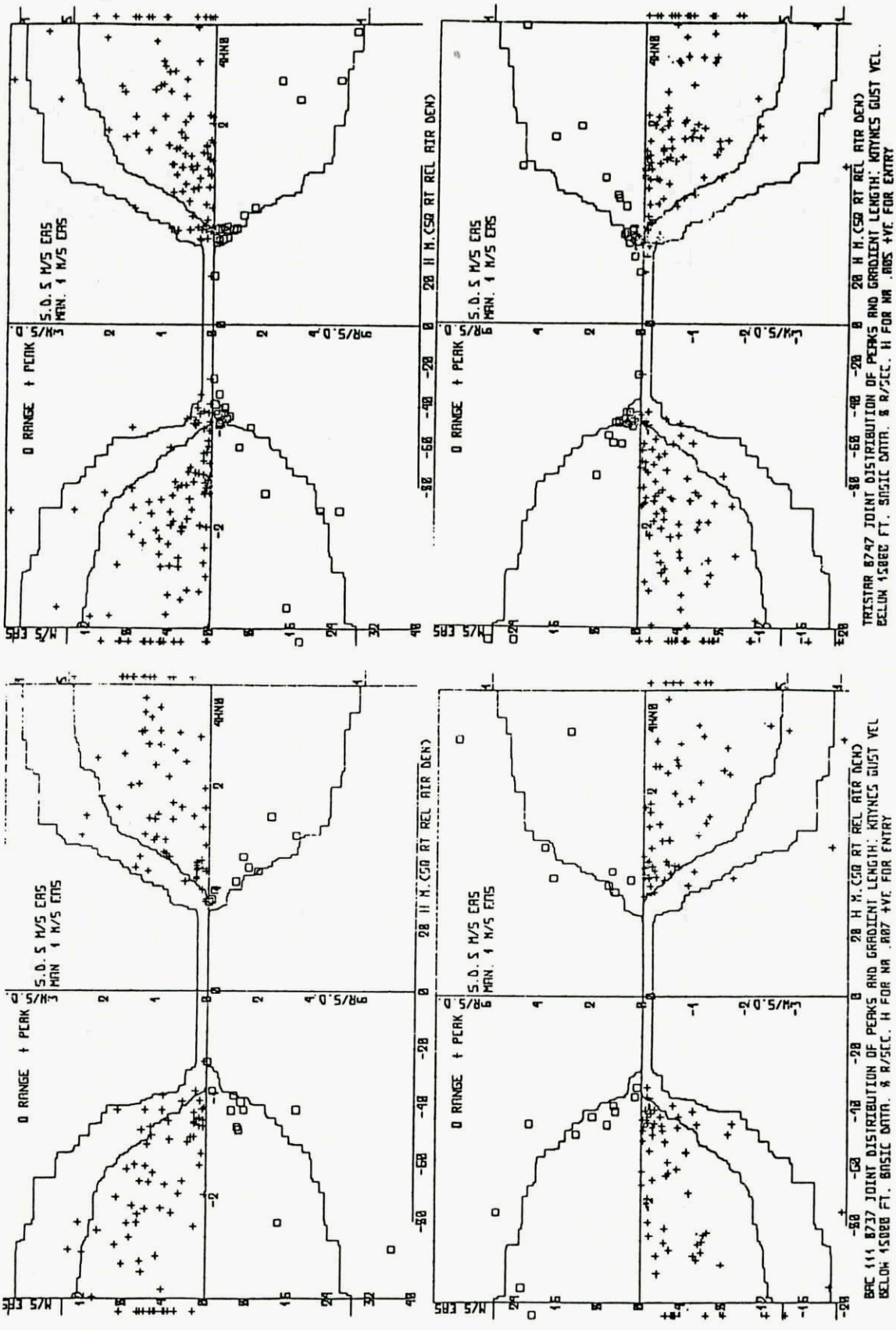

Fig.5A Gust Peaks and Gradient Distances for Severe Turbulence for all Aircraft below 15000 ft. Basic Data 0 to 2 HZ

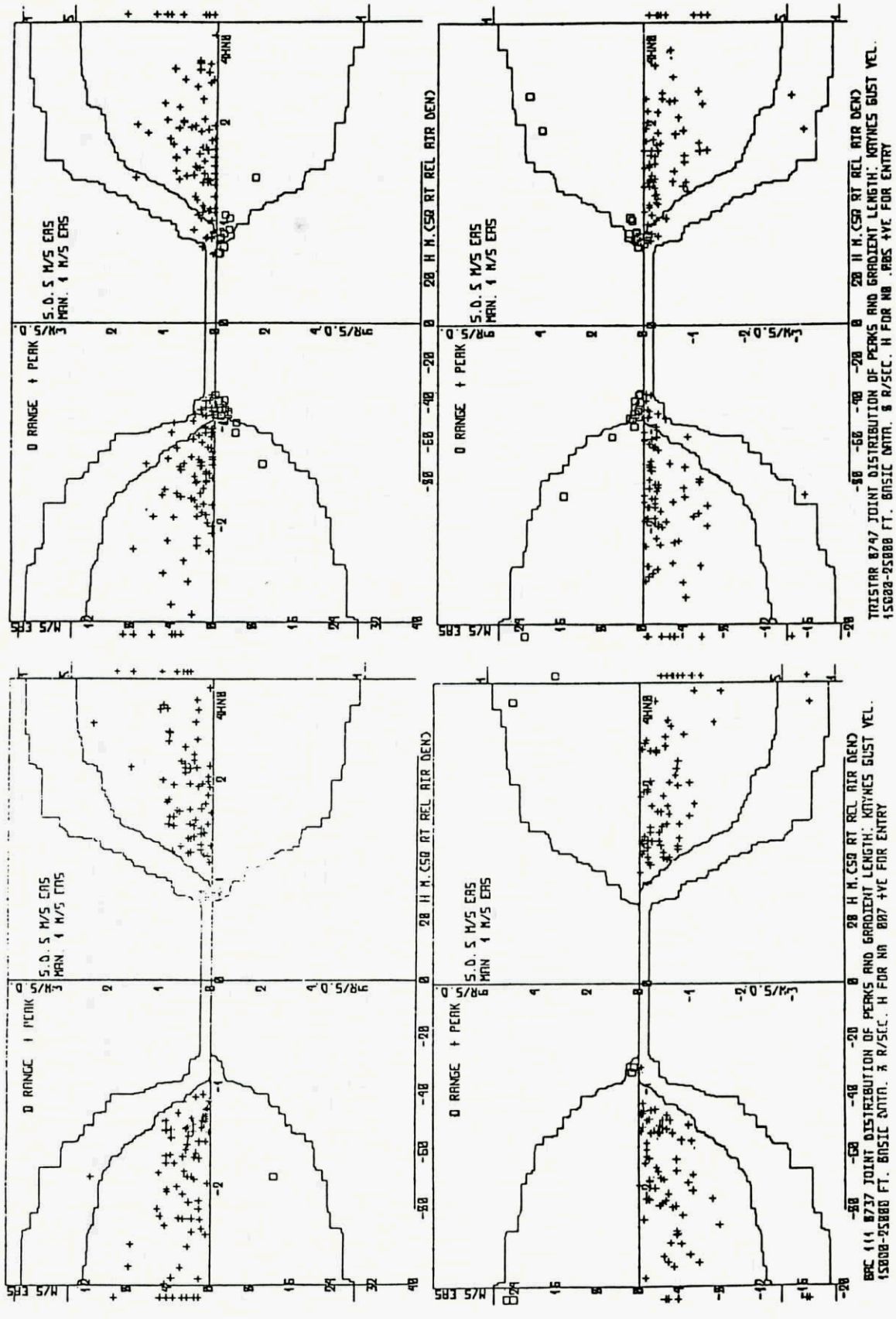

Fig.5B Gust Peaks and Gradient Distances for Severe Turbulence for all Aircraft at 15000—25000 ft. Basic Data 0 to 2 HZ

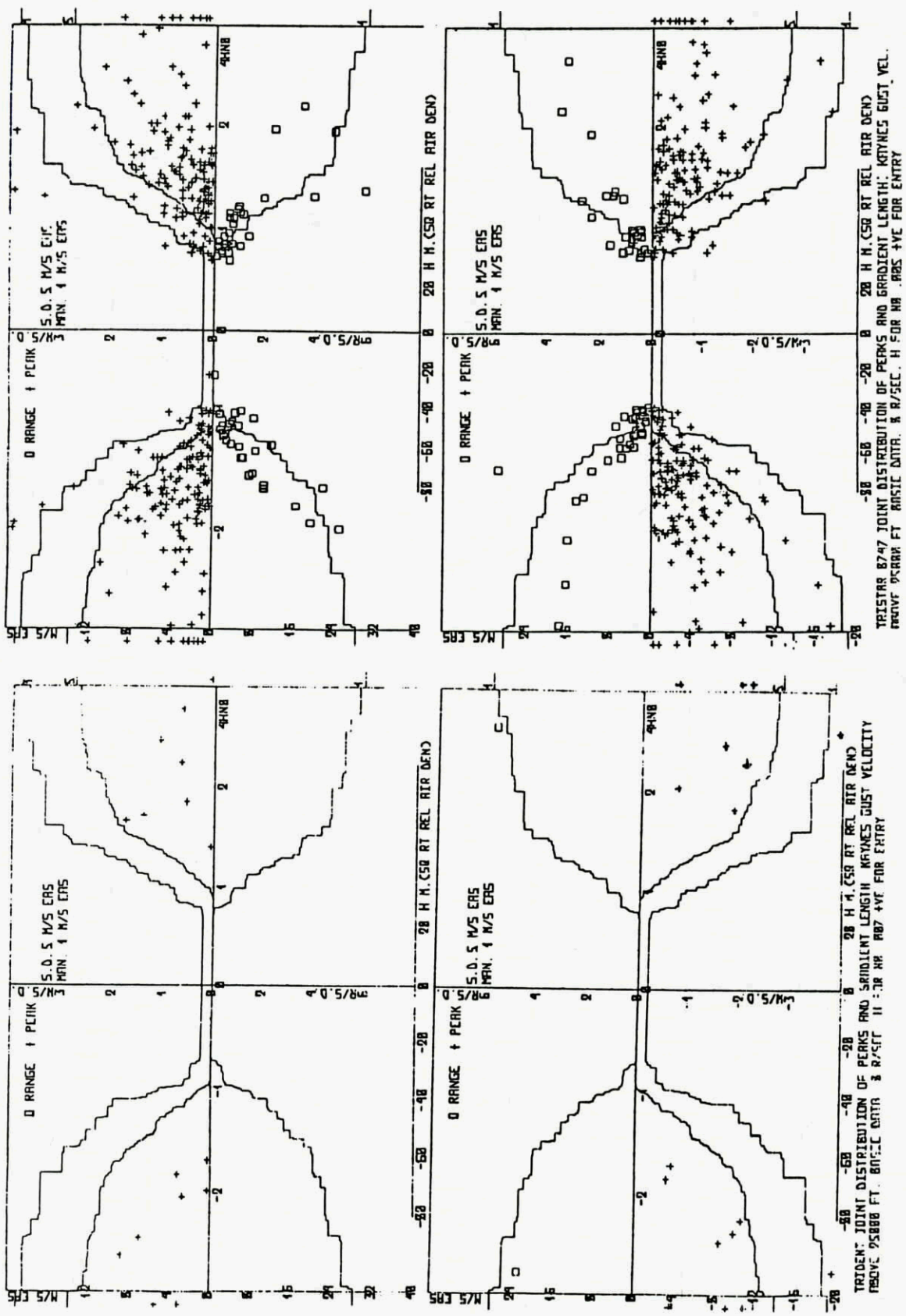

Fig.5C Gust Peaks and Gradient Distances for Severe Turbulence for all Aircraft above 25000 ft. Basic Data 0 to 2 HZ

THE NAE ATMOSPHERIC RESEARCH AIRCRAFT

by

J.I. MacPherson and S.W. Baillie
Flight Research Laboratory
National Aeronautical Establishment
National Research Council
Ottawa, Ontario, K1A 0R6
Canada

SUMMARY

The Flight Research Laboratory of the National Aeronautical Establishment of Canada operates a T-33 and a Twin Otter aircraft instrumented for atmospheric research studies. This paper describes the instrumentation in the aircraft with emphasis on the strapped-down inertial/Doppler system used to derive the mean and turbulent components of the atmospheric motion. Example data from several research projects are presented to demonstrate the measurement and analysis capabilities of the aircraft and their data playback facilities.

1. INTRODUCTION

The Flight Research Laboratory of the National Aeronautical Establishment of Canada (NAE) currently operates six fixed-wing aircraft and four helicopters in a variety of research programs. Two of these aircraft are instrumented specifically for atmospheric research studies. The NAE T-33 (Figure 1), a single-engine military jet trainer, was first instrumented in 1962. In its role as an atmospheric motion sensor, it has been employed in numerous studies on topics ranging from wake turbulence and cloud seeding to jet streams and terrain-induced turbulence. Throughout these projects, the aircraft measurement, data acquisition and playback systems have been continually updated to improve accuracy and capacity, as documented in References 1 to 3. The recording system, for example, has evolved from a continuous trace film device, to FM analog, to serial-digital and soon to a compact streamer tape drive.

The second NAE atmospheric research aircraft is a deHavilland of Canada Twin Otter STOL transport (Figure 1). Development of its on-board instrumentation began in 1974 when the NAE entered into a cooperative cloud physics research program with the Atmospheric Environment Service of Canada (AES). Over the intervening twelve years, its instrumentation and playback facilities have also undergone continuous expansion and refinement (Ref. 4). The aim of this development program was to produce a versatile research aircraft well equipped for flight dynamics experiments, as well as to create an atmospheric research platform capable of carrying and supporting other investigators' instruments and experiments. When in its cloud physics role, for example, the integration of the NAE air motion system and the AES particle spectrometers has made the Twin Otter a recognized state-of-the-art cloud physics research aircraft. Other applications of this aircraft have included air motion measurement around storms, air pollution studies and the determination of CO_2 fluxes above various crops in order to infer growth rates.

This paper will describe the current instrumentation in the NAE T-33 and Twin Otter and, by presenting example data from several research projects, demonstrate some of the measurement and analysis capabilities of the aircraft and their support systems. Some of the procedures used to ensure accuracy will be outlined, and the paper will close with a brief summary of the instrumentation improvements planned for both aircraft in the next two years.

2. AIRCRAFT AND INSTRUMENTATION

The T-33 and Twin Otter, with their very different flight envelopes (Table 1), complement one another in the atmospheric research role and together can meet most operational requirements. The low speed and manoeuvrability of the Twin Otter make it ideal for low altitude studies. Nevertheless, it has been fitted with an oxygen system and can make sensitive measurements to an altitude in excess of 20,000 feet. The T-33 is, of course, much faster and can be flown to about 41,000 feet, suitable for mountain wave and jet stream studies. Its higher wing loading and load limits of +7.3 and -3.0 G allow it to operate near severe storms, as well as to find application in flight mechanics experiments that require a military manoeuvring load envelope.

The measurement of atmospheric motion by an aircraft requires the computation of the vector difference between the aircraft's velocity relative to the air and its velocity relative to the ground. There are two basic methods to accomplish this, differing primarily by what means and in which axis system the inertial* velocity is sensed. The INS method utilizes the stable platform of an inertial navigation system to measure the aircraft's velocity in earth-relative axes. This is subtracted from the true airspeed (TAS) vector (resolved into earth axes using the aircraft heading and attitude) to derive the true air motion. In the strapped-down (SD) method, both the air-relative and the inertial velocity are measured in aircraft body axes, the differences are formed, and only the resultant wind components are resolved into earth axes.

At the NAE the SD method is used for both the Twin Otter and T-33. When these aircraft were being instrumented, this method offered several advantages for NAE's applications, the first being cost. The purchase of INS systems would have required prohibitive one-time expenses, whereas the SD systems have been built up through the use of existing hardware and timely purchases of the other necessary components. Early INS systems required more electrical power than could be spared, especially on the Twin Otter. Without the requirement for lengthy platform alignment, the SD method allows rapid launching of the aircraft, an advantage in some weather-related experiments. Finally, in flight mechanics studies the emphasis is on the aircraft forcing functions and responses, which are best measured directly in aircraft body axes.

The main steps in the application of the SD method to the computation of the true air motion are shown in Figure 2. The sensors currently used for air motion measurement on the Twin Otter and T-33 are listed in Table 2, with their locations illustrated in Figures 3 and 4. References 3 to 5 can be consulted for more detailed descriptions of the sensors and the equations used in these calculations.

The air velocity relative to the aircraft (the TAS vector) is sensed on both aircraft on a 1.9 m noseboom, however the instruments used to measure flow angles differ. On the T-33 the positions of balsa vanes are determined by synchros

---

* In this work the earth is assumed to be the inertial frame of reference.

to give the angles of attack and sideslip, while on the Twin Otter flow angles are measured by a Rosemount 858 5-hole probe and associated differential pressure transducers.

A third-order complementary filtering routine is used in the computation of the 3-axes inertial velocity components. The high frequency contribution originates with the accelerometer and rate gyro signals, is integrated as per the equations of motion and high-pass filtered to remove long term drifts. The complementary filtered low frequency component is provided by a 3-axis Doppler radar. The breakpoint of the filter is usually set at 0.02 Hz. The products of the filter routine are the 3-axes inertial velocities (e.g. Wmix) which have no long-term drift, that is, they are valid over the frequency range from D.C. to the upper limit determined by the anti-alias filters applied to the raw data signals (5 Hz on the Twin Otter, 10 Hz on the T-33). The three components of the true air motion are then calculated from the difference between the air-relative and the inertial velocity components. The resulting wind components can then be resolved into earth axes using the measured aircraft heading and the pitch and roll attitudes.

In addition to the air motion systems, each aircraft is equipped to make a considerable number of other measurements, which include atmospheric state parameters, radio-altimeter and pressure height and a multi-level event marker. (Table 3, Figs. 3 and 4). Both aircraft can record geographical position from a GNS-500A area navigation system. The Twin Otter has the optional capability of carrying a Loran-C system in areas of good coverage, while the T-33 can record glideslope and localizer deviations for specific studies at airports. The T-33 is also instrumented to measure the pilot's flight control inputs, throttle position and the engine RPM. Video and voice records are made on the Twin Otter by a VCR with three selectable camera positions, two with external fields of view and one focused on the colour weather radar. In the cloud physics role, the Twin Otter carries four wing-mounted PMS* laser spectrometers to measure aerosol, cloud droplet and precipitation particles over a size range from 0.1 to 6400 μm. These are owned and operated by the AES. It also has various inlets for airborne sampling and the collection of cloud water and precipitation. In weather modification experiments, the T-33 has served as the cloud seeding aircraft, carrying seven silver iodide flares in the pod under each wing (Fig. 1).

At present, the most significant difference in the project instrumentation on the two aircraft is the on-board computing capability, or more specifically, the display of real-time data and the degree of interaction with the computer available to the operator. The T-33 carries a DEC LSI-11/73 processor with software stored in core or EPROM, giving a limited capability for in-flight program changes. Wind speed and direction, TAS, static temperature and RMS vertical gust velocity can be calculated and displayed in the rear cockpit on 16 LED characters. Real-time computed data are not recorded. The Twin Otter carries two microprocessors, an LSI-11/23 performing the real-time computations of wind, fluxes etc., and a DEC Falcon which manages the recording of the sensor outputs and computed parameters. Full interaction with the main processor is provided by a console-mounted keyboard with programs loaded from a dual floppy disk unit. Alpha-numeric data are presented on 12 x 40-character plasma display units in the cockpit and the rear cabin.

The recorder on the T-33 is a rugged Nagra reel-to-reel device on which 10-bit digital data are written in serial format (Table 4). Thirty-two parameters are recorded at 32 samples/sec each on a single track of the 1/4-inch tape. A second track records voice from the intercom and the radios. The Twin Otter data acquisition system has recently been converted to a streamer tape drive, which has a capacity of 70 Mbytes on a 6 x 4-inch compact cartridge. The recording format is under computer control and is therefore very flexible. At present, 64 parameters, including the real-time computed winds, are written in 16-bit words at a rate of 16 samples/sec. Voice is recorded on separate stereo cassette recorders with voice-chip annotated time, and on the audio track of the VCR. When the Twin Otter is flown in cloud physics studies, a second data acquisition system developed by the AES is added to record the massive amount of data generated by the particle spectrometer probes. An interface between the NAE and AES microprocesors allows the exchange of data. The complete NAE data buffer is recorded by the AES system so that cloud particle measurements, for example, can be correlated with the motion and thermal structure of the atmosphere.

Ground support equipment for each aircraft includes portable LSI-11/23 or -11/73 field data playback systems (Refs. 3 and 4). Although some of the hardware differs, the capabilities of the two systems are similar. They permit development of the airborne software and provide initial data printout, chart recorder traces, flight track plots and other programmed calculations, such as heat and momentum fluxes. For more detailed numerical analysis, flight data can be transcribed to 9-track tape and sent to the NRC Computation Centre. Their IBM-3081 time-shared main frame has a large number of peripherals and an extensive library of system software, as well as a number of programs developed specifically to process the Twin Otter and T-33 data.

3. RESEARCH PROGRAMS AND EXAMPLE DATA

The T-33 and the Twin Otter have spent a total of 36 aircraft-years at the NAE instrumented as atmospheric research aircraft. They have been involved in numerous projects as research priorities have evolved through the years. Not all of these were directly related to the measurement of atmospheric turbulence for aeronautical applications, but most required good air motion sensing to achieve their objectives. Figure 5 depicts the time history of the major areas of research in which these aircraft have been involved. The reference sections in References 3 and 4 list resulting papers and reports from these activities through 1980, with a selection of publications since that time given as References 6 to 17 in this paper.

From being first instrumented in 1962 through to the mid 1970's, the T-33 was used primarily in basic research of the nature and energetics of turbulence generated by a variety of sources, including jet stream shears, mountain waves, thunderstorms, aircraft vortex wakes and terrain-induced effects upon the earth's boundary layer. In the last half of the 1970's, research on weather modification was important in North America, and both the T-33 and the Twin Otter were used in these studies. The T-33 served as the cloud seeding aircraft and collected a considerable amount of data on turbulence within the tops of towering cumulus clouds. The Twin Otter was outfitted as a cloud physics research aircraft with air motion sensing and laser particle spectrometers to record the dynamics and microphysics of clouds.

In the 1980's weather modifcation has become unpopular, and Canada's atmospheric priority has shifted to air pollution, in particular to the complicated processes that lead to the formation of acidic precipitation. Additional inlets, filters and chemical analyzers have been added to the Twin Otter for air pollution studies at several North American locations, including the high Arctic. Concern over the increasing concentration of CO_2 in the atmosphere has led to the development of instrumentation to measure CO_2 and H_2O fluxes above various ecosystems to parameterize the gaseous exchange rates between vegetation and the atmosphere. There is also a growing interest in severe storms, both the

---

* Manufactured by Particle Measuring Systems, Boulder, CO.

summertime convective complex and the wintertime mesoscale disturbance that sweeps up the east coast of North America and has a large impact on many major cities and the off-shore oil industry. This has led to further instrumentation refinements and participation in special studies of these phenomena.

The T-33 has been involved in a diverse series of experiments in the 1980's. These have included further low altitude turbulence measurements analyzed by the Statistical Discrete Gust Method, and parameter identification studies, that is, the computation of the aircraft stability derivatives. Its well-calibrated static pressure system has been applied to pressure surveys to 41,000 feet in the ICAO Flight Level Separation Program. The aircraft has also been used to expose Canadian astronauts to aerospace operational conditions, and has served as an instrumentation platform for basic research on voice recognition in an accelerating environment for future application to voice-dialogue systems in the cockpit.

In this section, example data from a few of these studies are presented to demonstrate some of the capabilities of the aircraft instrumentation and the products available from the data analysis software.

Figure 6 shows time histories for a T-33 seeding run at 15,000 feet through the top of a vigorous towering cumulus cloud. In fact, on this run the T-33 measured record turbulence levels unequaled in any other cloud penetration in the five years of this experiment (Refs. 6 - 11). A plot of the plan and elevation views of the gust vectors for this run (Fig. 7) more clearly illustrates the air motion within this cloud top. Downdrafts were measured on entry to the downwind side of the cloud, followed by a 650 m wide area of strong updraft centred just upwind of the mid-cloud position and smaller downdrafts within the upwind wall of the cloud. The peak vertical gust component reached 12.5 m s^{-1}, which, when combined with the longitudinal and lateral components, produced a gust vector of over 15 m s^{-1}. The RMS longitudinal and vertical gust levels within cloud were 5.2 and 5.4 m s^{-1} respectively. These gusts produced a peak vertical acceleration increment of 1.18 G and an RMS within cloud of 0.35 G.

The strongest gust yet measured by the Twin Otter was the result of a wave encounter over the Adirondack Mountains of northern New York State (Fig. 8). The aircraft was cruising south at 7000 feet with an abeam wind from the west averaging 38 m s^{-1} (73 knots). Prior to the onset of the turbulence, the aircraft entered a smooth, increasing downdraft (WGE) which reached 5 m s^{-1}. The peak gust (at t = 16 sec in Fig. 8) featured sharp excursions in the lateral and vertical components of -15.8 and -15.3 m s^{-1} within one second. During the reversal in the vertical gust component, the vertical acceleration registered excursions of +0.68 and -0.78 G from the level flight condition.

Contrasted with this event was another Twin Otter mountain wave encounter at 7000 feet over Maine (Fig. 9). On this occasion, the crew (including one of the authors) was unaware of an unusual occurrence until the wave patterns were observed in the data on playback. These data demonstrate the sensitivity of the instrumentation and its ability to measure long wave (~15 km), low amplitude (2.9 m s^{-1}) motions of the atmosphere.

In 1981 the Twin Otter joined 13 other instrumented aircraft in Montana in a major study of convective cloud systems (CCOPE). One of the most interesting cases was the study of the outflow of cool air from a dying thunderstorm. The Twin Otter was flown at 4000 ft msl (~1500 ft agl) back and forth on a north/south track 5 - 10 miles east of the storm. Although the storm did not appear very vigorous at this time, the gust front measured by the Twin Otter certainly was. Three penetrations of the cool outflow are shown in Figure 10. The temperature dropped about 5 deg C in each case and the wind speed increased by about 15 m s^{-1} (~30 knots) with little change in direction. Vertical gusts of $\pm$ 6 m s^{-1} produced a very rough ride in the Twin Otter. Part of this study involved a comparison of the aircraft-derived winds with those measured by a triangular array of Doppler radars. The low altitude wind shears associated with gust fronts of this nature are hazardous to aircraft during takeoff or approach. Well-calibrated Doppler weather radars offer promise as a means of early detection of these hazards, as has been demonstrated at Denver's Stapleton Airport (Ref. 18).

Several plotting routines have been developed to reproduce the aircraft flight paths relative to the ground or to the moving airmass. Figure 11 shows the ground track derived from the recorded GNS-500A data for a part of one Twin Otter flight. The aircraft was being flown in a study of the dispersion of a tracer gas released from a second aircraft. The Twin Otter airborne software has an 'airmass pointer' routine that presents the aircrew with command bearing and range to return to the parcel of air in which the routine was initiated. In this case the pointer was set while circling with the release aircraft in the upper left of Figure 11. After the gas release, the Twin Otter was held off to the northwest for a few minutes, and then, following the pointer, flown downwind to the southeast to intersect the pointer position at each of the 'P' event marks indicated on the flight track. In cloud physics studies, the pointer routine finds particular application in relocating a specific cloud in a cluttered sky in order to accomplish repeated penetrations.

At the request of Agriculture Canada, the NAE has been conducting annual experiments to measure the vertical flux of CO_2 and water vapour in the boundary layer above various types of vegetation (Refs. 12 and 13). The program has been concentrated on the development of airborne instrumentation and analytical techniques to measure gaseous exchange rates over wide areas to infer vegetation growth rates. In this experimental environment (low altitude, light winds and small vertical gusts damped by proximity to the ground), valuable experience is being gained on probing the aircraft's ability to make accurate gust and flux measurements.

Figure 12 shows time histories for one 7-km run at an altitude of 40 m over mixed farmland and forest. The vertical gust trace is typical of these runs, with an RMS value of only 0.6 m s^{-1}. The eddy correlation technique is used to derive CO_2 fluxes from the product of the vertical gust times fluctuations in the CO_2 concentration, as measured by an infrared radiation absorption device. The bottom three traces show 10-second running means of the contributions to the CO_2, heat and water vapour fluxes. The radiometer trace reveals that this run was flown in scattered cloud conditions. The vegetation and the atmosphere above it respond rapidly to changes in incident radiation. The patches of sunlight are clearly associated with increased activity on the temperature trace, the upward flux of heat and water vapour and the downward flux of CO_2. Average cospectra for CO_2 and sensible heat (Fig. 13) show that most of the contributions to the flux as measured by the Twin Otter fall in the wavelength range of 50-1000 m. Through comparison with ground-based measurements, estimates are being made to determine to what extent these cospectra may be truncated. The main limitation appears to be at long wavelengths, due largely to the restricted lengths of the runs. It appears that runs in excess of 10 km are required for accurate estimation of the fluxes (Ref. 17).

During the period 1982-1984, a considerable effort was expended on the investigation of low altitude turbulence modeling techniques. Turbulence data were collected by the T-33 over hilly and flat terrain to altitudes as low as 20 m. These data were then 'fitted' to two types of turbulence model, the power spectral representation and the Statistical Discrete Gust (SDG) model. Power spectral modeling appeared to fit most data sets very well, as typified by Figure 14.

On the other hand, the SDG analysis of the data showed a lack of convergence for the lower altitude turbulence (Fig. 15). It appears that this is a result of the breakdown of the self-similar scaling of the turbulent eddies when the measurement height is of the order of the scale length of the gust being considered (Ref. 14).

NATO air forces conduct low level training missions over Labrador, operating from the base at Goose Bay. In the late 1970's, there was a proposal for a cooperative low altitude turbulence research project in the same area. The NAE T-33 was flown there to make some preliminary measurements and to collect data over a terrain different from that near its home base. Figure 16 shows traces for a run at 50 m altitude from over Melville Lake (sea level) onto the shore, which rises steeply to about 600 m msl (the fourth trace shows terrain height computed from the difference between the radio altimeter height and pressure altitude). The traces show the expected increases in the mean wind and turbulence over the higher terrain. They also indicate that the air motion measurements are well compensated for the aircraft motion, for there are no significant disturbances in the gust traces during the 1/2-G pull-up and climb up the rising shore.

4. ACCURACY CHECKS

Operators of turbulence research aircraft face the constant vigil of maintaining or improving the accuracy of the measurements and, in particular, ensuring that the aircraft motion effects are minimized. Since the measured wind is the small difference between two relatively large vectors, even a small percentage error in either the TAS or the inertial velocity can produce a large percentage error in the computed wind components. To retain confidence in the measurements and detect the first signs of a deteriorating sensor or a software bug, the aircraft are routinely subjected to standard tests. Oscillations in pitch, roll and yaw are conducted in smooth air and any resultant excursions in the gust traces from the assumed steady wind values give an indication of inaccuracies in the compensation for aircraft motion (Fig. 17). Typical tests with the T-33 and Twin Otter have produced residual RMS gust velocities of 0.3 - 0.4 m s^{-1} (Refs. 3 and 4).

Accurate measurement of the mean wind is very important in many of the Twin Otter pollution studies . To test the precision of the system, a box pattern with 1 - 2 minute legs is flown at an altitude where the winds are expected to be relatively invariant. If the legs of the box are aligned along and across the wind direction, then the leg-averages of the winds, TAS and inertial velocities can be used to identify the source of an error in the measurements. A visual presentation of the wind vectors is also helpful. Figure 18 illustrates a Twin Otter flight track with the measured absolute wind vectors shown at a 6-second interval. If the measured mean wind vector is subtracted, there results a plot of the relative wind vectors, all of which would be zero in an ideal case. In this case (Fig. 19), there is a slight starboard bias in the wind measurements, which indicates a possible offset in the measurement of sideslip angle or a misalignment of the Doppler radar. Carefully timed reciprocal runs along a fixed ground track (such as a straight railway line) provide a method to discriminate a groundspeed error from one in the airspeed vector.

To maintain accuracy of the inertial velocity measurement, considerable care must be taken to ensure consistent calibrations of the accelerometers and rate gyros which contribute to the high frequency component. The low frequency contribution measured by the Doppler radar can be affected by the reflective properties of the earth's surface. For example, a two percent change is required in the Doppler calibration for flight over water, which is applied in the Twin Otter software through the use of a function switch. In a recent experiment over the Atlantic Ocean off Halifax, methods were developed to compensate for the effects of large waves and the current (Ref. 16). However, the most serious problems for the Doppler measurements are presented by flight in some types of precipitation, when the Doppler can lock onto the precipitation instead of the ground. In these cases, the Twin Otter software computes an optional inertial velocity with the low frequency contributions provided by the Loran-C and the rate of change of pressure altitude (Fig. 2).

There are also on-going efforts to maximize the accuracy of the airspeed vector measured by the aircraft. These focus on the flow angle sensors and the determination of the position errors for the static and dynamic pressure probes. Wind tunnel tests were used to ascertain the natural frequency and damping ratio for seven different designs of balsa and aluminum flow vanes (Ref. 19). Prior to its installation on the Twin Otter, the Rosemount 858 5-hole probe was carefully calibrated in the NAE 6 x 9-ft wind tunnel, primarily to verify the factors that relate the measured differential pressures to the flow angles and to document the airflow effects of the structure supporting the probe (Ref. 5). The effects of two methods of preventing blockage of the pressure lines in heavy precipitation or ice crystal clouds were also studied.

The presence of the aircraft and the disturbed airflow about it affect the accuracy of the measured airspeed vector, and hence the resultant wind components. Standard methods of determining these position errors have been used, which include tower flyby, trailing cone, aircraft intercomparison and tracking by a cinetheodolite camera (Ref. 20). Aircraft-generated flow disturbances can also distort the particle images and concentrations measured by the laser spectrometers. This has led to considerable theoretical and in-flight investigation of the aerodynamic influence of the wing on these measurements (Refs. 21 and 22).

5. TURBULENCE MEASUREMENT WITHOUT A GUST BOOM

Part of this workshop will address the use of commercial aircraft flight recorder data to derive atmospheric turbulence data. Prior to 1980, the NAE Twin Otter had its present inertial velocity capability but lacked a noseboom for the measurement of flow angles, and therefore was instrumented essentially the same as a modern commercial airliner. Vertical gusts were calculated using an angle of attack derived from the measured vertical acceleration, that is, the wing served as the angle of attack sensor through the lift expression utilizing airspeed, density, aircraft weight and the lift curve slope (Ref. 4). After the noseboom was installed, the approximate vertical gust (WZF) continued to be calculated for comparison with the vertical gust (WGE) computed using the boom-measured angle of attack. Both methods employed the same inertial velocity to correct for airplane motion.

A comparison of the RMS gust velocities produced by the two methods for 71 cumulus cloud penetrations showed excellent agreement, with a median difference of only 0.04 m s^{-1}. The WZF trace from one of these penetrations is shown in Figure 20 and closely approximates that for WGE, the vertical gust calculated using the angle of attack vane. Vertical gust spectra (e.g. Fig. 21) show close correlation up to about 1.0 Hz, where the high frequency content of the approximate gust is truncated because the aircraft does not fully respond to gusts at these frequencies. At the low speed of the Twin Otter, this means that only gusts of wavelengths shorter than about 70 m would not be well represented, which may not be a serious limitation for some studies. For a commercial airliner with a cruise TAS of about 240 m s^{-1} and a reduced response due to its higher wing loading, the wavelength limit for this approximate method may be of the order of 500 m.

6. PLANNED FUTURE DEVELOPMENTS

To maintain operations with highly instrumented atmospheric research aircraft requires continual development of the hardware and software and the acquisition of improved sensors as they become available. The miniaturization of computers and other supporting electronics, plus the scientists' desire to see real-time data to effectively direct the research flight, leads to more complete on-board processing and improved displays.

The NAE T-33 will shortly be undergoing a complete electrical rewiring as part of a life extension program being applied to all Canadian T-33 aircraft. This will provide an opportunity to install an entirely new, compact data acquisition system being built to fit the demanding confines of the T-33 nose bay and cockpit. It will employ an LSI-11/73 processor, dual floppy disks and a keyboard to provide a real-time computational capability similar to that on the Twin Otter. Data will be recorded in serial-digital format on a 70-Mbyte streamer. An advancement in real-time display is planned, using a Sharp EL unit with 2^{17} pixels to provide both an alpha-numeric and a graphic capability.

Major changes are also underway for the Twin Otter. In an effort to reduce weight and electrical power requirements while improving accuracy, a Litton-90 Inertial Reference System (IRS) has been ordered. It utilizes laser ring gyros and high quality accelerometers to provide an inertial velocity in the aircraft (SD) axes system. It is planned to employ Kalman filtering to mix the IRS data with low frequency components, to be provided initially by the Doppler radar and Loran-C. The IRS will have the capability to accept signals from the satellite-based Global Positioning System (GPS) when available, which can then be used to replace the Doppler radar and eliminate precipitation effects on the wind measurements. More flexibility is desired in the real-time software, which will likely require a new computer, possibly a Micro-Vax. Graphic displays are planned, compatible with the model being installed on the T-33. In the CO_2 flux program, there is a desire to improve short-wave gust resolution from 10 to 5 m. This will require a doubling of the recording rate to 32 Hz, with the anti-alias filters set with breakpoints of 10 Hz. An essential part of this improvement will be the fabrication of a new, stiffer noseboom with a natural frequency significantly higher than the 12 Hz of the current boom. Plans also call for further investigation of the position errors at the noseboom using the trailing cone and cinetheodolite tracking.

In the near future, the principal areas of research for the Twin Otter will continue to be atmospheric pollution (possibly including toxic chemicals) and the gaseous exchange between vegetation and the atmosphere. Flights are planned to compare measured winds with Canada's first Doppler weather radar, possibly as part of a larger study of wind shear. After its rewiring and re-instrumentation, the T-33 will continue to be applied to experiments in flight mechanics.

7. REFERENCES

1. Mather, G.K. — The NAE T-33 Turbulence Research Aircraft. NAE Aeronautical Report LR-474, National Research Council of Canada, Ottawa, Mar. 1967.

2. MacPherson, J.I. — A Description of the NAE T-33 Turbulence Research Aircraft, Instrumentation and Data Analysis. DME/NAE Quarterly Bulletin No. 1972(4), National Research Council of Canada, Ottawa, Jan. 1973.

3. Baillie, S.W. — A Description of the NAE T-33 Turbulence Research Aircraft (NTRA). NAE Laboratory Technical Report LTR-FR-90, National Research Council of Canada, Apr. 1984.

4. MacPherson, J.I.; Morgan, J.M.; Lum, K.K. — The NAE Twin Otter Atmospheric Research Aircraft. NAE Laboratory Technical Report LTR-FR-80, National Research Council of Canada, Mar. 1981.

5. MacPherson, J.I. — Wind Tunnel Calibrations of a PMS Canister Instrumented for Airflow Measurement. Aeronautical Note NAE-AN-32, National Research Council of Canada, Ottawa, Sept. 1985.

6. MacPherson, J.I.; Isaac, G.A. — Turbulence Characteristics of Some Canadian Cumulus Clouds. Journal of Applied Meteorology, Vol. 16, No. 1, Jan. 1977, pp. 81-90.

7. MacPherson, J.I. — A Comparison of the Turbulent Characteristics of Cumulus Clouds Measured Near Yellowknife and Thunder Bay. DME/NAE Quarterly Bulletin 1979(1), National Research Council of Canada, Ottawa, Apr. 1979.

8. Schemenauer, R.S.; MacPherson, J.I.; Isaac, G.A.; Strapp, J.W. — Canadian Participation in HIPLEX 1979. NAE Laboratory Technical Report LTR-FR-77, National Research Council of Canada, Ottawa, Oct. 1980.

9. Schemenauer, R.S.; MacPherson, J.I.; Isaac, G.A.; Strapp, J.W. — Canadian Participation in HIPLEX 1980. NAE Laboratory Technical Report LTR-FR-84, National Research Council of Canada, Ottawa, Oct. 1981.

10. Schemenauer, R.S.; Isaac, G.A.; Strapp, J.W.; MacPherson, J.I. — Aircraft Assessment of Weather Modification Potential. Proceedings of the Eighth Conference on Inadvertent and Planned Weather Modification, Reno, Oct. 1981, pp. 108-109.

11. Isaac, G.A.; Strapp, J.W.; Schemenauer, R.S.; MacPherson, J.I. — Summer Cumulus Cloud Seeding Experiments near Yellowknife and Thunder Bay, Canada. Journal of Applied Meteorology, Vol. 21, No. 9, Sept. 1982, pp. 1266-1285.

12. MacPherson, J.I. — Flight Tests of Instrumentation for Airborne Carbon Dioxide Flux Measurement. Aeronautical Note NAE-AN-16, National Research Council of Canada, Ottawa, Oct. 1983.

13. Alvo, P.; Desjardins, R.L.; Schuepp, P.H.; MacPherson, J.I. Aircraft Measurements of CO_2 Exchange Over Various Ecosystems. Boundary Layer Meteorology, Vol. 29, No. 2, June 1984.

14. Baillie, S.W. The Altitude Related Characteristics of Atmospheric Turbulence Displayed Through Statistical Discrete Gust Analysis. Paper 85-0343 AIAA 23rd Aerospace Sciences Meeting, Reno, Jan. 1985.

15. Isaac, G.A.; Leaitch, W.R.; Strapp, J.W.; Anlauf, K.G. Summer Aerosol Profiles Over Algonquin Park, Canada. Atmospheric Environment, Vol. 20, 1986, pp. 157-172.

16. Smith, P.C.; MacPherson, J.I. Lateral Variations of Near-Surface Wind Velocity and Atmospheric Turbulence at the Land-Sea Boundary During CASP. Submitted to Atmosphere Ocean, Aug. 1986.

17. MacPherson, J.I.; Desjardins, R.L.; Schuepp, P.H. Gaseous Exchange Measurements Using Aircraft-Mounted Sensors. To be Presented at the Sixth Symposium on Meteorological Observations and Instrumentation, New Orleans, Jan. 1987.

18. McCarthy, J. The Joint Airport Weather Studies Project: Current Analysis Highlights in the Aviation Safety Context. Paper 84-0111 AIAA 22nd Aerospace Sciences Meeting, Reno, Jan. 1984.

19. Baillie, S.W. The Dynamic Response Parameters of 7 Airflow Vane Designs. NAE Laboratory Memorandum FR-96, National Research Council of Canada, Ottawa, May 1984.

20. Aitken, J.F.; Baillie, S.W. Static Pressure Position Error Calibration of the NAE T-33 C-FSKH. Publication currently in editing.

21. Drummond, A.M.; MacPherson, J.I. Aircraft Flow Effects on Cloud Drop Images and Concentrations Measured by the NAE Twin Otter. Journal of Atmospheric and Oceanic Technology, Vol. 2, No. 4, Dec. 1985, pp. 633-643.

22. MacPherson, J.I.; Baumgardner, D. Studies of Aircraft Flow Effects About Wing-Mounted PMS Probes. To be Presented at the Sixth Symposium on Meteorological Observations and Instrumentation, New Orleans, Jan. 1987.

TABLE 1

NAE ATMOSPHERIC RESEARCH AIRCRAFT

Description and Performance

Type	**Canadair Silver Star T-33 Mk3**	**deHavilland DHC-6-200 Twin Otter**
Registration	C-FSKH	C-FPOK
Max Gross Weight, lb	16800	11579
Wing Span, ft	42.4	65.0
Wing Area, ft^2	237	420
Wing Loading, psf	71	28
Operational Ceiling, ft	41000	20000
Max Cruise Speed, IAS kt	505	150
Range, n mi	1000	500
Load Limits, G	+7.3	+3.5
	-3.0	-1.8

TABLE 2

NAE ATMOSPHERIC RESEARCH AIRCRAFT

Sensors for Air Motion Measurement

	T-33	Twin Otter
Flow Angles, α & β	6.1-ft gust boom Balsa vanes Synchros	6.1-ft gust boom Rosemount 858 5-hole probe Differential pressure transducers
Dynamic Pressure (Airspeed)	Differential transducer	Differential transducers (2)
Static Pressure	Quartz crystal temperature compensated transducer	Quartz crystal transducer Variable capacitance sensor
Inertial Velocity	3-axis servo accelerometers Rate gyros Marconi Doppler radar	3-axis servo accelerometers Rate gyros Decca Doppler radar
Body Angles	Attitude gyro	Attitude gyro
Heading	C-12 Compass	C-12 Compass
Total Temperature	Platinum element	Platinum element

TABLE 3

NAE ATMOSPHERIC RESEARCH AIRCRAFT

Other Measurements

	T-33	Twin Otter
Geographical Position	GNS-500A Localizer, Glide Slope	Loran-C or GNS 500A
Event Marker	10-level	16-level
Time	NAE clock	NAE clock
Absolute Height	Radio altimeter	Radio altimeter
Additional Temperatures	Dew point Reverse flow	Dew point Reverse flow
Additional Static Pressure	Fin-mounted trailing static cone	-
Control Inputs	Potentiometers on elevator, aileron, rudder and throttle	-
Engine RPM	Tachometer-generator	-
Cameras	Side-looking 16 mm	VCR with 3 cameras
Cloud Physics	AgI seeding pod	4 PMS laser spectrometers* JW, King liquid water* Air, cloud water and precipitation sampling systems
Weather radar	-	Bendix RDR-1300

* AES-owned

TABLE 4

NAE ATMOSPHERIC RESEARCH AIRCRAFT

Processor, Display and Recorder

		T-33	Twin Otter
Airborne Processor:		DEC LSI-11/73	DEC LSI-11/23, FALCON
		EPROM	Dual floppy disk Keyboard
Real-Time Display		16 LED characters	12 x 40 character Plasma display (cockpit & cabin)
		Fixed - winds, temperature, gust RMS, TAS	Programmable - winds, temperatures, fluxes, pointer etc.
Recorder:	Type	Nagra, reel	CDC Streamer, cartridge
	Data Format	Serial-Digital	Serial-Digital
	Resolution	10-bit	16-bit
	Parameters	32 (raw)	64 (including real-time computed data)
	Rate	32 Hz	16 Hz
	Capacity	2 hours	8 hours
	Voice	2nd track	On separate cassettes, VCR
	Cloud Physics	-	Particle data on AES recorder

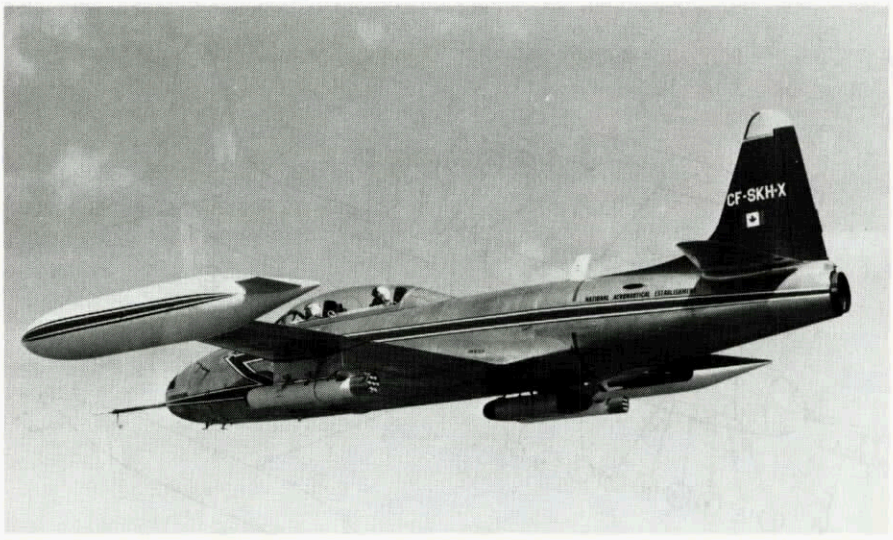

FIG. 1: NAE T-33 (TOP) AND TWIN OTTER ATMOSPHERIC RESEARCH AIRCRAFT

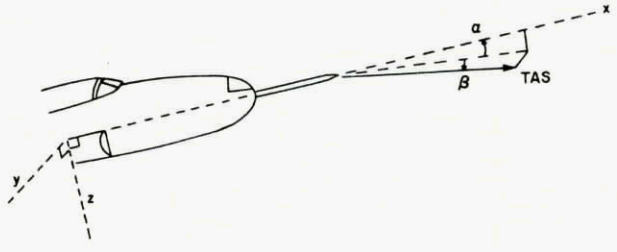

1 AIR VELOCITY RELATIVE TO AIRCRAFT

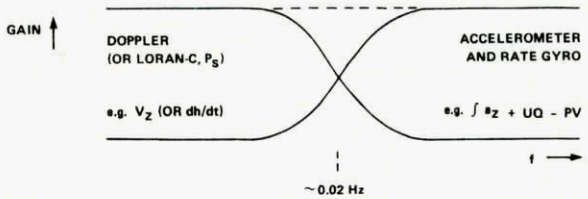

2 INERTIAL VELOCITY FROM COMPLEMENTARY FILTER
3 GUST IN A/C AXES, e.g. $W_g = U\alpha - W_{MIX}$
4 TRANSFORM TO EARTH AXES USING θ, ϕ AND Hdg

FIG. 2: AIR MOTION MEASUREMENT

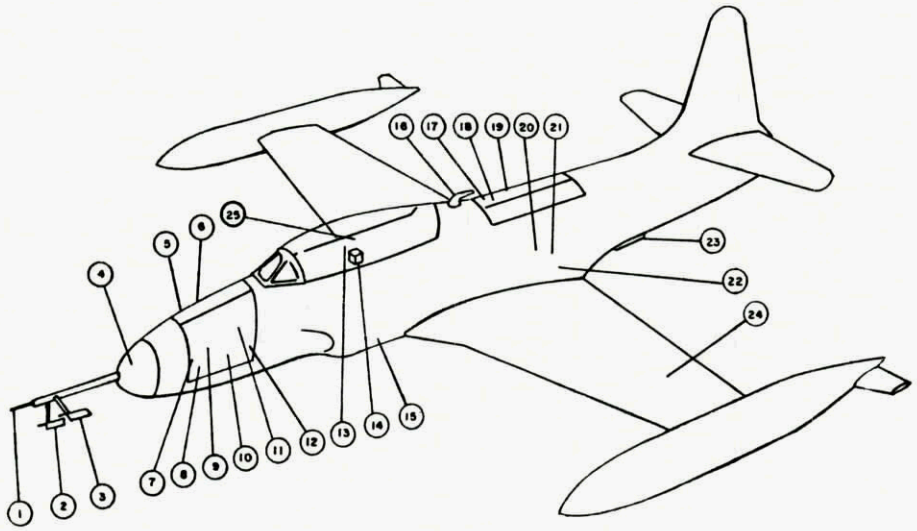

1. STATIC PROBE
2. BETA VANE
3. ALPHA VANE
4. VERTICAL GYRO
5. TOTAL TEMPERATURE PROBE
6. MAGNETIC TAPE RECORDER
7. RATE GYRO PACKAGE
8. PRESSURE SENSOR ΔP_T
9. PRESSURE SENSOR P_S
10. PRESSURE SENSOR P_D
11. SIGNAL CONDITIONING UNIT
12. PHASE ENCODER UNIT
13. PROJECT CONTROL UNIT
14. GNS 500A CDU
15. RADAR ALT. ANTENNA
16. GNS 500A ANTENNA
17. DOPPLER SDC
18. ELEVATOR POSITION POT.
19. RUDDER POSITION POT.
20. THROTTLE POSITION POT.
21. ACCELEROMETER PACKAGE
22. GNS 500 RCU
23. DOPPLER ANTENNA
24. AILERON POSITION POT.
25. MOVIE CAMERA

FIG. 3: INSTRUMENT LOCATIONS FOR NAE T-33

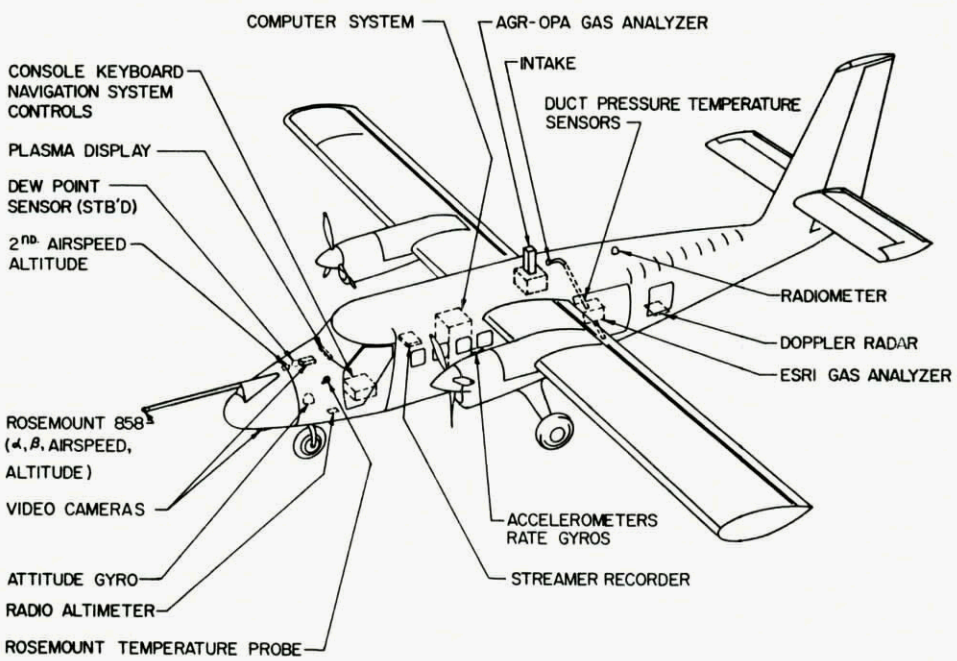

FIG. 4: NAE TWIN OTTER ATMOSPHERIC RESEARCH AIRCRAFT AS INSTRUMENTED FOR GASEOUS EXCHANGE MEASUREMENT

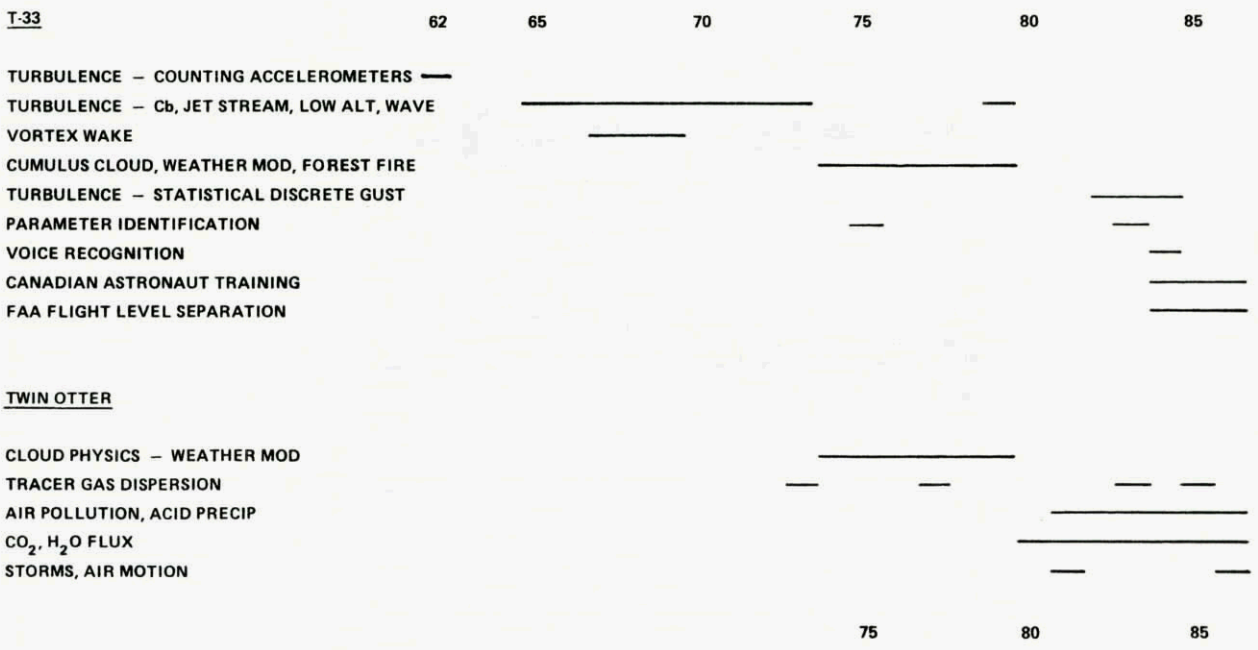

FIG. 5: NAE ATMOSPHERIC RESEARCH AIRCRAFT – PROGRAM HISTORY

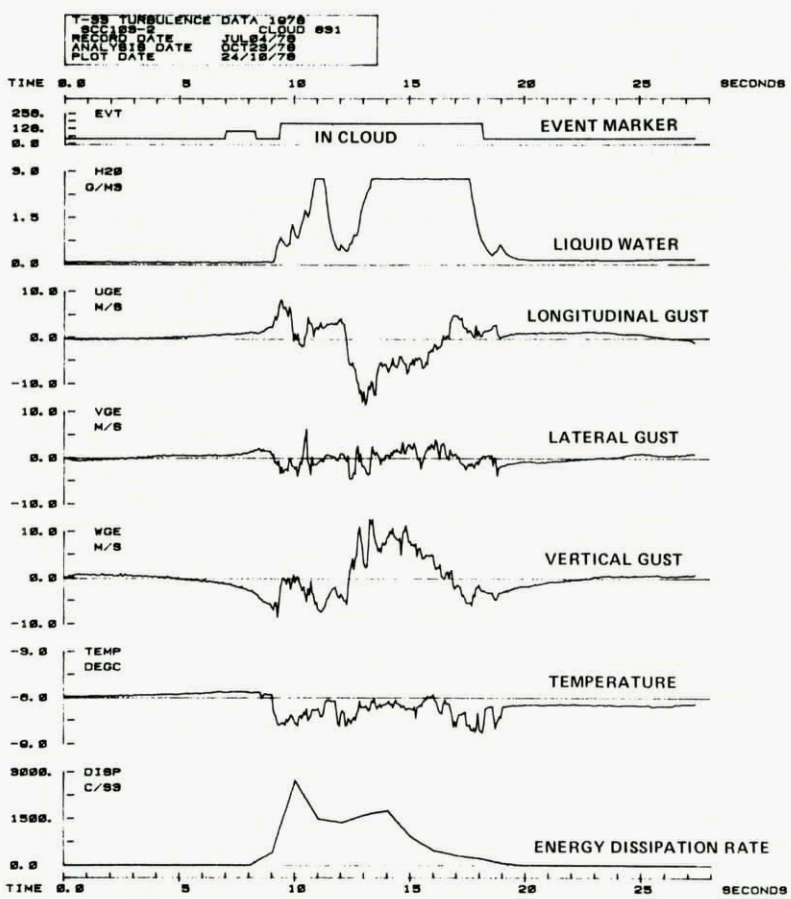

FIG. 6: TIME HISTORIES FOR THE MOST TURBULENT CLOUD PENETRATION IN EXPERIMENT

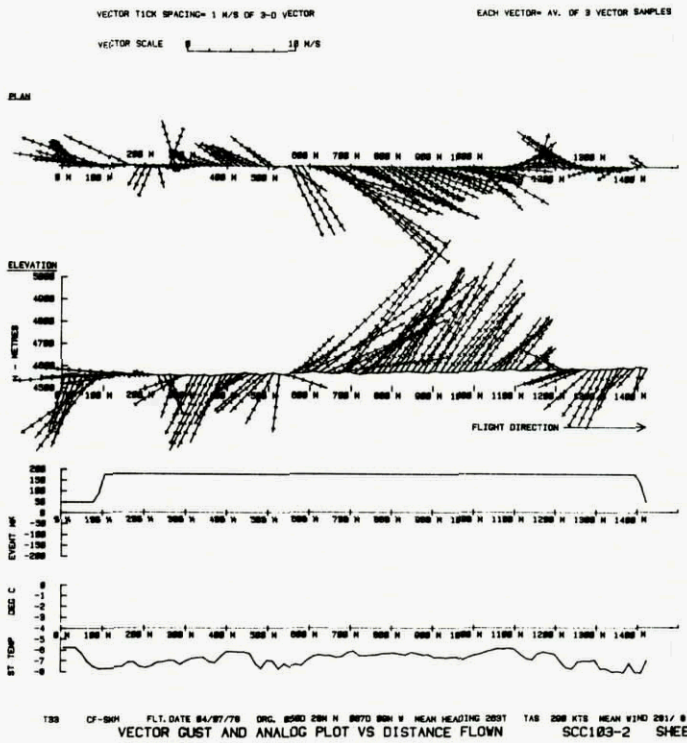

σ_u = 5.2 mps PEAK W_g = 12.5 mps σ_{A_Z} = 0.35G
σ_w = 5.4 mps VECTOR > 15 mps PEAK A_Z = 1.18G

FIG. 7: STRONGEST GUST MEASURED BY T-33 IN CUMULUS CLOUDS

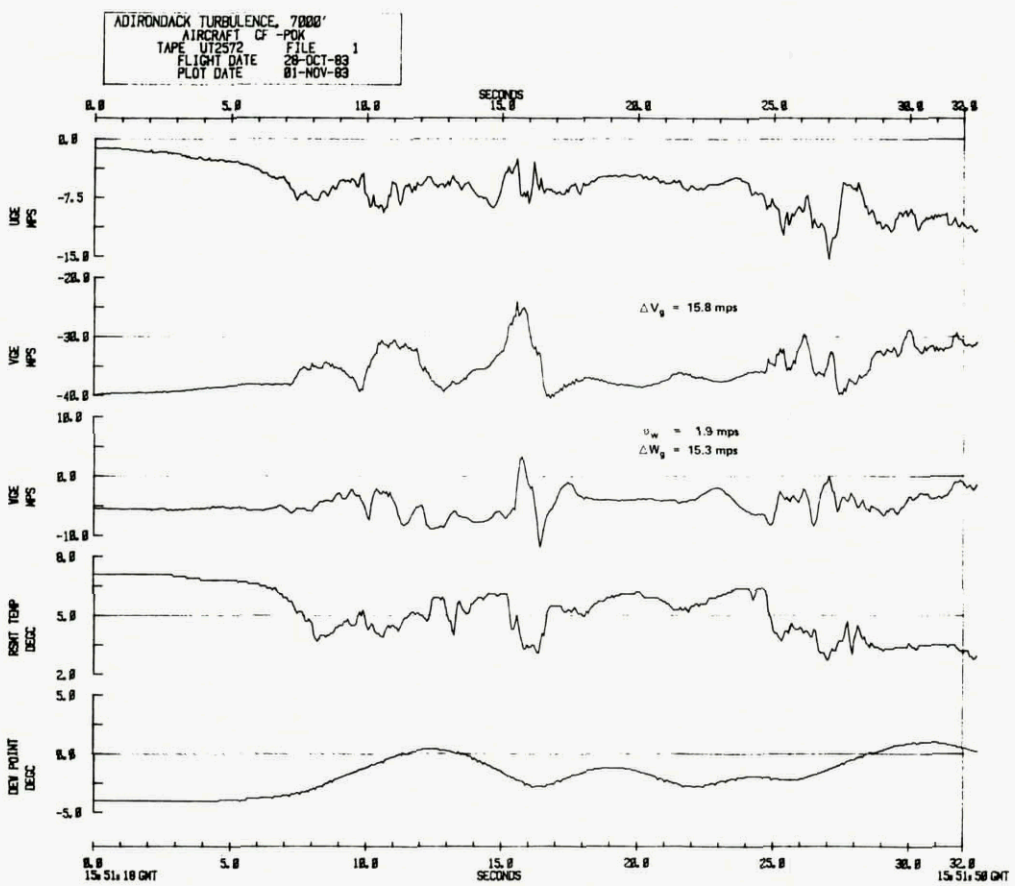

FIG. 8: TWIN OTTER TURBULENCE ENCOUNTER IN ADIRONDACKS

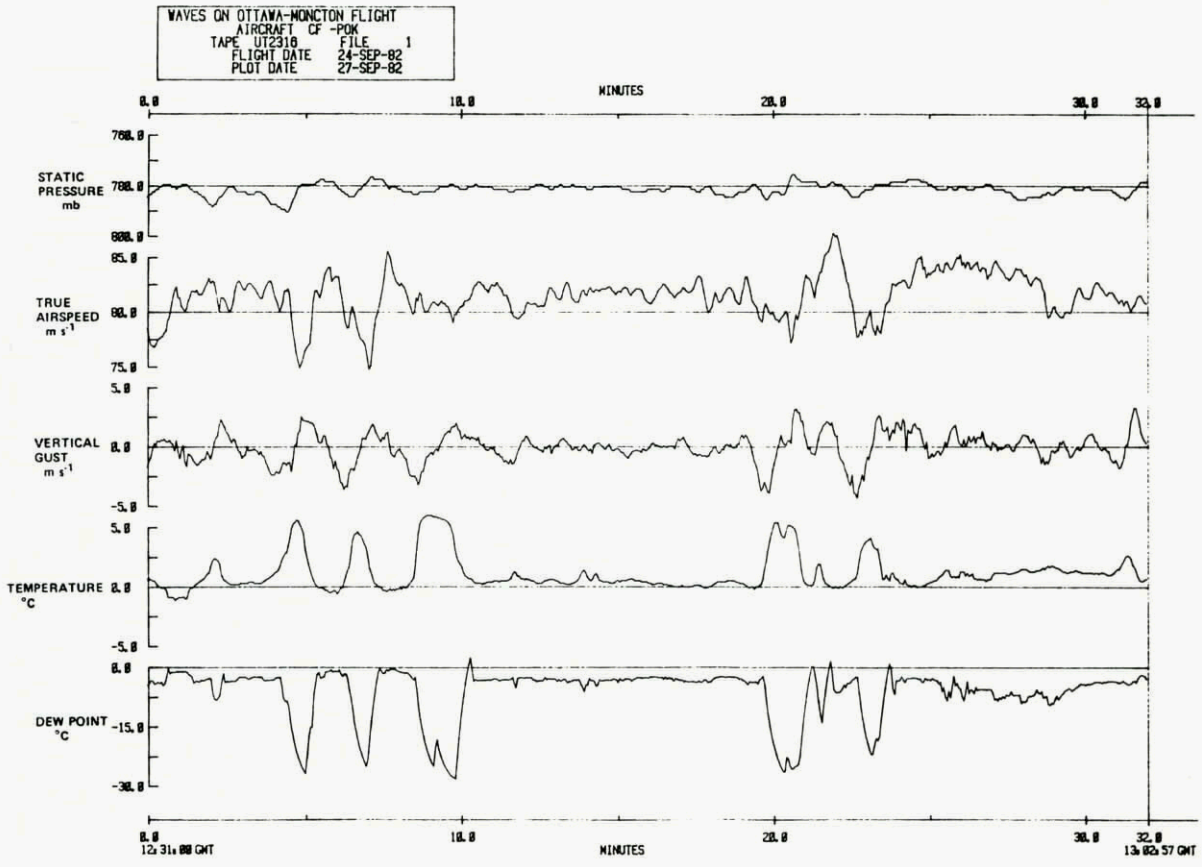

FIG. 9: MOUNTAIN WAVE ENCOUNTERED AT 7000' OVER MAINE. WAVELENGTH AND AMPLITUDE WERE CALCULATED TO BE 15 km AND 350 m RESPECTIVELY

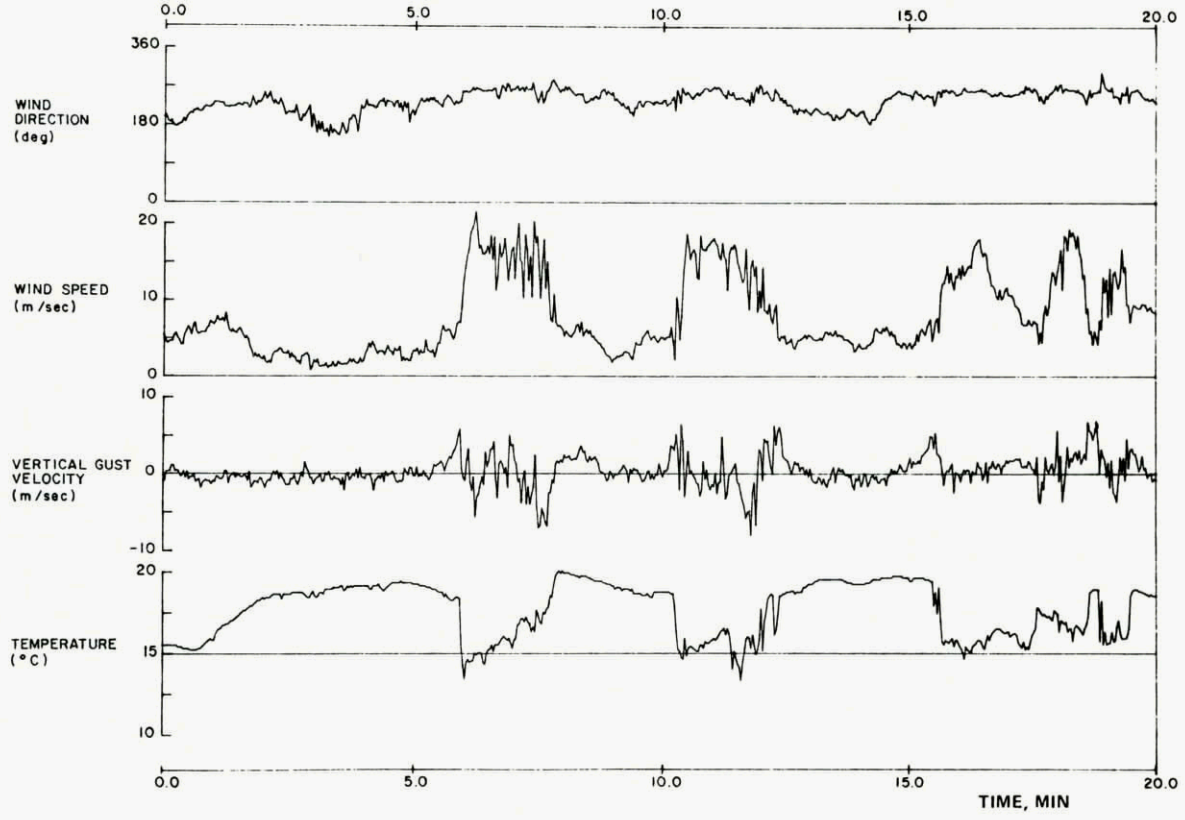

FIG. 10: TWIN OTTER GUST FRONT DATA MEASURED IN 1981 CCOPE EXPERIMENT IN MONTANA. ON THREE OCCASIONS THE AIRCRAFT PENETRATED THE COOL OUTFLOW FROM A DYING THUNDERSTORM

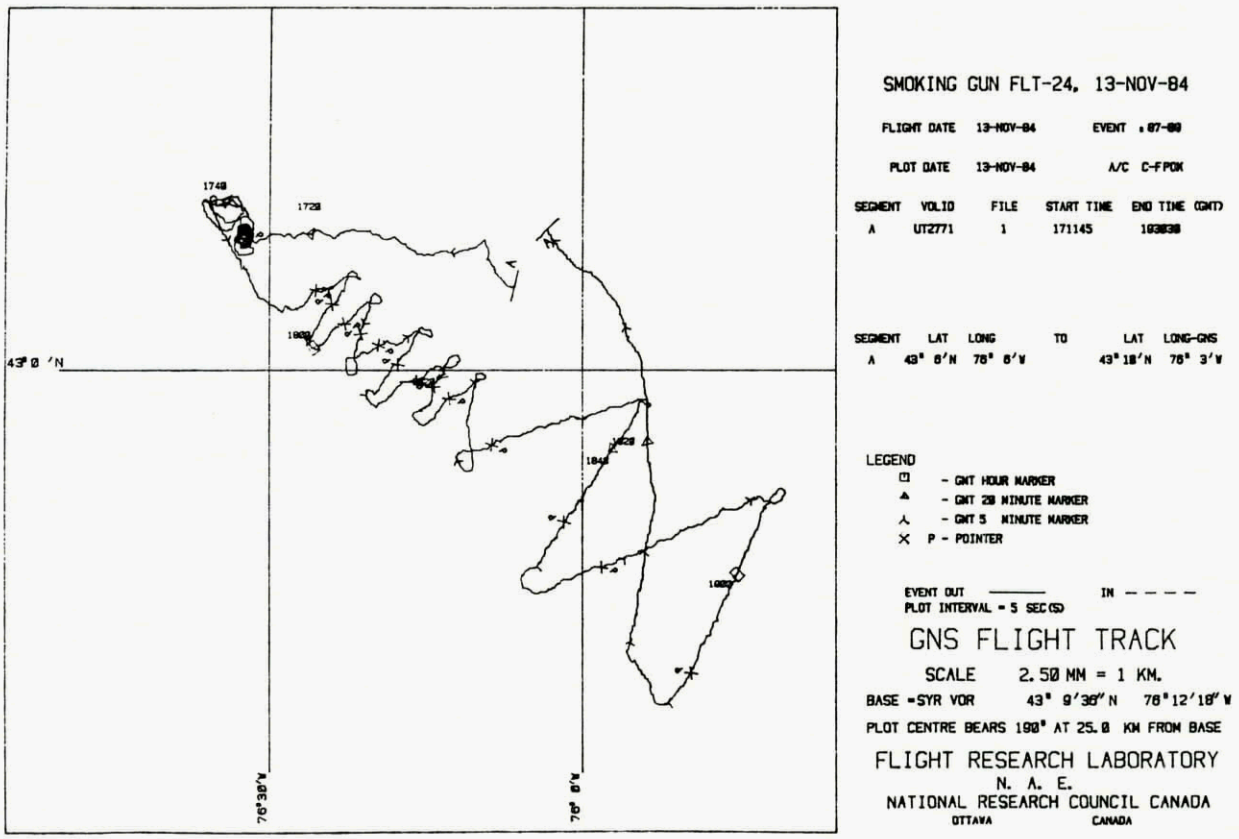

FIG. 11: TWIN OTTER FLIGHT TRACK DURING TRACER EXPERIMENT

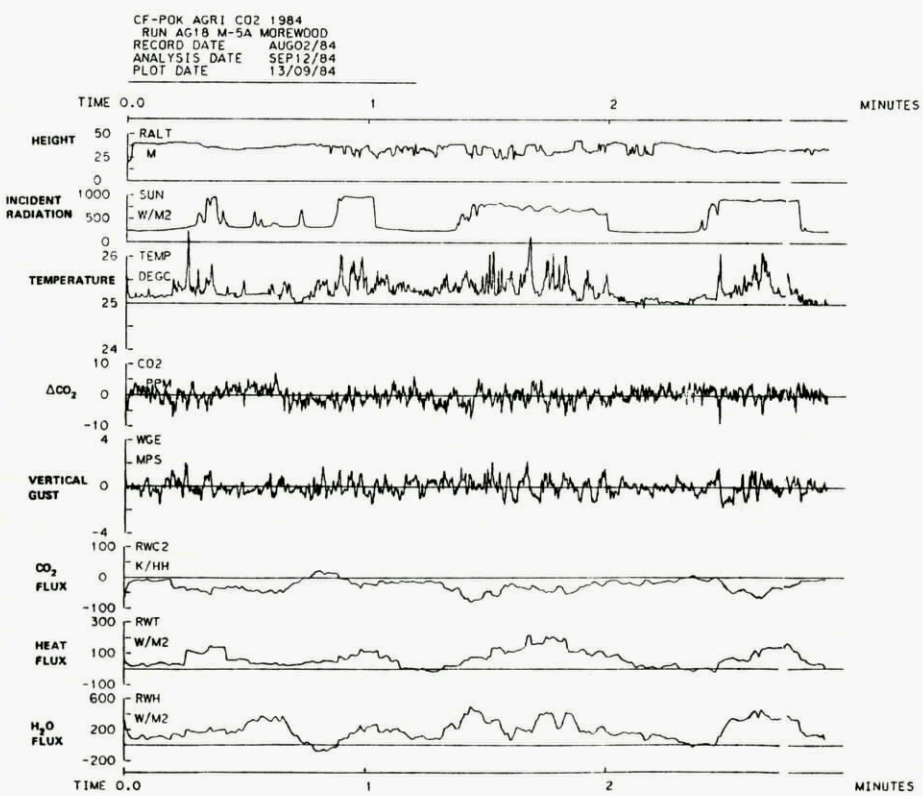

FIG. 12: TWIN OTTER DATA FROM CO_2 FLUX PROJECT. BOTTOM FOUR TRACES ARE 10-SEC RUNNING MEANS OF THE CONTRIBUTIONS TO THE CO_2, HEAT AND WATER VAPOUR FLUXES

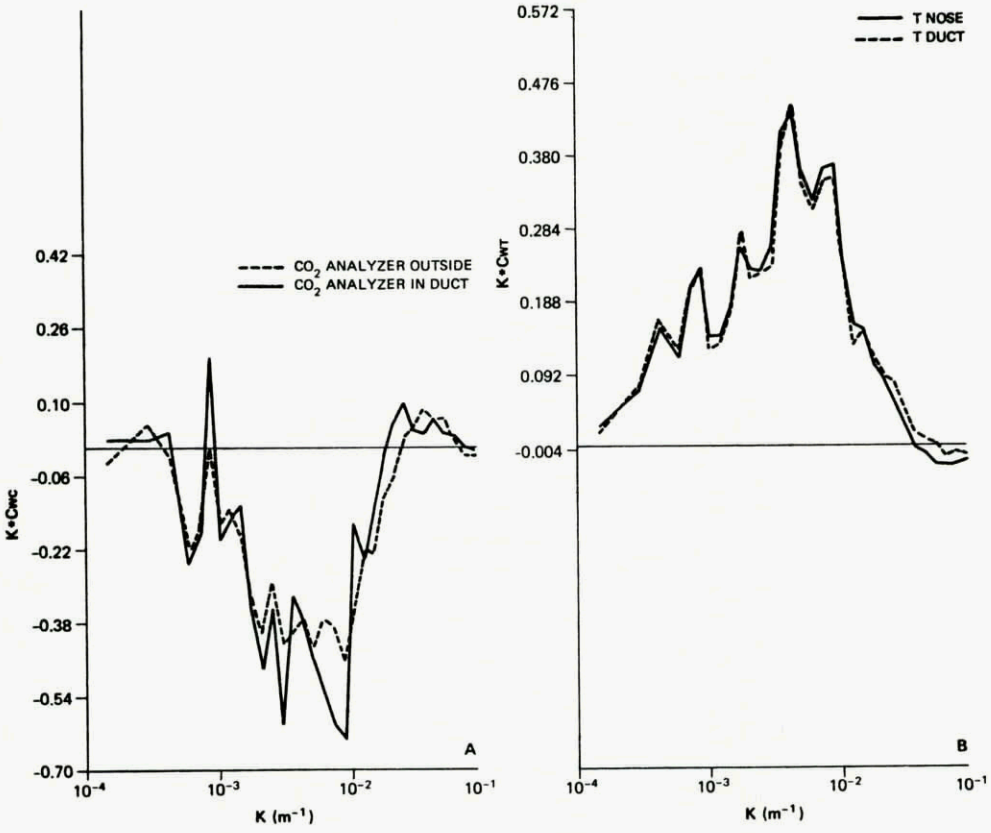

FIG. 13: TWIN OTTER MEASURED COSPECTRA FOR CO_2 FLUX (A) AND HEAT FLUX (B)

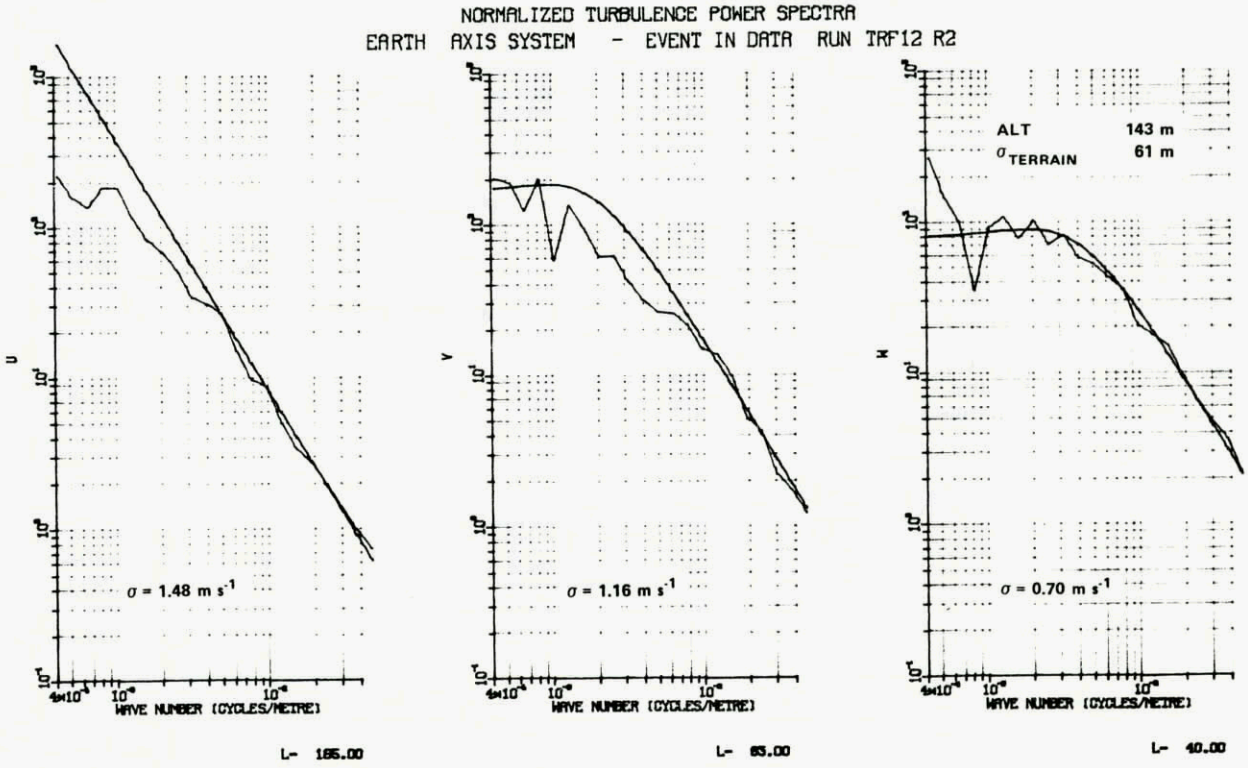

FIG. 14: T-33 GUST SPECTRA FROM LOW ALTITUDE TURBULENCE STUDY

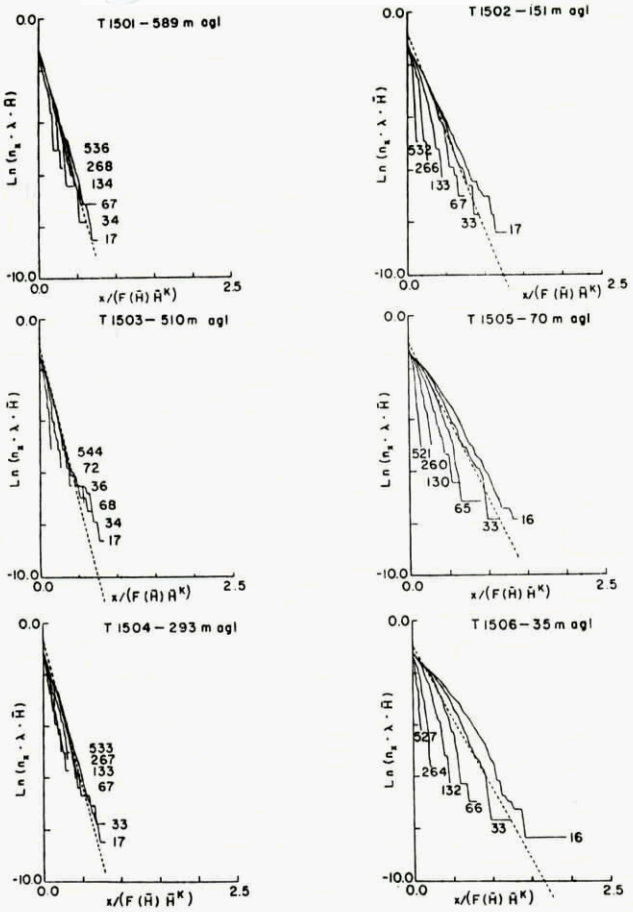

FIG. 15: EXAMPLE OF STATISTICAL DISCRETE GUST ANALYSIS OF T-33 DATA. THE ALTITUDE VARIATION OF THE VERTICAL TURBULENCE SMOOTHED TRANSITION FUNCTION PEAK RESPONSE DISTRIBUTION

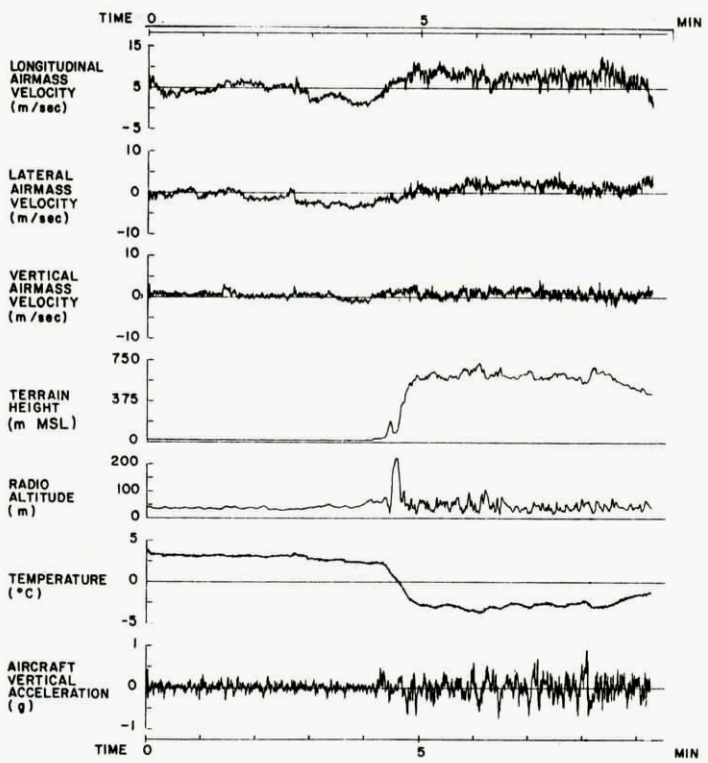

FIG. 16: T-33 LOW ALTITUDE TURBULENCE NEAR GOOSE BAY

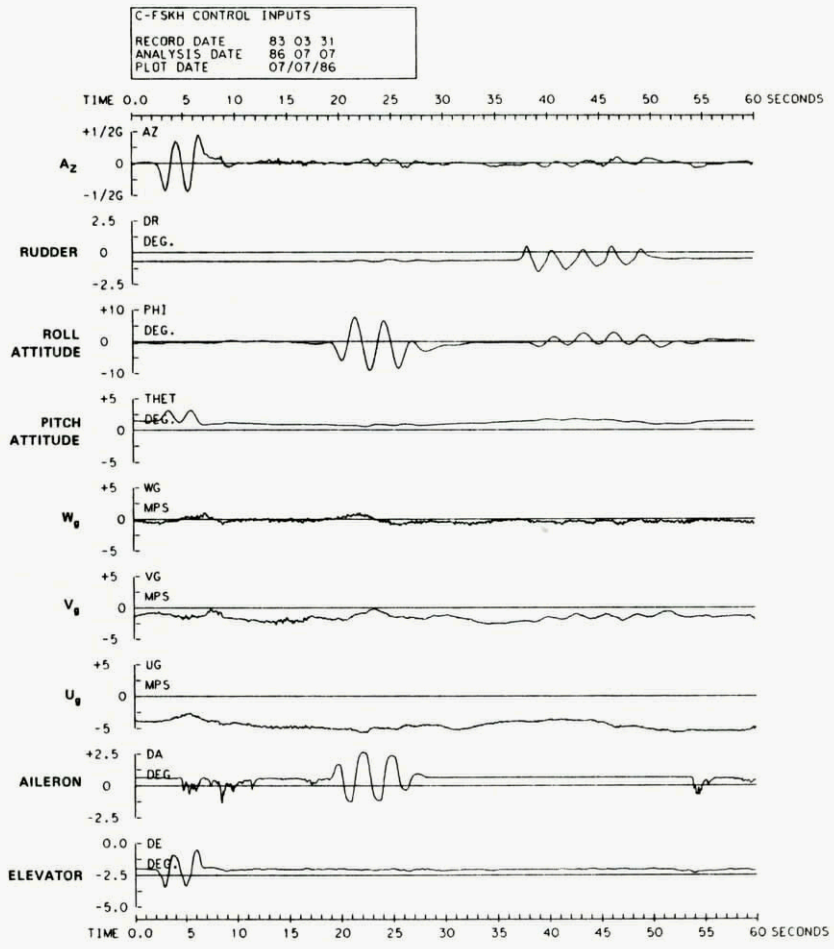

FIG. 17: T-33 CONTROL INPUTS

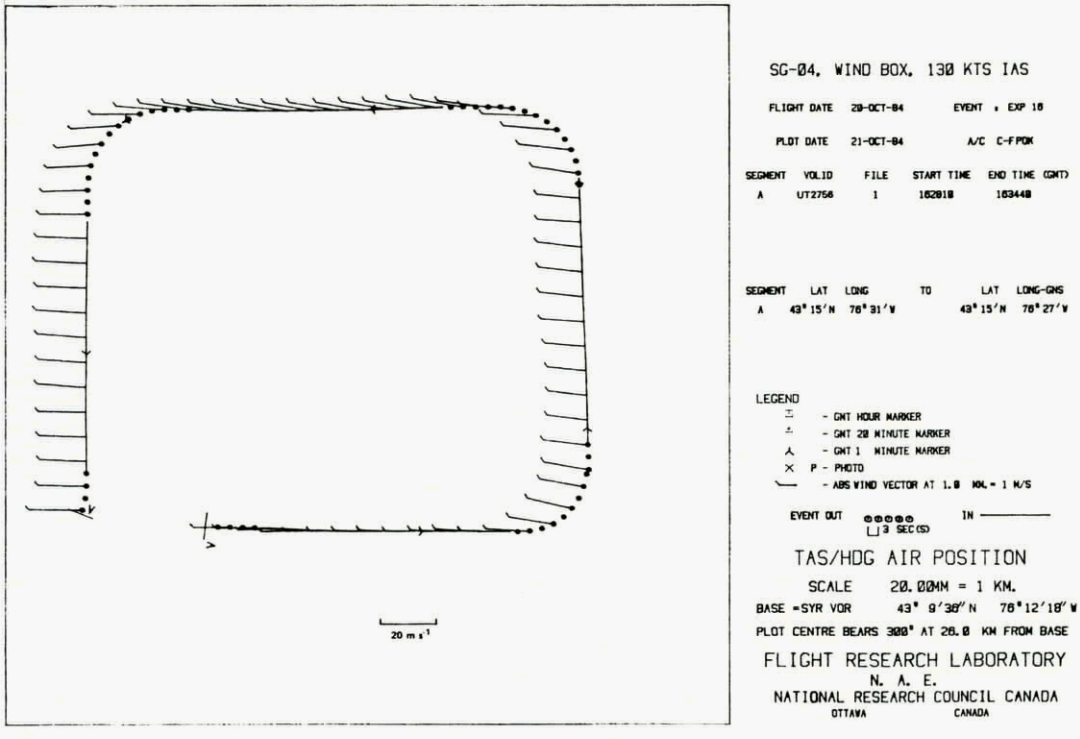

FIG. 18: TWIN OTTER WIND BOX

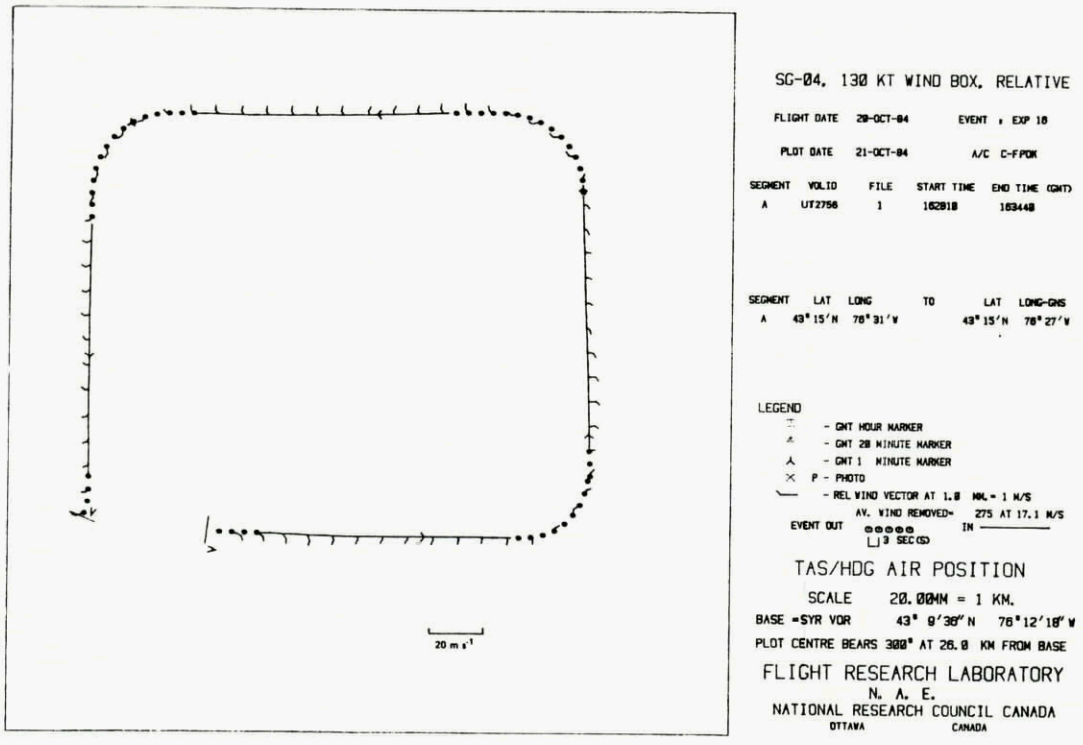

FIG. 19: TWIN OTTER RELATIVE WINDS

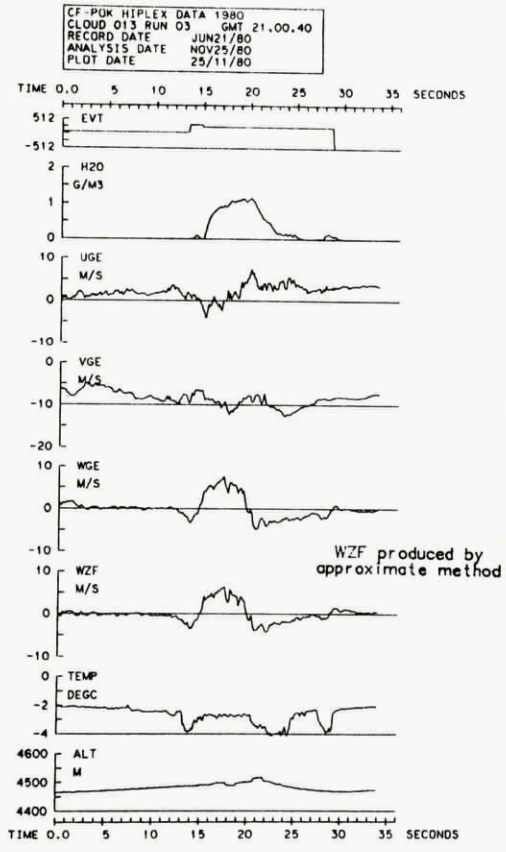

FIG. 20: TWIN OTTER CLOUD PENETRATION

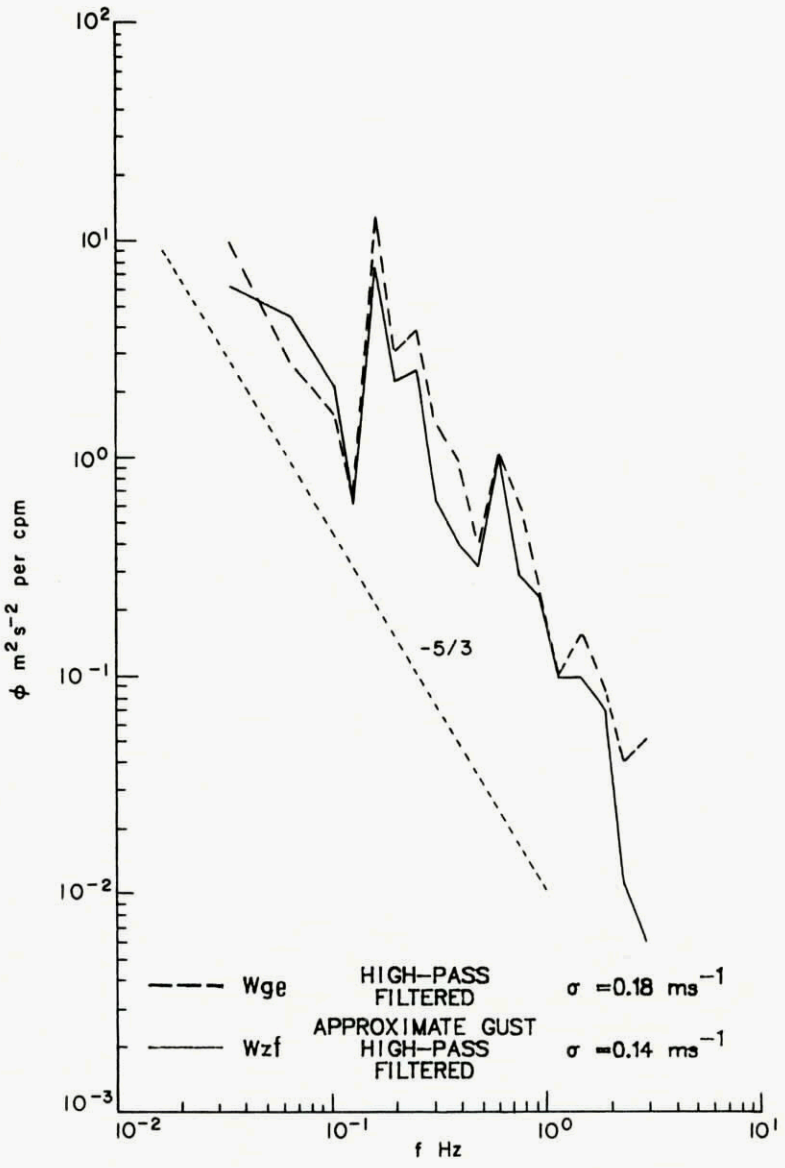

FIG. 21: POWER SPECTRA FOR VERTICAL GUSTS IN LIGHT TURBULENCE

AIRCRAFT DYNAMICS - AERODYNAMIC ASPECTS AND WIND TUNNEL TECHNIQUES

by
K.J. Orlik-Rückemann
Unsteady Aerodynamics Laboratory
National Research Council of Canada
Ottawa, Ontario, K1A 0R6, CANADA

1. INTRODUCTION

The dynamic behaviour of modern fighter aircraft depends much more on the unsteady aerodynamics considerations than in the past. Until quite recently an aircraft designer would display only a passing interest in that subject, concentrating probably on classical problems such as aeroelasticity and flutter. Dynamic stability parameters were most often determined by low angle-of-attack calculation methods, without much recourse to experiments; indeed suitable facilities were rather scarce and the priority habitually assigned to dynamic stability testing very low indeed. The results obtained from those few dynamic experiments that were performed were most often used to confirm that there were no particular problems present rather than to be applied as one of the design parameters or inputs. And yet, for most of the aircraft of the past, such a modest level of investment in unsteady aerodynamics and dynamic characteristics of aircraft was, in fact, quite adequate, and many excellent aircraft were successfully designed in this fashion.

It was only with the advent of modern advanced requirements for a fighter aircraft performance that this time-honoured methodology had become clearly inadequate. The new requirements include the ability to fly at high angles of attack in the presence of extensive regions of separated or vortical flows, relaxed static stability, greatly increased agility and the interest in unorthodox geometries such as closely-coupled-canard or tail-first configurations. There is also considerable interest in the ability to perform very rapid maneuvers and in the aerodynamic characteristics of large amplitude motions. The time lags and the unsteady phenomena associated with the resulting flow fields may significantly affect the dynamic behaviour of modern fighter aircraft and may become as important for aircraft design as the classical static performance criteria.

The unsteady aerodynamics involved is mostly very complex and, although considerable effort is now applied to the development of various analytical and numerical methods of calculations, the most important source of data - at the present time - consists of experimental techniques. Consequently, in this lecture, a review will first be made of the various aerodynamic aspects affecting aircraft dynamic behaviour, to be followed by a survey of the most pertinent experimental techniques. In both cases the presentation will emphasize applications to high performance fighters, such as are exemplified, for instance, by flight at high angles of attacks.

2. AERODYNAMIC ASPECTS

The aerodynamic aspects of aircraft dynamics were reviewed by the present author in an 1983 survey paper in the Journal of Aircraft (Ref. 1). For completeness, this reference is reproduced in full at the end of notes for this lecture. It therefore only remains to add a few remarks about some of the most recent developments in this field.

2.1 Rapid, Large-Amplitude, Pitch-up Motions

High-angular-rate, large-amplitude pitch-up motions may result in maximum lift coefficients far beyond the steady maximum values. In low speed experiments involving two-dimensional airfoils that perform pitch-up motions at constant pitch rate, $\dot{\alpha}$, up to a maximum angle of attack, α_{max}, and then remain at that angle, dynamic lift levels of three times the corresponding steady lift values have been observed (Ref. 2). This is illustrated in Fig. 1, where the maximum lift coefficient, $C_{L_{max}}$, is plotted versus a dimensionless pitch rate, $k=\dot{\alpha}c/2V$, for different values of α_{max}, where c is the airfoil chord and V the free stream velocity. As deduced from measurements of the unsteady pressure distributions during such motions, this lift augmentation is caused by an energetic separation vortex which originates at the leading edge and convects downstream as the angle of attack increases. This mechanism is similar to the well-known phenomenon of deep dynamic stall (Fig. 2), as described e.g. by McCroskey in his 1982 review of Unsteady Airfoils (Ref. 3). Although dynamic stall has previously been of interest mostly in connection with the helicopter blade oscillations and wind turbines, it may now prove to be very important also for the attainment of sustained dynamic maneuvering in the post-stall flight regime such as e.g. described by Herbst (Ref. 4) as "supermaneuverability" (Fig. 3). Of course, for such a purpose, the characteristics of complete configurations, rather than merely two-dimensional data, will be needed. Experiments are now being planned to obtain such information.

For performance evaluation it may be useful to present the effect of the aircraft motion-time history in some integrated fashion, rather than as the maximum lift coefficient that can be achieved only momentarily. One such possibility, proposed in Ref. 2, is to consider the area bounded by the lift-time curve from above and the static maximum lift from below, which may be said to define an effective impulse function, I_C, over a cycle. Such a representation allows for comparison of airfoil (or aircraft) performance between cases where the motion-time history is fundamentally different and this approach therefore lends itself well for lift optimization analysis. The variation of I_C with k for two airfoils is shown in Fig. 4. Results are depicted for several values of α_{max} and V. A rapid increase in I_C at low k is followed by a more gradual increase or even a gradual decrease at higher values of k. Furthermore, the maximum performance does not necessarily increase monotonously with α_{max}, but is achieved by terminating the unsteady motion and maintaining an α_{max} at or near the value for which, for a given k, the maximum C_L can be obtained. It is believed that such conditions correspond to the occurrence of the strongest and most persistent vortex.

2.2 Wing Rock

Wing rock is an undamped oscillation, primarily around the roll axis, that is exhibited by many modern fighter aircraft when flying at higher angles of attack. Several possible scenarios for the occurrence of wing rock have already been discussed in Ref. 1. Since wing rock is a very debilitating phenomenon, causing maneuver limitations ranging in severity from degradation in tracking effectiveness to loss of control, a considerable amount of work is currently being done to alleviate this problem by increasing our understanding of the underlying basic

aerodynamic phenomena. This work ranges all the way from efforts to postulate mathematical models for the prediction of wing rock characteristics, such as reported in Refs 5-7, to systematic low speed investigations, such as performed at NASA Langley Research Center and described by Nguyen et al in Ref. 8.

The NASA Langley studies comprise (a) wing rock encountered on highly-swept configurations, such as slender delta wings, and (b) wing rock induced by slender forebodies. The former type, already discussed in Ref. 1, seems to be associated with the alternating lifting-off and reattachment of leading edge vortices during each oscillation cycle. This results in the occurrence of incremental rolling moments which promote and oppose the oscillation in an alternating fashion. The latter type of wing rock is associated with the motion of forebody vortices and their interaction with the wing and empennage. In both cases strong vortex flows are present and it is the motion of these vortices, the mutual interaction of the two main forebody vortices or the two leading edge vortices (because of the slenderness of the wing), and possibly the phase lag between the motion of the vortices and the motion of the wing or aircraft, that provide the basic mechanism for the wing rock.

The importance of the forebody vortex flow for the occurrence of unstable damping in roll and, eventually, wing rock, is well illustrated in Figs 5 and 6. Damping in roll is shown for a range of angles of attack for an F-5 configuration with 3 alternative wings. The roll damping becomes highly unstable for all three wings in about the same range of angle of attack from 30° to 45°, indicating susceptibility to wing rock in that range of α. It is known that the full-scale F-5 aircraft is prone to large amplitude wing rock in the same angle-of-attack range. It is obvious that the planform of the wing is not responsible for the very unstable roll damping above $\alpha = 30^{o}$. Further corroboration was recently obtained during tests of a model of the X-29A Forward Swept Wing Airplane, which incorporates the exact fuselage forebody (which has a flat elliptical cross-section) of the F-5 but is completely different from the F-5 in almost every other aspect. Forced oscillation data for the X-29A showed the same lightly unstable roll damping in the 30° to 45° angle-of-attack range. It seems clear that the basic cause of the unstable roll damping in all these cases is the flow about the only common configuration feature, namely the forebody.

In order to generate sufficient rolling moments to cause wing rock, the basic forebody vortex flow must interact with some aircraft component further downstreams. This was illustrated during the Langley experiments during which the wing and vertical tail were alternatively removed from the model. It was shown that, with only the wing or only the vertical tail removed, the model still exhibited the wing rock, which only disappeared when both the wing and the vertical tail were removed at the same time.

With the forebody playing such a fundamental role in the generation of wing rock, it was only natural to investigate in some detail the effect of the forebody cross-section on the static lateral stability as well as on the wing rock occurrence and amplitude. This is now being done at NASA Langley (Ref. 8) on a generic fighter model, as part of a larger ongoing investigation, during which many forebodies and wings are systematically varied. Some preliminary results are shown in Figs 7 and 8 for the generic model configured with a trapezoidal wing with 26° leading-edge sweep and conventional tail. Four forebodies, all with the same 3.9:1 fineness ratio, but different cross-sectional shapes (circular, vertical ellipse, horizontal ellipse and triangular) were initially studied.

The preliminary results show that the forebody cross-section has a very strong influence on the static lateral stability, C_{l_β}, with the horizontal-ellipse and triangular cross-sections providing the stiffest "restoring spring" effects in the angle-of-attack range in which wing rock was observed in the free-to-roll tests. Above that range, the forebody/wing/tail flow fields appear to be no longer strongly coupled. It is noteworthy that the same two cross-sections were also found to be highly susceptible to wing rock, causing the highest wing-rock amplitudes, reaching 30°. It is also interesting that the horizontal-ellipse forebody is similar to the F-5 forebody discussed earlier and that the wing-rock characteristics for those two configurations are quite similar.

Work is continuing at NASA Langley to further explore the forebody induced wing-rock phenomenon. Although most of the present effort is conducted at low Reynolds numbers and certainly will have to be complemented by experiments at higher Reynolds numbers, certain similarities between the results obtained so far and flight test data (such as those mentioned above) seem to indicate that at least the basic mechanism is being properly identified.

2.3 Tumbling

Recent design trends for future combat aircraft, such as the use of tail-first or tailless configurations and highly relaxed static stability, have rekindled interest in a dangerous flight phenomenon known as tumbling. Last investigated during and immediately after World War II (see Ref. 9), tumbling was identified as a potential danger for aircraft with design features that included one or more of those mentioned above; it was also pointed out that accelerations in a tumble may be exceptionally dangerous. Since the conventional aircraft will not tumble, no more work in this area was conducted for approximately 35 years.

Last year, however, studies were conducted in the NASA Langley 20 - Feet Vertical Spin Tunnel on a dynamically scaled model of the X-29A aircraft, which makes use of canards and highly relaxed static stability. After initially confirming the occurrence of tumbling (which was coupled with cyclic variations in linear as well as angular rates) in a series of free - tumbling tests, more controlled experiments were conducted in single-degree-of-freedom, free-to-pitch tests (Refs 8 and 10). Autorotation was obtained by either imparting an initial rotation to the model in the proper direction, or by releasing the model from a proper attitude with zero rate. Once initiated, the autorotation persisted indefinitely. It was found that the canard and wing flap positions had little effect on the motion, while the strake flaps had a very large effect. For instance, with strake flaps fully down, only nose-down autorotation could be induced, regardless of the initial release conditions. Reversing the strake flaps to full up permitted a nose-up autorotation.

Figures 9 and 10 show the static pitching-moment and pitch damping data obtained from static and forced-oscillation experiments, respectively. The highly unstable pitching moment characteristics for angles of attack lower than $|45°|$ and higher than $|145°|$, as well as pitch undamping in the regions of around + 130° and -120°, are clearly visible. Using these data in a simulation programme, the time history of the motion for a full scale aircraft could be predicted (Fig. 11) and compared to scaled-up (in time) frame-by-frame readings of movies taken during the free-to-pitch tests (Fig. 12). Average pitch rate was about - 130°/sec, and maximum recycling values of axial and normal accelerations at the pilot station were 0 to - 3 g and + 1.5 g, respectively. Although the

attitude data are predicted quite closely, the match of velocity and acceleration data is not nearly as good, indicating the need for further work in both obtaining the basic data and improving the mathematical model.

The above experiments were all performed with the controls fixed. Although it is unlikely that in a highly augmented modern aircraft the controls would remain fixed through a large amplitude motion such as tumbling, the susceptibility to tumbling remains as a possible threat in off-nominal situations involving failures in the aircraft control system. Unfortunately, one of the best means to increase resistance to tumbling is to limit an aircraft's agility in pitch. However, control laws are now being developed at NASA Langley for highly-relaxed-stability fighter aircraft, which - assuming that some controls are still operational - would ensure a combination of high agility and good resistance to pitch departure.

2.4 Flow Control

Any attempt to achieve high agility and true supermaneuverability must include the ability to manage and control the time dependent, separated flows that are characteristic of such flight conditions. In the past such attempts were primarily aimed at reducing or eliminating regions of separation and promoting flow attachment, as exemplified by the use of vortex generators on wings of many current aircraft. For a high agility fighter, however, the separated-flow areas can be expected to dominate the flow around the aircraft, and it is the manipulation and even enhancement of that separated flow rather than its reduction or elimination that becomes the primary goal of any flow control procedure. For instance, if the residence time of the leading edge separation vortex mentioned in Section 2.1 could be extended, beneficial effects on the dynamic lift enhancement and its duration would result.

As discussed by Lang and Francis (Ref. 11) we are, at the present time, only taking the first steps in any such control attempts of the unsteady separated flows. Most of these first efforts use the idea of an oscillating spoiler to force and manipulate the flow. One of the earliest such studies dealt with the unsteady loading induced by a harmonically oscillating fence on one surface of the airfoil and its effect on both a fixed and a moving trailing edge flap (Ref. 12). A related investigation of the spoiler-generated flow field (Ref. 13) revealed the developing vortical character of the separation zone and described the behaviour of the suction peak on the airfoil surface. In an extension of these experiments to higher angles of attack (Ref. 14), a spoiler located at the 20% chord location was found to induce small spanwise vortices which greatly affected flowfield curvature, possibly increasing lift. Subsequent measurements confirmed a 60 to 110% unsteady load enhancement over the maximum steady flow value. It was also shown that a pulsed air jet may be successfully employed in place of a spoiler.

The management of a 2 D separated flow region has been systematically investigated at IIT (Ref. 15). Separated flow field was generated by using a wedge of a height equal to the local thickness of the turbulent boundary layer and the unsteady vorticity field was controlled by an oscillating flap with a variable waveform. Results have shown local surface pressure coefficient increases of nearly one hundred percent (Fig. 13) and a reduction of flow attachment length to thirty percent of the natural steady flow separation case. It was observed that the most effective reattachment control occurred for reduced frequencies of 0.07 to 0.08 (Fig. 14), and that the use of a triangular waveform, with a 90% duty cycle, resulted in a better organized, energetic and persistent vortex than some other cases having the same amplitude and period. Similar results were subsequently obtained for a separated flow generated by a backward facing step (Ref. 16); in that work it was also suggested that the control imparted by an active flap oscillation is independent of whether the incoming boundary layer is transitional or turbulent.

Separation control can also be achieved by actively stimulating the separated shear layer by sound at selected frequencies, as recently shown in Ref. 17.

An example of manipulating the flow in a 3 D case is provided in Ref. 18, which deals with the wing rock induced by leading edge vortices, that was already discussed in Ref. 1 and Section 2.2. It was shown that by mounting a small delta canard in front of a main delta wing, self-induced roll oscillations of the entire configuration (in a free-to-roll experiment) were obtained in a much larger range of angle of attack and with larger roll amplitude than with the main wing alone (Fig. 15). This was ascribed to the increased time lag (because of the larger length of the canard-wing) between the wing response and the movement of leading-edge vortices. Up to 30° the vortices from the canard and the wing were combined, while at higher angles of attack the resulting vortex breakdown at the wing trailing edge was providing a damping which reduced the roll angle amplitude. In the range $44° < \alpha < 46°$ an interesting unstable asymmetric oscillation was recorded (Fig. 16), which could easily flip from the positive to the negative roll angles and viceversa, and which was related to the capturing of one of the canard's vortices by the opposite semiwing while the other vortex was shed into the flow. Also at the lower semiwing, a major vortex breakdown was detected. These observations, although, in a sense, describing undesirable results of controlling the flow, provide a useful insight into the fluid dynamics of these rather complex phenomena.

2.5 Digital Datcom

Some of the static and dynamic stability derivatives may be obtained from a computerized version of the USAF Stability and Control Datcom, called Digital Datcom. This includes the direct and the cross derivatives, but not any cross-coupling derivatives. The configurations and speed regimes for which Digital Datcom methods for dynamic derivative prediction are available are listed in Fig. 17. More details, including a comparison with wind tunnel data for several configurations and Mach numbers (see examples in Fig. 18), can be found in Ref. 19. All Datcom methods for dynamic derivatives, however, assume attached flow and hence are restricted to the low angle of attack regime.

3. WIND TUNNEL TESTING TECHNIQUES

As mentioned in the Introduction, the most important source of dynamic stability data for the advanced flight conditions or unorthodox configurations which are of interest for the modern fighter design, lies in experimental investigations. Although, in principle, experiments can be performed both in wind tunnels and in free flight, the latter cannot be rigorously carried out until a prototype is built and even then it usually does not provide the well-defined experimental conditions which are available in a laboratory. On the other hand, of course, although wind-tunnel testing is usually conducted at too low a Reynolds number and may be subject to some form of wind-tunnel or support-interference effects, it does, by and large, provide valuable information, obtained under

well controlled test conditions. It is often only through a combination of both wind tunnel and flight data with some additional data sources such as dynamic model flight tests, analytical studies and piloted simulation that a complete data set required for a satisfactory design can be obtained (Fig. 19). However, as discussed by Chambers et al (Ref. 20), dynamic wind tunnel tests are also to some extent involved in each of these procedures. For example, conduct of piloted simulator studies cannot be accomplished without dynamic stability parameters, and the interpretation and analysis of dynamic model flight tests and airplane flight tests may be subject to considerable question without dynamic wind tunnel data. Dynamic wind-tunnel experiments appear, therefore, to constitute the most important experimental source for dynamic data and the remainder of this paper will be devoted to examining the various techniques that are presently available or under development for such testing.

Reviews of the wind-tunnel techniques for dynamic stability testing have been presented by the present author at several occasions in the past (Refs 21-24). Since Refs 23 and 24 are easily accessible to the AGARD community, the material presented therein will not be reproduced here but will only be included by a suitable reference, as appropriate. Of the multitude of techniques available (Fig. 20), only those that, in the author's opinion, are currently the most important or the most promising for the future, will be listed.

3.1 Single DOF Forced Oscillation - Measurement of Reactions

This is commonly referred to as the "forced oscillation" technique, and is, by far, the most often encountered and most versatile technique in use today. It can be used for angular oscillation, such as in pitch, yaw or roll, as well as for translational oscillation, such as in plunge or in lateral translation. In the former case, the dynamic derivatives around a fixed axis, i.e. composite derivatives (such as $C_{mq} + C_{m\dot{\alpha}}$) (see Ref. 1), can be obtained while in the latter case derivatives due to linear acceleration (such as $C_{m\ddot{z}}$), - which in a linear situation are approximately equal to the derivatives due to the time rate of change of the angle in the same plane of motion (such as $C_{m\dot{\alpha}}$) are measured. In most cases the drive is inexorable (of the hydraulic or mechanical type), resulting in a constant amplitude sinusoidal oscillation. In some cases, an electromagnetic drive is used, resulting in a constant amplitude of the applied torque (or force), unless a motion-amplitude stabilizing circuitry is used. Although in all the cases the motion is in a single degree-of-freedom (DOF), all three aerodynamic moments and two aerodynamic forces (normal force and side force) can be measured, usually with a single-piece construction strain-gauge balance. The derivatives are obtained from the in-phase and quadrature components of the measured aerodynamic reactions with respect to the model motion, and the frequency and amplitude data. All direct, cross and cross-coupling derivatives can be obtained using this technique in various degrees of freedom. The direct derivatives can also be obtained from the measurement of the torque and its phase with relation to the induced motion. Examples of the instrumentation used at NAE and AEDC and of the required data acquisition and reduction systems are given in Ref. 25. Numerous applications of this technique, as used at NASA Langley, ONERA Chalais-Meudon, ONERA Modane, AEDC-VKF, AEDC-PWT, DFVLR and NAE, are described in Section 5 of Ref. 24. The technique is also used in Sweden (FFA, Ref. 26) and China (SARI, NAI and BIA). A recent sting-mounted Swedish pitch/yaw apparatus is shown in Fig. 21.

3.2 Multi DOF Forced Oscillation - Measurement of Motion

In this technique, the model is suspended elastically in such a way that it can oscillate in several degrees of freedom simultaneously, although one degree of freedom (choice depends on the oscillation frequency) is usually predominant. The amplitude and phase of the various motions (rather than of the various reactions, as in the preceding section), together with the information about the driving force or torque and frequency, are measured and fed into a system of equations of motion, which is then solved for the unknown stability derivatives. In the limiting case of a single DOF oscillation, the above technique reduces to the "constant-amplitude torque" subgroup of the preceding section, where the direct derivatives can be obtained from the amplitude and phase of the forced motion and the forcing torque and frequency (in the same DOF) by means of a direct calculation rather than indirectly by solving a system of equations. That type of technique is used at RAE - Bedford, DFVLR-AVA and NASA - Langley, as described in Section 6 of Ref. 24. In the latter case the model is elastically suspended for multi-DOF experiments by a system of cables, whereas at RAE and DFVLR the model is mounted on a spring unit (attached to the sting) which limits the number of DOF's to 2 or 3 (Ref. 27).

3.3 Single DOF Free Oscillation - Measurement of Motion

This technique is the oldest and the simplest of the various oscillatory techniques. It involves the evaluation of a decaying oscillatory motion performed by an elastically suspended model following some initial disturbance. No complicated drive or control system are usually required and the data reduction is relatively straight forward. Although the results are representative of an amplitude range rather than of a discrete value of amplitude, with modern instrumentation this amplitude range can be made sufficiently small so that any variations of the results with amplitude can be obtained as conveniently as with other methods. The technique, however, is limited to the measurement of the direct derivatives (damping and stiffness) only, and in its simplest form is not suitable for use under conditions of dynamic instability or in the presence of large static moments. For these reasons the free-oscillation technique is now gradually being replaced by the various forced-oscillation techniques. Some examples of its use in the past are given in Section 7 of Ref. 24.

3.4 Half-Model Testing

The use of half models (semi-span models) for testing of symmetrical configurations at symmetric flow conditions has been a recognized experimental procedure for a long time. The technique eliminates interference problems usually associated with the presence and with the motion of the sting, permits the use of models larger than otherwise possible and allows for a more convenient arrangement of the test equipment (utilizing the space outside of the wind tunnel). On the other hand, the use of half models has some problems of its own, such as the possible effect of the gap between the model and the wind tunnel wall and, at higher speeds, the effect of an interaction between the shock and the wall boundary layer. Since all applications are strictly limited to symmetrical flow conditions, the technique cannot be used at higher angles of attack, even for symmetrical configurations.

Half models can be used for experiments involving pitching or plunging oscillation using appropriate free- or forced - oscillation techniques described before. The technique is particularly recommended for cases

where static or dynamic sting interference effects may be significant or when the shape of the model afterbody is incompatible with a sting mounting. Other possible applications include the determination of the dynamic interference between two oscillating models and the measurement of the effect of the jet exhaust plume on the pitching or plunging oscillations of a model (Ref. 28). The technique is used for oscillatory testing in many countries, including Sweden (FFA), Canada (NAE), USA (AEDC), China (SARI, BIA) and Japan (NAL).

3.5 Rotary Motion

There are a number of wind tunnel techniques where the model is performing a continuous rotary rather than oscillatory motion, as discussed so far. The two most important varieties of such a rotary motion are as follows:

3.5.1 Rolling - a rotary motion of the model around the body axis or around the wind axis, at zero to moderate angles of attack, usually at zero sideslip and at low to moderate rotation rates. The main purpose of the rolling experiments is to determine stability derivatives due to rolling, such as encountered during a rolling maneuver. Although - strictly speaking - quite different, such derivatives are sometimes used interchangeably with those obtained from roll oscillation experiments. Rolling techniques can be further subdivided into techniques using steady roll and those using free decay of the roll rate. Apparatuses employing these techniques can be found at NASA - Langley, AEDC, FFA, BAC - Warton and DFVLR-Köln, and are described in Section 9.1 of Ref. 24.

3.5.2 Coning - a rotary motion of the model around the wind axis, at arbitrary angle of attack, usually non-zero angle of sideslip and low to moderate rotation rates. Such a motion is sometimes referred to as the lunar motion and the apparatuses employed for such experiments are usually called rotary balances. The main purpose of the coning experiments is to obtain the aerodynamic coefficients (rather than derivatives) as functions of the coning rate. These are required for a better simulation of the aerodynamic phenomena that are associated with the steady spin motion of aircraft and spin recovery. The coning motion is also one of the fundamental characteristic motions derived in the mathematical models of Tobak and Schiff (Ref. 29) and the aerodynamic moments measured during such a motion are required for prediction of even nonspinning maneuvers. It should be noted that many apparatuses used for steady roll about the wind axis can be used interchangeably as rotary balances, that is for the purpose of obtaining the various aerodynamic reactions as functions of the roll rate. The difference lies mainly in the instrumentation and in the data reduction. Several rotary balances are now in existence for both low-speed and high-speed wind tunnels, including those at NASA Langley, NASA-Ames, BAC-Warton, DFVLR-Köln, Aeronautica Macchi and IMF. These were described in Section 9.2 of Ref. 24 and in Ref. 30. A new rotary balance at RAE-Bedford (Ref. 31) is shown in Fig. 22.

All rotary balances, of course, can be used to obtain derivatives due to the rate of roll. In addition, by slightly tilting the axis of a rotary balance with respect to the wind axis, it is possible to superimpose an oscillatory motion in pitch and yaw on the main rotary motion. Such a motion, called "oscillatory coning", may permit the determination of additional derivatives, viz. those due to oscillatory pitch and yaw (Ref. 32).

3.6 Pure Rotation

Since the results of oscillatory experiments (such as in pitch) around a fixed axis are in the form of composite derivatives which contain derivatives due to pure rotation (such as q) and derivatives due to the time-rate-of-change of the angular deflection in the same plane of motion (such as $\dot{\alpha}$), there is a need to separate such component derivatives so that each can be inserted at its proper position in the equations of motion. To separate the two parts, additional experiments are required, in which either a pure angular motion (with the appropriate aerodynamic deflection angles remaining constant) or a pure translation (with the appropriate angular rates remaining zero) is simulated. As already discussed, under certain conditions the translational acceleration is aerodynamically equivalent to the time-rate-of-change of the aerodynamic angle in the same plane of motion. Effects of translational acceleration can be measured by single DOF forced oscillation experiments in vertical or lateral translation, as done at NAE, using methods described in Section 3.1. Simulation of pure angular motion (or pure rotation) in pitch or yaw can be achieved by snaking motion experiments or experiments in a suitably curved flow, while pure rolling can be simulated by experiments in a suitably arranged rolling flow. These latter techniques, which were all developed at NASA-Langley in the 1950's and have now been transferred, together with the 6 ft Stability Tunnel, to the Virginia Polytechnic Institute, will be briefly described in the following paragraphs. More details can be found in Ref. 33.

3.6.1 Snaking Motion - This combines yawing and lateral motions of a model in such a manner as to produce pure yawing. The apparatus (Fig. 23) generates an oscillatory motion in the xy plane so that the model always heads into the relative wind or, in other words, so that the instantaneous angle of yaw - which includes vector components generated by the two basic motions - remains constant at all times. This occurs when $\dot{y} = V \sin \psi$, at which condition the angle of yaw contributed by the yawing oscillation is exactly cancelled by the angle of yaw induced by the lateral oscillation. A comparison of data obtained by algebraic summation of snaking and translational oscillation tests with the data obtained from angular oscillation tests (around a fixed axis) is shown in Fig 24.

3.6.2 Curved Flow - This technique is based on the concept of simulating a steady curved-flight condition by using a fixed model and arranging the wind-tunnel flow in such a way that it is curved in a circular path in the vicinity of the model and that it has the velocity variation normal to the streamlines in direct proportion to the local radius of curvature. This is achieved by using flexible side walls for curving the flow and by employing special vertical-wire drag screens upstream of the test section for producing the desired velocity gradient in the flow across the tunnel (Fig. 25). These screens vary in size across the wind tunnel, with the most dense portion of the screens located at the inner radius of the curved test section. The technique allows measuring pure yawing (due to r only) or pure pitching (due to q only) derivatives with a fixed model mounted on a static balance. The simulation of the steady curved flight is not exact, however, and usually corrections have to be applied for the buoyancy effect caused by the static pressure gradient normal to the streamlines (which does not exist in curved flight). In addition, there are dissimilarities in the behaviour of the model boundary layer (which on the model in a curved flow tends to move towards the center of curvature, contrary to its normal tendency in curved flight), and possible problems due to a rather high degree of turbulence behind the wire screens. Hopefully, however, in many cases these phenomena may be considered to have only a minor effect on the measurements of the purely-rotary derivatives.

3.6.3 Rolling Flow - When a model at an angle of attack performs a rolling motion about a fixed body axis, the

resulting aerodynamic reactions are functions of both the roll rate and the simultaneously occurring time rate of change of the angle of sideslip. This is similar to the previously discussed composite effect resulting from pitching or yawing oscillation around a fixed axis. To obtain aerodynamic derivatives due to "pure" rolling, one can use a stationary model immersed in a rolling flow. The rolling flow must be generated in such a way that its velocity component normal to the tunnel axis increases proportionally to the radial distance. This can be achieved by using, upstream of the test section, a large rotor with several vanes that are specially shaped in order to impart a suitable solid core vortex motion to the flow. One fascinating future application of this technique would be to impart pitching or yawing oscillation to the model and obtain measurements of the various damping, cross and cross-coupling derivatives in the presence of the rolling flow, thereby providing valuable data for studies of the incipient spin and spin entry and, in particular, oscillatory spin (Ref. 33).

3.7 Control Surface Oscillation

So far we have dealt with dynamic stability testing of full or half models of complete configurations. A brief comment should also be included about the stability characteristics related to the oscillation or motion of the various control surfaces. These are normally of two kinds: (1) the hinge moment derivatives of an oscillating surface and (2) the derivatives of the aerodynamic reactions imparted to the model by the oscillation of a control surface. Although the main interest lies usually in the static control derivatives, the trend is increasing towards also obtaining some dynamic control derivatives, which may become important in connection with high-rate maneuvers and quick-acting controls. The necessary experiments are most conveniently performed using a half model of the aircraft configuration; the hinge moment measurements can be performed with any single DOF oscillation method mentioned before, whereas the aerodynamic reactions on the model itself can be obtained using methods similar to those employed for cross and cross-coupling derivative measurements. Some suitable experimental techniques are mentioned in Section 14 of Ref. 23.

3.8 Non-Linear Dynamic Loads

The various wind-tunnel techniques previously mentioned are characterized by the relatively small amplitude motion that they impart to the model. It has traditionally been assumed that under these conditions the resulting aerodynamic phenomena are linearly related to the model motion, implying that if a sinusoidal motion is used, as is typically the case, the aerodynamic reactions are also sinusoidal and of the same frequency as that of the model oscillation. In such a case the desired aerodynamic information can be represented in the form of stability derivatives that can be obtained using procedures like the ones discussed in Refs 25 and 28.

The applicability of the locally linearized aerodynamics model, implicit in the derivative formulation, to large amplitude and high rate maneuvers, has been increasingly questioned over the last few years. Consequently, a new wind-tunnel technique, specifically designed to investigate the aerodynamic loads acting on a model subjected to large amplitude and/or high rate motions has been recently developed at NAE.

3.8.1 Data Reduction - The goal is to measure the instantaneous value of the reactions in terms of the corresponding instantaneous value of the pertinent motion variables. Since no assumption of linearity is made, the components of the reactions at the oscillation frequency as well as at its harmonics need to be determined. Therefore the technique basically consists of measuring the Fourier coefficients of the balance outputs (deflections), which are converted into their causative loads by using the appropriate model-balance system mechanical transfer functions. The inverse Fourier Transform is then applied to the above coefficients in order to represent the reactions in the time domain. This apparently round-about approach is required in order to account for the dynamic response of the model-balance system, which can have a substantial impact on the observed balance outputs. Inertial effects are eliminated by means of tare measurements. Further details on the technique can be found in Ref. 34. The current implementation of the instrumentation system and data reduction procedures are described in Ref. 35.

3.8.2 Reaction Representation - Once the concept of stability derivatives can no longer be used, it becomes imperative to formulate an appropriate representation of the non-linear aerodynamic data in order to effectively utilize it in flight mechanics computations. One possible representation (Ref. 36) is based on the assumption that there is a well defined (although not necessarily single valued) relationship between the instantaneous value of any given aerodynamic reaction and the corresponding instantaneous value of the motion variables. In a topological sense, this representation implies the existence of a unique (again not necessarily single valued) "reaction hypersurface" that defines the reaction in terms of n motion variables.

If the hypersurface could be experimentally obtained in its entirety - e.g. by means of the technique summarized in the previous section - it could be used to carry out simulations without resorting to mathematical models. Practical considerations, however, limit the number of experiments that can be performed to obtain the very large data base required to suitably define the hypersurface, therefore necessitating some level of mathematical modelling to supplement the empirical data.

A detailed description of the hypersurface representation with its rather wide-ranging implications can be found in the above reference and is, therefore, not included here. However an example of how the representation can be applied to the simple case of a single DOF motion is briefly mentioned here for completeness. Let us consider a hypothetical case of a motion about the roll body axis where the reaction C_l is a function of ϕ and p only, in which case the reaction surface becomes three dimensional and can thus be readily visualized. A schematic hysteretical surface is arbitrarily postulated as an illustration (Fig. 26). The motion of the model is represented by a trajectory in the ϕ- p phase plane and the corresponding value of the reaction is defined by the reaction surface. The surface depicted in Fig. 26 is characterized by threshold values that are independent of the rate, corresponding to the case of "static hysteresis", as opposed to the situation shown in Fig. 27 where the thresholds are a linear function of rate, indicating a convective time lag effect on the threshold values. Both reaction surfaces are single valued everywhere except at the line defining the "step" indicating that "minor loops" are permissible under oscillation amplitudes below the threshold value. A double valued reaction surface where such minor loops do not occur is shown in Fig. 28, in which case the only way to transfer from one branch of the hysteresis curve to the other is by exceeding the threshold value.

The reaction surface for an 80 degree delta wing in subsonic flow has been approximately determined (Ref. 37), on the basis of experimental data obtained by Nguyen et al. (Ref. 38). Although sufficient information

was not available to precisely define the surface, the results indicate that the surface concept is applicable to this case.

4. CONCLUDING REMARKS

In this lecture a brief review was presented of some of the aerodynamic aspects of the dynamic behaviour of a modern, high performance fighter aircraft and of some of the more important experimental techniques that are available for measuring the dynamic stability parameters of an aircraft in a wind tunnel. Because of space limitations many topics had to be omitted and the reader is referred to the three volumes listed in "Bibliography", and in particular to Refs 1, 23 and 24 by the present author, for further details. More recent pertinent information can be found in Refs 39-46. It is hoped that the present review, together with the above additional material, may provide a useful insight into the aerodynamics of a maneuvering modern fighter and may serve as a guide to the large variety of wind tunnel methods that have to be used in order to obtain the dynamic data required for the design of such an aircraft.

5. REFERENCES

1. Orlik-Rückemann, K.J., "Aerodynamic Aspects of Aircraft Dynamics at High Angles of Attack", J. of Aircraft, Vol. 20, No. 9 Sept. 1983, pp 737-752.

2. Francis, M.S. and Keesee, J.E., "Airfoil Dynamic Stall Performance with Large- Amplitude Motions", AIAA Journal, Vol. 23, No. 11, Nov. 1985, pp 1653-1659.

3. McCroskey, W.J., "Unsteady Airfoils", Ann. Rev. Fluid Mech. 1982, 14, pp 285-311.

4. Herbst, W.B., "Supermaneuverability", Proc. of AFOSR-FJSRL - Univ. of Colorado Workshop on Unsteady Separated Flow, USAF Academy, Colorado Springs, August 1983, pp 1-9.

5. Ericsson, L.E., "The Fluid Mechanics of Slender Wing Rock", J. of Aircraft, Vol. 21, No. 5, May 1984, pp 322-328.

6. Lan, C.E., "Theoretical Prediction of Wing Rocking", AGARD CP-386, May 1985, Paper 32.

7. Hsu, C.H. and Lan, C.E., "Theory of Wing Rock", J. of Aircraft, Vol. 22, No. 10, October 1985, pp 920-924.

8. Nguyen, L.T., Whipple, R.D. and Brandon, J.M., "Recent Experiences of Unsteady Aerodynamic Effects on Aircraft Flight Dynamics at High Angles of Attack", AGARD CP-386, May 1985, Paper 28.

9. Stone, R.W., Jr. and Bryant, R.L., "Summary of Results of Tumbling Investigations Made in the Langley 20 - Feet Free Spinning Tunnel on 14 Dynamic Models", NACA RM L8 J 28, December 1948.

10. Whipple, R.D., Green, M.A. and Fears, S.P., "Preliminary Results of Experimental and Analytical Investigations of the Tumbling Phenomenon for an Advanced Configuration" AIAA 84-2108, August 1984.

11. Lang, J.D. and Francis, M.S., "Unsteady Aerodynamics and Dynamic Aircraft Maneuverability", AGARD CP-386, May 1985, Paper 29.

12. Lang, J.D., "The Interaction of an Oscillating Airfoil and/or Flap with a Separating Flow", Ph.D. Thesis, Cranfield Inst. of Tech. January 1975.

13. Francis, M.S., Keesee, J.E., Lang, J.D. Sparks, G.W. and Sisson, G.E., "Aerodynamic Characteristics of an Unsteady Separated Flow", AIAA Journal, Vol. 17, 1979, pp 1332-1339.

14. Luttges, M.W. Robinson, M.C. and Kennedy, D.A., "Control of Unsteady Separated Flow Structures on Airfoils", AIAA-85-0531, AIAA Shear Flow Control Conference, March 1985.

15. Koga, D.J., Reisenthel, P.H. and Nagib, H.M., "Control of Seperated Flowfields using Forced Unsteadiness", IIT Fluids Heat Transfer Report R 84-1, January 1984.

16. Reisenthel, P.H., "Reattachment Control behind a Rearward Facing Step Using Forced Unsteadiness", IIT M.Sc. Thesis, Dec. 84.

17. Ahuja, K.K., "Basic Experimental Study of the Coupling Between Flow Instabilities and Incident Sound", NASA CR 3789, March 1984.

18. Katz, J. and Levin, D., "Measurements of Canard-Induced Roll Oscillations", AIAA 85-1830, Snowmass, CO, August 1985.

19. Blake, W.B., "Prediction of Fighter Aircraft Dynamic Derivatives using Digital Datcom", AIAA-85-4070, Colorado Springs, October 1985.

20. Chambers, J.R., Dicarlo, D.J. and Johnson, J.L. Jr., "Applications of Dynamic Stability Parameters to Problems in Aircraft Dynamics", AGARD-LS-114, March 1981, Lecture 17.

21. Orlik-Rückemann, K.J., "Methods of Measurements of Aircraft Dynamic Stability Derivatives". NRC Canada LR-254, 1959.

22. Orlik-Rückemann, K.J., "Dynamic Stability Testing of Aircraft - Needs versus Capabilities". Progress in Aerospace Sciences 1975, Vol 16, No 4, pp 431-447.

23. Orlik-Rückemann, K.J., "Techniques for Dynamic Stability Testing in Wind Tunnels", AGARD-CP-235, May 1978, Paper 1.

24. Orlik-Rückemann, K.J., "Review of Techniques for Determination of Dynamic Stability Parameters in Wind Tunnels", AGARD-LS-114, March 1981, Lecture 3.

25. Hanff, E.S., "Direct Forced Oscillation Techniques for the Determination of Stability Derivatives in Wind Tunnels", AGARD-LS-114, 1981, Lecture 4.

26. Jansson, T. and Torngren, L., "New Dynamic Testing Techniques and Related Results at FFA", AGARD-CP-386, 1985, Paper 20.

27. O'Leary, C.O. "Wind Tunnel Measurement of Aerodynamic Derivatives Using Flexible-Sting Rigs", AGARD-LS-114, 1981, Lecture 5.

28 Hanff, E.S., "Applications of Half-Model Technique in Dynamic Stability Testing", AGARD-LS-114, 1981, Lecture 9.

29. Tobak, M. and Schiff, L.B., "Aerodynamic Mathematical Modeling - Basic Concepts", AGARD-LS-114, 1981, Lecture 1.

30. Malcolm, G.N., "Rotary and Magnus Balances", AGARD-LS-114, 1981, Lecture 6.

31. O'Leary, C.O. and Rowthorn, E.N., "New Rotary Rig at RAE and Experiments on HIRM". AGARD-CP-386, 1985, Paper 19.

32. Tristrant, D. and Renier, O. "Récents développements des techniques de simulation dynamique appliquées a l'identification des parametres de stabilité", AGARD-CP-386, 1985, Paper 22.

33. Chambers, J.R., Grafton, S.B., and Lutze, F.H., "Curved-Flow, Rolling-Flow, and Oscillatory Pure-Yawing Wind Tunnel Test Methods for Determination of Dynamic Stability Derivatives", AGARD-LS-114, 1981, Lecture 7.

34. Hanff, E.S. "Determination of Non-Linear Loads on Oscillating Models in Wind Tunnels", ICIASF '83 Record, pp 145-151, Sept. 1983.

35. Hanff, E.S., "Instrumentation and Other Issues in Non-Linear Dynamic Testing in Wind Tunnels", ICIASF '85 Record, pp 200-208, Aug. 1985.

36. Hanff. E.S., "Dynamic Nonlinear Airloads - Representation and Measurement", AGARD-CP-386, 1985, Paper 27.

37. Hanff, E.S., "Non-Linear Representation of Aerodynamics of Wing Rock of Slender Delta Wings", AIAA-85-1931, Snowmass, Co. August 1985.

38. Nguyen, L.T., Yip, L. and Chambers, J.R., "Self-Induced Wing Rock of Slender Delta Wings", AIAA Paper 81-1883, August 1981.

39. Ericsson, L.E. and Reding J.P., "Review of Support Interference in Dynamic Tests", AIAA Journal, Vol 21, No 12, December 1983, pp 1652-1666.

40. Uselton, B.L. and Haberman, D.R., "Summary of Sting Interference Effects for Cone, Missile and Aircraft Configurations as Determined by Dynamic and Static Measurements", AIAA-82-1366, August 1982.

41. Graham, G.M. and Strickland, J.H., "An Experimental Investigation of an Airfoil Pitching at Moderate to High Rates to Large Angles of Attack", AIAA-86-0008, January 1986.

42. Jumper, E.J., Shreck, S.J. and Dimmick, R.L., "Lift-Curve Characteristics for an Airfoil Pitching at Constant Rate", AIAA-86-0117, January 1986.

43. Robinson, M.C. and Luttges, M.W., "Vortices Produced by Air Pulse Injection from the Surface of an Oscillating Airfoil", AIAA-86-0118, January 1986.

44. Brandon, J.M. and Nguyen, L.T., "Experimental Study of Effects of Forebody Geometry on High Angle of Attack Static and Dynamic Stability", AIAA-86-0331, January 1986.

45. Gera, J., "Dynamics and Controls Flight Testing of the X-29A Airplane", AIAA-86-0167, January 1986.

46. Beyers, M.E., "SDM Pitch - and Yaw - Axis Stability Derivatives", AIAA-85-1827, August 1985.

6. BIBLIOGRAPHY

1. Orlik-Rückemann, K.J. (Ed.) "Dynamic Stability Parameters", AGARD FDP Symposium, Athens (Greece), AGARD-CP-235, May 1978.

2. Orlik-Rückemann, K.J. (Ed.) "Dynamic Stability Parameters", AGARD FDP Lecture Series, NASA Ames (USA) and von Karman Institute (Belgium), AGARD-LS-114, March 1981.

3. Orlik-Rückemann K.J. (Ed.), "Unsteady Aerodynamics - Fundamentals and Applications to Aircraft Dynamics", AGARD FDP Symposium, Göttingen (Germany), AGARD-CP-386, May 1985.

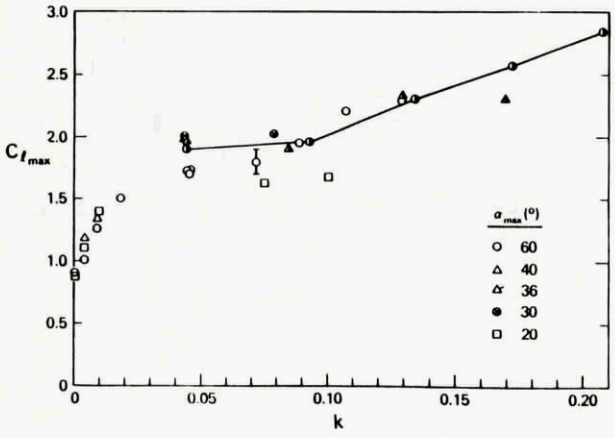

Fig. 1. Maximum lift coefficient vs pitch rate for NACA 0012 (open symbols) and NACA 64 A012 (13) (half solid symbols) (Ref. 2)

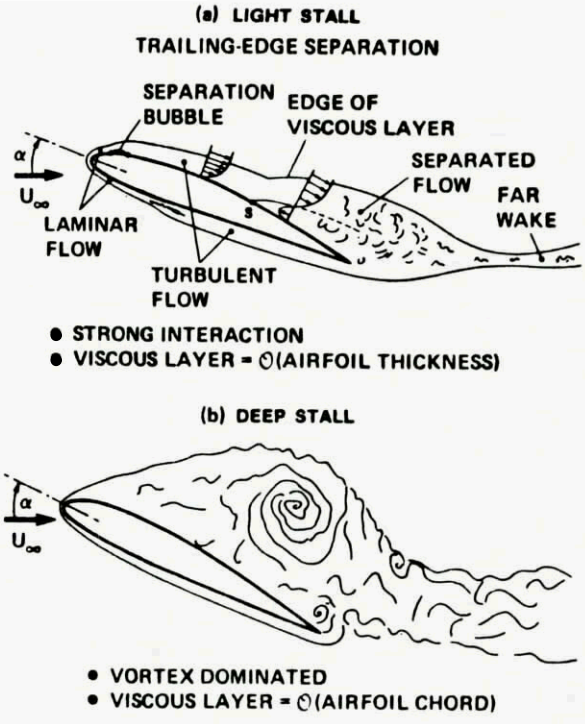

Fig. 2. Sketches of flow fields during dynamic stall (Ref.3)

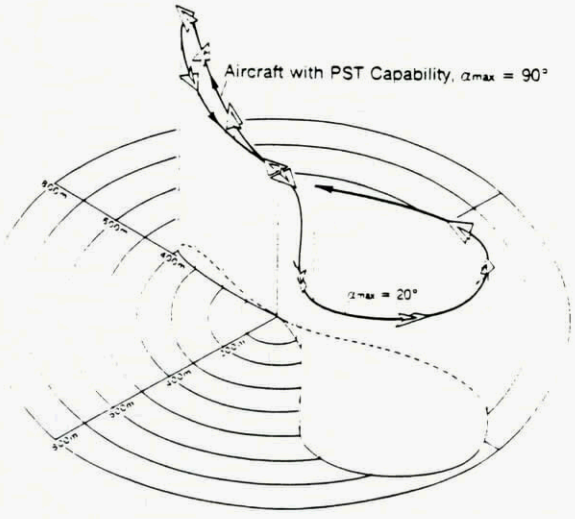

(a) Trajectory comparison

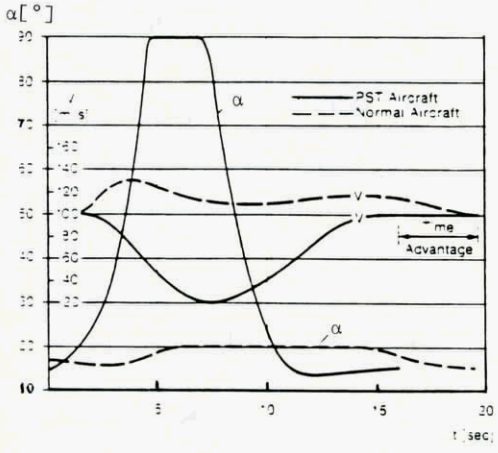

(b) Time histories

Fig. 3. Supermaneuverability. Minimum time maneuvers (Ref. 4)

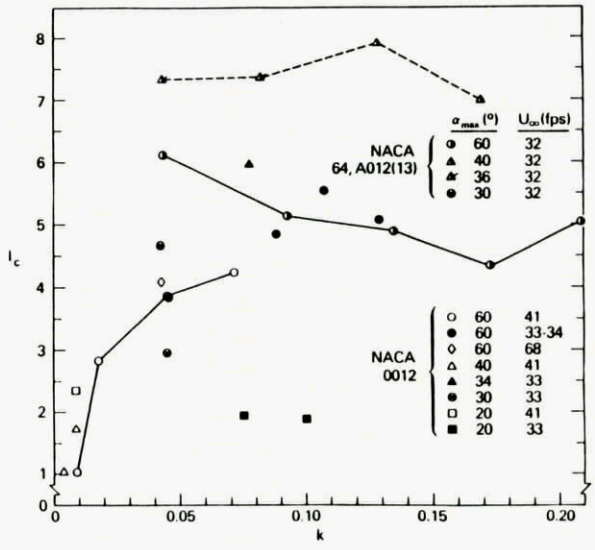

Fig. 4. Impulse function vs pitch rate (Ref. 2)

Fig. 5. Wing models tested with model based on F-5 configuration (Ref. 8)

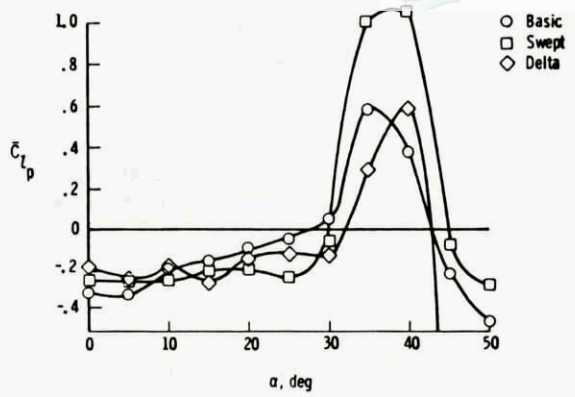

Fig. 6. Low-speed damping in roll for models of Fig 5 (Ref. 8)

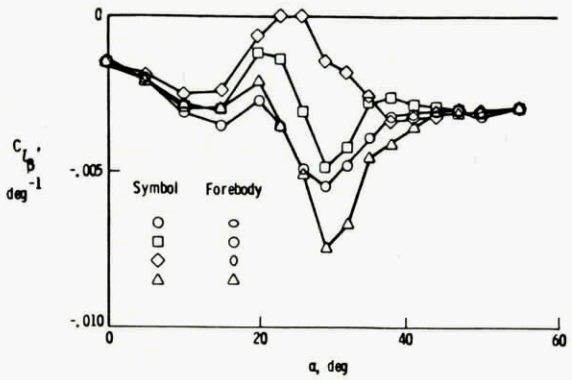

Fig. 7. Effect of forebody cross-section on static lateral stability. Generic fighter model (Ref. 8)

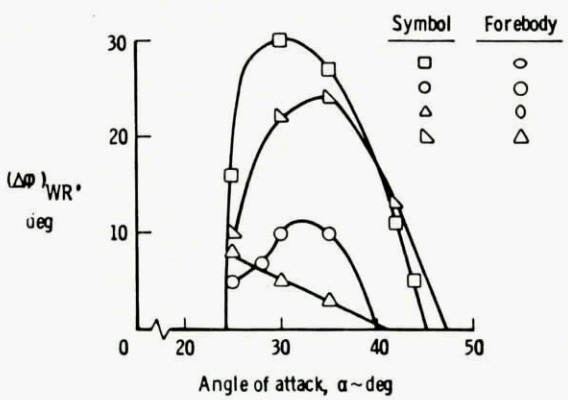

Fig. 8. Effect of forebody cross-section on wing rock amplitude. Generic fighter model (Ref. 8)

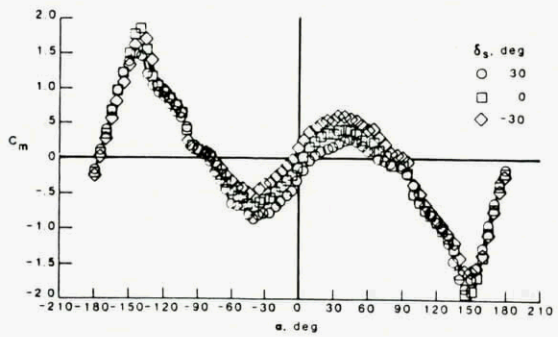

Fig. 9. Pitching moment coefficient for X-29 A model (Ref. 8)

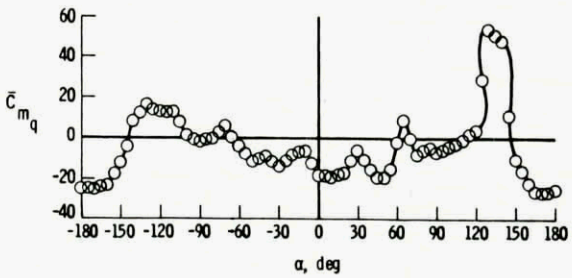

Fig. 10. Damping in pitch parameter for X-29 A model (Ref. 8)

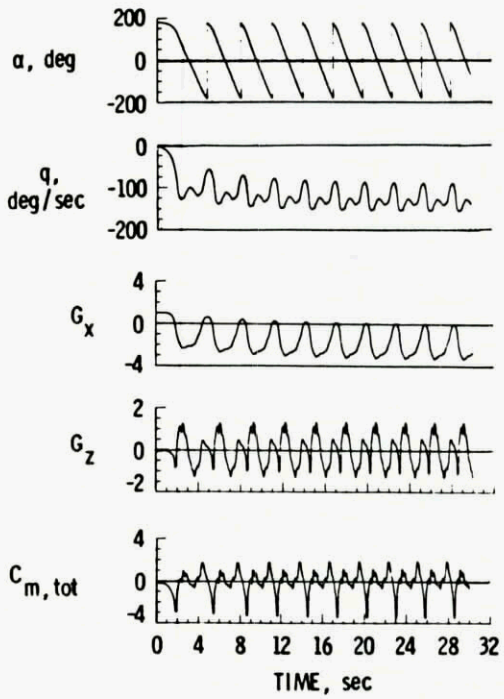

Fig. 11. Time histories of a computed tumbling motion, X-29 A configuration (Ref. 8)

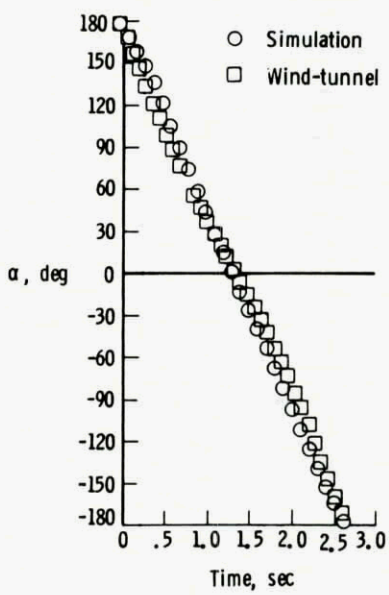

Fig. 12. One cycle of X-29 A tumbling - experiment vs computation (Ref. 8)

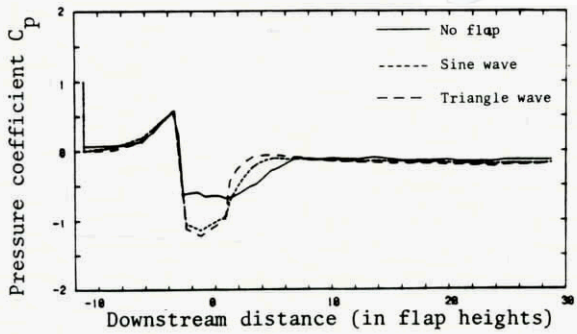

Fig. 13. Effect of oscillating flap on flow separation resulting from an upstream wedge, X'/H=-3, (Ref. 15)

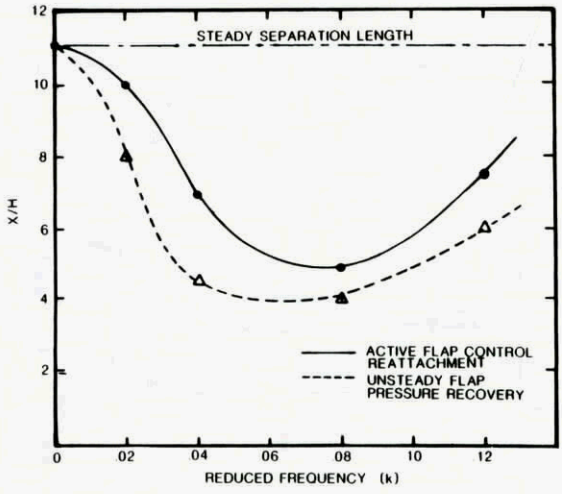

Fig. 14. Effect of reduced frequency on flow attachment length (Ref. 15)

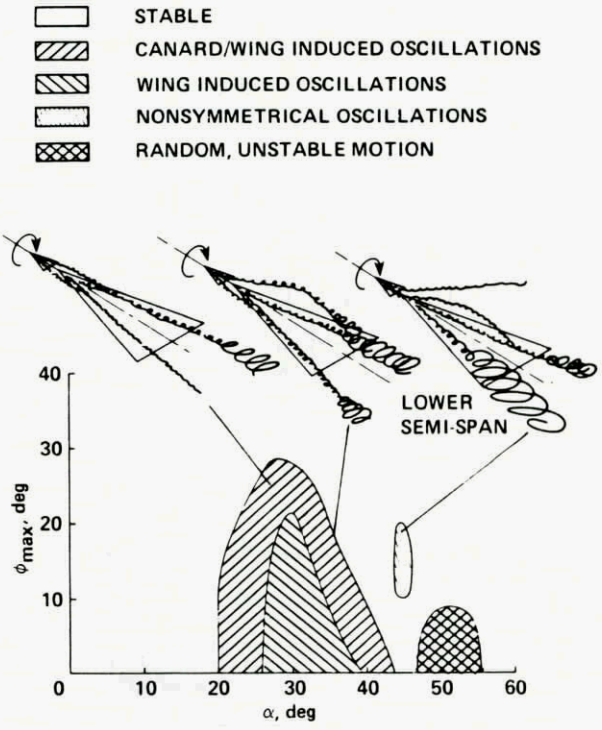

Fig. 15. Angle of attack range for self-induced roll oscillations for a 76° delta wing (Ref. 18)

Configuration	Speed Regime	C_{L_q}	C_{m_q}	$C_{L_{\dot{\alpha}}}$	$C_{m_{\dot{\alpha}}}$	C_{ℓ_p}	C_{n_p}	C_{Y_p}	C_{n_r}	C_{ℓ_r}
Body	Subsonic	o	o	o	o					
	Transonic	o	o	o	o					
	Supersonic	o	o	o	o					
Wing	Subsonic	o	o	o	o	o	o	o	o	o
	Transonic	✓	✓	✓	✓					
	Supersonic	o	✓	o	o	o	o	o		
Horizontal Tail	Subsonic	o	o	o	o	o				
	Transonic	✓	✓	✓	✓					
	Supersonic	o	✓	o	o	o				
Vertical Tail-Ventral Fin	Subsonic					o	o	o	o	o
	Transonic									
	Supersonic									
Wing-Body	Subsonic	o	o	o	o	o	o	o	o	o
	Transonic	✓	✓	✓	✓					
	Supersonic	o	✓	o	o	o	o	o		
Wing-Body-Horizontal Tail	Subsonic	✓	✓	✓	✓	o	o	o	o	o
	Transonic	✓	✓	✓	✓					
	Supersonic	✓	✓	✓	✓	o	o	o		
Wing-Body-Vertical Tail-Ventral-Fin	Subsonic	o	o	o	o	o	o	o	o	o
	Transonic	✓	✓	✓	✓					
	Supersonic	o	✓	o	o					
Wing-Body-Horizontal Tail-Vertical Tail-Ventral Fin	Subsonic	✓	✓	✓	✓	o	o	o	o	o
	Transonic	✓	✓	✓	✓					
	Supersonic	✓	✓	✓	✓					

o output available
✓ output only for configurations with straight-tapered wings

Fig. 17. Configurations and speed regimes for which Digital Datcom can be used for prediction of dynamic direct and cross derivatives in the attached flow region (Ref. 19)

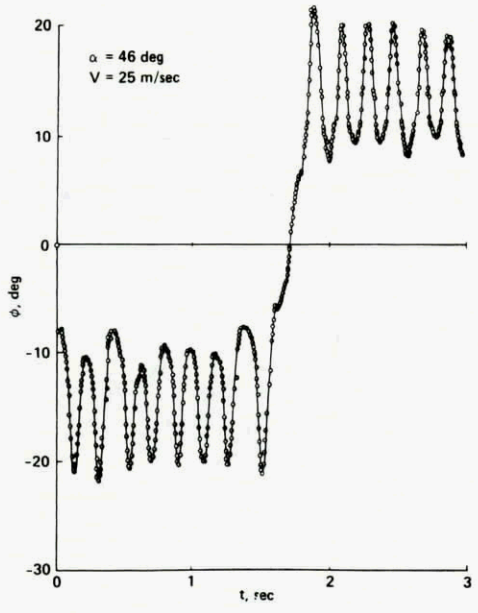

Fig. 16. Rolling angle vs time for asymmetric oscillation (Ref. 18)

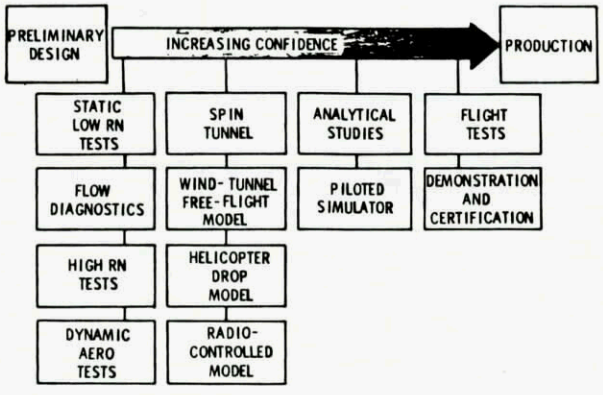

Fig. 19. Methodology for prediction and analysis of high α- characteristics (Ref. 20)

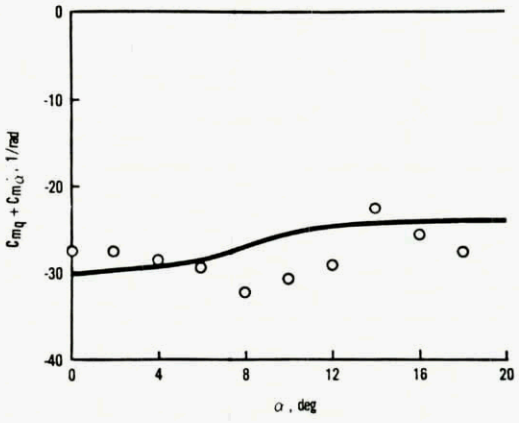

(a) F-111, M = 0.4

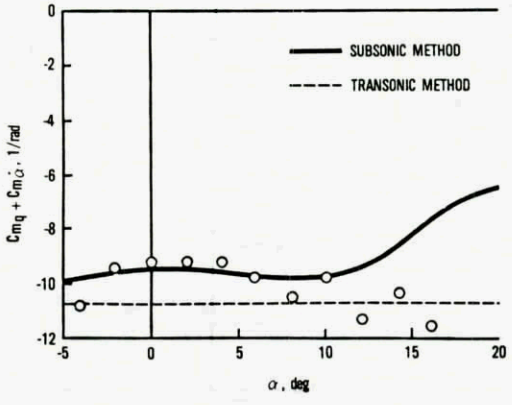

(b) Standard Dynamics Model, M = 0.8

Fig. 18.Comparison of Digital Datcom predictions with experiment (Ref. 19)

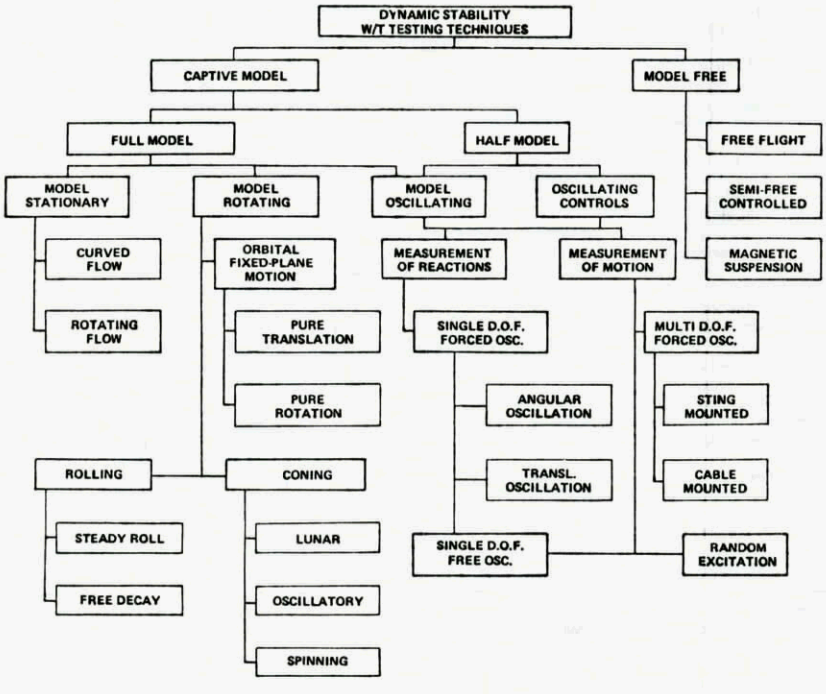

Fig. 20. Wind tunnel techniques for dynamic stability testing

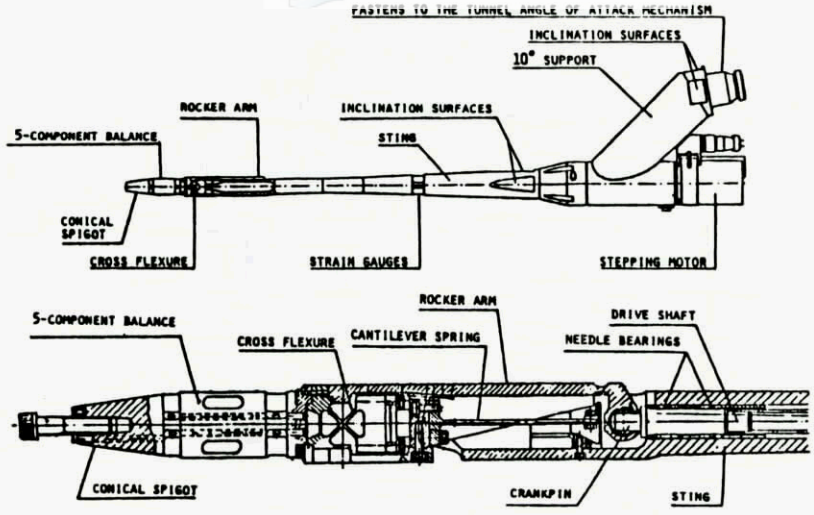

Fig. 21. FFA pitch/yaw forced oscillation apparatus (Ref. 26)

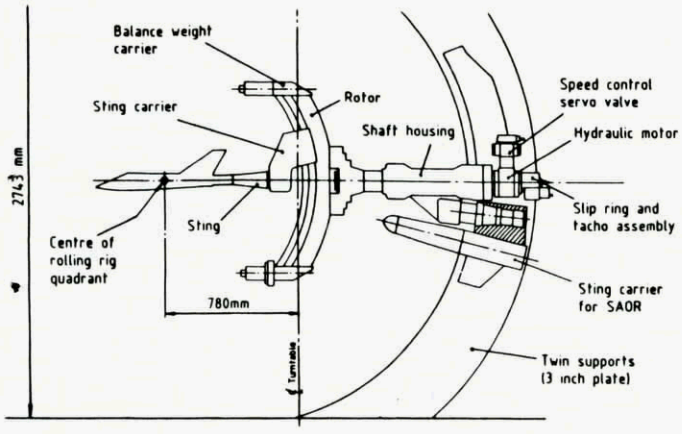

(a) Rotary balance mounted in RAE 4 m x 2.7 m wind tunnel

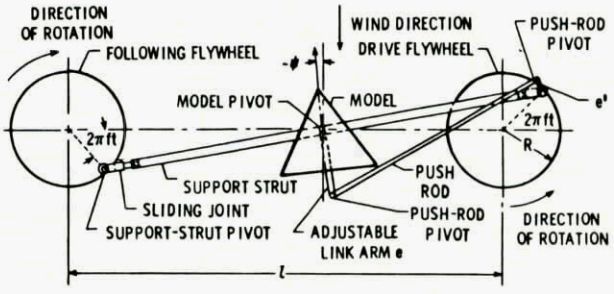

Fig. 23. NACA/VPI apparatus for snaking motion (Ref. 33)

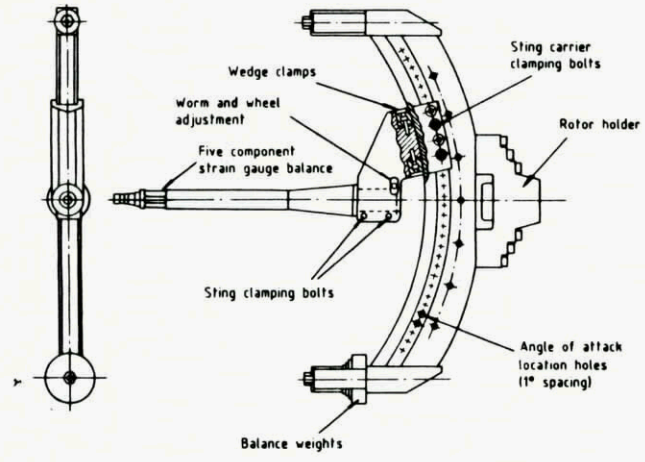

(b) Details of rotor and sting

Fig. 22. RAE - Bedford rotary balance (Ref. 31)

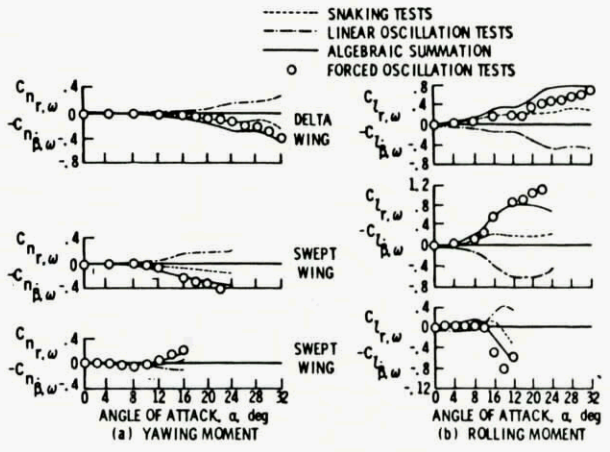

Fig. 24. Comparison of combined snaking and linear test results with forced oscillation results (Ref. 33)

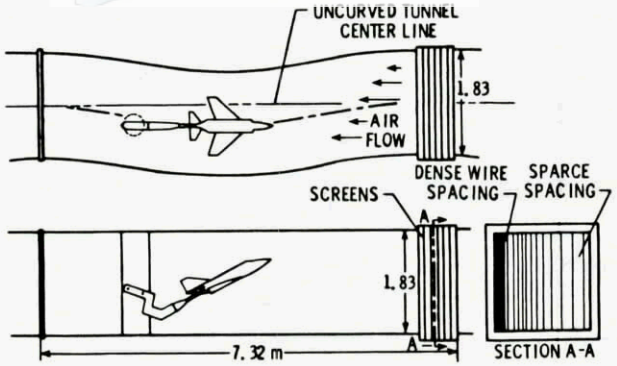

Fig. 25. NACA/VPI curved flow test section (Ref. 33)

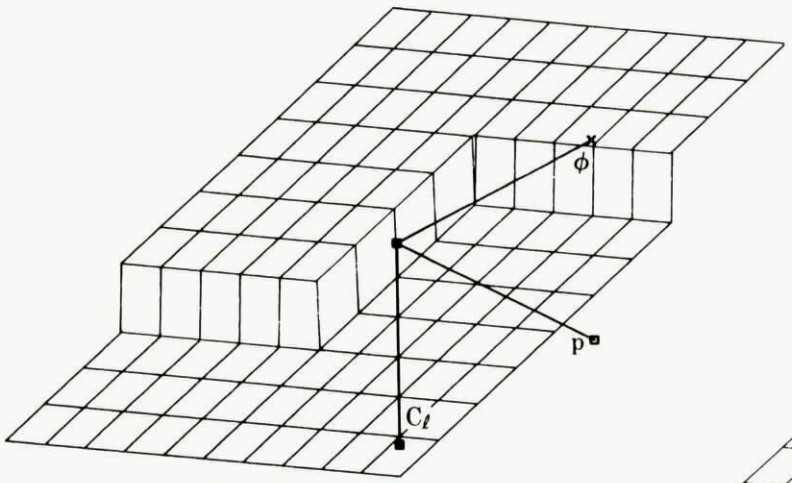

Fig. 26. Schematic reaction surface - threshold values independent of rate (static hysteresis); minor loops permitted (Ref. 36)

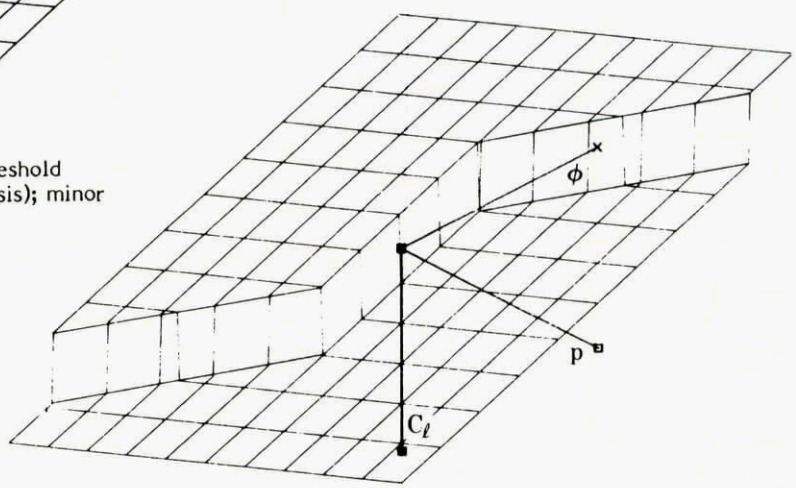

Fig. 27. Schematic reaction surface - threshold values linearly dependent on rate (Ref. 36)

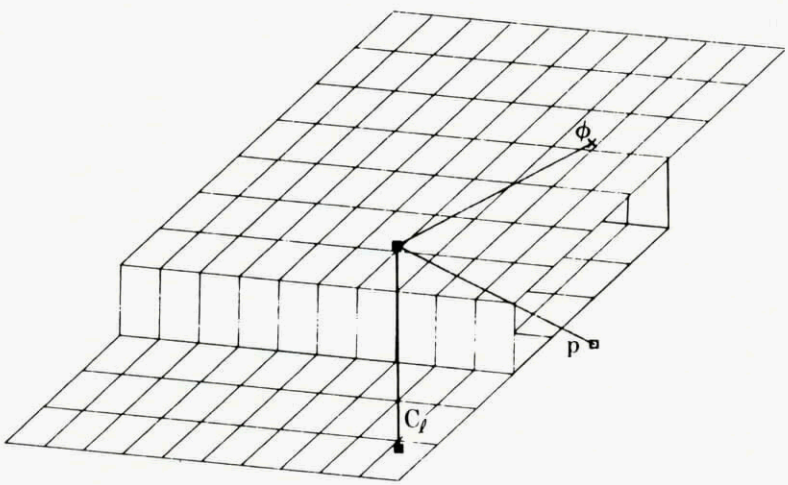

Fig. 28. Schematic reaction surface - threshold values independent of rate, minor loops not permitted (Ref. 36)

RE-ASSESSMENT OF GUST STATISTICS USING CAADRP DATA

by
B.W.Payne, A.E.Dudman and K.C.Griffiths
British Aerospace plc
Military Aircraft Division
Weybridge, Surrey, UK

1.0 INTRODUCTION

During the past fifteen years the Dynamics Department at BAe Weybridge have carried out a number of detailed investigations into a wide range of gust design procedures, varying from discrete gust to continuous turbulence on a number of different aircraft.

As a result of a study (Ref. 1) into a unified procedure for meeting power spectral density and statistical discrete gust requirements for flight in turbulence (Ref. 2), it was recommended that additional flight measurement evidence on the structure of high intensity turbulence events needed to be obtained on a more routine basis in order to support the gust parameters used in gust prediction procedures.

Thus in the early eighties it was agreed by the Civil Airworthiness Authority (CAA) and BAe that a reassessment of the gust statistics should be undertaken together with a study of turbulence events taken from routine operational flights.

The first part of the contract was to reassess the American and British gust statistical data. This data was collected in the most part prior to 1950 and formed a large part of the gust probability information upon which the current discrete gust airworthiness requirements are based. Whereas the second part was set to re-assess the current high vertical acceleration response data and routine data from the CAA Data Recording Programme (CAADRP) as has been measured upon the BAC 1-11 500 Series on standard airline routes, reference Figure 1.

The first part covered the 'Re-assessment of American Data and British Data' and was reported in Reference 3. It concluded that the earlier derived gust velocities were over estimated because of the limitations in the aircraft modelling techniques at the time, implying that the probability of meeting the design gust is lower than was intended.

The second part of the contract, 'Analysis of High Acceleration and Routine CAADRP Data' compared it with the predicted 'Mission Analysis' theoretical gust exceedance results.

Therefore the main topics of the report covers comparison of the predicted gust loads for a probability of 2 x 10-5 exceedances per hour (as defined in JAR 25.305(d)) with those analysed from the measured data.

However it should be noted that the measured and predicted analyses were concerned only with the BAC 1-11 500 Series aircraft in order to reduce the required amount of formal aircraft mathematical modelling.

Also the original assessment of the American data measured prior to 1950 (against which the certification requirements for gust loads are based) and British data measured in 1966 have also been compared with the 1981 re-assessment of the earlier data (Ref. 3), as well as the measured distributions of maximum derived gust velocities from CAADRP data.

These are the topics of this report and presentation to the 1986 AGARD workshop on 'Turbulence'.

2.0 OBJECTIVES

The objective of this report is to compare the measured incremental c.g. accelerations of the BAC 1-11 operating on scheduled flights with the equivalent theoretical predictions in a gust environment.

3.0 ANALYSIS OF MEASURED DATA

The raw data used in this analysis was obtained from the CAADRP programme, which has great potential as a source of information on gust statistics, covering many thousands of hours of scheduled flight operations, using modern operational techniques.

In addition to the 'special event' (CAADRP 'B') flights of each encounter of severe turbulence, giving a c.g. acceleration greater than 0.50 'g', there also existed records of 'routine' (CAADRP 'A') flights which, together with research into the airline operations, were used to define exact operating procedures for Mission Analyses studies. Therefore it was possible to define accurately the pattern of 'g' exceedances in the mission segments of total operational characteristics for comparison on a Mission Analyses basis, with the derived c.g. acceleration exceedances. The raw CAADRP data for c.g. acceleration consisted of standard flight data and it should be noted that the data was only available at eight samples per second. The basic theory associated with the analyses was to identify the speed, weight and altitude together with the time and then obtain only the response due to a gust encounter. This data was then evaluated for an accurate assessment of the probability of exceedance for the aircraft c.g. acceleration.

A 'g' counting algorithm was developed for analysing the routine BAC 1-11 collected data, which counted positive and negative level crossings in one pass. However in order to separate true gust contributions on the trace from manoeuvre induced accelerations, a digital high pass filter with a corner frequency at 0.1 Hz was used, thus allowing two sets of level counts to be measured; one for the raw record and the other for the 'gust only' acceleration.

The 'routine' flight CAADRP 'A' data was broken down in order to determine the average mission, including inside the Berlin Corridor, with confidence limits such that the following parameters could be identified :-

- Average take-off weight
- Average altitude
- Average speed
- Average time in each reduced mission segment
- Exceedance counts of c.g. acceleration for each segment

Regarding the 'special event' CAADRP 'B' data, these were also broken down into the average flight conditions and exceedance counts evaluated for each segment.
The analyses of the measured data is basically split into four parts, the first and second for the determination of flight segments and incremental c.g. acceleration data from 'routine' CAADRP 'A' data respectively, and the third for the incremental c.g. acceleration data obtained from the 'special event' CAADRP 'B' data. The fourth part relates to the data collected on flights inside the Berlin Corridor. The determination of the flight segment data was taken from the routine flights.

In view of all the detailed data that was available, only a random sample of 124 flights, involving 95 flight hours, reference Figure 2, and covering the period July 1978 to October 1980, was obtained from the CAADRP programme.

These flights included those inside and outside the Berlin Corridor, and it should be noted that during this period the airline's BAC 1-11 fleet made 24,028 departures from Berlin out of a total of 93,852, thus approximately 50% of the BAC 1-11 flights involved a trip through the Berlin Corridor. The altitude limitations in the corridor were constrained to be below 9,500 feet.

From this data it was possible to determine the average mission for the BAC 1-11 500 Series, consisting of 14 flight segments, covering take-off, climb, cruise, descent and approach conditions. The flight envelope, up to 30,000 feet was split up into approximately 5000 feet bands. A breakdown of all the flight segments showing the average altitude, condition, speed and flap position for each segment are shown in Figure 3. This shows the average conditions, including the standard deviation, in terms of time, altitude, speed and weight for all flights, with the average mission approximating to 46.4 minutes.

Figure 4 shows the number of flights inside and outside the Berlin Corridor where the average mission times are approximately 44.1 and 50.3 minutes respectively.

It should be noted that a segment defined as 13 (descent) was also considered, but no data could be successfully analysed within this segment and was omitted from any further analyses.

(a) Routine Data — CAADRP 'A' — Incremental c.g. Accelerations

The measured incremental c.g. accelerations exceedances from the 'routine' CAADRP data are shown as CAADRP 'A' in Figure 5 and covered accelerations up to 0.3g during this period for the random sample of 124 flights, approximating to 95 Flight hours.

However the data did include accelerations up to 0.7g, reference Figure 6, however because the sample above 0.3g was so insignificant they were not included in the final analysis.

(b) Special Event Data — CAADRP 'B' — Incremental c.g. Acceleration

The special event data was evaluated in two parts, firstly defined as CAADRP 'B' covering the period May 1980 to April 1983, and secondly defined as CAADRP 'C' which covers the period from May 1980 to October 1983.

CAADRP 'B' measured data covered high incremental c.g. acceleration events greater than 0.5g from 49,395 flight hours, reference Figure 2 and the analysed results in terms of acceleration exceedances are shown Figure 5.

The detailed information of the c.g. accelerations in terms of the probability of excedances per hour for the segments is defined in Figure 7. This figure shows that segment exceedance results are well grouped together, but that Segment 12 gives the most significant results, although it should be noted it is based upon a very small period of time. CAADRP 'C' measured data is similarly based but includes an extra six months of data, therefore representing 58,733 flight hours, reference Figure 2. All the points, including CAADRP 'B' have been used for the exceedance calculations and the results, in terms of incremental c.g. acceleration exceedances are shown in Figure 5 together with the CAADRP 'A' and 'B' results.

Regarding the additional six months of flight data in isolation, it can be seen that the results are very similar to those obtained from three years of analysis, except for one point that gave an incremental value of 1.30g compared to the highest values seen in the earlier data of 1.10g. However the difference between 1.13g and 1.25g respectively is small at the probability of 2 x 10-5 exceedances per hour (defined as the datum exceedance).

(c) Berlin Corridor Data

Since flights through the Berlin Corridor were restricted to flying below 9500 feet, it was considered that this could be an important aspect in the correlation of results, so CAADRP 'B' data were split into flights inside and outside of the Berlin Corridor.

This was achieved by breaking down the data into flights that arrived at or departed from Berlin, and flights to and from other airfields, reference Figure 4. Figure 8 shows the measured differences in the probability of exceedances per hour for inside and outside the Corridor are very small.

4.0 THEORETICAL PREDICTIONS

The mathematical models used in this work were consistent and similar to those used in the various design stages of the BAC 1-11 other than that these models used up-to-date information with regard to structural stiffness and aerodynamic data.

Standard symmetric gust response calculations in the frequency plane were used to carry out the necessary Continuous Turbulence Mission and Discrete 1-Cosine Gusts analyses.

Also a review was made to evaluate the effect of the autopilot and the accelerometer transfer function.

(a) Mission Weights

The missions were broken down into two weight cases, a heavy weight case corresponding to take-off climb and cruise, and a lighter weight case corresponding to descent and landing.

The take-off weight was an average weight over the corresponding flight segments (Ref. 6), whereas the landing weight allowed for fuel burn during the average mission length of flight.

The two weight cases used in the analysis are detailed as follows in terms of basic aircraft weight, payload and fuel.

	Light Weight lb	Heavy Weight lb
Basic A/C	54,600	54,600
Payload	17,500	17,500
Fuel	8,100	2,400
Total AUW	80,200	74,500

Noting that the fuel weight included 2,400 lbs of reserve.

(b) Structural

Basically the analyses were performed using a symmetric structural model, the structure being treated as a series of branches, front fuselage, rear fuselage, wings, fin, tail and engines.

Normal modes were calculated for each of the branches using standard 'lumped mass' representation and stiffness influence coefficients.

Sub-sets of these branch modes together with the rigid body modes, joint flexibilities and control surfaces were built to form a 'normal mode' representation of the whole aircraft.

A table of frequencies for the branch modes and definition of the mode shapes are given in Figure 9.

Figure 10 shows the first 12 symmetric normal modes (including rigid heave and pitch) which were used in the gust analyses.

(c) Aerodynamic

The aerodynamic forces were calculated using two-dimensional strip theory, with three-dimensional quasi static stiffness derivatives calculated from the current rigid aircraft aerodynamic loading data. In the case of the BAC 1-11 aerodynamic forces on the wing, tail and nacelles were included and found sufficient to give the symmetric rigid body characteristics in the short period pitching mode.

The model also included representation of gust input delays by use of 'Kussner' applied gust lag functions and a 'Wagner' lift growth function for each lifting surface.

(d) Autopilot

It can be seen from Figure 3, which defines details regarding the measured data that for most of the segments the autopilot was engaged, therefore there was a need to study the effect of the autopilot on the response.

From earlier response work carried out on the BAC 1-11 (Ref. 4) where similar mathematical modelling techniques were used, the effect of autopilot has been calculated for symmetrical gust loads. The exceedance curves presented in this report show for acceleration, that although there were some variation in the results for the front fuselage and tailplane, with and without autopilot, there were insignificant differences at the c.g. position.

Therefore, it was assumed in this study, that the effect of autopilot can be neglected and the predicted results can be assumed valid for c.g. acceleration without autopilot.

(e) Aircraft Accelerometer Transfer Function

All the CAADRP c.g. acceleration data, taken from the BAC 1-11 500 Series aircraft, was measured using a Plessey PV 714 accelerometer, and a full description of the accelerometer may be found in Reference 5.

In order to match the measured results, the characteristics of the PV 714 accelerometer needed to be modelled. Therefore a model incorporating a second order filter with characteristics of 1.85 Hz and 34% critical damping was used, and the compared measured and predicted frequency responses shown on Figure 9 are very similar. It should be noted that the recording system in the aircraft provided c.g acceleration data at eight points per second, thus only low frequency information is contained in the measured data.

(f) Mission Analysis Method

Solutions of the aircraft equations of motion were undertaken in the frequency plane in order to derive the transfer functions relating the response of various parts of the aircraft (Interesting Quantity) to unit gust input. These transfer functions were then used to derive the Continuous Turbulence coefficients A and No. for Mission Analysis, and for checking purposes the response to Discrete 1-Cosine Gusts was also calculated.

The Mission Analysis procedure used in these analyses are as those defined in JAR 25.305. Although the Mission Analysis method has been used basically to predict only the exceedance curves for c.g. acceleration, response forces were also evaluated for checking the response.

The values of P1, P2, b1 and b2, reference Figure 11, have been determined at the average altitudes shown in Figure 3 for each Mission segment together with the times for each segment factored such that the total Mission time equalled one hour.

(g) Analyses

Using the mathematical models of the BAC 1-11 500 Series aircraft for the two AUW's of 80,200 lbs and 74,500 lbs together with two sets of aerodynamic data for Mach No. 0.5 and 0.78, the responses of the aircraft for each segment have been analysed. The data nearest to the measured segment data was then used, such that Segments 2 to 5 (Climb) and 9 to 12 (Descent) used equivalent 0.5 Mach No. data, whereas for Segments 5 (Cruise) to 8 (Descent) used the data associated with Mach No. 0.78.

Due to the complexities of setting up the detailed aerodynamic data for other speed and flap conditions, the take-off and approach condition segments have not been modelled.

Using the measured altitude and speeds for each segment the dynamic response was calculated in terms of A and No. for c.g. acceleration, the Mission Analysis method was applied for calculation of the incremental acceleration exceedance curves.

5.0 COMPARISON OF THEORETICAL PREDICTIONS

(a) Mission and Segment Response

The predicted c.g. acceleration exceedance curves were determined for 'All' flights, for flights in and outside the Berlin corridor together with the detailed segment curves without autopilot as defined in Figure 3.

The comparison of the segments, without autopilot, in terms of exceedances, are shown in Figure 12, where it is noted that the maximum incremental accelerations of 2.59g at the datum exceedance value is for Segment 10 (Descent). On Figure 13, the Segment 3 BC, the Vc case and the 16 segment Mission have been compared showing that the Vc case has the largest incremental c.g. acceleration of 2.93g at the datum exceedance value.

The response for the single Segment 3BC (which has the longest time in a segment) and 'All' segments are very comparable at 2.42g and 2.38g respectively, but, as expected, lower than the Vc case for the similar exceedance. However the segment exceedance results at low incremental acceleration are higher than the Vc case.

It also should be noted that the exceedance curves for seven flight segments with the longest times are almost identical to those produced for the sixteen segment mission presented in Figure 13.

(b) Berlin Corridor

As stated in Section 3 more than half of the CAADRP 'B' were flown through the Berlin Corridor at a restricted height of below 9500 feet which was considered to be an important aspect in the correlation of the measured results.

Figure 14 presents the predicted effects of such flights compared with 'All' flights and it can be seen that although the results for the Berlin Corridor give the highest exceedances they are only marginal different to those outside the Corridor and 'All' flight exceedances. At the datum exceedance, the results are 2.39g and 2.36g inside and outside of the Berlin Corridor compared with 2.38g for 'All' flights.

(c) Parameter Variations

The effect of the standard deviations changes (about the datum value) on the predicted exceedance values were evaluated in this study and found to be small and can be neglected as a significant variation in the analysis of the measured data.

(d) Effect of Accelerometer Transfer Function

Results were obtained using the filtered and unfiltered c.g. acceleration data from the analysis for the flight segments. It was shown that the filter reduces the effective acceleration results by 0.07g relative to the 'All' flights acceleration of 2.38g at the datum.

6.0 COMPARISON OF PREDICTED AND MEASURED RESULTS

(a) Mission Analysis

The measured incremental c.g. acceleration CAADRP data and the equivalent Mission Analysis prediction results were compared in terms of probability of exceedance per hour. Figure 15 shows this comparison and it can be seen from the results that the predicted Mission Analysis values were approximately twice the measured CAADRP values, all of which was based upon approximately 59,000 flight hours of BAC 1-11 Series 500. That is, at the datum probability of 2 x 10-5 exceedances per hour, the measured value of 1.25g can be compared with the predicted value for 'All' flight data of 2.38g.

For comparison purposes the predicted exceedance curve for the Vc Mission case were also shown which has the equivalent acceleration of 2.93g. At low incremental c.g. accelerations, the Mission Analysis results compared fairly well with the CAADRP data, although the accelerations for a given exceedance were still larger than the predicted data.

(b) Berlin Corridor

The exceedance values for the Berlin Corridor can be compared by reviewing Figures 8 and 14 respectively, where it is shown that there was very little difference between flights inside and outside of the Berlin Corridor for both the measured and predicted data.

The predicted values were shown to have an approximate factor of two greater than the measured exceedances values.

(c) Comparison with Design Condition Results

Calculations were carried out of c.g. acceleration response to design gust velocity using the various Airworthiness requirements for transport aircraft. Figure 16 shows the differences in the incremental c.g. acceleration results at the datum exceedance for the Pratt, Tuned Discrete, 12.5c Discrete and PSD (DEA & Mission) analyses compared with the equivalent measured CAADRP results.

It can be seen that the Mission Analysis '1' (16 segment) generally gives comparable results to those from the Pratt, Tuned Discrete Gust and the PSD method approximating to 2.2g for the datum exceedance value. However the Mission Analysis '2' results for the Vc segment were large, as expected, at 2.9g. All these predicted design results were compared with the CAADRP analysis and showed that the Design values were aproximately twice the measured result of 1.3g at the datum probability.

7.0 COMPARISON OF CAADRP MEASURED DATA WITH EARLIER DATA

(a) Earlier Data from 1950

The gust velocities used in Airworthiness Certification were based upon aircraft c.g. acceleration data collected prior to 1950. Reference 4 presents some of the results, taken from a DC-3 and Martin 2-0-2, upon which values of derived gust velocities were calculated.

These original Airworthiness assessments were based on a 'Pratt' solution with a rigid aircraft. However during the re-assessments of the gust velocities for these aircraft and additional measured data taken from a Viscount aircraft, modern flexible aircraft calculations were used for assessing the gust velocities. The results from this re-assessment can be seen in Figure 17, where it was noted that the re-assessed maximum derived gust velocities relative to the average flight miles were approximately 25% less than those obtained using the original 'Pratt' assessment.

(b) Measured CAADRP Data

The measured CAADRP results for the BAC 1-11 aircraft have also been compared with the original assessments, reference Figure 18. In determining the ratio of incremental c.g. accelerations to gust velocity, the results from three methods, 'Pratt', 12.5 Discrete and Tuned Discrete Gust have been included.

All the methods were based upon incremental accelerations, with Pratt using rigid aircraft data for all flight segments, whereas the Discrete Gust used flexible aircraft and were based upon flight segment 3BC.

It should be noted that the concept for converting accelerations to gust velocities uses the same level of probability as used in the original assessment of the American data, (Ref. 3). Flight Segment 3BC was used to obtain typical average values of incremental acceleration for given gust velocities. The average statute flight miles for the BAC 1-11 were based upon the 58,733 hours of flight time together with the speed data from CAADRP.

The tuned Discrete Gust of equal probability to the 12.5c Discrete Gust gives a further reduction in derived gust velocity relative to the reassessed 'Pratt' estimate, which is fully consistent with the 25% reduction derived in Ref. 3 for the DC-3, Martin 2-0-2 and the Viscount.

8.0 CONCLUSIONS

The results of this study of the BAC 1-11 500 Series measured and predicted analyses were concluded as follows

- An analysis of the measured CAADRP data, based upon a significant 58,733 flying hours, gave an incremental vertical c.g. acceleration of 1.25g at the datum probability value of 2 x 10-5 exceedances per hour.
- The theoretical predictions from all the flight segments in the 'Mission Analysis' gave an incremental c.g. acceleration of 2.38g at the datum exceedance value.
- Therefore in the comparison between the measured and predicted analyses for a similar mission considerably differences were found with measured frequencies of exceedance of about one half those predicted using current airworthiness requirements.
- The measured differences from the CAADRP analysis for flights inside and outside of the Berlin Corridor were small which was consistent with the predicted differences. This to some degree was unexpected since it was assumed that flying inside the Berlin Corridor at the restricted altitude of 9,500 feet would provide higher accelerations at a given exceedance value.
- A comparison of the frequency distribution of maximum derived gust velocities for the measured CAADRP data and the original American data obtained prior to 1950 shows that the gust velocities have been approximately halved.

9.0 REFERENCES

1) V Card BAe/WBD/D/M/32

Gust Design Procedures Development of Improved Gust Load Requirements incorporating the Statistical Discrete Gust Method

2) G G Jones RAeS/CASI/AIAA

A Unified Discrete Gust and Power Spectral Treatment of Conference Atmospheric Turbulence. London 1971

3) V Card BAe/WBD/D/P/120

Re-assessment of Gust Statistics Aug-Nov 1981

4) T G Pearce VTO/D/BAC1-11/17

The Longitudinal Response of the BAC 1-11 to Continuous Turbulence. Issue 2

5) E J Vincent BAe/WBD/D/M/389

Investigation into Frequency Characteristics of Two A I D S Accelerometers

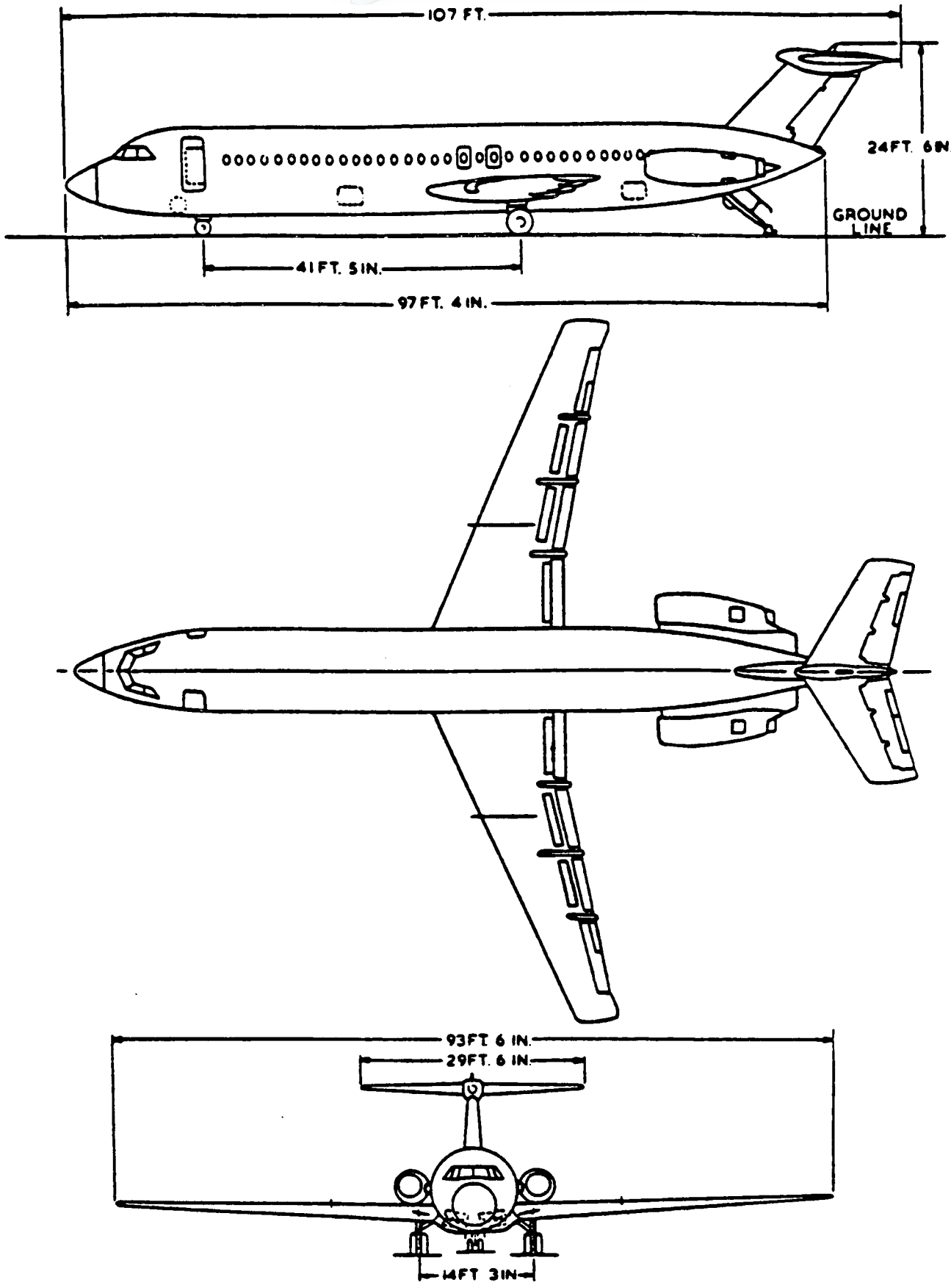

Fig.1 BAC One-Eleven — 500 Series

CAADRP 'A'
ROUTINE DATA — JULY 1978 to OCTOBER 1980
95 FLIGHT HOURS (124 FLIGHTS) — $\Delta G < 0.3$ G ONLY

CAADRP 'B'
HIGH G EVENTS — MAY 1980 to APRIL 1983
49395 FLIGHT HOURS — $\Delta G > 0.5$ G ONLY

CAADRP 'C' (INCLUDES CAADRP 'B')
HIGH G EVENTS — MAY 1980 to OCTOBER 1983
58733 FLIGHT HOURS — $\Delta G > 0.5$ G ONLY

Fig.2

FLIGHT SEGMENT	FLAP POSITION	AUTO-PILOT	ALTITUDE RANGE ft	A/C CONDITION	SPEED kts EAS	ALTITUDE t	SPEED kts TAS	MACH No
1	8°/18°	OUT	0—⩽ 5000	T/O	168.1	1705	172.4	0.26
2	0	OUT	⩽ 10000	CLIMB	265.4	4696	284.6	0.44
3	0	IN	⩽ 15000	CLIMB	286.8	9755	332.5	0.52
3BC	0	IN	⩽ 15000	CRUISE BC	306.3	8939	350.6	0.55
3	0	IN	⩽ 15000	CRUISE	311.2	12327	375.8	0.60
4	0	IN	15000—20000	CLIMB	281.2	17018	366.5	0.59
4	0	IN	15000—20000	CRUISE	301.5	16785	391.5	0.63
5	0	IN	20000—25000	CLIMB	268.8	21821	379.9	0.62
5	0	IN	20000—25000	CRUISE	282.0	22857	405.8	0.67
6	0	IN	25000—30000	CLIMB	252.5	26472	387.3	0.65
6	0	IN	25000—30000	CRUISE	271.3	27978	427.6	0.72
7	0	IN	30000—25000	DESCENT	286.1	26436	438.5	0.73
8	0	IN	25000—20000	DESCENT	293.3	21642	413.3	0.68
9	0	IN	20000—15000	DESCENT	301.6	17162	394.0	0.64
10	0	IN	15000—10000	DESCENT	308.6	12387	373.0	0.59
11	0	IN	⩽ 10000	DESCENT	292.2	6723	323.2	0.50
12	0	OUT	⩽ 10000	DESCENT	290.7	6377	319.8	0.50
14	26°/45°	OUT	⩽ 1000	APPROACH	141.0	500	142.0	0.22

Fig.3 Routine CAADRP Flight Segment Data

CAADRP 'A' ROUTINE DATA

124 FLIGHTS

77 IN BERLIN CORRIDOR

47 NOT IN BERLIN CORRIDOR

CAADRP 'B' HIGH G EVENT

808 SAMPLES

304 IN BERLIN CORRIDOR

324 NOT IN BERLIN CORRIDOR

180 DO NOT KNOW

BERLIN CORRIDOR

ALTITUDE CONSTRAINED TO BELOW 9,500 FEET

Fig.4

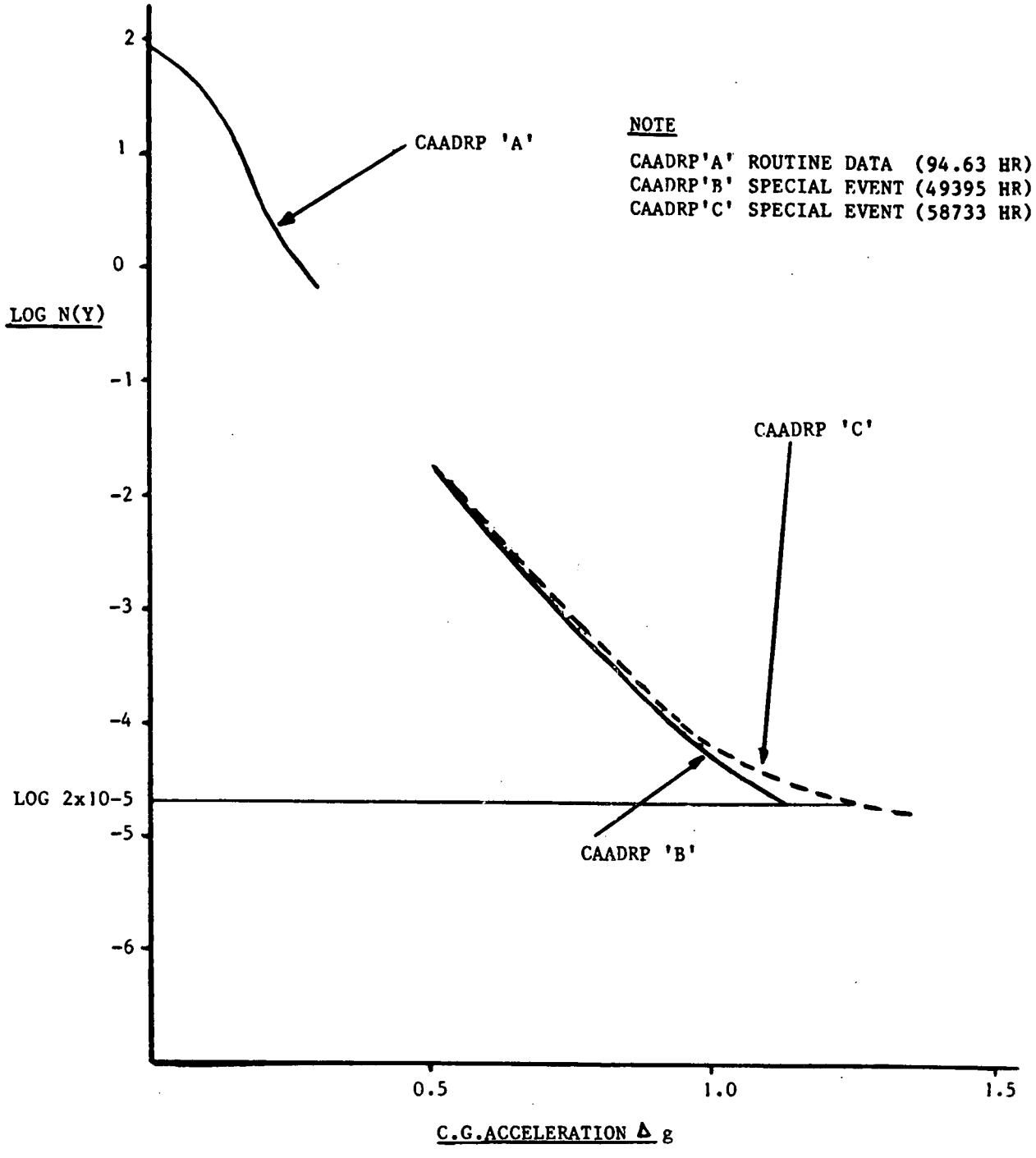

Fig.5 CAADRP

G	TOTAL NUMBER OF EXCEEDANCES N (Y)	LOG N (Y)
0.	8340	1.95
0.1	3103	1.52
0.2	328	0.54
0.3	64	-0.17
0.4	37	-0.41
0.5	18	-0.72
0.6	13	-0.86
0.7	6	-1.20

Fig.6 CAADRP 'A'

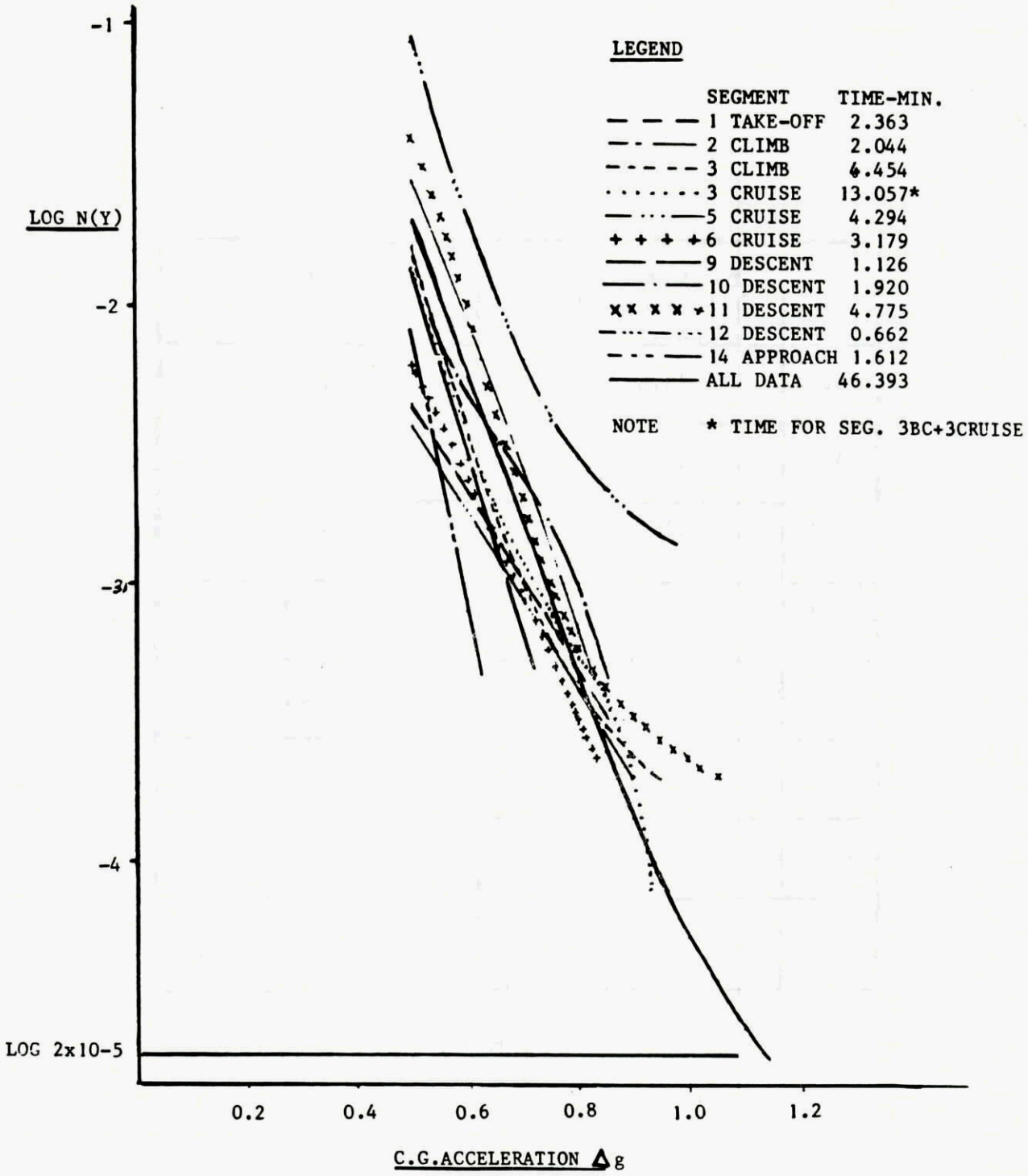

Fig.7 Summary of CAADRP 'B' Data Using the Time in Each Segment

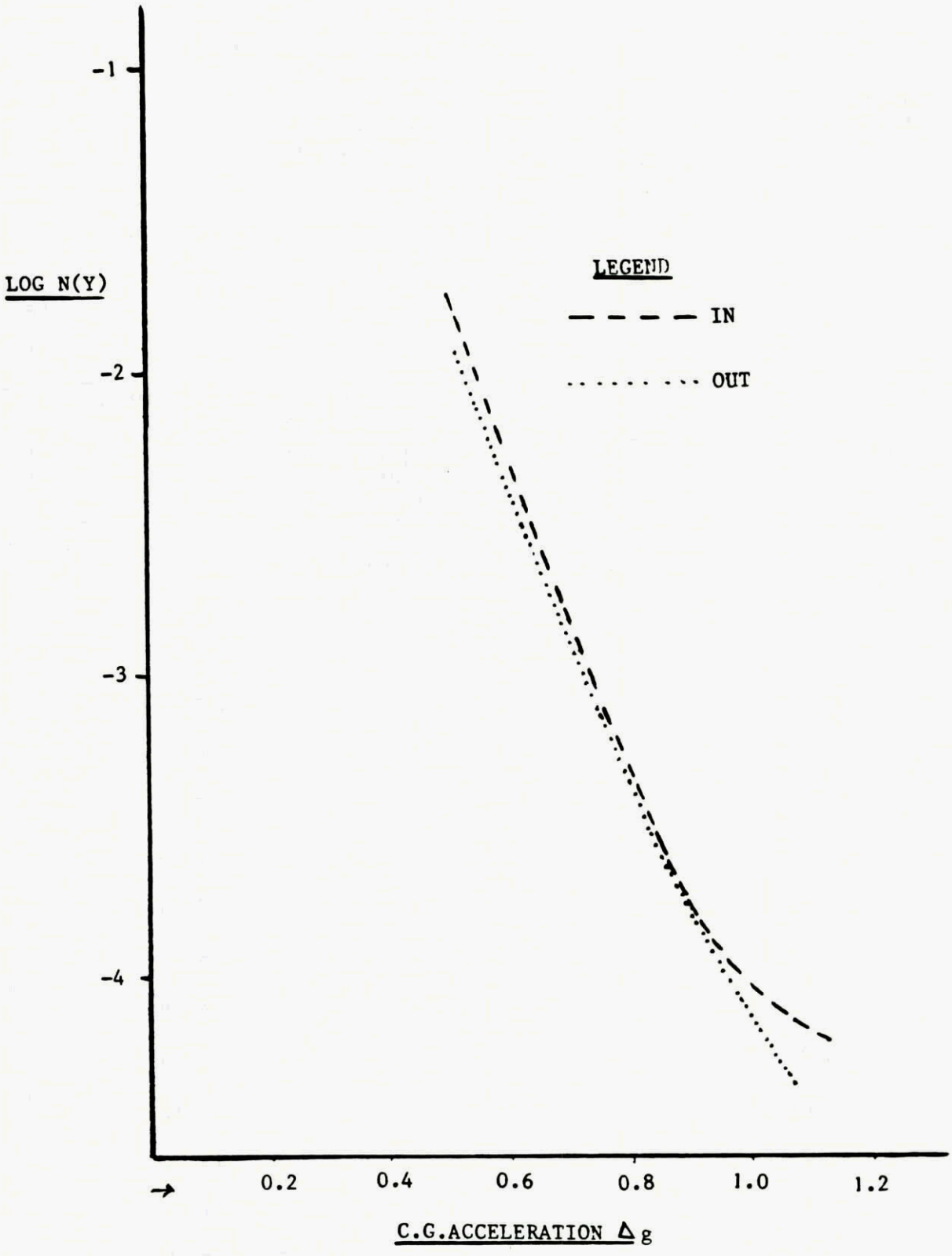

Fig.8 CAADRP DATA 'B' Comparison of Flights In and Out of Berlin Corridor

BRANCH	FREQUENCY (Hz)	DESCRIPTION
RIGID BODY	0 0	HEAVE PITCH
FRONT FUSELAGE	4.45 26.0	VERTICAL BENDING VB2 — TORSION
WING (2400 LB FUEL/8100 LB FUEL)	3.42 3.34 11.8 10.6 20.5 19.7 25.5 22.8 36.9 33.9 42.3 38.3	BENDING 2nd BENDING BENDING TORSION
ENGINE	6.27 8.49 20.4 26.4 32.7 46.5	
FIN	3.66 10.4	FIN ROTATION @ FUS. ATTACHMENT FIN F/A BENDING
TAIL	10.1 8.39 28.8	TAIL ROTATION @ FIN PIVOT BENDING BENDING — TORSION

Fig.9 Branch Modes Included in the Structural Model

NORMAL MODES

AUW 74500 LB	AUW 80200 LB
0	0
0	0
3.23	3.19
3.58	3.54
6.28	6.29
6.94	6.78
8.24	8.23
10.28	10.25
12.00	11.00
19.58	19.08
20.65	20.05
20.80	20.69

Fig.10 BAC 1-11 Gust Statistics

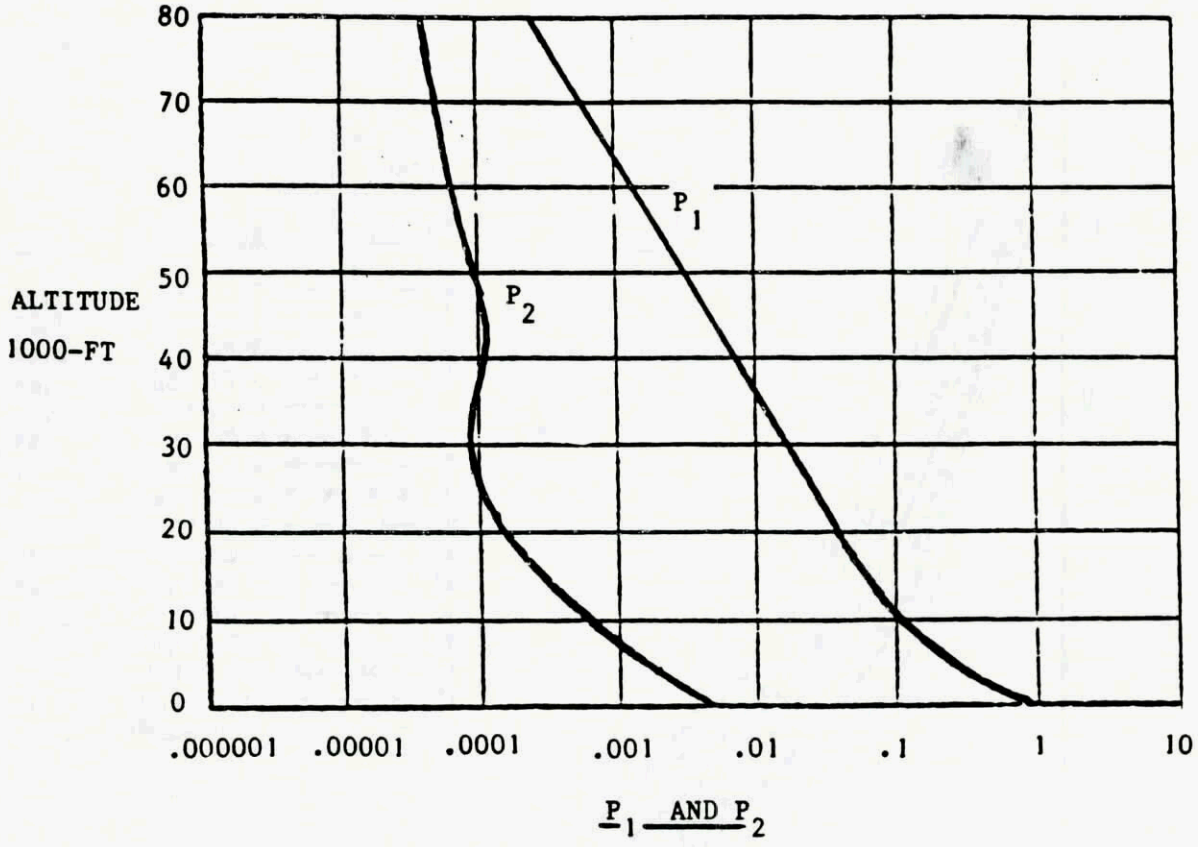

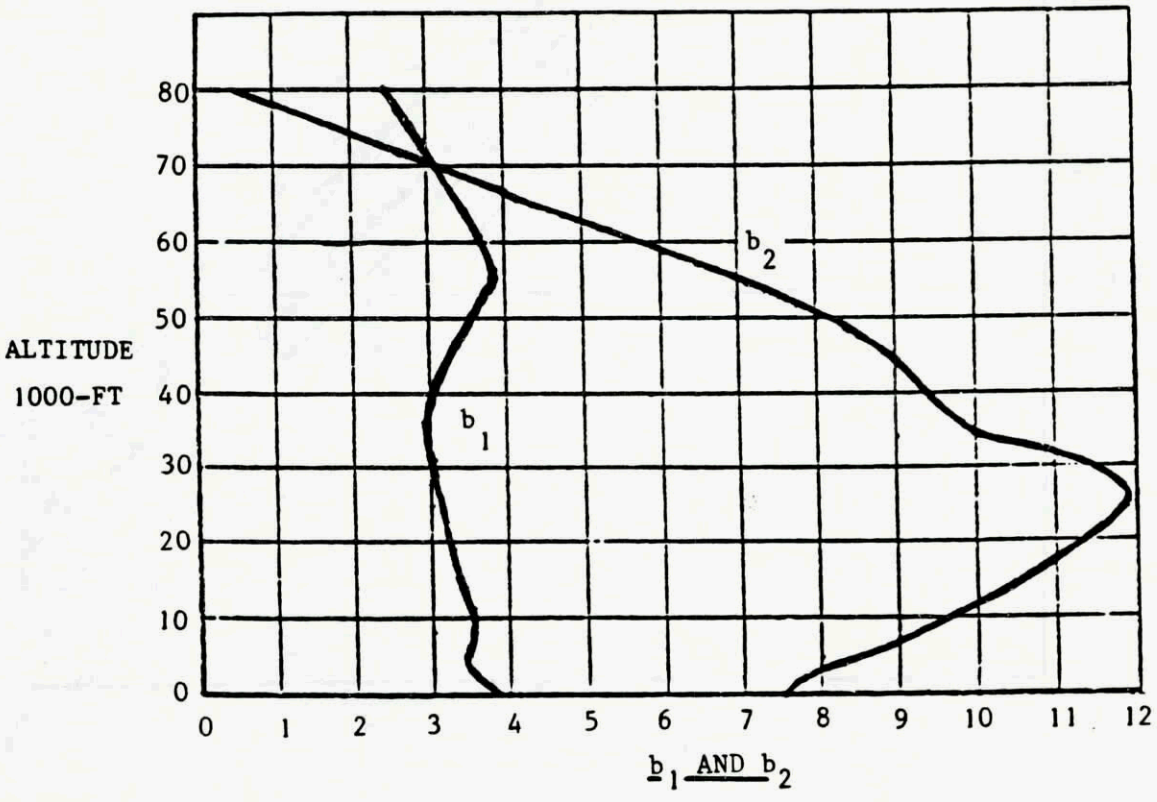

Fig.11 Mission Analysis — Values of P1, P2, b1 and b2

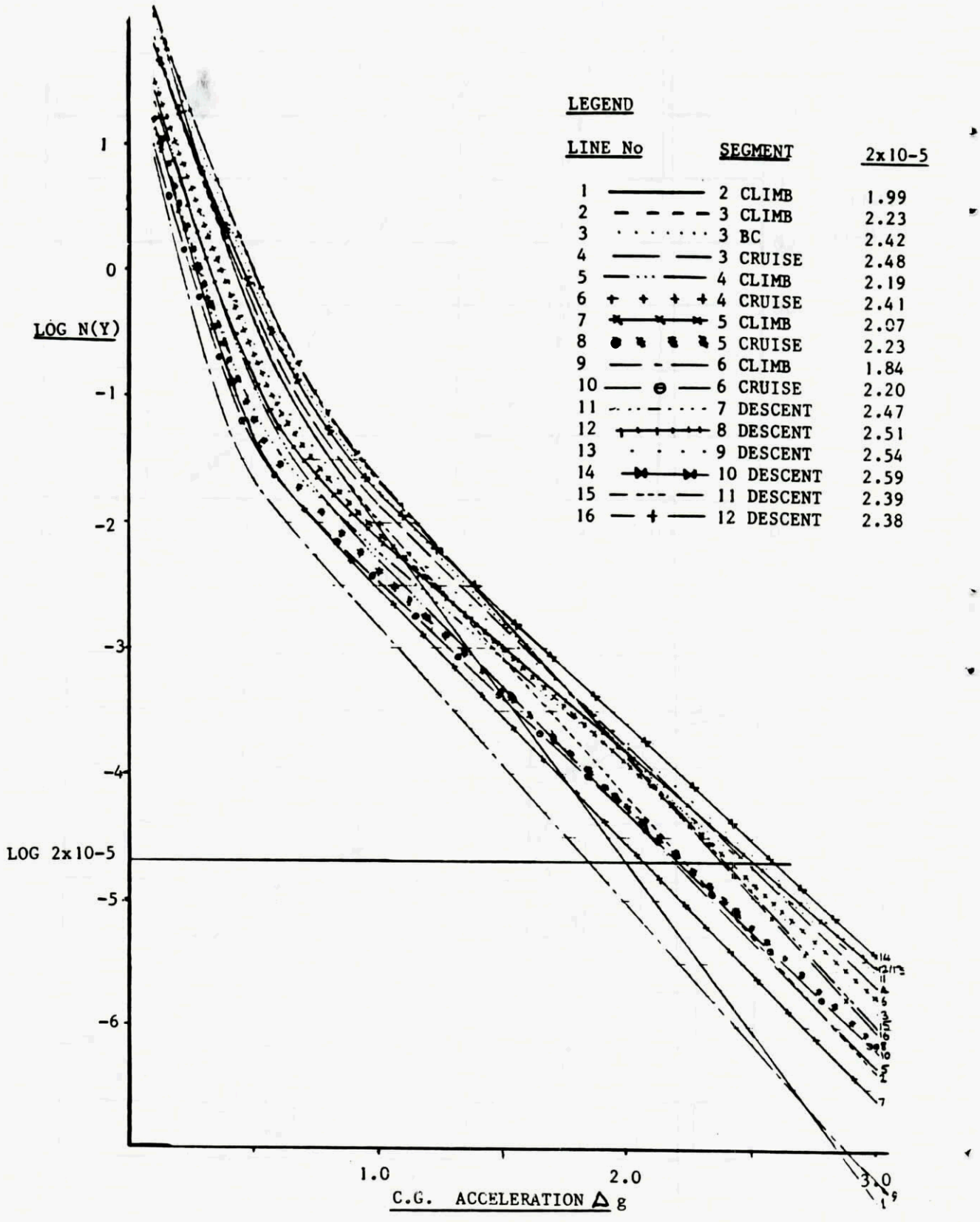

Fig.12 Mission Analysis Comparison of Flight Segments

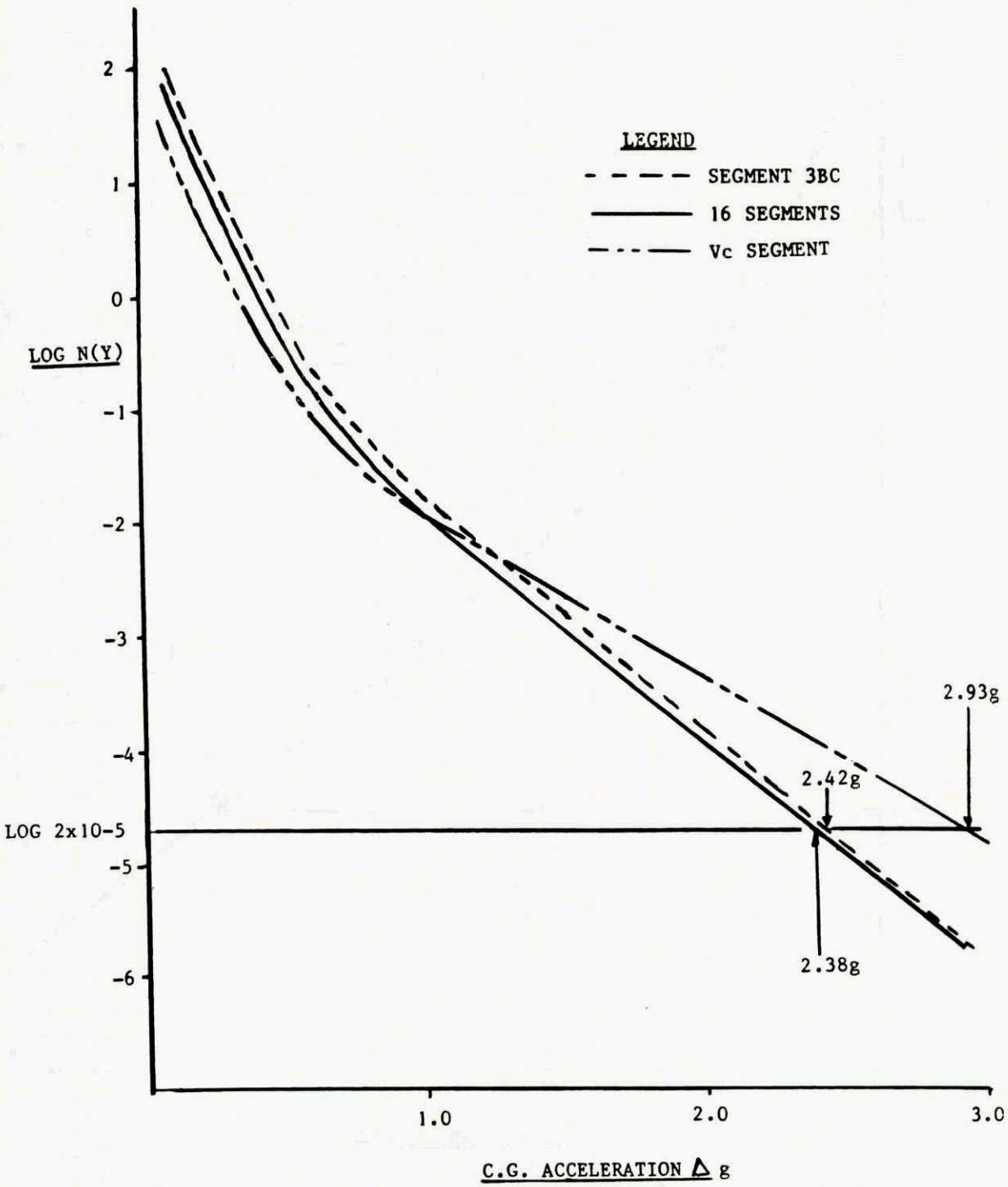

Fig.13 Mission Analysis Predictions for Flight Segments

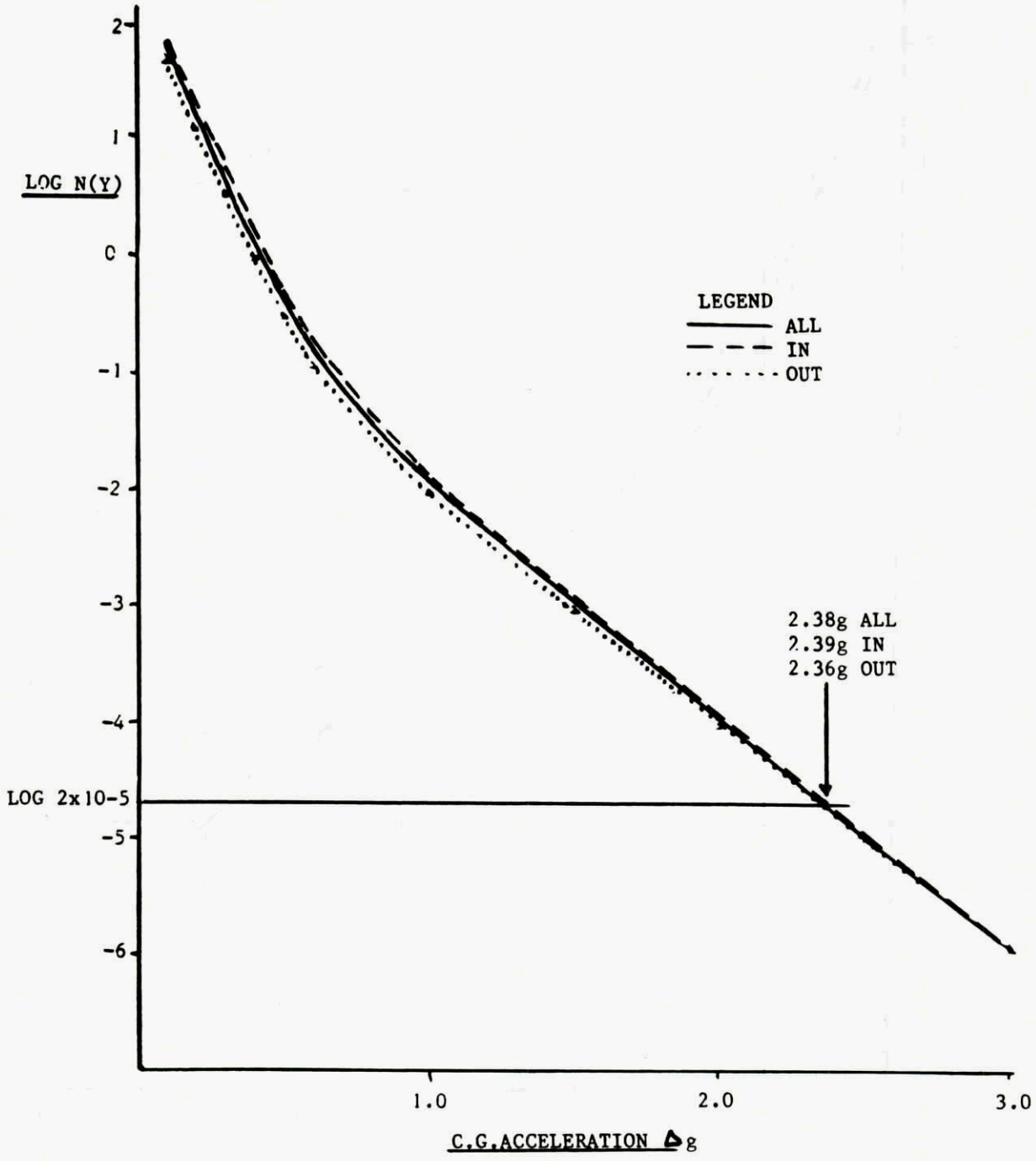

Fig.14 Mission Analysis for Flights In and Out of the Berlin Corridor

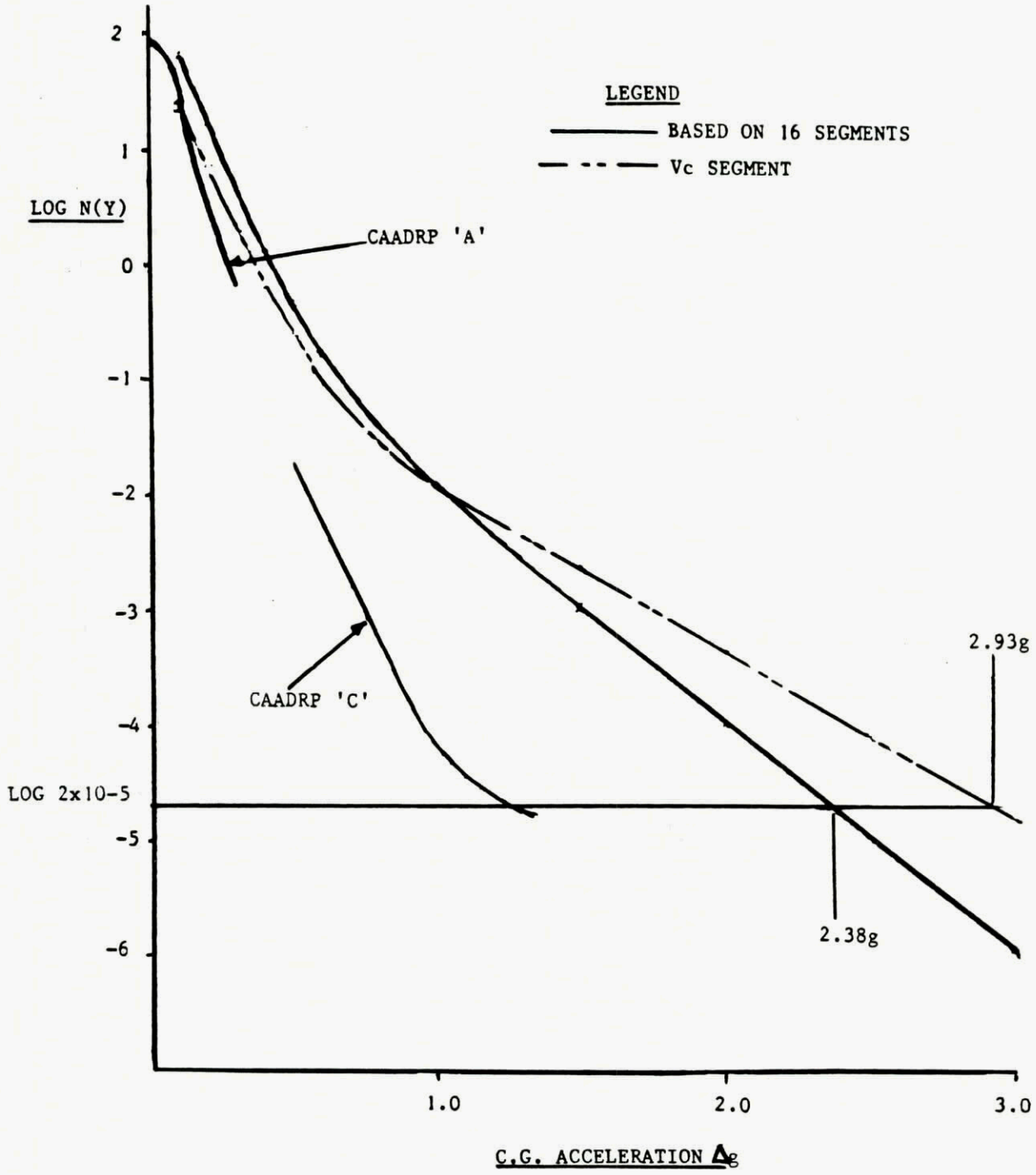

Fig.15 Mission Analysis — Comparison of Measured and Predicted Data

	ΔG
PRATT	2.2
DISCRETE GUST ($12\frac{1}{2}\bar{c}$)	1.6
DISCRETE GUST (TUNED)	+ 2.0 @ 29 $\bar{c}$ - 3.1 @ 40 $\bar{c}$
DESIGN ENVELOPE (U_σ = 85ft/sec)	2.2
MISSION ANALYSIS 1	2.4
MISSION ANALYSIS 2	2.9
CAADRP 'C'	1.3

MISSION ANALYSIS Δ G AT 2 x 10 $^{-5}$ EXCEEDANCES PER HOUR

1. USING 16 SEGMENTS
2. ONE SEGMENT @ Vc

Fig.16 Comparison of C.G. Accelerations at Design Condition

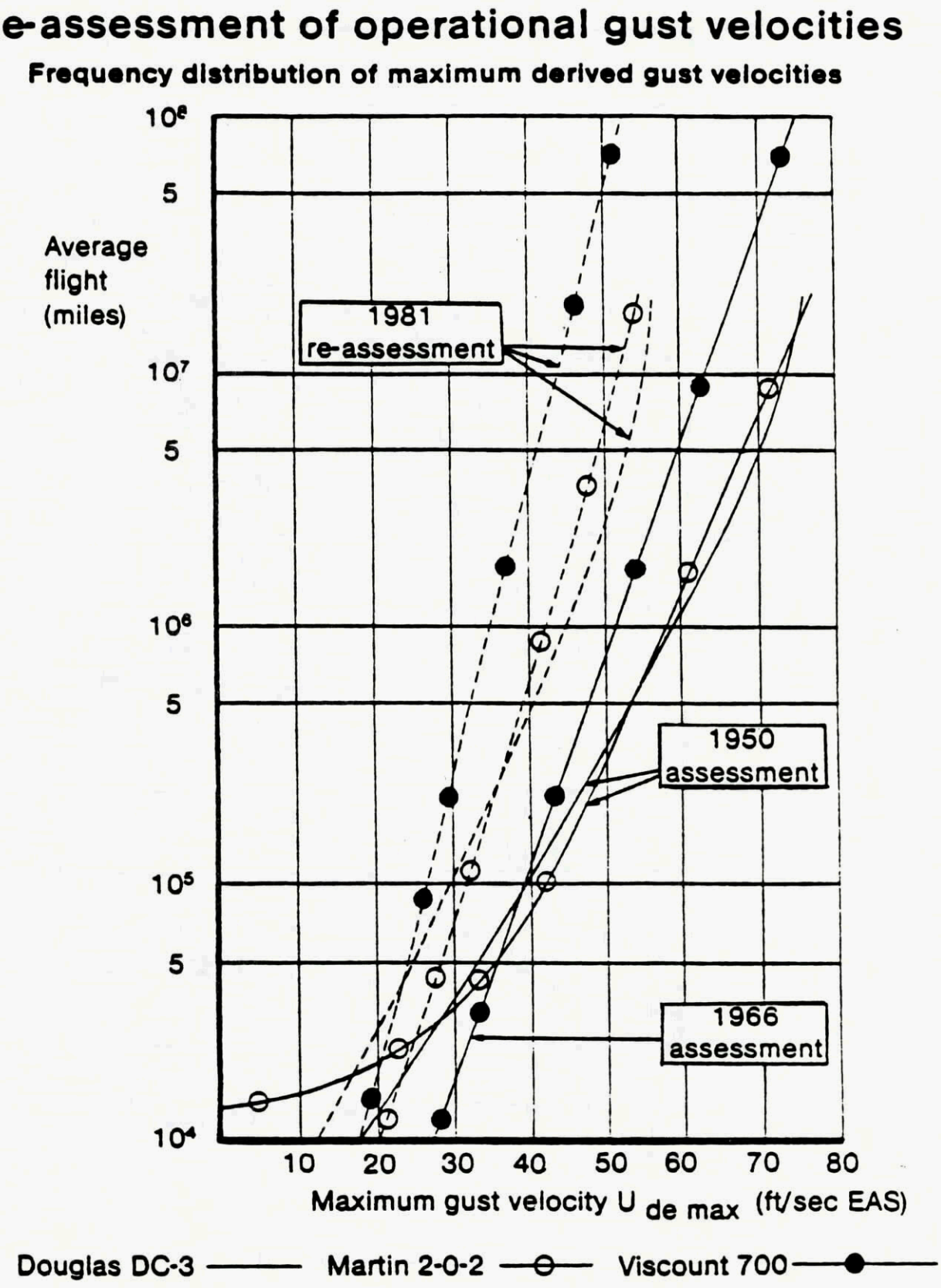

Fig.17 Comparison of Gust Velocities from an Early Assessment on a DC-3, Martin 2-0-2 and Viscount with those from an Assessment using the Latest Modelling Techniques

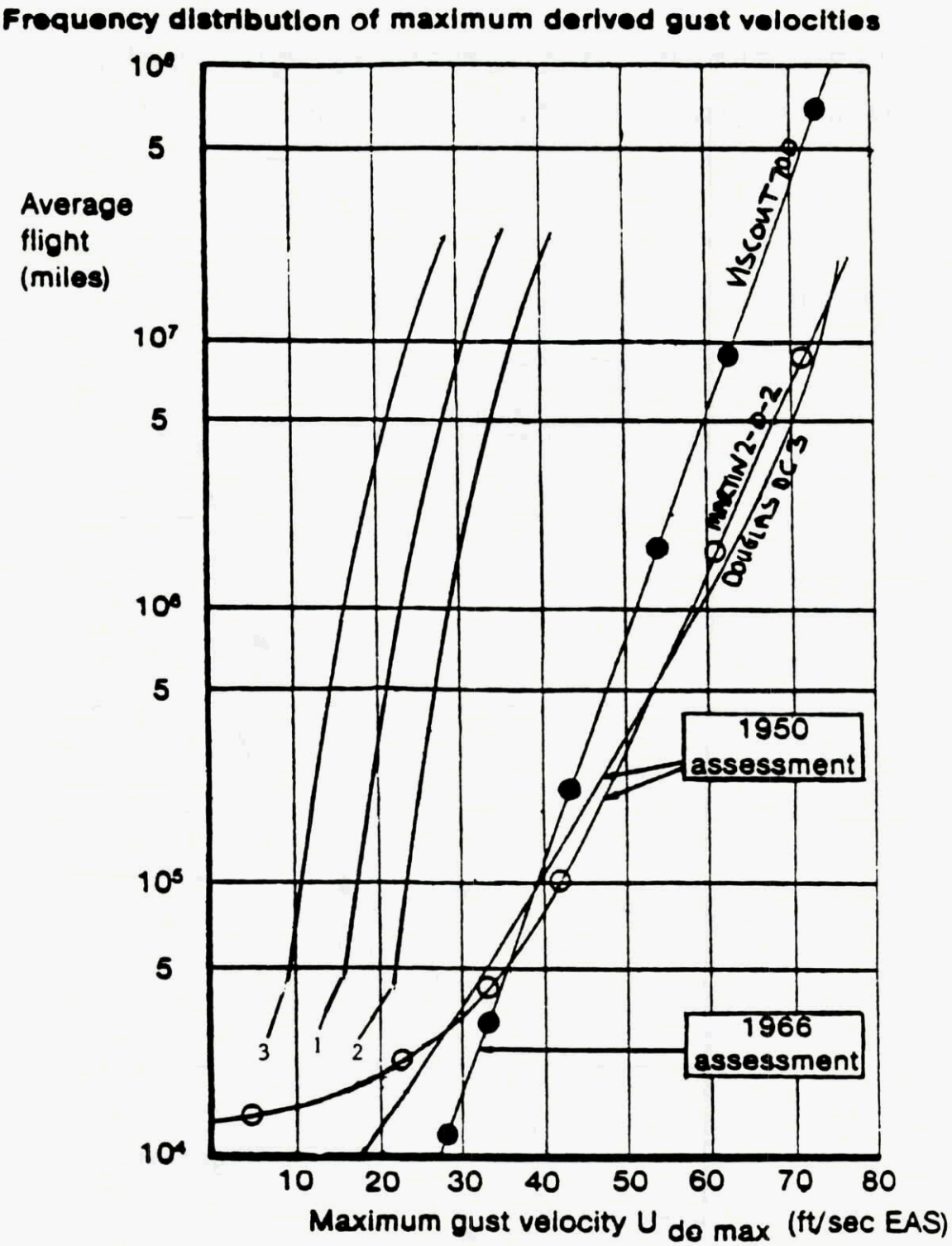

LINE 1 PRATT RIGID A/C

LINE 2 FLEXIBLE A/C 12.5 CHORD GUST

LINE 3 FLEXIBLE A/C TUNED (+ve PEAK) GUST OF 23C OF EQUAL PROBABILITY TO A 12.5C GUST

Re-assessment of operational gust velocities

Fig.18 Comparisons of Gust Velocities from an Early Assessment on a DC-3, Martin 2-0-2 and Viscount with those from the 1-11 CAADRP Special Event Data

ACQUISITION OF GUST STATISTICS FROM AIDS-RECORDED DATA

by
J.B. de Jonge, A.J.P. v.d. Wekken and R. Noback
National Aerospace Laboratory NLR
Anthony Fokkerweg 2, 1059 CM Amsterdam
The Netherlands

ABSTRACT

Since more than ten years, service load data, including c.g. acceleration peaks, recorded in B747 aircraft have been stored at NLR in the so-called AIDS-Fatigue Data Base.

This paper describes the procedures applied to reduce the acceleration data to "derived gust velocities". The results are presented and compared with other data sources.

The validity of the assumptions made in the derivation are discussed.

LIST OF SYMBOLS

a	speed of sound (m/s)
$\bar{A}$	PSD response factor (s/m)
b_1, b_2	gust intensity parameters, referring to non-storm turbulence and storm turbulence respectively (m/s)
$\bar{C}$	discrete response factor (s/m)
c	mean wing chord (m)
C_{L_α}	lift curve slope (degree^{-1})
ΔC_{L_α} flap	increase in lift curve slope due to the flap angle (degree^{-1})
$F(\mu g)$	gust alleviation factor
$F_{PSD}(\mu g)$	continuous alleviation factor
g	gravity constant (m/s^2)
h	altitude (m)
L	scale of turbulence (m)
m	airplane mass (kg)
Δn_z	incremental load factor
N_o	PSD frequency response parameter; number of positive zero crossings per unit distance flown
P_1, P_2	gust frequency parameters; relative time spent in non-storm turbulence and storm-turbulence respectively
S	wing area (m^2)
U_{de}	$\frac{\Delta n_z}{\bar{C}}$, derived gust velocity (m/s EAS)
U_σ	$\frac{\Delta n_z}{\bar{A}}$, derived PSD gust velocity (m/s EAS)
V	velocity (m/s)
V_e	equivalent velocity = $V \cdot \sqrt{\frac{\rho}{\rho_o}}$ (m/s)
ρ	air density (kg/m^3)
ρ_o	air density at sea level (kg/m^3)
μg	mass ratio = $\frac{2m}{\rho\, C_{L_\alpha} .c\, S}$

1. INTRODUCTION

Since more than ten years, service load data have been retrieved from AIDS-recordings obtained in Boeing 747 aircraft operated by the KSSU-group (KLM, Swissair and SAS). These data have been stored at NLR in the so-called AIDS Fatique Data Base.

Currently, this Data Base covers more than 20000 flights, or 100.000 flight hours. The Data provide detailed statistical information about the aircraft usage and load experience (refs. 1, 2, 3).
On the other hand, as the information stored includes the values of c.g. acceleration peaks that have occurred, the Data Base can be used to provide statistical information about atmospheric turbulence.

The present paper describes the procedures applied to reduce the acceleration data to "derived gust velocities". The results are presented and compared with other data sources.

In a discussion, the assumptions made in the data reduction and the associated limitations on validity of the obtained data are reviewed. It is recommended to define common standard reduction procedures, which are based on a more realistic representation of gustiness and aircraft response.

2. DESCRIPTION OF THE DATA BASE

A complete description of the AIDS Fatigue Data Base and the procedures followed for its creation have been presented in the refs. 1 and 2. The present description will be restricted to those aspects that are relevant in the context of this paper.

The AIDS-system used for KSSU-747, performs a continuous scanning of a large number of parameters, including speed, altitude, instantaneous weight and c.g. acceleration. The latter parameter is scanned eight times per second.

This (very large) data stream is not always recorded but only then if specific criteria are met. One of these criteria is the occurrence of an incremental acceleration $|\Delta n_z| \geq 0.18$. Hence, one may say that all periods of turbulence of any importance are recorded.

The AIDS-recordings are processed by KSSU-operators in their respective computer facilities through a number of application programs. One of these programs is the "Fatigue Data Program", which extracts the required data to be stored in the Fatigue Data Base.

The AIDS-data are analysed and the extracted data are stored on a flight-by-flight basis. The analysis includes a search of the recorded acceleration histories for peaks and valleys (maxima and minima), whereby a range-filter of 0.18 g is maintained. That means, successive "recognized" peaks and valleys differ at least 0.18 g from each other.

The values of the successive acceleration peaks and valleys are stored in the Fatigue Data Base, together with their time of occurrence, and flap setting and roll angle at time of occurrence*.
From the additional data stored, the altitude, speed and instantaneous A/C weight at any time, and hence at the instant of each acceleration peak/valley, can be obtained.

Because the exact weight at the acceleration peak is known, one may say that the data available is more complete than provided by the "classical" VGH recorders used by NACA/NASA (ref. 4).
The current Data Base includes 20205 flights, covering 101157 flight hours and 47,066,322 nautical miles of flight.
It may be noticed that this data sample is considerably larger than the NASA VGH data sample of 42188 flight hours presented in ref. 4.

However, as shown in the table below, a very large part of the data refers to the altitude band from 30000 to 40000 feet, being the cruise altitude for the 747 aircraft.

Distribution of Data over altitude bands

	Flight hours	Distance (NM)
0- 5000	3530.25	681,441
5-15000	4888.50	1,530,607
15-30000	10,836.61	4,928,235
30-40000	81,667.49	39,812,982
> 40000	234.00	113,056
All altitudes	101,156.85	47,066,322

Main statistics of the flights contained in the AIDS-fatigue data base have been presented in table 1.

3. REDUCTION PROCEDURES

It was decided that the deduction of statistical gust data from the AIDS data base should be done in such a manner as to allow a comparison of the results with already available turbulence statistics.
This means that the assumptions to be made with regard to gust "nature" and shape and aircraft response should preferably be the same as those underlying existing turbulence descriptions.

* The roll angle has recently been added to the list of stored data, as a possible means to distinguish (turning) manoeuvre induced accelerations.

The existing descriptions can be divided into two types, namely those based on a Discrete gust model and those assuming a continuous turbulence, further indicated as "PSD-model".
The discrete gust statistics are presented as exceedance frequencies per mile of "derived gust velocities" as a function of altitude.

There are two major data sources namely the data presented by NASA, based on VGH recordings, and the RAE data, based on fatigue meter readings.

In both cases, acceleration peak values have been reduced to "derived gust velocities", assuming a rigid airplane responding in plunge motion only. However, the NASA derivations assumes a 1-cos gust with 25 chords length, whereas the British assume a ramp gust with a constant length of 100 ft. Moreover, a difference exists in that the NASA data consider acceleration peaks that have been filtered according to a "peak between means" criterion, whereas the British acceleration peaks are filtered according to what has been defined as "restricted level cross count criterion" (ref. 5).

The PSD-turbulence environment is usually defined by means of the parameters P_1, P_2 and b_1, b_2 as a function of altitude (refs. 6, 7).

Although the PSD-description is based on a completely different model of turbulence, it should be recognized that continuous turbulence measurements have served so far essentially to justify the model as such (normality, spectrum shape, turbulence scale L): the statistical parameters P and b were actually determined from the same VGH-data batch forming the basis of the NASA U_{de} statistics (see ref. 6 and ref. 8).

To allow comparison with both "discrete" and "PSD"-gust descriptions it was decided to reduce the AIDS-acceleration data in a manner comparable to the reduction of the VGH-data.

For this purpose, the acceleration peaks in the AIDS-data base were first filtered using the "peak between means" criterion, see figure 1. The resulting acceleration peak values (classified according to magnitude and altitude band) are presented in table 2. These acceleration values were then reduced to derived gust velocities, both on a "discrete" basis and a PSD-basis. The PSD-data were then further processed to obtain P- and b-values.
The procedures will be described in some more detail below.

a. Discrete gust model

Acceleration values Δn_z were reduced to derived gust velocities U_{de} according to:

$$U_{de} = \frac{\Delta n_z}{\bar{C}} \quad \text{(m/s EAS)}$$

where

$$\bar{C} = \frac{C_{L_\alpha} \rho_o V_e}{2\ mg/S} F(\mu g)$$

$$F(\mu g) = \frac{.88\ \mu g}{5.3 + \mu g}$$

and

$$\mu g = \frac{2m}{\rho\ C_{L_\alpha}\ c\ S}$$

C_{L_α} is calculated as a function of M, ρa^2, C_L and flap position:

$$C_{L_\alpha} = \frac{C_{L_\alpha\ rig}}{1 + C_{L_{\alpha\ rig}} \left[\tfrac{1}{2}\rho a^2 M^2 K_L - \frac{K_n}{C_L} \right]} + \Delta C_{L_{\alpha\ flap}}$$

with, for the 747 aircraft, $K_L = 1.23 \times 10^{-4}$ $(m^2.N^{-1}.\ degrees)$
$K_n = 0.31$ (degrees)

where $C_{L_{\alpha\ rig}}$ is the following function of Machnumber:

M	$C_{L_{\alpha\ rig}}$
0.30	0.087
0.40	0.088[5]
0.50	0.090
0.60	0.092
0.70	0.093
0.80	0.094
0.85	0.101
0.90	0.118

In the configuration with flaps down the C_{L_α} value is considerably higher than with flaps up. To calculate the increase in lift curve slope as a function of flap angle the following table is used:

flap angle (degrees)	ΔC_{L_α} flap ($degree^{-1}$)
0	0.
1	.005
5	.015
10	.017
20	.019
25	.020
30	.020

The effect of the flap position in the calculation of gust spectra is not negligible. Approximately 30 % of all recorded load factor peaks occur in a flap down configuration (see Ref. 11).
The C_{L_α} expression for flaps up fits the curves presented in figure 2, that were originally provided by Boeing (ref. 9).

For all variables in the above equations, the value prevailing at the time of the acceleration peak can either be directly taken or calculated from the AIDS data base.

The resulting distribution of U_{de}-occurrences, according to altitude band and magnitude, is presented in table 3.

b. PSD-gust model

The acceleration values Δn_z were reduced to "derived PSD-gust velocities" U_σ according to

$$U_\sigma = \frac{\Delta n_z}{\bar{A}} \quad \text{(m/s EAS)}$$

where the PSD response factor $\bar{A}$ is given by

$$\bar{A} = \frac{C_{L_\alpha}\, \rho_o\, V_e}{2\, mg/S} \cdot F_{PSD}\ (\mu g)$$

The response parameter $\bar{A}$, or rather F_{PSD} (μg) was calculated under the following assumptions:
i rigid aircraft*, with plunge response freedom only
ii "Von Karman" turbulence spectrum with scale length L = 765 m at all altitudes
iii finite span and sweep back effects are taken into account (see ref. 10)

The result could be approximated by the following expression:

$$F_{PSD}\ (\mu g) = -0.086 + .413\ {}^{10}\log \mu g$$

The reader will have noticed that actually

$$U_\sigma = U_{de} \cdot \frac{\bar{C}}{\bar{A}}, \text{ or } U_\sigma = U_{de} \cdot \frac{F(\mu g)}{F_{PSD}\ (\mu g)}$$

The resulting distribution of U_σ occurrences has been presented in table 4.
The reader should note that U_σ has been presented in EAS instead of TAS as is often the case in other publications.
Next, the U_σ-distributions were used to establish values for the parameters b_1, b_2 and P_1, P_2 for the various altitude bands.
The procedure which is illustrated in figure 3, is based on the assumption that the number of exceedings $N(U_\sigma)$ of gust level U_σ at a specific altitude is given by:

$$N(U_\sigma) = \bar{N}_o \left[P_1 \exp\left(-\frac{U_\sigma}{b_1}\right) + P_2 \exp\left(\frac{-U_\sigma}{b_2}\right) \right]$$

In this equation, $\bar{N}_o$ is an average N_o-value for the particular altitude band and the recording aircraft (in this case the 747).

* Flexibiliby effects on C_{L_α} are included, as described under a.

As shown in figure 3, the $N(U_g)$-curve, drawn in a semi-logarithmic grid is approximated as the sum of the two straight lines. The slopes of these lines define b_1 and b_2, and the intersections with the vertical axis give $\overline{N_o}.P_1$ and $\overline{N_o}.P_2$.

In order to find a value for $\overline{N_o}$, an analysis was made of a set of "unreduced" acceleration traces obtained from the AIDS-recordings. An example of such a trace, showing a relatively long turbulence patch, is given in figure 4.

By calculating the Power Spectrum of these traces and dividing by the Von Karman turbulence spectrum, the shape of the A/C transfer function was estimated. Figure 5 gives the result, showing a peak at a frequency of appr. 4 cycles per km.

This value has been further adopted as $\overline{N_o}$-value.

The resulting values of P_1, P_2, b_1 and b_2 found for the various altitude intervals have been tabulated in table 5 and are depicted in the figures 9, 10 together with the parameter values defined in ref. 6. Note that b_1 and b_2 are given in m/s TAS.

4. REVIEW OF OBTAINED GUST DATA

Figure 6 presents the obtained U_{de} exceedance curves for all altitude bands considered.
In the figures 7 and 8, these data are compared with the data presented in NACA TN 4332 (ref. 8), for altitudes below 10000 ft and above 10000 ft respectively. The data were regrouped to (wider) altitude bands, corresponding with those considered in ref. 8.

Figure 7 shows that the 747-data at low altitude are considerably more severe than those presented in ref. 8.

Possible contributing factors to this difference are:

- The 747 data include manoeuvre-induced load factor increments, which were essentially filtered out from the NASA-VGH data.
  Manoeuvring is concentrated in lower altitude bands and largely results in positive load factor increments. Indeed, the load data for the lower altitudes show the expected asymmetry (more upward than downward loads). However, the inclusion of manoeuvres alone is insufficient to explain the difference with the ref. 8 data. In fact, the downward gust data alone are already more severe than NACA TN 4332.
- The 747 data at lower altitude refer to climb and descent phases, largely in the direct neighbourhood of the departure or destination airport. Turbulence avoidance is hardly possible. The NACA 4332 data in the 2000-10000 ft altitude band probably exist for a major part of cruise data for piston engined feeder liners and include turbulence avoidance procedures.

Figure 8 shows that the present gust data for the altitudes above 10000 ft are slightly less severe than those in NACA TN 4332.

Taking into account that, specifically the data above 30000 ft refer to cruise conditions, and that the current means for predicting and thus avoiding turbulence are considerably better than in the late fifties, the observed lower gust load experience for 747 at higher altitude is in accordance with expectations.
The continuous gust parameters b_1, b_2, P_1 and P_2 have been compared in the figures 9 and 10 with the values defined in ref. 6.

Looking first at the "non-storm" parameter values b_1 and P_1 it may be noted that like in ref. 6 the intensity parameter b_1 appears to be only slightly dependent on altitude. The values for b_1 presently found are approximately 1.5 times larger than those given in ref. 6. The present P_1-values, which are approximately the same at very low altitude, are for higher altitudes appr. 10 times lower than those of ref. 6.

With regard to the "storm"-parameters b_2 and P_2 figure 9 shows considerably higher b_2 values at the lower altitudes. On the other hand, the P_2's presently found are considerably less than those given in ref. 6 for all altitude levels.

In summary, the present data suggest that atmospheric turbulence is more intense than specified in ref. 6, but that it is considerably less frequently encountered.

5. DISCUSSION

The majority of modern transport aircraft are equipped with multichannel flight recorders. So, every day thousands of flight hours, including many hours of flight in turbulence, are being recorded.

The programme described in this paper has shown that it is relatively easy and inexpensive to obtain large amounts of "rough" statistical information about gustiness from such recordings.

Fortunately, severe turbulence encounters are rare: deduced P_2-values were less than 10^{-4}, so storm type turbulence conditions are prevailing less than 0.01 percent of the time. This implies that very large samples are required to establish reliable statistical information on the probability of specifically the more severe gust encounters, and the gathering of such data, preferable on a cooperative basis, should be stimulated.

To be able to compare data stemming from different sources, agreement on methods to be applied in reduction and processing of the recorded data is urgently required.

As explained previously, the data reduction procedures used in the present study were not selected because of their "physical relevance", but primarily to obtain compatibility with other data sources, specifically the NACA VGH data.
It is felt that this aim has been fulfilled: a data set of significant size has become available that could be compared with previous data.

However, at the same time, the limitations of the data obtained, associated with the "weaknesses" in the data reduction procedures should be recognized.

It may be recalled that the procedures applied were essentially based on the following (simplifying) assumptions:

a. A "discrete" gust concept: the recorded acceleration traces are reduced to "discrete acceleration bumps" using the peak between means criterion. Each "acceleration bump" is due to a "discrete gust" of specified shape and length. It must be recognized that the "PSD-data" were actually derived from the "discrete" data and are hence still "quasi discrete" in nature; the essential difference is that in U_{de} derivation a constant gust length of 25 chords is assumed; the U_{σ} is calculated on the basis of a "weighted average response, considering all possible gust lengths and taking into account their relative probability.
It must be admitted, however, that actually recorded acceleration traces, like the one presented in figure 4, show the continuous nature of turbulence response and shed serious doubt on the ultimate validity of discrete gust approaches.

b. The airplane is assumed rigid and responding only in plunge.
In the present analysis of the 747-data the flexibility has been taken into account by using a "$C_{L_{\alpha\ \text{flex}}}$", that means the effect of the wing deformation under load on the overall $C_{L_{\alpha}}$ was included.
Figure 2 shows that this effect is really very large and cannot be ignored. In fact, one of the problems encountered in the data reduction was to obtain trustworthy $C_{L_{\alpha\ \text{flex}}}$-data.

The effect of elastic mode excitations has not been included. In our opinion, these elastic modes will have in general a limited effect on the c.g. acceleration response (but they may be important for e.g. wing bending moment or torsion).
With regard to the neglection of response in pitch, it is our feeling that this assumption may be justified in a discrete gust concept in so far as pitch response may have little influence on the maximum value of the incremental acceleration caused by a discrete gust-bump; the c.g.-acceleration response on continuous turbulence, however, may be heavily influenced by pitch motion. The transfer function shown in figure 5 indicates a pitch response at 4 cycles per kilometer, as discussed previously.

To conclude this discussion, it is our conviction that a possible "standard" procedure for reduction of gust load data, to be commonly agreed upon, should be based on a more realistic gust model and better aircraft response representation than the "classical" procedures described in this paper.

6. CONCLUSIONS

1. Modern transport aircraft are usually equipped with multichannel flight recorders. Thus, thousands of flight hours are recorded every day.

2. This paper has shown how the recordings may be used to yield in a relatively easy and inexpensive way, statistical gust load data.

3. In order to be able to compare data from different sources, agreement should be reached on common "standard" data reduction procedures.

4. These procedures should be based on a more realistic gust presentation, and a better aircraft response model than the "classical" procedures used in the past.

7. ACKNOWLEDGEMENT

The analyses presented in this paper have been made under contract with the Netherlands Department of Civil Aviation (RLD). Their permission to publish the results is gratefully acknowledged here.

8. REFERENCES

1. Jonge, J.B. de, and Spiekhout, D.J.; Assessment of Service Load Experience Using AIDS-Recorded Data. Paper presented at 9th ICAF symposium, Darmstadt, 1977, ICAF-Doc. No. 960. Also published as NLR MP 77011 U.
2. Jonge, J.B. de, and Spiekhout, D.J.; Use of AIDS-Recorded Data for Assessing Service Load Experience. In ASTM SP671, 1979.
3. Spiekhout, D.J., and Lummel, C.W.J. van; Operational Loads on B-747 Aircraft: Design Assumptions, Actual Experience and Maintenance Aspects. NLR MP 83051 U, DFVLR Mitt. 84.01.
4. Coleman, T.L.; Trends in Repeated Loads on Transport Airplanes, Paper presented at 4th ICAF Symposium, Munich, June 1965. Also NASA TN D-4586.
5. Dijk, G.M. van; Statistical Load Data Processing. Paper presented at 6th ICAF Symposium, Miami NASA SP-309, 1972. Also NLR MP 71007 U.
6. Hoblitt, F.M. et al; Development of a Power Spectral Gust Design Procedure for Civil Transport, FAA-ADS-53, 1966.
7. FAR Part 25, Appendix G.
8. Press, H., Steiner, R.; An Approach to the Problem of Estimating Severe and Repeated Gust Loads for Missile Operations. NACA TN 4332, 1958.
9. Private Communication with Dr. G. Coupry, Onera, 1982.
10. Kaynes, I.W.; Aircraft Centre of Gravity Response to Two-Dimensional Spectra of Turbulence, ARC R and M 3665, 1971.
11. Spiekhout, D.J., and Lummel, C.W.J. van; Assessment of load factor experience for B-747 aircraft as a function of flap position using AIDS-recorded data, NLR TR 79079 L, 1979.

TABLE 1

Statistics of flights in fatigue data base

	FLIGHT TYPE	FLIGHT DURATION INTERVALS (HRS)													ALL FLIGHT DURATIONS
		.0-.5	.5-1	1-1.5	1.5-2	2-3	3-4	4-5	5-6	6-7	7-8	8-9	9-10	>10	
NUMBER OF	A	1279	1475	908	1331	1013	1331	599	1369	4152	3912	1629	360	277	19635
FLIGHTS OF	B	9	41	25	53	87	43	26	4	17	14	21	10	0	350
INDICATED	C	0	1	2	0	0	0	0	0	0	0	0	0	0	3
FLIGHT TYPE	D	1	4	3	10	7	10	0	0	1	0	0	0	0	36
	X	21	34	4	11	21	5	4	4	35	21	16	5	0	181
	ALL	1310	1555	942	1405	1128	1389	629	1377	4205	3947	1666	375	277	20205
AVERAGE FLIGHT DURATION (HRS)		.44	.77	1.26	1.72	2.60	3.49	4.49	5.57	6.53	7.52	8.36	9.52	10.52	5.01
AVERAGE BLOCK TIME (HRS)		.78	1.15	1.68	2.17	3.08	3.97	5.01	6.03	7.05	8.01	8.82	9.93	10.92	5.47
AVERAGE TOW (X 1000 KG)		220.60	224.28	231.79	230.19	248.99	263.64	280.94	290.74	302.05	316.88	324.54	335.09	342.49	281.40
STAND. DEV. TOW (X 1000 KG)		12.92	21.04	24.16	20.26	18.35	22.34	21.03	17.63	15.72	17.97	16.15	16.27	11.35	42.41
AVERAGE FUEL CONSUMPTION (X 1000 KG)		6.55	10.02	15.16	18.83	28.60	38.42	51.20	62.43	74.76	87.79	97.81	109.56	122.70	57.79
STAND. DEV. FUEL CONSUMPTION (X 1000 KG)		5.34	5.44	7.05	5.35	5.82	5.78	7.18	5.64	6.01	6.91	6.79	7.20	7.04	33.56

FLIGHT TYPE LEGEND: A = SCHEDULED COMMERCIAL
B = CHARTER
C = TEST
D = TRAINING
X = MISCELLANEOUS

TABLE 2
Survey of recorded acceleration peaks
(reduced according to the peak-between-means criterion)

NUMBER OF FLIGHTS CONSIDERED 20205

ALTITUDE INTERVAL (FT)	TOTAL DISTANCE FLOWN (NM)	TOTAL TIME SPENT (HRS)	NUMBER OF PEAK OCCURRENCES IN INDICATED DELTA-G. INTERVALS U P W A R D									
			.15-.20	.20-.25	.25-.30	.30-.40	.40-.50	.50-.60	.60-.75	.75-.90	.90-1.10	> 1.10
< 1500	164144	1036.24	15184	4948	1470	574	68	21	2	1		4
1500- 3000	217974	1161.64	12023 ε	4360	1362	493	69	4	4			3
3000- 5000	299323	1332.37	9382 ε	3825	1249	550	80	10	1			2
5000-10000	731005	2618.93	9486 ε	4049	1495	795	149	33	8	4		2
10000-15000	799602	2269.57	3514 ε	1671	697	415	100	26	16	4		
15000-20000	787312	1973.36	1740 ε	758	309	205	51	16	11	3	1	
20000-25000	1058572	2417.90	1432 ε	616	257	146	49	21	8	3		
25000-30000	3082351	6445.35	2639 ε	1127	392	261	50	19	10	1		
30000-35000	21421269	43841.93	11238 ε	4285	1459	877	154	46	21	2	1	5
35000-40000	18391713	37825.56	8154 ε	3293	1161	617	124	36	12	1		2
> 40000	113056	234.00	105 ε	46	22	10	2					
ALL ALTITUDES	47066322	101156.85	74897 ε	28978	9873	4943	896	232	93	19	2	18

ALTITUDE INTERVAL (FT)	TOTAL DISTANCE FLOWN (NM)	TOTAL TIME SPENT (HRS)	NUMBER OF PEAK OCCURRENCES IN INDICATED DELTA-G. INTERVALS D O W N W A R D									
			.15-.20	.20-.25	.25-.30	.30-.40	.40-.50	.50-.60	.60-.75	.75-.90	.90-1.10	> 1.10
< 1500	164144	1036.24	7443	1523	324	168	21	9	7	1		
1500- 3000	217974	1161.64	6635 ε	1523	364	99	27	24	13	11	1	
3000- 5000	299323	1332.37	4981 ε	1454	446	179	28	14	3	3		
5000-10000	731005	2618.93	5751 ε	2099	739	428	80	15	8	3	1	
10000-15000	799602	2269.57	2820 ε	1044	391	267	64	24	12	3		
15000-20000	787312	1973.36	1590 ε	564	249	144	31	9	6	3	1	
20000-25000	1058572	2417.90	1291 ε	428	169	107	17	9	6	2		
25000-30000	3082351	6445.35	2378 ε	814	341	205	49	19	4	1	1	
30000-35000	21421269	43841.93	10145 ε	3526	1323	667	135	44	17	2		
35000-40000	18391713	37825.56	7338 ε	2695	923	523	114	36	8	4		
> 40000	113056	234.00	101 ε	33	14	10		1				
ALL ALTITUDES	47066322	101156.85	50473 ε	15703	5283	2797	566	204	84	33	4	

ε STATISTICALLY UNRELIABLE DATA DUE TO RECORDING THRESHOLD OF 0.18 G

TABLE 3
Survey of recorded U_{de}-peaks

NUMBER OF FLIGHTS CONSIDERED 20205

ALTITUDE INTERVAL (FT)	TOTAL DISTANCE FLOWN (NM)	TOTAL TIME SPENT (HRS)	NUMBER OF GUST "OCCURRENCES" IN INDICATED VELOCITY INTERVALS ("M/SEC", EQUIV.) U P W A R D									
			2-3	3-4	4-5	5-7	7-9	9-11	11-13	13-16	16-20	> 20
< 1500	164144	1036.24	21251	20021	10406	5739	760	130	33	17	4	5
1500- 3000	217974	1161.64	20006 ε	12757 ε	4752 ε	2235	232	25	4		1	3
3000- 5000	299323	1332.37	14564 ε	8210 ε	2863	1153	115	19			1	1
5000-10000	731005	2618.93	13664 ε	6933	2369	978	81	20	3	1		2
10000-15000	799602	2269.57	4391 ε	1557	517	231	40	5	3			
15000-20000	787312	1973.36	1979 ε	557	195	86	19	5	2	1		
20000-25000	1058572	2417.90	1558	409	112	68	17	3	1			
25000-30000	3082351	6445.35	2946	783	199	84	14	4				
30000-35000	21421269	43841.93	13208	3077	746	285	43	8	2	2	1	2
35000-40000	18391713	37825.56	9001	1968	447	166	22	3				2
> 40000	113056	234.00	104	29	5	2						
ALL ALTITUDES	47066322	101156.85	102672 ε	56301 ε	22611 ε	11027	1343	222	48	21	7	15

ALTITUDE INTERVAL (FT)	TOTAL DISTANCE FLOWN (NM)	TOTAL TIME SPENT (HRS)	NUMBER OF GUST "OCCURRENCES" IN INDICATED VELOCITY INTERVALS ("M/SEC", EQUIV.) D O W N W A R D									
			2-3	3-4	4-5	5-7	7-9	9-11	11-13	13-16	16-20	> 20
< 1500	164144	1036.24	27251	12903	4092	1314	198	49	13	10	3	1
1500- 3000	217974	1161.64	18619 ε	8638 ε	2421 ε	772	58	20	24	11	8	
3000- 5000	299323	1332.37	11013 ε	4354 ε	1250	454	46	12	5	2	4	
5000-10000	731005	2618.93	10230 ε	4039	1228	485	57	14	8	1	2	
10000-15000	799602	2269.57	3524 ε	1017	303	154	22	8	1			
15000-20000	787312	1973.36	1780 ε	416	134	56	10	3	2	1		
20000-25000	1058572	2417.90	1363	318	78	22	10	1				
25000-30000	3082351	6445.35	2651	622	173	73	15	2				
30000-35000	21421269	43841.93	11890	2699	613	263	38	5				
35000-40000	18391713	37825.56	7859	1588	398	140	22	2	2			
> 40000	113056	234.00	92	24	5	2						
ALL ALTITUDES	47066322	101156.85	96272 ε	36618 ε	16506 ε	3735	476	116	55	25	17	1

ε STATISTICALLY UNRELIABLE DATA DUE TO RECORDING THRESHOLD OF 0.18 G

TABLE 4
Survey of recorded U_σ-peaks

NUMBER OF FLIGHTS CONSIDERED 20205

ALTITUDE INTERVAL (FT)	TOTAL DISTANCE FLOWN (NM)	TOTAL TIME SPENT (HRS)	NUMBER OF GUST "OCCURRENCES" IN INDICATED VELOCITY INTERVALS ("M/SEC", EQUIV.) U P W A R D									
			3-4	4-5	5-7	7-9	9-12	12-15	15-18	18-23	23-30	> 30
< 1500	164144	1036.24	9213	15758	22570	8618	3091	506	106	41	10	5
1500- 3000	217974	1161.64	11392 ε	12349 ε	13208 ε	3636	1134	138	19	2		4
3000- 5000	299323	1332.37	9593 ε	8194 ε	8070 ε	1898	478	52	12			2
5000-10000	731005	2618.93	9418 ε	7214 ε	6248	1411	364	34	12	1		2
10000-15000	799602	2269.57	3309 ε	1699	1168	267	78	14	4			
15000-20000	787312	1973.36	1462	570	374	76	27	6	2	1		
20000-25000	1058572	2417.90	1048	371	208	53	20	4	1			
25000-30000	3082351	6445.35	1832	605	287	52	19	3				
30000-35000	21421269	43841.93	7167	2147	953	156	38	7	1	2	1	1
35000-40000	18391713	37825.56	4753	1354	553	74	20	2				2
> 40000	113056	234.00	57	17	6	1						
ALL ALTITUDES	47066322	101156.85	59244 ε	50278 ε	53645 ε	16242 ε	5269	766	157	47	11	16

ALTITUDE INTERVAL (FT)	TOTAL DISTANCE FLOWN (NM)	TOTAL TIME SPENT (HRS)	NUMBER OF GUST "OCCURRENCES" IN INDICATED VELOCITY INTERVALS ("M/SEC", EQUIV.) D O W N W A R D									
			3-4	4-5	5-7	7-9	9-12	12-15	15-18	18-23	23-30	> 30
< 1500	164144	1036.24	18160	15259	13154	2871	595	152	23	13	8	2
1500- 3000	217974	1161.64	13482 ε	10091 ε	8331 ε	1563	302	34	16	28	15	
3000- 5000	299323	1332.37	8463 ε	5396 ε	3866 ε	758	174	26	10	5	4	
5000-10000	731005	2618.93	7820 ε	4731 ε	3301	682	171	21	10	3	3	
10000-15000	799602	2269.57	2772 ε	1159	674	156	52	15	1			
15000-20000	787312	1973.36	1291	425	256	48	17	3	2	1		
20000-25000	1058572	2417.90	883	277	145	15	11	2				
25000-30000	3082351	6445.35	1558	489	244	47	17	2				
30000-35000	21421269	43841.93	6331	1882	765	141	41	3				
35000-40000	18391713	37825.56	3981	1075	474	86	20	2	1			
> 40000	113056	234.00	43	10	6	1						
ALL ALTITUDES	47066322	101156.85	64784 ε	40794 ε	31216 ε	6368	1400	260	63	50	30	2

ε STATISTICALLY UNRELIABLE DATA DUE TO RECORDING THRESHOLD OF 0.18 G

TABLE 5
Values of the turbulence parameters P_1, P_2, b_1, b_2

Altitude band	P_1	P_2	b_1 (m/s TAS)	b_2 (m/s TAS)
< 1500 ft	.61	1.10^{-3}	1.58	4.99
1500- 3000 ft	.35	$2.5.10^{-4}$	1.45	5.98
3000- 5000 ft	.18	$1.3.10^{-4}$	1.38	4.91
5000-10000 ft	$5.3.10^{-2}$	$5.0.10^{-5}$	1.49	5.22
10000-15000 ft	$9.2.10^{-3}$	$5.6.10^{-5}$	1.60	4.16
15000-20000 ft	$6.0.10^{-3}$	$5.8.10^{-5}$	1.46	4.07
20000-25000 ft	$3.1.10^{-3}$	$6.3.10^{-5}$	1.53	3.37
25000-30000 ft	$2.5.10^{-3}$	$3.8.10^{-5}$	1.55	3.34
30000-35000 ft	$1.9.10^{-3}$	$1.1.10^{-5}$	1.54	3.90
35000-40000 ft	$1.5.10^{-3}$	$7.9.10^{-6}$	1.61	3.97

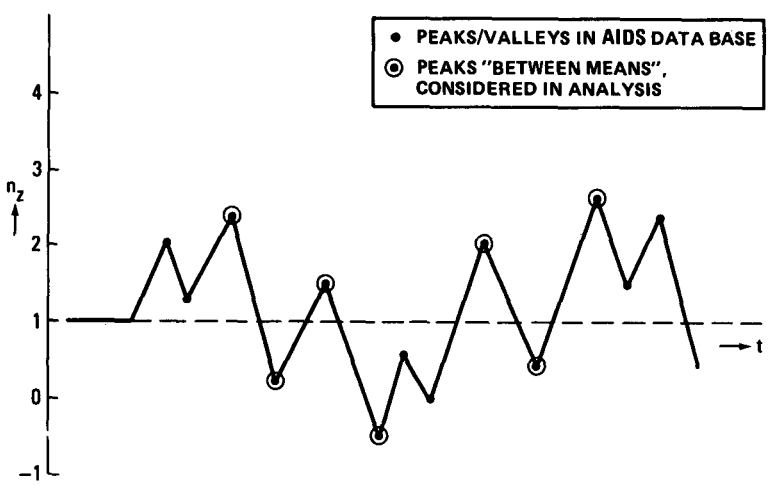

Fig. 1 Reduction of peak data by "peak between means" criterion

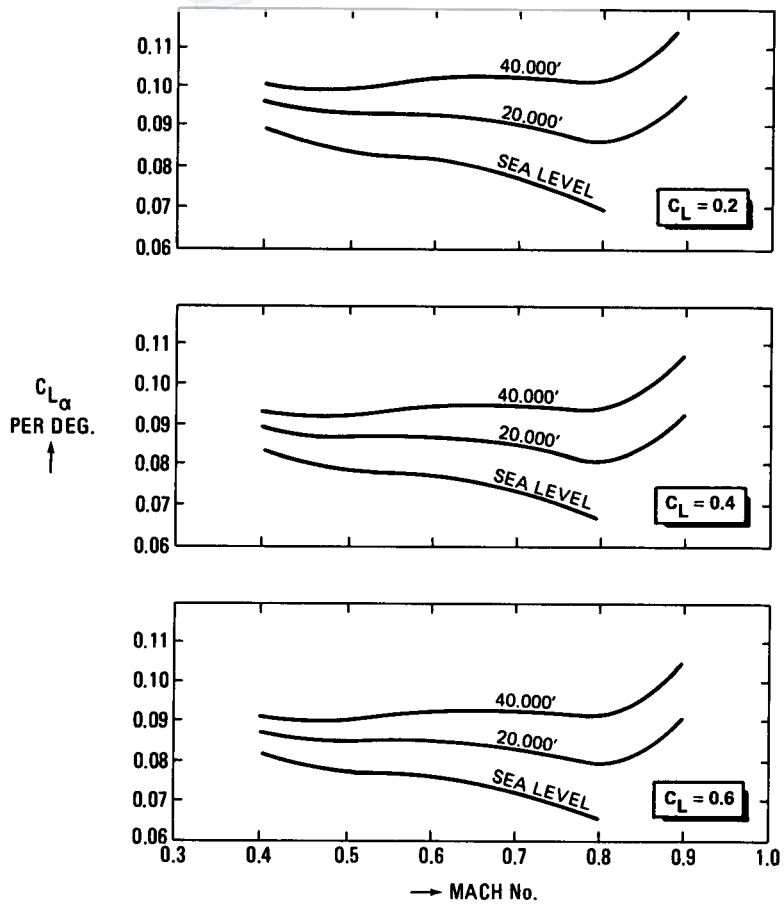

Fig. 2 C_{L_α} as function of Mach nr., altitude and C_L

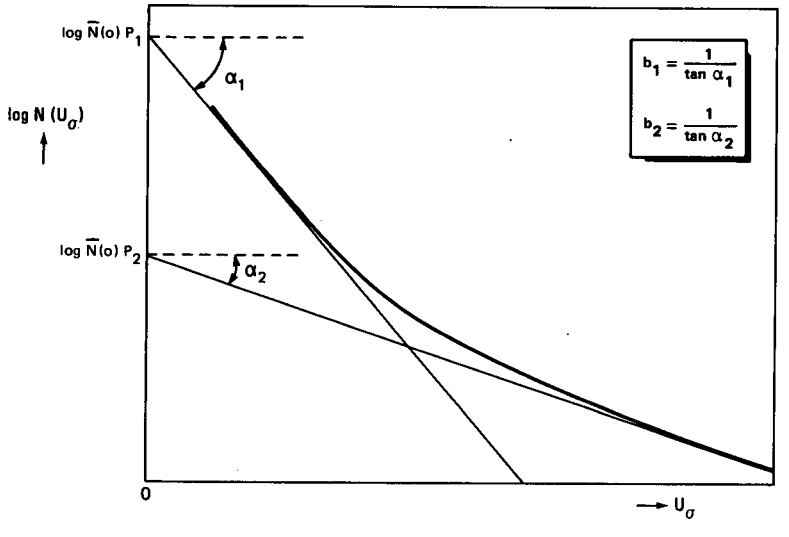

Fig. 3 Graphical determination of turbulence parameters

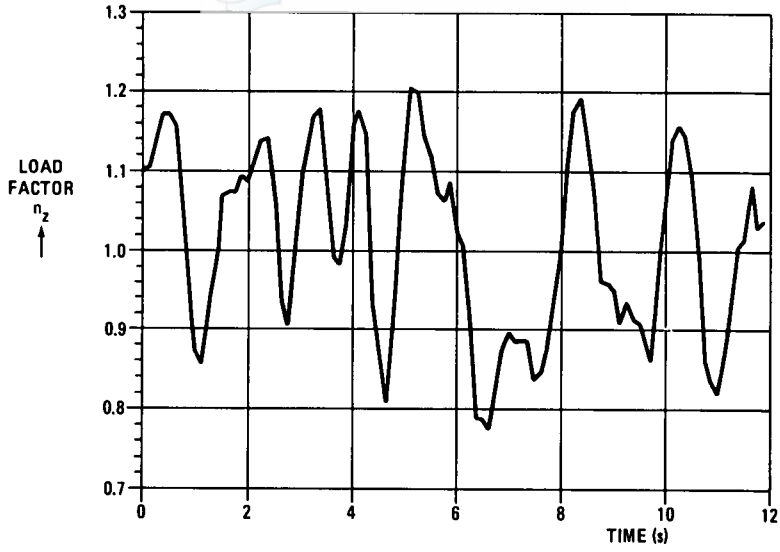

Fig. 4 Example of recorded acceleration trace

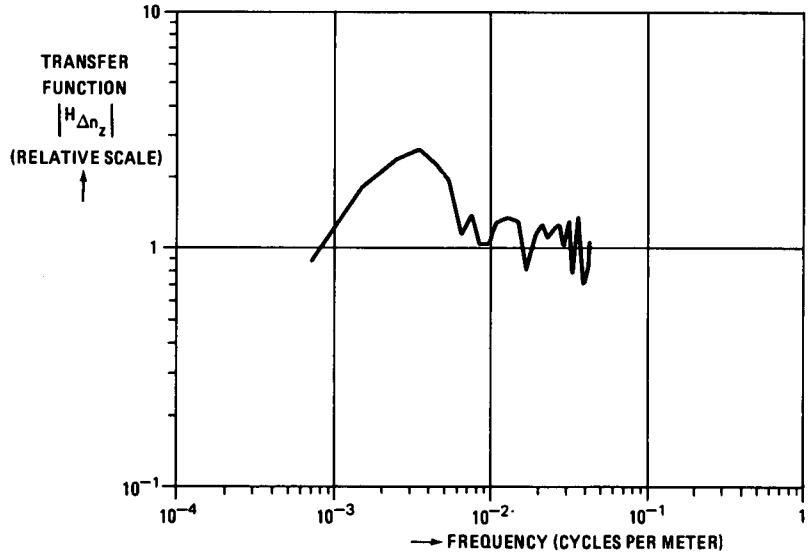

Fig. 5 Relative transfer function, determined from 19 turbulence-patches

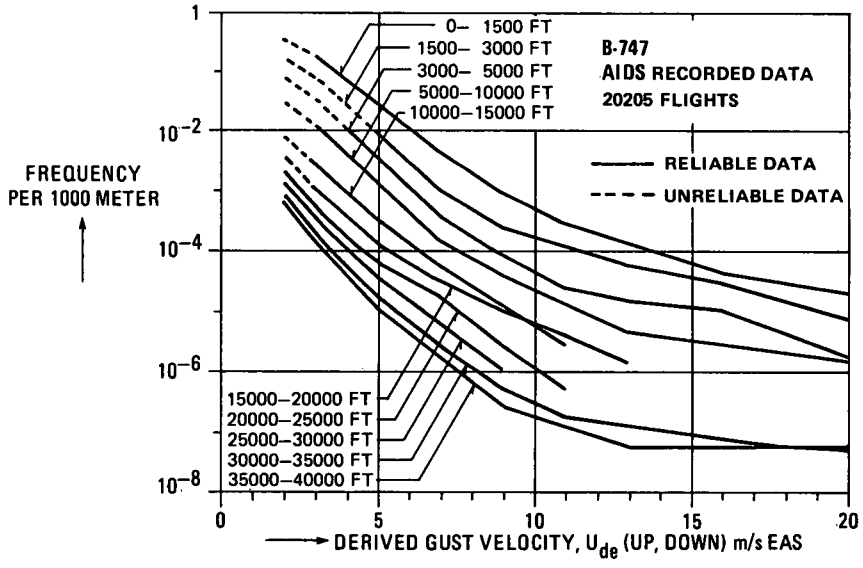

Fig. 6 U_{de}-exceedance curves

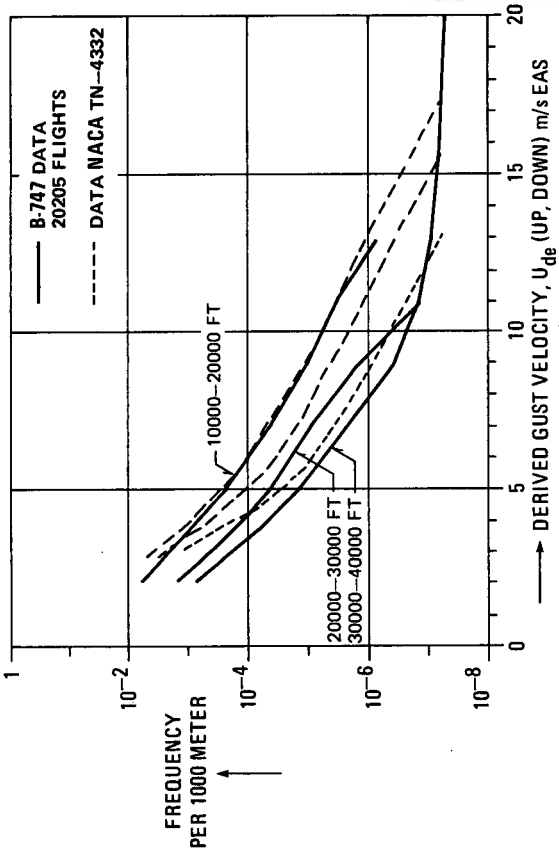

Fig. 8 Comparison of present data with NACA TN-4332, altitudes > 10000 ft

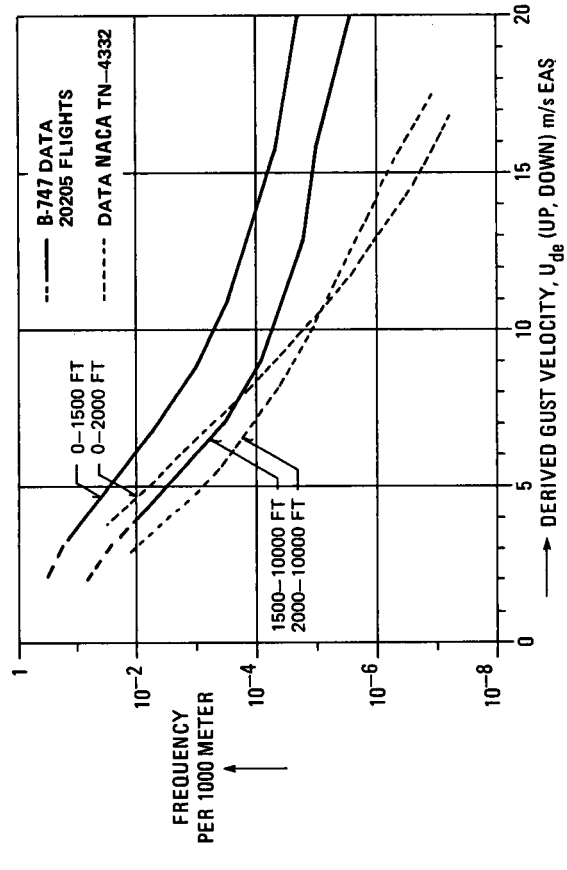

Fig. 7 Comparison of present data with NACA TN-4332, altitudes < 10000 ft

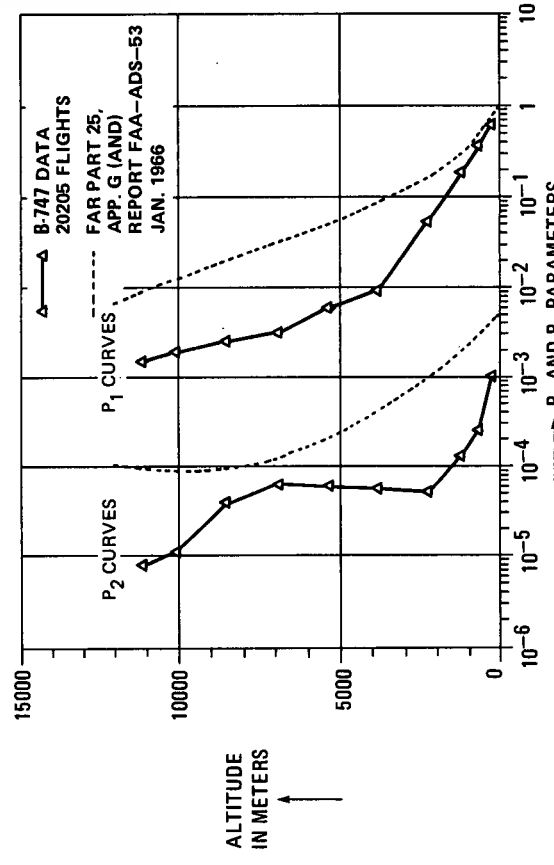

Fig. 10 The parameters P_1 and P_2

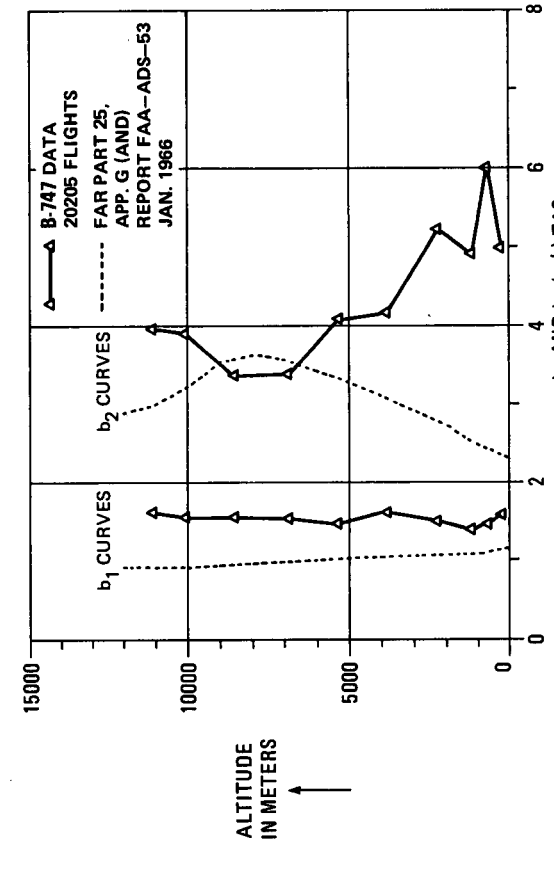

Fig. 9 The parameters b_1 and b_2

PRESENTATION DES TURBULENCES ATMOSPHERIQUES EXTREMES

par Gabriel COUPRY

Office National d'Etudes et de Recherches Aérospatiales (ONERA)
92322 Châtillon Cedex - France

RESUME

L'analyse de près d'un million d'heures de vols effectuée pendant 5 ans sur la flotte de British Airways, pour des facteurs de charge supérieurs à 0,5 g a permis de proposer une description nouvelle des turbulences atmosphériques extrêmes. L'apparition de paquets de turbulence pour lesquels un niveau de turbulence élevé est dépassé obéit à une loi de Poisson ; la moyenne de cette loi de Poisson décroît elle-même exponentiellement avec l'amplitude. On en déduit que les turbulences extrêmes obéissent à la statistique des valeurs extrêmes de Gumbel, avec toutes les possibilités d'extrapolation qu'offre une telle formulation.

EXTREME GUSTS DISTRIBUTION

SUMMARY

The reduction of about one million of flight hours flown during 5 years by British Airways, for events where the load factor has exceeded 0,5 has made it possible to propose a new description of atmospheric turbulence in extreme conditions. Encounter of patches of turbulence where gusts are greater than a given value obeys a Poisson distribution, the mean of which decreases exponentially with amplitude. This means that the probability of very big gusts can be represented by the Gumbel's extreme value theory.

INTRODUCTION

La motivation pour des recherches nouvelles sur la modélisation de la turbulence atmosphérique est fondée sur les remarques suivantes :

- La réglementation pour le calcul des avions aux rafales est basée sur une description de l'atmosphère déduite d'un faible nombre d'heures de vol (de l'ordre de 60000 heures) à partir d'avions souvent limités en altitude, de dimensions et de vitesses très différentes de celles des avions actuels, et non équipés de radars d'orage.

- L'installation sur les avions de nombreuses Compagnies Aériennes d'enregistreurs embarqués sophistiqués (AIDS par Aircraft Integrated Data System) permet une analyse automatique rapide de différents paramètres de vols.

A la demande de l'ONERA, la CAA et British Airways ont accepté de fournir à l'Office l'ensemble des informations de vol relatives aux dépassements dus à la turbulence d'un seuil de 0,5 g de variation d'accélération, et ceci pendant 5 ans. C'est ainsi que près d'un million d'heures de vol (dont 500000 pour les seuls Boeing 747) ont été analysées et plus de 6000 évènements observés, correspondant tous à de très fortes turbulences.

Le passage des accélérations aux turbulences a été effectué par la formule de Hall qui a permis d'obtenir des descriptions de l'atmosphère cohérentes, quelque soit le type d'avion considéré, ce qui n'était pas le cas pour la formule de Pratt.

L'analyse systématique, par tranche d'altitude, de la probabilité de rencontre d'un paquet de turbulence d'un niveau supérieur à un seuil donné a fait apparaître des distributions de Poisson dont la moyenne décroissait exponentiellement avec l'amplitude. On en déduit que cette probabilité obéit à la théorie des valeurs extrêmes de Gumbel.

I - CALCUL DES TURBULENCES

I.1 - Banque de données d'accélérations

British Airways indique le nombre d'heures analysées chaque mois pour chaque type d'appareil et fournit, pour chaque évènement, l'ensemble des paramètres de vol (Date, segment de vol, aéroports de départ et d'arrivée, masse, vitesse, altitude, configuration, $C_{L,\alpha}$, ...).

Par ailleurs, le profil moyen de vol des Boeing 747 a été établi en collaboration entre l'ONERA et la CAA à partir de plus d'une centaine de vols caractéristiques.

I.2 - Stationnarité

Avant toute analyse détaillée, on s'est assuré que le phénomène présentait un certain degré de stationnarité. Cette stationnarité est très bien illustrée dans le tableau 1 qui présente, pour la flotte des Boeing 747, le nombre de fois en 1000 vols où une accélération de 0,5 g a été dépassée, pour chacune des 5 années de collection de données.

ANNEE / ALTITUDE	1	2	3	4	5
0 - 5000 ft	.37	.35	.63	.68	.63
5000 - 10000 ft	2.85	1.72	1.89	2.48	1.71
10000 - 15000 ft	1.30	1.49	1.63	1.75	1.13
15000 - 20000 ft	1.30	.34	.82	1.13	.63
20000 - 30000 ft	1.36	1.26	1.26	1.64	1.25
> 30000 ft	4.65	3.56	4.40	4.79	3.54

Tableau 1 - Nombre d'évènements par 1000 vols

I.3 - Calcul de la turbulence

Le traitement de plusieurs milliers d'informations interdit tout calcul précis de la turbulence à partir des facteurs de charge, calcul par ailleurs impossible du fait que certaines informations (telles que le centrage ou la répartition du carburant) ne sont pas accessibles. On est donc amené à se servir de formules simplifiés qui ne considèrent que le degré de liberté de pompage de l'avion.

En conséquence, on n'aboutit surement pas à une description de la turbulence réelle, mais plutôt aux statistiques de "quelque chose" dont on espère qu'elle est significative, c'est-à-dire telle que ses statistiques, déduites d'un type d'avion, permettent de prévoir les facteurs de charge subis par un autre type d'avion, même très différent.

On relie classiquement la turbulence w à l'accélération γ d'un avion de masse M à la vitesse V par la formule :

$$M\gamma = \rho/2\, S K C_{L,\alpha} V w$$

dans laquelle K représente le facteur d'atténuation de rafale, et $C_{L,\alpha}$ la pente de la portance de l'avion flexible.

La formule de Pratt, fondée sur le calcul de la réponse de l'avion à une rafale de forme $1-\cos 2\pi L/V$ de longueur L égale à 25 cordes a abouti à des descriptions différentes de l'atmosphère à partir des accélérations mesurées respectivement sur Boeing 747, Bac 111 et Boeing 737.

La formule de Hall, que nous avons utilisée par la suite, part d'un modèle de turbulence continue pour lequel on calcule le rapport de l'écart type d'accélération à l'écart type de turbulence. L'utilisation d'une formule fondée sur la notion de turbulence continue pour l'analyse d'évènements isolés se justifie par le fait que l'avion traverse des rafales de longueurs aléatoires dont la répartition est fixée par la densité spectrale de turbulence choisie.

Les calculs effectués ici, pour une échelle de turbulence :

$$\Lambda = 440 \sqrt{\frac{\rho_o}{\rho}} \text{ (en mètres)}$$

ont permis d'aboutir à des descriptions de l'atmosphère très voisines quelque soit l'avion sur lequel les informations ont été recueillies.

I.4 - Résultats

L'ensemble des résultats déduits des vols analysés des flottes de Boeing 747, Bac 111 et Boeing 737 est présenté dans les figures 1 à 6, pour les 6 tranches d'altitude considérées. Le nombre de dépassements par mile nautique en fonction de l'amplitude de rafale est présenté par une droite dans la représentation semi-logarithmique, ce qui veut dire que le nombre de dépassements par mile nautique décroît exponentiellement avec l'amplitude, tout au moins pour les turbulences extrêmes envisagées ici.

On remarquera par ailleurs que ces fonctions sont très cohérentes pour les trois types d'avions considérés, ce qui est un argument en faveur de la formule de Hall, pour une distribution en altitude de l'échelle compatible avec les connaissances actuelles.

II - MODELISATION DE LA TURBULENCE

II.1 - Distribution de Poisson des turbulences extrêmes

On a vérifié que l'apparition d'évènements (dépassements d'un seuil W de turbulence) obéissait à une loi de Poisson. Pour ce faire, on a procédé de la manière suivante : pour la tranche d'altitude considérée, on a compté le nombre total d'évènements supérieurs à une valeur W, mesurés pour une flotte d'avions ; on en a déduit le nombre moyen d'évènements par semaine et, dant l'hypothèse d'une loi de Poisson, la probabilité théorique P_T (K) pour qu'une semaine appartienne à la classe K (K évènements dans la semaine). On a par ailleurs déterminé, à partir de la banque de données, la distribution statistique réelle P_E (K) des semaines de classe K.

Les résultats de la comparaison entre statistiques théoriques et expérimentales sont présentés dans les tableaux 2, 3 et 4.

CLASSE	0	1	2	3	4
P_T (K)	.5113	.3344	.1222	.0322	0
P_E (K)	.5090	.3437	.1160	.0261	.0044

Tableau 2 - Lois de Poisson - Altitudes comprises entre 5000 et 10000ft.

CLASSE	0	1	2	3	4
P (K)	.7010	.2508	.0354	.0129	0
P (K)	.6976	.2512	.0452	.0054	.0005

Tableau 3 - Lois de Poisson - Altitudes comprises entre 20000 et 30000ft.

CLASSE	0	1	2	3	4
P (K)	.3473	.4051	.1415	.0643	.0289
P (K)	.3439	.3971	.1659	.0697	.0186

Tableau 4 - Lois de Poisson - Altitudes supérieures à 30000ft.

L'ensemble des résultats est relatif, pour toutes les altitudes, aux dépassements de 8m/s de turbulence. Ils montrent à l'évidence que les turbulences intenses obéissent à une loi de Poisson.

II.2 - Théorie des valeurs extrêmes

Les conclusions des discussions précédentes sont les suivantes :
- les très fortes turbulences obéissent à une loi de Poisson,
- la moyenne de cette loi de Poisson décroît expérientiellement avec l'amplitude.

Ces deux conditions suffisent pour s'assurer que les très fortes turbulences sont décrites par la théorie des valeurs extrêmes de Gumbel.

Dans ces conditions, la probabilité de rencontrer, dans une tranche d'altitude, K dépassement d'un seuil W de turbulence intense pour une distance D parcourue est donnée par :

$$P_{D,W}(K) = \frac{(\mu(W)D)^K}{K!} \exp(-\mu(W)D)$$

où $\mu(W)$ est de la forme :

$$\mu(W) \square \mu_o \exp(-VW)$$

En conséquence :

$$P_{D,W}(K) = \frac{(\mu_o D)^K}{K!} \exp(-KUW) \exp(-\mu_o D \exp(-VW))$$

ce qui est classiquement la distribution des valeurs extrêmes.

Les valeurs, pour chaque tranche d'altitude, de μ_o et V sont déduites des figures 1 à 6 dans le tableau 5 :

ALTITUDES	μ_o	V
<10000ft	.00686	.525
10000 - 20000ft	.00526	.585
20000 - 30000ft	.00057	.617
> 30000ft	.00027	.627

Tableau 5 - Valeurs de μ et de V .

CONCLUSIONS

L'étude qui a été présentée dans ce rapport repose sur l'analyse de près d'un million d'heures de vol d'avions commerciaux. Elle a mis en lumière les points suivants :

- La formule de Pratt doit être abandonnée, car elle aboutit à des descriptions de l'atmosphère incohérentes, c'est-à-dire différentes suivant le type d'avion sur lequel les informations ont été collectées.

- La formule de Hall, avec un choix approprié et raisonnable de l'échelle, aboutit à une description cohérente de la turbulence relativement indépendante des types d'avions considérés.

- Pour les fortes turbulences, seules considérées ici, le nombre moyen de dépassements par mile nautique d'un seuil de référence décroît exponentiellement avec ce seuil.

- L'apparition de fortes turbulences obéit à une loi de Poisson dont la moyenne décroît exponentiellement avec l'amplitude ; elle est donc parfaitement décrite par la théorie des valeurs extrêmes de Gumbel.

Les résultats devront être comparés, par des tranches d'altitude plus étroites, avec la description de la turbulence forte proposée par la règlementation (coefficients P_2 et b_2).

REFERENCES

[1] - Joint Airworthiness Requirements, JAR 25, Large Airplanes, Civil Aviation Authority - Cheltenham -

[2] - J. Taylor
Manual on Aircraft Loads, 1965, Pergamon Press -

[3] - B. Etkin
Turbulent Wind and its Effects on Flight - J. Aircraft, May 1981 -

[4] - E.H Vanwooke
Random Field : Analysis and Synthesis - M.I.T. Press, Cambridge, 1983

[5] - R. Noback
Review and Comparison of Discrete and Continuous Gust Methods for the Determination of Airplane Design Loads - N.L.R. - TR 82134 U, 1982

[6] - G. Coupry
Progrès dans la connaissance de la turbulence atmosphérique - AGARD Report 738 - 1985

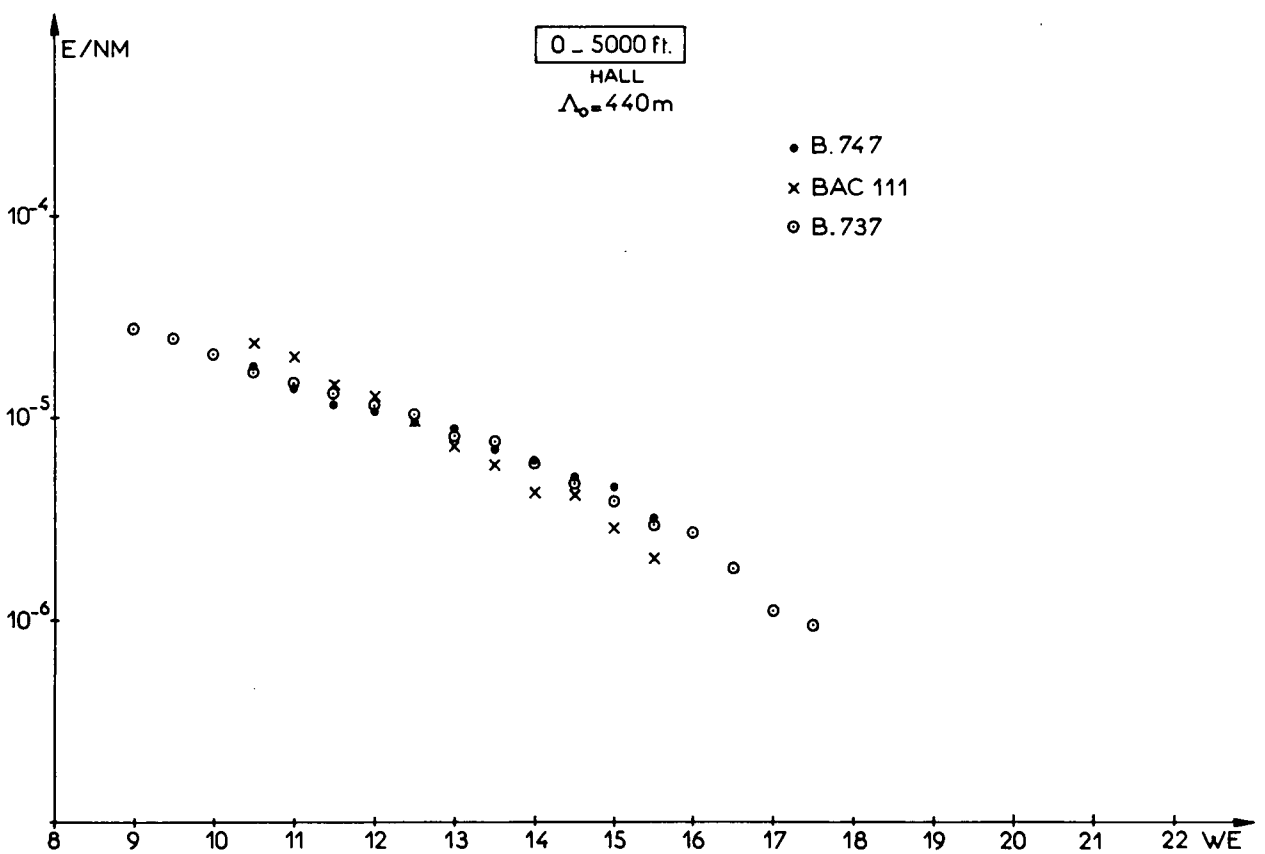

Fig.1 _ Dépassements par mile nautique

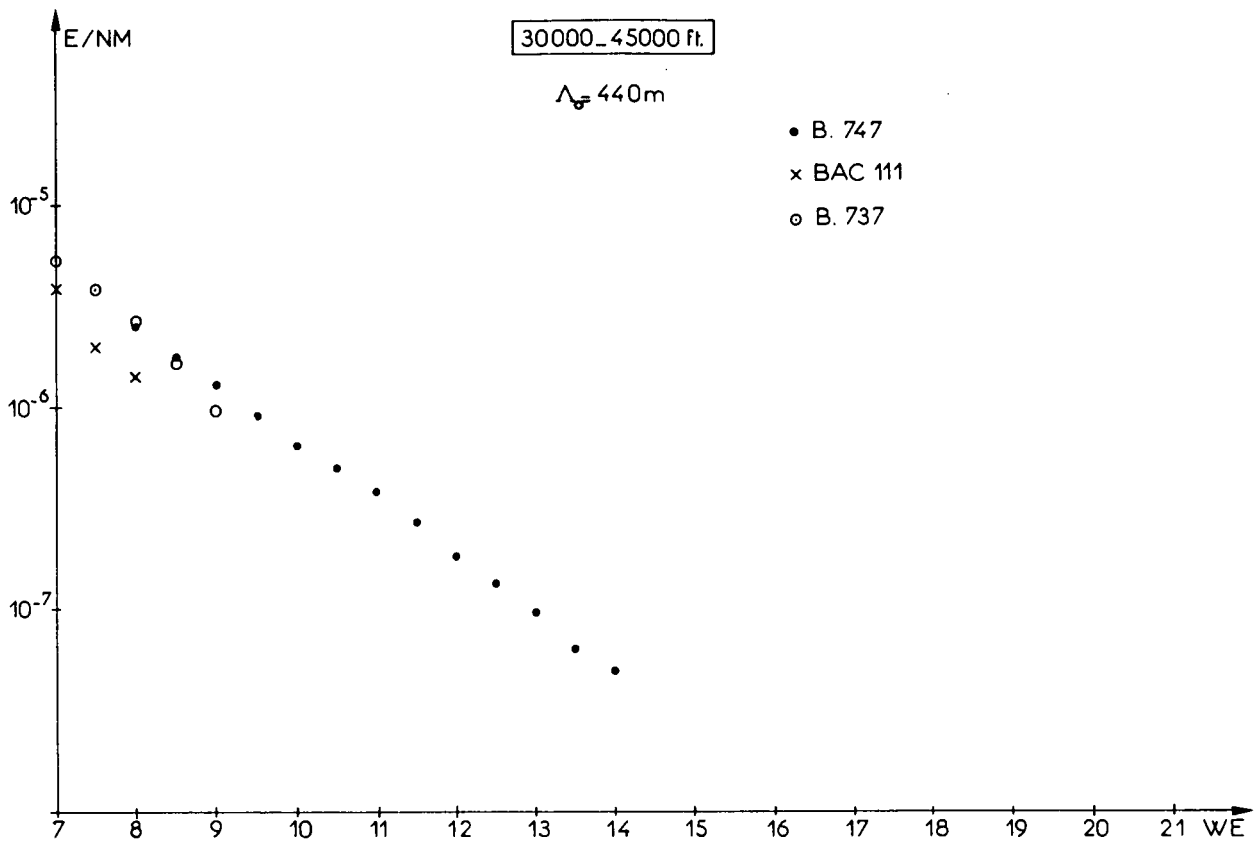

Fig.6_Dépassements par mile nautique

REPORT DOCUMENTATION PAGE

1. Recipient's Reference	2. Originator's Reference	3. Further Reference	4. Security Classification of Document
	AGARD-R-734	ISBN 92-835-0426-7	UNCLASSIFIED

5. Originator Advisory Group for Aerospace Research and Development
North Atlantic Treaty Organization
7 rue Ancelle, 92200 Neuilly sur Seine, France

6. Title THE FLIGHT OF FLEXIBLE AIRCRAFT IN TURBULENCE — STATE-OF-THE-ART IN THE DESCRIPTION AND MODELLING OF ATMOSPHERIC TURBULENCE

7. Presented at the 63rd Meeting of the Structures and Materials Panel of AGARD in Athens, Greece, 28 September—3 October 1986

8. Author(s)/Editor(s)	9. Date
Various	December 1987
10. Author's/Editor's Address	**11. Pages**
Various	188

12. Distribution Statement This document is distributed in accordance with AGARD policies and regulations, which are outlined on the Outside Back Covers of all AGARD publications.

13. Keywords/Descriptors

Turbulence
Aircraft
Flight characteristics
Surveys
Data reduction
Accelerometers
Airborne equipment

14. Abstract

The Structures and Materials Panel of AGARD is studying the Flight of Flexible Aircraft in Turbulence. This, the first section of a two-part report, contains presentations given at the first of two Workshops on the subject; topics covered here are (a) Measurements of Turbulence by Specially-equipped Aircraft and (b) Data Collection and Reduction of Incremental Accelerations observed in Commercial Flights.

AGARD Report No.734 Advisory Group for Aerospace Research and Development, NATO THE FLIGHT OF FLEXIBLE AIRCRAFT IN TURBULENCE — STATE-OF-THE-ART IN THE DESCRIPTION AND MODELLING OF ATMOSPHERIC TURBULENCE Published December 1987 188 pages The Structures and Materials Panel of AGARD is studying the Flight of Flexible Aircraft in Turbulence. This, the first section of a two-part report, contains presentations given at the first of two Workshops on the subject; topics covered here are (a) Measurements of Turbulence by Specially-equipped Aircraft and (b) Data P.T.O	AGARD-R-734 Turbulence Aircraft Flight characteristics Surveys Data reduction Accelerometers Airborne equipment	AGARD Report No.734 Advisory Group for Aerospace Research and Development, NATO THE FLIGHT OF FLEXIBLE AIRCRAFT IN TURBULENCE — STATE-OF-THE-ART IN THE DESCRIPTION AND MODELLING OF ATMOSPHERIC TURBULENCE Published December 1987 188 pages The Structures and Materials Panel of AGARD is studying the Flight of Flexible Aircraft in Turbulence. This, the first section of a two-part report, contains presentations given at the first of two Workshops on the subject; topics covered here are (a) Measurements of Turbulence by Specially-equipped Aircraft and (b) Data P.T.O	AGARD-R-734 Turbulence Aircraft Flight characteristics Surveys Data reduction Accelerometers Airborne equipment
AGARD Report No.734 Advisory Group for Aerospace Research and Development, NATO THE FLIGHT OF FLEXIBLE AIRCRAFT IN TURBULENCE — STATE-OF-THE-ART IN THE DESCRIPTION AND MODELLING OF ATMOSPHERIC TURBULENCE Published December 1987 188 pages The Structures and Materials Panel of AGARD is studying the Flight of Flexible Aircraft in Turbulence. This, the first section of a two-part report, contains presentations given at the first of two Workshops on the subject; topics covered here are (a) Measurements of Turbulence by Specially-equipped Aircraft and (b) Data P.T.O	AGARD-R-734 Turbulence Aircraft Flight characteristics Surveys Data reduction Accelerometers Airborne equipment	AGARD Report No.734 Advisory Group for Aerospace Research and Development, NATO THE FLIGHT OF FLEXIBLE AIRCRAFT IN TURBULENCE — STATE-OF-THE-ART IN THE DESCRIPTION AND MODELLING OF ATMOSPHERIC TURBULENCE Published December 1987 188 pages The Structures and Materials Panel of AGARD is studying the Flight of Flexible Aircraft in Turbulence. This, the first section of a two-part report, contains presentations given at the first of two Workshops on the subject; topics covered here are (a) Measurements of Turbulence by Specially-equipped Aircraft and (b) Data P.T.O	AGARD-R-734 Turbulence Aircraft Flight characteristics Surveys Data reduction Accelerometers Airborne equipment

Collection and Reduction of Incremental Accelerations observed in Commercial Flights.

Papers presented at the 63rd Meeting of the Structures and Materials Panel of AGARD in Athens, Greece, 28 September—3 October 1986.

ISBN 92-835-0426-7

Collection and Reduction of Incremental Accelerations observed in Commercial Flights.

Papers presented at the 63rd Meeting of the Structures and Materials Panel of AGARD in Athens, Greece, 28 September—3 October 1986.

ISBN 92-835-0426-7

Collection and Reduction of Incremental Accelerations observed in Commercial Flights.

Papers presented at the 63rd Meeting of the Structures and Materials Panel of AGARD in Athens, Greece, 28 September—3 October 1986.

ISBN 92-835-0426-7

Collection and Reduction of Incremental Accelerations observed in Commercial Flights.

Papers presented at the 63rd Meeting of the Structures and Materials Panel of AGARD in Athens, Greece, 28 September—3 October 1986.

ISBN 92-835-0426-7

AGARD

NATO OTAN

7 rue Ancelle · 92200 NEUILLY-SUR-SEINE

FRANCE

Telephone (1)47.38.57.00 · Telex 610 176

DISTRIBUTION OF UNCLASSIFIED AGARD PUBLICATIONS

AGARD does NOT hold stocks of AGARD publications at the above address for general distribution. Initial distribution of AGARD publications is made to AGARD Member Nations through the following National Distribution Centres.Further copies are sometimes available from these Centres, but if not may be purchased in Microfiche or Photocopy form from the Purchase Agencies listed below.

NATIONAL DISTRIBUTION CENTRES

BELGIUM
Coordonnateur AGARD — VSL
Etat-Major de la Force Aérienne
Quartier Reine Elisabeth
Rue d'Evere, 1140 Bruxelles

CANADA
Director Scientific Information Services
Dept of National Defence
Ottawa, Ontario K1A 0K2

DENMARK
Danish Defence Research Board
Ved Idraetsparken 4
2100 Copenhagen Ø

FRANCE
O.N.E.R.A. (Direction)
29 Avenue de la Division Leclerc
92320 Châtillon

GERMANY
Fachinformationszentrum Energie,
Physik, Mathematik GmbH
Karlsruhe
D-7514 Eggenstein-Leopoldshafen 2

GREECE
Hellenic Air Force General Staff
Aircraft Support Equipment Directorate
Department of Research and Development
Holargos, Athens, 15500

ICELAND
Director of Aviation
c/o Flugrad
Reyjavik

ITALY
Aeronautica Militare
Ufficio del Delegato Nazionale all'AGARD
3 Piazzale Adenauer
00144 Roma/EUR

LUXEMBOURG
See Belgium

NETHERLANDS
Netherlands Delegation to AGARD
National Aerospace Laboratory, NLR
P.O. Box 126
2600 AC Delft

NORWAY
Norwegian Defence Research Establishment
Attn: Biblioteket
P.O. Box 25
N-2007 Kjeller

PORTUGAL
Portuguese National Coordinator to AGARD
Gabinete de Estudos e Programas
CLAFA
Base de Alfragide
Alfragide
2700 Amadora

TURKEY
Millî Savunma Bakanlığı (MSB)
ARGE Daire Başkanlığı (ARGE)
Ankara

UNITED KINGDOM
Defence Research Information Centre
Kentigern House
65 Brown Street
Glasgow G2 8EX

UNITED STATES
National Aeronautics and Space Administration (NASA)
Langley Research Center
M/S 180
Hampton, Virginia 23665

THE UNITED STATES NATIONAL DISTRIBUTION CENTRE (NASA) DOES NOT HOLD STOCKS OF AGARD PUBLICATIONS, AND APPLICATIONS FOR COPIES SHOULD BE MADE DIRECT TO THE NATIONAL TECHNICAL INFORMATION SERVICE (NTIS) AT THE ADDRESS BELOW.

PURCHASE AGENCIES

National Technical
Information Service (NTIS)
5285 Port Royal Road
Springfield
Virginia 22161, USA

ESA/Information Retrieval Service
European Space Agency
10, rue Mario Nikis
75015 Paris, France

The British Library
Document Supply Division
Boston Spa, Wetherby
West Yorkshire LS23 7BQ
England

Requests for microfiche or photocopies of AGARD documents should include the AGARD serial number, title, author or editor, and publication date. Requests to NTIS should include the NASA accession report number. Full bibliographical references and abstracts of AGARD publications are given in the following journals:

Scientific and Technical Aerospace Reports (STAR)
published by NASA Scientific and Technical
Information Branch
NASA Head
Washington I

Government Reports Announcements (GRA)
published by the National Technical

ISBN 92-835-0426-7